

Copyright

By

Dragoslav Vidović

2007

The Dissertation Committee for Dragoslav Vidović certifies that this is the  
approved version of the following dissertation:

**The Chemistry of  $\beta$ -Diketiminato-Supported Boron,  
Aluminum, Gallium and Phosphorus Compounds**

**Committee:**

---

Alan H. Cowley, Supervisor

---

Richard A. Jones

---

Bradley J. Holliday

---

Ben A. Shoulders

---

Jason A. C. Clyburne

**The Chemistry of  $\beta$ -Diketiminato-Supported Boron,  
Aluminum, Gallium and Phosphorus Compounds**

by

**Dragoslav Vidović, B.S.**

**Dissertation**

Presented to the Faculty of the Graduate School of

The University of Texas at Austin

in Partial Fulfillment

of the Requirements

for the Degree of

**Doctor of Philosophy**

The University of Texas at Austin

May 2007

**Dedicated to:**

my Father, mother and brother for endless love and support

**Посвећено:**

мом Оцу, мајци и брату на бескрајној љубави и подршци

## Acknowledgements

First and foremost, I would like to thank Professor Alan H. Cowley for not hesitating even for a moment to accept me as a part of his research group. His endless knowledge, insights, instructions and enthusiasm are truly inspirational. All of the Cowley group members with whom I had the privilege to work certainly played an important role in my achievement. Thus, I would like to thank Dr. Jeffery Pietryga, Silvia Filliponi, Lucille Mullins, Zheng Lu, Dr. Christopher Entwistle, Dr. Leonardo Apostolico, Kalyan Vasudevan, Clint Hoberg and Adam Powell. The toughest times are usually at the beginning but Dr. Piyush Shukla's help and guidance eased lots of those first jitters and concerns when I joined the Cowley group. Special thanks go to Dr. Jamie Jones, Dr. Jennifer Moore, Dr. Nick Hill, Dr. Gregor Reeske and Michael Findlater for sacrificing their valuable time for the X-ray crystallographic analyses of the compounds included in this work. I also greatly appreciate the time Jamie, Jennifer and Michael invested to perform computational studies of several compounds included in this work. Even though Jamie was understandably "uptight" when she was finishing her PhD, I arguably had the best times dancing down on 6<sup>th</sup> Street during her numerous visits from South Carolina. I am thankful to Jennifer not only for insightful chemistry related discussions but also for all of the delicious home-made cooking I loved so much.

Pete Webber, a member of the Krische group, performed an organic transformation reaction involving one of the compounds described in this work. He was also probably one of the subconscious reasons I kept showing up at the Gregory gym at

6 am every morning. I really did enjoy our time working out together but I had much more fun watching the Longhorns-Buckeyes clashes over the years.

Dr. Kenneth Matthews and I met thanks to the common passion that is The Sacramento Kings. However, we later discovered that we had much more in common than just being die-hard Kings fans. He did allow me to be his wing-man when he was rebuilding a car engine which I treasure as invaluable experience. He was also instrumental for the introduction of many US specific events/experiences such as trips to the Texas State Fair and Rodeo and NHRA Drag Racing.

Finally, I want to thank my family for helping me become the man I am today. For various life lessons and more importantly for emphasizing the importance of education, I would like to thank my father. For infinite love and encouragement, I would like to thank my mother. To my brother, I am thankful for simply being an exceptional brother.

# **The Chemistry of $\beta$ -Diketimate-Supported Boron, Aluminum, Gallium and Phosphorus Compounds**

Publication No. \_\_\_\_\_

Dragoslav Vidović, Ph.D.

The University of Texas at Austin, 2007

Supervisor: Alan H. Cowley

Six synthetic methods have been explored for the preparation of several boron, aluminum, gallium and phosphorus compounds supported by the  $C_6F_5$ -substituted  $\beta$ -diketimate ligand. The most significant advance was achieved in the synthesis of  $\beta$ -diketiminato boron dihalide complexes ( $LBX_2$ , L =  $\beta$ -diketimate ligand, X = halide) because only a handful of compounds with this general formula were known. These syntheses were carried out in virtually quantitative yields by treatment of an N-trimethylsilyl aminoimine intermediate with the appropriate boron trihalides.

The synthesis and characterization of the elusive monomeric oxoborane, a compound with formal double bond between boron and oxygen, was also achieved by

employing the  $\text{C}_6\text{F}_5$ -substituted  $\beta$ -diketiminato ligand. The overall stability of the resulting monomeric oxoborane was enhanced by complexation of the Lewis acid  $\text{AlCl}_3$  to the oxoborane oxygen atom. Successful synthetic approaches to the boron, aluminum and gallium bistriflate complexes of the general formula  $\text{LE}(\text{OTf})_2$ , where  $\text{E} = \text{B}, \text{Al}$  or  $\text{Ga}$ , were also developed and preliminary studies involving the use of these compounds as catalysts in organic transformations gave promising results. These bistriflate group 13 compounds also proved to be effective reagents for the synthesis of the first examples of boron, aluminum and gallium dications. The boron and aluminum dications were characterized by single-crystal X-ray diffraction.

Finally, the use of the pentamethylcyclopentadienyl group as the boron substituent has allowed the synthesis and structural characterization of a new cationic terminal borylene complex. This complex, together with the two previously reported cationic terminal borylene complexes, demonstrate that the boron-metal bond order is sensitive to the electronic properties of the boron substituents and can vary from 1 to 2.



## Table of Contents:

List of Figures.....	xi
List of Schemes.....	xix
List of Tables.....	xxi
Index of Compounds.....	xxvii
<b>CHAPTER 1: Synthetic Approaches to C<sub>6</sub>F<sub>5</sub>-Substituted β-Diketimate Complexes of Boron, Aluminum, Gallium and Phosphorus.....</b>	<b>1</b>
<i>INTRODUCTION.....</i>	<i>1</i>
<i>Results and Discussion.....</i>	<i>14</i>
Section 1.1. <i>Methane Elimination Method.....</i>	<i>14</i>
Section 1.2. <i>Dehydrohalogenation Method.....</i>	<i>16</i>
Section 1.3. <i>Salt Metathesis Methods.....</i>	<i>18</i>
Section 1.4. <i>Trimethylsilyl Halide Elimination Method.....</i>	<i>24</i>
Section 1.5. <i>Discussion of X-Ray Crystallographic Data .....</i>	<i>28</i>
<i>CONCLUSIONS.....</i>	<i>42</i>
<b>CHAPTER 2, Part I: Synthesis and Characterization of a Coordinated Oxoborane. Lewis Acid Stabilization of a Boron-Oxygen Double Bond.....</b>	<b>44</b>
<i>INTRODUCTION.....</i>	<i>44</i>
<i>Results and Discussion.....</i>	<i>49</i>
<b>CHAPTER 2, Part II: A Single-Bonded Cationic Terminal Borylene Complex....</b>	<b>59</b>
<i>INTRODUCTION.....</i>	<i>59</i>
<i>Results and Discussion.....</i>	<i>65</i>

<i>CONCLUSIONS</i> .....	71
<b>CHAPTER 3: Synthesis, Characterization, and Reactivity of <math>\beta</math>-Diketiminato-Supported Boron, Aluminum and Gallium Bistriflate Complexes</b> .....	72
<i>INTRODUCTION</i> .....	72
<i>Results and Discussion</i> .....	80
Section 3.1. <i>Boron Triflates</i> .....	80
Section 3.2. <i>Aluminum Triflates</i> .....	88
Section 3.3. <i>Gallium Triflates</i> .....	96
Section 3.4. <i>Hydrolysis products</i> .....	101
Section 3.5. <i>Organic Transformation</i> .....	104
<i>CONCLUSIONS</i> .....	106
<b>CHAPTER 4: Experimental</b> .....	108
Section 4.1. <i>General Procedures</i> .....	108
Section 4.2. <i>Physical Measurements</i> .....	108
Section 4.3. <i>X-Ray Crystallography</i> .....	109
Section 4.4. <i>DFT calculations</i> .....	110
Section 4.5. <i>Experimental Procedures and Spectroscopic Data</i> .....	111
Section 4.6. <i>Figures and Tables of X-ray Crystallographic Data</i> .....	134
<b>References</b> .....	221
<b>Vita</b> .....	228

## List of Figures

<b>Figure 1.1.</b> General structure for a $\beta$ -diketiminato ligand.....	1
<b>Figure 1.2.</b> Different binding modes of $\beta$ -diketiminato ligands.....	2
<b>Figure 1.3.</b> (a) Structure of the Dipp-substituted $\beta$ -diketiminato ligand. (b) General structure of the group 13 carbene analogues.....	5
<b>Figure 1.4.</b> Structure of the $C_6F_5$ -substituted $\beta$ -diketiminato ligand.....	7
<b>Figure 1.5.</b> Examples of $\beta$ -diketiminato-supported boron difluoride complexes.....	8
<b>Figure 1.6.</b> (a) Phosphanyl-substituted $\beta$ -diketiminato complexes (b) Dipp-substituted $\beta$ -diketiminato ligand incorporating different phosphorus moieties.....	10
<b>Figure 1.7.</b> General structure of the targeted compounds.....	12
<b>Figure 1.8.</b> Molecular structure of $(CH(CMe_2)_2(NC_6F_5)_2)H$ , <b>1.1</b> .....	28
<b>Figure 1.9.</b> Molecular structure of $(CH(CMe_2)_2(NC_6F_5)_2)BCl_2$ , <b>1.6</b> . All hydrogen atoms have been omitted for clarity.....	29
<b>Figure 1.10.</b> Molecular structure of $(CH(CMe_2)_2(NC_6F_5)_2)BBr_2$ , <b>1.7</b> . All hydrogen atoms have been omitted for clarity.....	31
<b>Figure 1.11.</b> Molecular structure of $(CH(CMe_2)_2(NC_6F_5)_2)BI_2$ , <b>1.8</b> . All hydrogen atoms have been omitted for clarity.....	32
<b>Figure 1.12.</b> Molecular structure of $(CH(CMe_2)_2(NC_6F_5)_2)AlMe_2$ , <b>1.9</b> . All hydrogen atoms have been omitted for clarity.....	33
<b>Figure 1.13.</b> Molecular structure of $(CH(CMe_2)_2(NC_6F_5)_2)AlCl_2$ , <b>1.11</b> . All hydrogen atoms have been omitted for clarity.....	34
<b>Figure 1.14.</b> Molecular structure of $(CH(CMe_2)_2(NC_6F_5)_2)AlI_2$ , <b>1.12</b> . All hydrogen atoms have been omitted for clarity.....	36
<b>Figure 1.15.</b> Molecular structure of $(CH(CMe_2)_2(NC_6F_5)_2)GaMe_2$ , <b>1.13</b> . All hydrogen atoms have been omitted for clarity.....	37
<b>Figure 1.16.</b> Molecular structure of $(CH(CMe_2)_2(NC_6F_5)_2)GaCl_2$ , <b>1.14</b> . All hydrogen atoms have been omitted for clarity.....	38

<b>Figure 1.17.</b> Molecular structure of $(\text{PCl}_2)\text{CH}(\text{CMe}_2)_2(\text{NC}_6\text{F}_5)_2$ , <b>1.16a</b> . All hydrogen atoms, except that on the $\gamma$ -carbon, have been omitted for clarity.....	39
<b>Figure 1.18.</b> View of the skeleton of <b>1.16a</b> showing the short $\text{P}\cdots\text{N}$ contacts.....	40
<b>Figure 1.19.</b> Molecular structure of $(\text{PhPCl})\text{CH}(\text{CMe}_2)_2(\text{NC}_6\text{F}_5)_2$ , <b>1.17a</b> . All hydrogen atoms, except that on the $\gamma$ -carbon, have been omitted for clarity.....	41
<b>Figure 2.1.</b> Postulated intermediates in the oxidation of a four-membered boracycle with (a) dimethyl sulfoxide (b) diphenylsulfoxide.....	45
<b>Figure 2.2.</b> Structure of the $\text{C}_6\text{F}_5$ -substituted $\beta$ -diketiminate ligand, $\text{L}^-$ .....	48
<b>Figure 2.3.</b> Molecular structure of $[\text{LBCl}]^+$ cation of <b>2.1</b> . The $[\text{AlCl}_4]^-$ anion and all hydrogen atoms have been omitted for clarity.....	50
<b>Figure 2.4.</b> Molecular structure of $[\text{LBPh}]^+$ cation of <b>2.2</b> . The $[\text{AlCl}_4]^-$ cation and all hydrogen atoms have been omitted for clarity.....	51
<b>Figure 2.5.</b> Molecular structure of monomeric oxoborane $\text{LB}=\text{O}\rightarrow\text{AlCl}_3$ , <b>2.3</b> . Hydrogen atoms have been omitted for clarity.....	52
<b>Figure 2.6.</b> Results of DFT calculations at the B3LYP level of theory and the 6-311+G(d) basis set for $\text{LB}=\text{O}\rightarrow\text{AlCl}_3$ , <b>2.3a</b> , and $\text{LB}=\text{O}$ , <b>2.3b</b> . Bond lengths and angles are expressed in Å and degrees, respectively .....	53
<b>Figure 2.7.</b> Selected MO's for $\text{LB}=\text{O}\rightarrow\text{AlCl}_3$ ( <b>2.3a</b> ) and $\text{LB}=\text{O}$ ( <b>2.3b</b> ).....	54
<b>Figure 2.8.</b> Molecular structure of $[\text{LH}_2][\text{AlCl}_4]$ , <b>2.4</b> . All hydrogen atoms, except those on the nitrogen atoms, and the $[\text{AlCl}_4]^-$ anion have been omitted for clarity.....	56
<b>Figure 2.9.</b> Molecular structure of $[\text{LB}-\text{OH}]^+$ cation of <b>2.5</b> . All hydrogen atoms, except that on the hydroxide group, have been omitted for clarity.....	57
<b>Figure 2.10.</b> Proposed structure of one of the products ( <b>2.6</b> ) of the reaction of $\text{LBI}_2$ with $\text{Ag}_2\text{O}$ .....	58
<b>Figure 2.11.</b> Examples of neutral terminal borylene complexes .....	61
<b>Figure 2.12.</b> Examples of (a) dicyclohexylamido ( <b>2.8b</b> ) and (b) diisopropylamido ( <b>2.8c</b> ) substituted cationic terminal borylene complexes. The corresponding anions are not shown.....	63

<b>Figure 2.13.</b> (a) Structure of the cation of <b>2.8</b> (the thermal ellipsoids are drawn at 30% probability and all hydrogen atoms and the anion have been omitted for clarity). (b) The HOMO-4 MO of $[(\eta^5\text{-C}_5\text{H}_5)\text{Fe}(\text{CO})_2(\text{B}(\eta^5\text{-C}_5\text{Me}_5))]^+$ as calculated by the DFT method at the B3LYP level of theory showing the B—Fe $\sigma$ -bond.....	67
<b>Figure 3.1.</b> Coordination geometries of borinium ( <b>A</b> ), borenium ( <b>B</b> ) and boronium ( <b>C</b> ) monocations.....	73
<b>Figure 3.2.</b> Examples of borinium monocations that employ bulky (a) amido and (b) phosphinimide ligands. Corresponding anions have been omitted for clarity.....	73
<b>Figure 3.3.</b> Examples of borenium monocations stabilized by (a) $\beta$ -diketiminato ligands, (b) a phosphazene ligand and (c) non-nitrogen-based boracycle ligands. In each case, the corresponding anions have been omitted for clarity.....	74
<b>Figure 3.4.</b> Examples of boronium cations that are stabilized by bipyridine molecule. Corresponding anions have been omitted for clarity.....	75
<b>Figure 3.5.</b> Examples of (a) a seven-coordinate aluminum monocation and (b) an dialuminum dication. The corresponding anions have been omitted for clarity.....	76
<b>Figure 3.6.</b> Examples of gallium(I) cations. The corresponding anions omitted for clarity.....	78
<b>Figure 3.7.</b> Molecular structure of $\text{LB}(\text{OTf})_2$ , <b>3.1</b> . All hydrogen atoms have been omitted for clarity.....	81
<b>Figure 3.8.</b> Molecular structure of one of the two independent cations of $[\text{LB}(\text{bipy})][2\cdot\text{OTf}]$ , <b>3.2</b> . All hydrogen atoms and both triflate anions have been omitted for clarity.....	82
<b>Figure 3.9.</b> (a) HOMO and (b) LUMO for <b>3.2</b> .....	84
<b>Figure 3.10.</b> Optimized structure of the free boron dication, <b>3.2a</b> . Computed bond distances [ $\text{\AA}$ ] and angles [ $^\circ$ ]: B(1)-N(1) 1.418, B(1)-N(2) 1.393, B(1)-F(1) 1.507, F(1)-C(7) 1.536, N(1)-C(1) 1.401, N(2)-C(3) 1.404, C(1)-C(2) 1.402, C(2)-C(3) 1.404, N(1)-B(1)-N(2) 127.1, B(1)-N(1)-C(1) 116.9, N(1)-C(1)-C(2) 116.1, C(1)-C(2)-C(3) 126.5, C(2)-C(3)-N(2) 117.9, B(1)-N(2)-C(3) 115.4.....	85
<b>Figure 3.11.</b> Molecular structure of one of the two independent units of $[\text{LB}(\text{terpy})][2\cdot\text{OTf}]$ , <b>3.3</b> . All hydrogen atoms and the two triflate anions have been omitted for clarity.....	86

<b>Figure 3.12.</b> Molecular structure of one of the independent molecules of $\text{LAl(OTf)Me}$ , 3.6. All hydrogen atoms, except those on the Al-Me group, have been omitted for clarity.....	89
<b>Figure 3.13.</b> Proposed structures for 3.7 (a) with all bridging triflates, (b) with bridging and terminal triflates.....	90
<b>Figure 3.14.</b> Molecular structures of (a) 3.8, (b) 3.9 and (c) 3.10. In each case, the $\text{C}_6\text{F}_5$ -groups and all hydrogen atoms have been omitted for clarity. The counteranions for 3.9 and 3.10 have also been omitted.....	93
<b>Figure 3.15.</b> Postulated solution phase structures for (a) 3.8a and (b) 3.8b .....	95
<b>Figure 3.16.</b> Postulated solution phase structures for 3.9a.....	95
<b>Figure 3.17.</b> Molecular structure of 3.11. The $\text{C}_6\text{F}_5$ groups of the $\beta$ -diketiminato ligands and all hydrogen molecules have been omitted for clarity.....	97
<b>Figure 3.18.</b> Molecular structures of (a) 3.12 and (b) 3.13. In each case, the $\text{C}_6\text{F}_5$ -groups and all hydrogen atoms have been omitted for clarity. The counteranion for 3.13 has also been omitted .....	99
<b>Figure 3.19.</b> Proposed solution phase structures for (a) 3.13a, (b) 3.12a and (c) 3.12b.....	100
<b>Figure 3.20.</b> Proposed structure for the $\beta$ -diketiminato gallium dication supported by the tren ligand.....	101
<b>Figure 3.21.</b> Molecular structures of (a) 3.15 and (b) 3.16. The $\text{C}_6\text{F}_5$ groups of the $\beta$ -diketiminato ligands and all hydrogen atoms have been omitted for clarity.....	102
<b>Figure 4.1.</b> Molecular structure of $\text{CH(CMe}_2)_2(\text{NC}_6\text{F}_5)(\text{HNC}_6\text{F}_5)$ , 1.1, showing the atom number scheme for selected atoms. The thermal ellipsoids are shown at the 30 % probability level.....	133
<b>Figure 4.2.</b> Molecular structure of $(\text{CH(CMe}_2)_2(\text{NC}_6\text{F}_5)_2\text{BCl}_2)$ , 1.6, showing the atom number scheme for selected atoms. The thermal ellipsoids are shown at the 30 % probability level. All hydrogen atoms have been omitted for clarity.....	136
<b>Figure 4.3.</b> Molecular structure of $(\text{CH(CMe}_2)_2(\text{NC}_6\text{F}_5)_2\text{BBr}_2)$ , 1.7, showing the atom number scheme for selected atoms. The thermal ellipsoids are shown at the 30 % probability level. All hydrogen atoms have been omitted for clarity.....	139

**Figure 4.4.** Molecular structure of  $(\text{CH}(\text{CMe}_2)_2(\text{NC}_6\text{F}_5)_2)\text{BI}_2$ , **1.8**, showing the atom number scheme for selected atoms. The thermal ellipsoids are shown at the 30 % probability level. All hydrogen atoms have been omitted for clarity.....142

**Figure 4.5.** Molecular structure of  $(\text{CH}(\text{CMe}_2)_2(\text{NC}_6\text{F}_5)_2)\text{AlMe}_2$ , **1.9**, showing the atom number scheme for selected atoms. The thermal ellipsoids are shown at the 30 % probability level. All hydrogen atoms have been omitted for clarity.....145

**Figure 4.6.** Molecular structure of  $(\text{CH}(\text{CMe}_2)_2(\text{NC}_6\text{F}_5)_2)\text{AlCl}_2$ , **1.11**, showing the atom number scheme for selected atoms. The thermal ellipsoids are shown at the 30 % probability level. All hydrogen atoms have been omitted for clarity.....148

**Figure 4.7.** Molecular structure of  $(\text{CH}(\text{CMe}_2)_2(\text{NC}_6\text{F}_5)_2)\text{AlI}_2$ , **1.12**, showing the atom number scheme for selected atoms. The thermal ellipsoids are shown at the 30 % probability level. All hydrogen atoms have been omitted for clarity.....151

**Figure 4.8.** Molecular structure of  $(\text{CH}(\text{CMe}_2)_2(\text{NC}_6\text{F}_5)_2)\text{GaMe}_2$ , **1.13**, showing the atom number scheme for selected atoms. The thermal ellipsoids are shown at the 30 % probability level. All hydrogen atoms have been omitted for clarity.....154

**Figure 4.9.** Molecular structure of  $(\text{CH}(\text{CMe}_2)_2(\text{NC}_6\text{F}_5)_2)\text{GaCl}_2$ , **1.14**, showing the atom number scheme for selected atoms. The thermal ellipsoids are shown at the 30 % probability level. All hydrogen atoms have been omitted for clarity.....157

**Figure 4.10.** Molecular structure of  $(\text{Cl}_2\text{P})\text{CH}(\text{CMe}_2)_2(\text{NC}_6\text{F}_5)_2$ , **1.16a**, showing the atom number scheme for selected atoms. The thermal ellipsoids are shown at the 30 % probability level. All hydrogen atoms, except that on the  $\gamma$ -carbon, have been omitted for clarity.....160

**Figure 4.11.** Molecular structure of  $(\text{ClPhP})\text{CH}(\text{CMe}_2)_2(\text{NC}_6\text{F}_5)_2$ , **1.17a**, showing the atom number scheme for selected atoms. The thermal ellipsoids are shown at the 30 % probability level. All hydrogen atoms, except that on the  $\gamma$ -carbon, have been omitted for clarity.....163

**Figure 4.12.** Molecular structure of  $[(\text{CH}(\text{CMe}_2)_2(\text{NC}_6\text{F}_5)_2)\text{BCl}][\text{AlCl}_4]$ , **2.1**, showing the atom number scheme for selected atoms. The thermal ellipsoids are shown at the 30 % probability level. All hydrogen atoms have been omitted for clarity.....166

**Figure 4.13.** Molecular structure of one of the independent units of  $[(\text{CH}(\text{CMe}_2)_2(\text{NC}_6\text{F}_5)_2)\text{BCl}][\text{AlCl}_4]$ , **2.1**, showing the atom number scheme for selected atoms. The thermal ellipsoids are shown at the 30 % probability level. All hydrogen atoms have been omitted for clarity.....166

**Figure 4.14.** Molecular structure of  $[(CH(CMe_2)_2(NC_6F_5)_2)BPh][AlCl_4]$ , **2.2**, showing the atom number scheme for selected atoms. The thermal ellipsoids are shown at the 30 % probability level. All hydrogen atoms have been omitted for clarity.....169

**Figure 4.15.** Molecular structure of  $(CH(CMe_2)_2(NC_6F_5)_2)B=O \rightarrow AlCl_3$ , **2.3**, showing the atom number scheme for selected atoms. The thermal ellipsoids are shown at the 30 % probability level. All hydrogen atoms have been omitted for clarity.....172

**Figure 4.16.** Molecular structure of  $[CH(CMe_2)_2(HNC_6F_5)_2][AlCl_4]$ , **2.4**, showing the atom number scheme for selected atoms. The thermal ellipsoids are shown at the 30 % probability level. All hydrogen atoms, except those on the nitrogen atoms, have been omitted for clarity.....175

**Figure 4.17.** Molecular structure of  $[(CH(CMe_2)_2(NC_6F_5)_2)B(OH)][AlCl_4]$ , **2.5**, showing the atom number scheme for selected atoms. The thermal ellipsoids are shown at the 30 % probability level. All hydrogen atoms, except those on the oxygen atoms, have been omitted for clarity .....178

**Figure 4.18.** Molecular structure of one of the independent units of  $[(CH(CMe_2)_2(NC_6F_5)_2)B(OH)][AlCl_4]$ , **2.5**, showing the atom number scheme for selected atoms. The thermal ellipsoids are shown at the 30 % probability level. All hydrogen atoms, except that on the oxygen atom, have been omitted for clarity.....178

**Figure 4.19.** Molecular structure of  $[(\eta^5-C_5H_5)Fe(CO)_2B(\eta^5-C_5Me_5)][AlCl_4]$ , **2.8**, showing the atom number scheme for selected atoms. The thermal ellipsoids are shown at the 30 % probability level. All hydrogen atoms have been omitted for clarity.....181

**Figure 4.20.** Molecular structure of  $(CH(CMe_2)_2(NC_6F_5)_2)B(OTf)_2$ , **3.1**, showing the atom number scheme for selected atoms. The thermal ellipsoids are shown at the 30 % probability level. All hydrogen atoms have been omitted for clarity.....184

**Figure 4.21.** Molecular structure of  $[(CH(CMe_2)_2(NC_6F_5)_2)B(bipy)][2 \cdot OTf]$ , **3.2**, showing the atom number scheme for selected atoms. The thermal ellipsoids are shown at the 30 % probability level. All hydrogen atoms have been omitted for clarity.....187

**Figure 4.22.** Molecular structure of one of the two independent units of  $[(CH(CMe_2)_2(NC_6F_5)_2)B(bipy)][2 \cdot OTf]$ , **3.2**, showing the atom number scheme for selected atoms. The thermal ellipsoids are shown at the 30 % probability level. All hydrogen atoms and the two triflate anions have been omitted for clarity.....187

**Figure 4.23.** Molecular structure of  $[(CH(CMe_2)_2(NC_6F_5)_2)B(terpy)][2 \cdot OTf]$ , **3.3**, showing the atom number scheme for selected atoms. The thermal ellipsoids are shown at the 30 % probability level. All hydrogen atoms have been omitted for clarity.....190



**Figure 4.24.** Molecular structure of one of the two independent units of  $[(\text{CH}(\text{CMe}_2)_2(\text{NC}_6\text{F}_5)_2)\text{B}(\text{terpy})][2\text{-OTf}]$ , **3.3**, showing the atom number scheme for selected atoms. The thermal ellipsoids are shown at the 30 % probability level. All hydrogen atoms and the two triflate anions have been omitted for clarity.....190

**Figure 4.25.** Molecular structure of  $(\text{CH}(\text{CMe}_2)_2(\text{NC}_6\text{F}_5)_2)\text{Al}(\text{OTf})\text{Me}$ , **3.6**, showing the atom number scheme for selected atoms. The thermal ellipsoids are shown at the 30 % probability level. All hydrogen atoms except those on the Al-Me group have been omitted for clarity.....193

**Figure 4.26.** Molecular structure of one of the two independent units of  $(\text{CH}(\text{CMe}_2)_2(\text{NC}_6\text{F}_5)_2)\text{Al}(\text{OTf})\text{Me}$ , **3.6**, showing the atom number scheme for selected atoms. The thermal ellipsoids are shown at the 30 % probability level. All hydrogen atoms, except those on the Al-Me group, have been omitted for clarity.....193

**Figure 4.27.** Molecular structure of  $(\text{CH}(\text{CMe}_2)_2(\text{NC}_6\text{F}_5)_2)\text{Al}(\text{OTf})_2(\text{bipy})$ , **3.8**, showing the atom number scheme for selected atoms. The thermal ellipsoids are shown at the 30 % probability level. All hydrogen atoms have been omitted for clarity.....196

**Figure 4.28.** Molecular structure of  $[(\text{CH}(\text{CMe}_2)_2(\text{NC}_6\text{F}_5)_2)\text{Al}(\text{OTf})(\text{terpy})][\text{OTf}]$ , **3.9**, showing the atom number scheme for selected atoms. The thermal ellipsoids are shown at the 30 % probability level. All hydrogen atoms and the solvent molecules have been omitted for clarity.....199

**Figure 4.29.** Molecular structure of  $[(\text{CH}(\text{CMe}_2)_2(\text{NC}_6\text{F}_5)_2)\text{Al}(\text{tren})][2\text{-OTf}]$ , **3.10**, showing the atom number scheme for selected atoms. The thermal ellipsoids are shown at the 30 % probability level. All hydrogen atoms have been omitted for clarity.....202

**Figure 4.30.** Molecular structure of  $((\text{CH}(\text{CMe}_2)_2(\text{NC}_6\text{F}_5)_2)\text{Ga}(\text{OTf})_2(\text{CH}_3\text{CN}))_2$ , **3.11**, showing the atom number scheme for selected atoms. The thermal ellipsoids are shown at the 30 % probability level. All hydrogen atoms have been omitted for clarity.....205

**Figure 4.31.** Molecular structure of  $((\text{CH}(\text{CMe}_2)_2(\text{NC}_6\text{F}_5)_2)\text{Ga}(\text{OTf})_2(\text{CH}_3\text{CN}))_2$ , **3.11**, showing the atom number scheme for selected atoms. The thermal ellipsoids are shown at the 30 % probability level. All hydrogen atoms and the  $\text{C}_6\text{F}_5$ -substituents have been omitted for clarity.....205

**Figure 4.32.** Molecular structure of  $(\text{CH}(\text{CMe}_2)_2(\text{NC}_6\text{F}_5)_2)\text{Ga}(\text{OTf})_2(\text{bipy})$ , **3.12**, showing the atom number scheme for selected atoms. The thermal ellipsoids are shown at the 30 % probability level. All hydrogen atoms have been omitted for clarity.....208

**Figure 4.33.** Molecular structure of  $[(\text{CH}(\text{CMe}_2)_2(\text{NC}_6\text{F}_5)_2)\text{Ga}(\text{OTf})(\text{terpy})][\text{OTf}]$ , **3.13**, showing the atom number scheme for selected atoms. The thermal ellipsoids are shown at the 30 % probability level. All hydrogen atoms and the solvent molecules have been omitted for clarity.....211

**Figure 4.34.** Molecular structure of  $((\text{CH}(\text{CMe}_2)_2(\text{NC}_6\text{F}_5)_2)\text{Al}(\text{OTf})(\text{OH}))_2$ , **3.15**, showing the atom number scheme for selected atoms. The thermal ellipsoids are shown at the 30 % probability level. All hydrogen atoms have been omitted for clarity.....214

**Figure 4.35.** Molecular structure of  $((\text{CH}(\text{CMe}_2)_2(\text{NC}_6\text{F}_5)_2)\text{Ga}(\text{OTf}))_2\text{O}$ , **3.16**, showing the atom number scheme for selected atoms. The thermal ellipsoids are shown at the 30 % probability level. All hydrogen atoms have been omitted for clarity.....217

## List of Schemes

<b>Scheme 1.1.</b> First reported synthesis of a $\beta$ -diketiminate ligand.....	3
<b>Scheme 1.2.</b> Synthesis of a $\beta$ -diketiminate ligand from tetraalkoxypropane.....	4
<b>Scheme 1.3.</b> Synthesis of a $\beta$ -diketiminato boron dichloride complex.....	8
<b>Scheme 1.4.</b> General description of the methane elimination route.....	14
<b>Scheme 1.5.</b> Possible ligand scrambling process for $\text{Me}_2\text{AlCl}$ .....	15
<b>Scheme 1.6.</b> General description of the dehydrohalogenation method.....	16
<b>Scheme 1.7.</b> General description of the salt elimination method.....	18
<b>Scheme 1.8.</b> Equilibrium between diimine and aminoimine forms of phosphorus compounds.....	21
<b>Scheme 1.9.</b> General description of the trimethylsilyl halide elimination method.....	24
<b>Scheme 1.10.</b> Possible reaction scheme for the formation of $\beta$ -diketiminate-supported group 13 dihalide complexes by the reaction of the silyl-based reagent 1.5 with $\text{MX}_3$ . (i) coordination of $\text{MX}_3$ to the imine nitrogen; (ii) silane elimination; (iii) ring closure.....	25
<b>Scheme 2.1.</b> Oxidation of a four-membered boracycle by dimethyl sulfoxide (DMSO) and trapping of postulated $\text{Tbt-B=O}$ .....	44
<b>Scheme 2.2.</b> Oxidation of a four-membered boracycle by diphenyl sulfoxide (DPSO) and trapping of postulated $\text{Tbt-B=O}$ .....	45
<b>Scheme 2.3.</b> Photolysis of a dioxodiboretane in presence of trapping agents.....	46
<b>Scheme 2.4.</b> Thermolysis of tris(trimethylsilyl)boranes.....	47
<b>Scheme 2.5.</b> Evidence for the existence of a monomeric oxoborane as a reactive intermediate.....	48
<b>Scheme 2.6.</b> A possible reaction pathway in the synthesis of $[\text{LBOH}][\text{AlCl}_4]$ , <b>2.5</b> .....	57
<b>Scheme 2.7.</b> Trapping of a reactive borylene.....	60

<b>Scheme 2.8.</b> Synthesis of the first bridging borylene complex.....	60
<b>Scheme 2.9.</b> Synthesis of the first cation terminal borylene.....	62
<b>Scheme 2.10.</b> The synthesis of $[(\eta^5\text{-C}_5\text{H}_5)\text{Fe}(\text{CO})_2(\text{B}(\eta^5\text{-C}_5\text{Me}_5))][\text{AlCl}_4]$ , <b>2.8</b> , by a halide abstraction reaction.....	66
<b>Scheme 2.11.</b> (a) addition of a chloride anion to <b>2.8</b> does not regenerate <b>2.7</b> but instead the intermediate <b>2.9</b> (b) dissolution of <b>2.7</b> in $\text{CH}_2\text{Cl}_2$ results in a mixture of <b>2.9</b> and an analogue of <b>2.8</b> , $[\text{2.8}^+][\text{Cl}^-]$ ; addition of $[\text{Ph}_4\text{P}]\text{Cl}$ leads to <b>2.9</b> only while addition of $\text{AlCl}_3$ produces <b>2.8</b> .....	69
<b>Scheme 3.1.</b> Hydrolysis of a borenium cation led to the isolation of the first example of diboron dication. The corresponding anions have been omitted for clarity.....	75
<b>Scheme 3.2.</b> Summary of the reactions of aluminum bistriflate <b>3.7</b> with the neutral Lewis bases bipy, terpy and tren.....	92
<b>Scheme 3.3.</b> Summary of the reactions of gallium bistriflate <b>3.11</b> with the neutral Lewis bases bipy and terpy.....	98
<b>Scheme 3.4.</b> Hydrolysis products of the aluminum and gallium bistriflates, <b>3.15</b> and <b>3.16</b> .....	102
<b>Scheme 3.5.</b> Amination of the epoxide.....	105

## List of Tables

<b>Table 1.1.</b> Bond dissociation energies in kJ/mol.....	26
<b>Table 4.1.</b> Crystal data and structure refinement for CH(CMe <sub>2</sub> ) <sub>2</sub> (NC <sub>6</sub> F <sub>5</sub> ) (HNC <sub>6</sub> F <sub>5</sub> ), 1.1.....	134
<b>Table 4.2.</b> Selected bond lengths (Å) for CH(CMe <sub>2</sub> ) <sub>2</sub> (NC <sub>6</sub> F <sub>5</sub> )(HNC <sub>6</sub> F <sub>5</sub> ), 1.1.....	135
<b>Table 4.3.</b> Selected bond angles (°) for CH(CMe <sub>2</sub> ) <sub>2</sub> (NC <sub>6</sub> F <sub>5</sub> )(HNC <sub>6</sub> F <sub>5</sub> ), 1.1.....	135
<b>Table 4.4.</b> Crystal data and structure refinement for (CH(CMe <sub>2</sub> ) <sub>2</sub> (NC <sub>6</sub> F <sub>5</sub> ) <sub>2</sub> )BCl <sub>2</sub> , 1.6.....	137
<b>Table 4.5.</b> Selected bond lengths (Å) for (CH(CMe <sub>2</sub> ) <sub>2</sub> (NC <sub>6</sub> F <sub>5</sub> ) <sub>2</sub> )BCl <sub>2</sub> , 1.6.....	138
<b>Table 4.6</b> Selected bond angles (°) for (CH(CMe <sub>2</sub> ) <sub>2</sub> (NC <sub>6</sub> F <sub>5</sub> ) <sub>2</sub> )BCl <sub>2</sub> , 1.6.....	138
<b>Table 4.7.</b> Crystal data and structure refinement for (CH(CMe <sub>2</sub> ) <sub>2</sub> (NC <sub>6</sub> F <sub>5</sub> ) <sub>2</sub> )BBr <sub>2</sub> , 1.7.....	140
<b>Table 4.8.</b> Selected bond lengths (Å) for (CH(CMe <sub>2</sub> ) <sub>2</sub> (NC <sub>6</sub> F <sub>5</sub> ) <sub>2</sub> )BBr <sub>2</sub> , 1.7.....	141
<b>Table 4.9.</b> Selected bond angles (°) for (CH(CMe <sub>2</sub> ) <sub>2</sub> (NC <sub>6</sub> F <sub>5</sub> ) <sub>2</sub> )BBr <sub>2</sub> , 1.7.....	141
<b>Table 4.10.</b> Crystal data and structure refinement for (CH(CMe <sub>2</sub> ) <sub>2</sub> (NC <sub>6</sub> F <sub>5</sub> ) <sub>2</sub> )BI <sub>2</sub> , 1.8.....	143
<b>Table 4.11.</b> Selected bond lengths (Å) for (CH(CMe <sub>2</sub> ) <sub>2</sub> (NC <sub>6</sub> F <sub>5</sub> ) <sub>2</sub> )BI <sub>2</sub> , 1.8.....	144
<b>Table 4.12.</b> Selected bond angles (°) for (CH(CMe <sub>2</sub> ) <sub>2</sub> (NC <sub>6</sub> F <sub>5</sub> ) <sub>2</sub> )BI <sub>2</sub> , 1.8.....	144
<b>Table 4.13.</b> Crystal data and structure refinement for (CH(CMe <sub>2</sub> ) <sub>2</sub> (NC <sub>6</sub> F <sub>5</sub> ) <sub>2</sub> )AlMe <sub>2</sub> , 1.9.....	146
<b>Table 4.14.</b> Selected bond lengths (Å) for (CH(CMe <sub>2</sub> ) <sub>2</sub> (NC <sub>6</sub> F <sub>5</sub> ) <sub>2</sub> )AlMe <sub>2</sub> , 1.9.....	147
<b>Table 4.15.</b> Selected bond angles (°) for (CH(CMe <sub>2</sub> ) <sub>2</sub> (NC <sub>6</sub> F <sub>5</sub> ) <sub>2</sub> )AlMe <sub>2</sub> , 1.9.....	147
<b>Table 4.16.</b> Crystal data and structure refinement for (CH(CMe <sub>2</sub> ) <sub>2</sub> (NC <sub>6</sub> F <sub>5</sub> ) <sub>2</sub> )AlCl <sub>2</sub> , 1.11.....	149
<b>Table 4.17.</b> Selected bond lengths (Å) for (CH(CMe <sub>2</sub> ) <sub>2</sub> (NC <sub>6</sub> F <sub>5</sub> ) <sub>2</sub> )AlCl <sub>2</sub> , 1.11.....	150

<b>Table 4.18.</b> Selected bond angles (°) for (CH(CMe <sub>2</sub> ) <sub>2</sub> (NC <sub>6</sub> F <sub>5</sub> ) <sub>2</sub> )AlCl <sub>2</sub> , <b>1.11</b> .....	150
<b>Table 4.19.</b> Crystal data and structure refinement for (CH(CMe <sub>2</sub> ) <sub>2</sub> (NC <sub>6</sub> F <sub>5</sub> ) <sub>2</sub> )AlI <sub>2</sub> , <b>1.12</b> .....	152
<b>Table 4.20.</b> Selected bond lengths (Å) for (CH(CMe <sub>2</sub> ) <sub>2</sub> (NC <sub>6</sub> F <sub>5</sub> ) <sub>2</sub> )AlI <sub>2</sub> , <b>1.12</b> .....	153
<b>Table 4.21.</b> Selected bond angles (°) for (CH(CMe <sub>2</sub> ) <sub>2</sub> (NC <sub>6</sub> F <sub>5</sub> ) <sub>2</sub> )AlI <sub>2</sub> , <b>1.12</b> .....	153
<b>Table 4.22.</b> Crystal data and structure refinement for [CH(CMe <sub>2</sub> ) <sub>2</sub> (NC <sub>6</sub> F <sub>5</sub> ) <sub>2</sub> ]GaMe <sub>2</sub> , <b>1.13</b> .....	155
<b>Table 4.23.</b> Selected bond lengths (Å) for (CH(CMe <sub>2</sub> ) <sub>2</sub> (NC <sub>6</sub> F <sub>5</sub> ) <sub>2</sub> )GaMe <sub>2</sub> , <b>1.13</b> .....	156
<b>Table 4.24.</b> Selected bond angles (°) for (CH(CMe <sub>2</sub> ) <sub>2</sub> (NC <sub>6</sub> F <sub>5</sub> ) <sub>2</sub> )GaMe <sub>2</sub> , <b>1.13</b> .....	156
<b>Table 4.25.</b> Crystal data and structure refinement for (CH(CMe <sub>2</sub> ) <sub>2</sub> (NC <sub>6</sub> F <sub>5</sub> ) <sub>2</sub> )GaCl <sub>2</sub> , <b>1.14</b> .....	158
<b>Table 4.26.</b> Selected bond lengths (Å) for (CH(CMe <sub>2</sub> ) <sub>2</sub> (NC <sub>6</sub> F <sub>5</sub> ) <sub>2</sub> )GaCl <sub>2</sub> , <b>1.14</b> .....	159
<b>Table 4.27.</b> Selected bond angles (°) for (CH(CMe <sub>2</sub> ) <sub>2</sub> (NC <sub>6</sub> F <sub>5</sub> ) <sub>2</sub> )GaCl <sub>2</sub> , <b>1.14</b> .....	159
<b>Table 4.28.</b> Crystal data and structure refinement for (Cl <sub>2</sub> P)CH(CMe <sub>2</sub> ) <sub>2</sub> (NC <sub>6</sub> F <sub>5</sub> ) <sub>2</sub> , <b>1.16a</b> .....	161
<b>Table 4.29.</b> Selected bond lengths (Å) for (Cl <sub>2</sub> P)(CH(CMe <sub>2</sub> ) <sub>2</sub> (NC <sub>6</sub> F <sub>5</sub> ) <sub>2</sub> ), <b>1.16a</b> .....	162
<b>Table 4.30.</b> Selected bond angles (°) for (Cl <sub>2</sub> P)CH(CMe <sub>2</sub> ) <sub>2</sub> (NC <sub>6</sub> F <sub>5</sub> ) <sub>2</sub> , <b>1.16a</b> .....	162
<b>Table 4.31.</b> Crystal data and structure refinement for (ClPhP)CH(CMe <sub>2</sub> ) <sub>2</sub> (NC <sub>6</sub> F <sub>5</sub> ) <sub>2</sub> , <b>1.17a</b> .....	164
<b>Table 4.32.</b> Selected bond lengths (Å) for (ClPhP)CH(CMe <sub>2</sub> ) <sub>2</sub> (NC <sub>6</sub> F <sub>5</sub> ) <sub>2</sub> , <b>1.17a</b> .....	165
<b>Table 4.33.</b> Selected bond angles (°) for (ClPhP)CH(CMe <sub>2</sub> ) <sub>2</sub> (NC <sub>6</sub> F <sub>5</sub> ) <sub>2</sub> , <b>1.17a</b> .....	165
<b>Table 4.34.</b> Crystal data and structure refinement for [(CH(CMe <sub>2</sub> ) <sub>2</sub> (NC <sub>6</sub> F <sub>5</sub> ) <sub>2</sub> )BCl] [AlCl <sub>4</sub> ], <b>2.1</b> .....	167
<b>Table 4.35.</b> Selected bond lengths (Å) for [(CH(CMe <sub>2</sub> ) <sub>2</sub> (NC <sub>6</sub> F <sub>5</sub> ) <sub>2</sub> )BCl][AlCl <sub>4</sub> ], <b>2.1</b> ..	168
<b>Table 4.36.</b> Selected bond angles (°) for [(CH(CMe <sub>2</sub> ) <sub>2</sub> (NC <sub>6</sub> F <sub>5</sub> ) <sub>2</sub> )BCl][AlCl <sub>4</sub> ], <b>2.1</b> .....	168

<b>Table 4.37.</b> Crystal data and structure refinement for $[(\text{CH}(\text{CMe}_2)_2(\text{NC}_6\text{F}_5)_2)\text{BPh}][\text{AlCl}_4]$ , <b>2.2</b> .....	170
<b>Table 4.38.</b> Selected bond lengths (Å) for $[(\text{CH}(\text{CMe}_2)_2(\text{NC}_6\text{F}_5)_2)\text{BPh}][\text{AlCl}_4]$ , <b>2.2</b> ..	171
<b>Table 4.39.</b> Selected bond angles (°) for $[(\text{CH}(\text{CMe}_2)_2(\text{NC}_6\text{F}_5)_2)\text{BPh}][\text{AlCl}_4]$ , <b>2.2</b> ....	171
<b>Table 4.40.</b> Crystal data and structure refinement for $(\text{CH}(\text{CMe}_2)_2(\text{NC}_6\text{F}_5)_2)\text{B}=\text{O} \rightarrow \text{AlCl}_3$ , <b>2.3</b> .....	173
<b>Table 4.41.</b> Selected bond lengths (Å) for $(\text{CH}(\text{CMe}_2)_2(\text{NC}_6\text{F}_5)_2)\text{B}=\text{O} \rightarrow \text{AlCl}_3$ , <b>2.3</b> ...	174
<b>Table 4.42.</b> Selected bond angles (°) for $(\text{CH}(\text{CMe}_2)_2(\text{NC}_6\text{F}_5)_2)\text{B}=\text{O} \rightarrow \text{AlCl}_3$ , <b>2.3</b> .....	174
<b>Table 4.43.</b> Crystal data and structure refinement for $[\text{CH}(\text{CMe}_2)_2(\text{HNC}_6\text{F}_5)_2][\text{AlCl}_4]$ , <b>2.4</b> .....	176
<b>Table 4.44.</b> Selected bond lengths (Å) for $[\text{CH}(\text{CMe}_2)_2(\text{HNC}_6\text{F}_5)_2][\text{AlCl}_4]$ , <b>2.4</b> .....	177
<b>Table 4.45.</b> Selected bond angles (°) for $[\text{CH}(\text{CMe}_2)_2(\text{HNC}_6\text{F}_5)_2][\text{AlCl}_4]$ , <b>2.4</b> .....	177
<b>Table 4.46.</b> Crystal data and structure refinement for $[(\text{CH}(\text{CMe}_2)_2(\text{NC}_6\text{F}_5)_2)\text{B}(\text{OH})][\text{AlCl}_4]$ , <b>2.5</b> .....	179
<b>Table 4.47.</b> Selected bond lengths (Å) for $[(\text{CH}(\text{CMe}_2)_2(\text{NC}_6\text{F}_5)_2)\text{B}(\text{OH})][\text{AlCl}_4]$ , <b>2.5</b> .....	180
<b>Table 4.48.</b> Selected bond angles (°) for $[(\text{CH}(\text{CMe}_2)_2(\text{NC}_6\text{F}_5)_2)\text{B}(\text{OH})][\text{AlCl}_4]$ , <b>2.5</b> .....	180
<b>Table 4.49.</b> Crystal data and structure refinement for $[(\eta^5\text{-C}_5\text{H}_5)\text{Fe}(\text{CO})_2\text{B}(\eta^5\text{-C}_5\text{Me}_5)][\text{AlCl}_4]$ , <b>2.8</b> .....	182
<b>Table 4.50.</b> Selected bond lengths (Å) for $[(\eta^5\text{-C}_5\text{H}_5)\text{Fe}(\text{CO})_2\text{B}(\eta^5\text{-C}_5\text{Me}_5)][\text{AlCl}_4]$ , <b>2.8</b> .....	183
<b>Table 4.51.</b> Selected bond angles (°) for $[(\eta^5\text{-C}_5\text{H}_5)\text{Fe}(\text{CO})_2\text{B}(\eta^5\text{-C}_5\text{Me}_5)][\text{AlCl}_4]$ , <b>2.8</b> .....	183
<b>Table 4.52.</b> Crystal data and structure refinement for $(\text{CH}(\text{CMe}_2)_2(\text{NC}_6\text{F}_5)_2)\text{B}(\text{OTf})_2$ , <b>3.1</b> .....	185
<b>Table 4.53.</b> Selected bond lengths (Å) for $(\text{CH}(\text{CMe}_2)_2(\text{NC}_6\text{F}_5)_2)\text{B}(\text{OTf})_2$ , <b>3.1</b> .....	186
<b>Table 4.54.</b> Selected bond angles (°) for $(\text{CH}(\text{CMe}_2)_2(\text{NC}_6\text{F}_5)_2)\text{B}(\text{OTf})_2$ , <b>3.1</b> .....	186

<b>Table 4.55.</b> Crystal data and structure refinement for $[\text{CH}(\text{CMe}_2)_2(\text{NC}_6\text{F}_5)_2\text{B}(\text{bipy})][2\cdot\text{OTf}]$ , <b>3.2</b> .....	188
<b>Table 4.56.</b> Selected bond lengths (Å) for $[(\text{CH}(\text{CMe}_2)_2(\text{NC}_6\text{F}_5)_2\text{B}(\text{bipy}))][2\cdot\text{OTf}]$ , <b>3.2</b> .....	189
<b>Table 4.57.</b> Selected bond angles (°) for $[(\text{CH}(\text{CMe}_2)_2(\text{NC}_6\text{F}_5)_2\text{B}(\text{bipy}))][2\cdot\text{OTf}]$ , <b>3.2</b> .....	189
<b>Table 4.58.</b> Crystal data and structure refinement for $[\text{CH}(\text{CMe}_2)_2(\text{NC}_6\text{F}_5)_2\text{B}(\text{terpy})][2\cdot\text{OTf}]$ , <b>3.3</b> .....	191
<b>Table 4.59.</b> Selected bond lengths (Å) for $[(\text{CH}(\text{CMe}_2)_2(\text{NC}_6\text{F}_5)_2\text{B}(\text{terpy}))][2\cdot\text{OTf}]$ , <b>3.3</b> .....	192
<b>Table 4.60.</b> Selected bond angles (°) for $[(\text{CH}(\text{CMe}_2)_2(\text{NC}_6\text{F}_5)_2\text{B}(\text{terpy}))][2\cdot\text{OTf}]$ , <b>3.3</b> .....	192
<b>Table 4.61.</b> Crystal data and structure refinement for $(\text{CH}(\text{CMe}_2)_2(\text{NC}_6\text{F}_5)_2\text{Al}(\text{OTf})(\text{Me}))$ , <b>3.6</b> .....	194
<b>Table 4.62.</b> Selected bond lengths (Å) for $(\text{CH}(\text{CMe}_2)_2(\text{NC}_6\text{F}_5)_2\text{Al}(\text{OTf})\text{Me})$ , <b>3.6</b> ....	195
<b>Table 4.63.</b> Selected bond angles (°) for $(\text{CH}(\text{CMe}_2)_2(\text{NC}_6\text{F}_5)_2\text{Al}(\text{OTf})\text{Me})$ , <b>3.6</b> .....	195
<b>Table 4.64.</b> Crystal data and structure refinement for $(\text{CH}(\text{CMe}_2)_2(\text{NC}_6\text{F}_5)_2\text{Al}(\text{OTf})_2(\text{bipy}))$ , <b>3.8</b> .....	197
<b>Table 4.65.</b> Selected bond lengths (Å) for $(\text{CH}(\text{CMe}_2)_2(\text{NC}_6\text{F}_5)_2\text{Al}(\text{OTf})_2(\text{bipy}))$ , <b>3.8</b> .....	198
<b>Table 4.66.</b> Selected bond angles (°) for $(\text{CH}(\text{CMe}_2)_2(\text{NC}_6\text{F}_5)_2\text{Al}(\text{OTf})_2(\text{bipy}))$ , <b>3.8</b> ..	198
<b>Table 4.67.</b> Crystal data and structure refinement for $[(\text{CH}(\text{CMe}_2)_2(\text{NC}_6\text{F}_5)_2\text{Al}(\text{OTf})(\text{terpy}))][\text{OTf}]$ , <b>3.9</b> .....	200
<b>Table 4.68.</b> Selected bond lengths (Å) for $[(\text{CH}(\text{CMe}_2)_2(\text{NC}_6\text{F}_5)_2\text{Al}(\text{OTf})(\text{terpy}))][\text{OTf}]$ , <b>3.9</b> .....	201
<b>Table 4.69.</b> Selected bond angles (°) for $[(\text{CH}(\text{CMe}_2)_2(\text{NC}_6\text{F}_5)_2\text{Al}(\text{OTf})(\text{terpy}))][\text{OTf}]$ , <b>3.9</b> .....	201
<b>Table 4.70.</b> Crystal data and structure refinement for $[(\text{CH}(\text{CMe}_2)_2(\text{NC}_6\text{F}_5)_2\text{Al}(\text{tren}))][2\cdot\text{OTf}]$ , <b>3.10</b> .....	203



<b>Table 4.71.</b> Selected bond lengths (Å) for [(CH(CMe <sub>2</sub> ) <sub>2</sub> (NC <sub>6</sub> F <sub>5</sub> ) <sub>2</sub> )Al(tren)][2·OTf], <b>3.10</b> .....	204
<b>Table 4.72.</b> Selected bond angles (°) for [(CH(CMe <sub>2</sub> ) <sub>2</sub> (NC <sub>6</sub> F <sub>5</sub> ) <sub>2</sub> )Al(tren)][2·OTf], <b>3.10</b> .....	204
<b>Table 4.73.</b> Crystal data and structure refinement for ((CH(CMe <sub>2</sub> ) <sub>2</sub> (NC <sub>6</sub> F <sub>5</sub> ) <sub>2</sub> )Ga (OTf) <sub>2</sub> (CH <sub>3</sub> CN)) <sub>2</sub> , <b>3.11</b> .....	206
<b>Table 4.74.</b> Selected bond lengths (Å) for ((CH(CMe <sub>2</sub> ) <sub>2</sub> (NC <sub>6</sub> F <sub>5</sub> ) <sub>2</sub> )Ga(OTf) <sub>2</sub> (CH <sub>3</sub> CN)) <sub>2</sub> , <b>3.11</b> .....	207
<b>Table 4.75.</b> Selected bond angles (°) for ((CH(CMe <sub>2</sub> ) <sub>2</sub> (NC <sub>6</sub> F <sub>5</sub> ) <sub>2</sub> )Ga(OTf) <sub>2</sub> (CH <sub>3</sub> CN)) <sub>2</sub> , <b>3.11</b> .....	207
<b>Table 4.76.</b> Crystal data and structure refinement for (CH(CMe <sub>2</sub> ) <sub>2</sub> (NC <sub>6</sub> F <sub>5</sub> ) <sub>2</sub> )Ga (OTf) <sub>2</sub> (bipy), <b>3.12</b> .....	209
<b>Table 4.77.</b> Selected bond lengths (Å) for (CH(CMe <sub>2</sub> ) <sub>2</sub> (NC <sub>6</sub> F <sub>5</sub> ) <sub>2</sub> )Ga(OTf) <sub>2</sub> (bipy), <b>3.12</b> .....	210
<b>Table 4.78.</b> Selected bond angles (°) for (CH(CMe <sub>2</sub> ) <sub>2</sub> (NC <sub>6</sub> F <sub>5</sub> ) <sub>2</sub> )Ga(OTf) <sub>2</sub> (bipy), <b>3.12</b> .....	210
<b>Table 4.79.</b> Crystal data and structure refinement for [(CH(CMe <sub>2</sub> ) <sub>2</sub> (NC <sub>6</sub> F <sub>5</sub> ) <sub>2</sub> )Ga (OTf)(terpy)][OTf], <b>3.13</b> .....	212
<b>Table 4.80.</b> Selected bond lengths (Å) for [(CH(CMe <sub>2</sub> ) <sub>2</sub> (NC <sub>6</sub> F <sub>5</sub> ) <sub>2</sub> )Ga(OTf)(terpy)] [OTf], <b>3.13</b> .....	213
<b>Table 4.81.</b> Selected bond angles (°) for [(CH(CMe <sub>2</sub> ) <sub>2</sub> (NC <sub>6</sub> F <sub>5</sub> ) <sub>2</sub> )Ga(OTf)(terpy)][OTf], <b>3.13</b> .....	213
<b>Table 4.82.</b> Crystal data and structure refinement for ((CH(CMe <sub>2</sub> ) <sub>2</sub> (NC <sub>6</sub> F <sub>5</sub> ) <sub>2</sub> )Al (OTf)(OH)) <sub>2</sub> , <b>3.15</b> .....	215
<b>Table 4.83.</b> Selected bond lengths (Å) for ((CH(CMe <sub>2</sub> ) <sub>2</sub> (NC <sub>6</sub> F <sub>5</sub> ) <sub>2</sub> )Al(OTf)(OH)) <sub>2</sub> , <b>3.15</b> .....	216
<b>Table 4.84.</b> Selected bond angles (°) for ((CH(CMe <sub>2</sub> ) <sub>2</sub> (NC <sub>6</sub> F <sub>5</sub> ) <sub>2</sub> )Al(OTf)(OH)) <sub>2</sub> , <b>3.15</b> .....	216

<b>Table 4.85.</b> Crystal data and structure refinement for ((CH(CMe <sub>2</sub> ) <sub>2</sub> (NC <sub>6</sub> F <sub>5</sub> ) <sub>2</sub> )Ga(OTf)) <sub>2</sub> O, <b>3.16</b> .....	218
<b>Table 4.86.</b> Selected bond lengths (Å) for ((CH(CMe <sub>2</sub> ) <sub>2</sub> (NC <sub>6</sub> F <sub>5</sub> ) <sub>2</sub> )Ga(OTf)) <sub>2</sub> O, <b>3.16</b> .....	219
<b>Table 4.87.</b> Selected bond angles (°) for ((CH(CMe <sub>2</sub> ) <sub>2</sub> (NC <sub>6</sub> F <sub>5</sub> ) <sub>2</sub> )Ga(OTf)) <sub>2</sub> O, <b>3.16</b> ...	219

## Index of Compounds

- 1.1  $\text{CH}(\text{CMe}_2)_2(\text{NC}_6\text{F}_5)(\text{HNC}_6\text{F}_5)$
- 1.2  $(\text{CH}(\text{CMe}_2)_2(\text{NC}_6\text{F}_5)_2)\text{Li}\cdot\text{OEt}_2$
- 1.3  $(\text{CH}(\text{CMe}_2)_2(\text{NC}_6\text{F}_5)_2)\text{Na}$
- 1.4  $(\text{CH}(\text{CMe}_2)_2(\text{NC}_6\text{F}_5)_2)\text{SnCl}$
- 1.5  $\text{CH}(\text{CMe}_2)_2(\text{NC}_6\text{F}_5)(\text{Me}_3\text{Si}-\text{NC}_6\text{F}_5)$
- 1.6  $(\text{CH}(\text{CMe}_2)_2(\text{NC}_6\text{F}_5)_2)\text{BCl}_2$
- 1.7  $(\text{CH}(\text{CMe}_2)_2(\text{NC}_6\text{F}_5)_2)\text{BBr}_2$
- 1.8  $(\text{CH}(\text{CMe}_2)_2(\text{NC}_6\text{F}_5)_2)\text{BI}_2$
- 1.9  $(\text{CH}(\text{CMe}_2)_2(\text{NC}_6\text{F}_5)_2)\text{AlMe}_2$
- 1.10  $(\text{CH}(\text{CMe}_2)_2(\text{NC}_6\text{F}_5)_2)\text{AlMeCl}$
- 1.11  $(\text{CH}(\text{CMe}_2)_2(\text{NC}_6\text{F}_5)_2)\text{AlCl}_2$
- 1.12  $(\text{CH}(\text{CMe}_2)_2(\text{NC}_6\text{F}_5)_2)\text{AlI}_2$
- 1.13  $(\text{CH}(\text{CMe}_2)_2(\text{NC}_6\text{F}_5)_2)\text{GaMe}_2$
- 1.14  $(\text{CH}(\text{CMe}_2)_2(\text{NC}_6\text{F}_5)_2)\text{GaCl}_2$
- 1.15  $(\text{CH}(\text{CMe}_2)_2(\text{NC}_6\text{F}_5)_2)\text{GaI}_2$
- 1.16  $(\text{PCl}_2)\text{CH}(\text{CMe}_2)_2(\text{NC}_6\text{F}_5)_2$
- 1.17  $(\text{PhPCl})\text{CH}(\text{CMe}_2)_2(\text{NC}_6\text{F}_5)_2$
- 2.1  $[(\text{CH}(\text{CMe}_2)_2(\text{NC}_6\text{F}_5)_2)\text{BCl}][\text{AlCl}_4]$
- 2.2  $[(\text{CH}(\text{CMe}_2)_2(\text{NC}_6\text{F}_5)_2)\text{BPh}][\text{AlCl}_4]$
- 2.3  $(\text{CH}(\text{CMe}_2)_2(\text{NC}_6\text{F}_5)_2)\text{B}=\text{O}\rightarrow\text{AlCl}_3$
- 2.4  $[(\text{CH}(\text{CMe}_2)_2(\text{HNC}_6\text{F}_5)_2)][\text{AlCl}_4]$

- 2.5  $[(\text{CH}(\text{CMe}_2)_2(\text{NC}_6\text{F}_5)_2)\text{B}(\text{OH})][\text{AlCl}_4]$
- 2.6  $((\text{CH}(\text{CMe}_2)_2(\text{NC}_6\text{F}_5)_2)\text{BO})_2$
- 2.7  $(\eta^5\text{-C}_5\text{H}_5)\text{Fe}(\text{CO})_2\text{BCl}(\eta^5\text{-C}_5\text{Me}_5)$
- 2.8  $[(\eta^5\text{-C}_5\text{H}_5)\text{Fe}(\text{CO})_2\text{B}(\eta^5\text{-C}_5\text{Me}_5)] [\text{AlCl}_4]$
- 2.9  $(\eta^5\text{-C}_5\text{H}_5)\text{Fe}(\text{CO})_2\text{BCl}(\eta^3\text{-C}_5\text{Me}_5)$
- 3.1  $(\text{CH}(\text{CMe}_2)_2(\text{NC}_6\text{F}_5)_2)\text{B}(\text{OTf})_2$
- 3.2  $[(\text{CH}(\text{CMe}_2)_2(\text{NC}_6\text{F}_5)_2)\text{B}(\text{bipy})][2\cdot\text{OTf}]$
- 3.3  $[(\text{CH}(\text{CMe}_2)_2(\text{NC}_6\text{F}_5)_2)\text{B}(\text{terpy})][2\cdot\text{OTf}]$
- 3.4  $[(\text{CH}(\text{CMe}_2)_2(\text{NC}_6\text{F}_5)_2)\text{B}(\text{bipy})][2\cdot\text{I}]$
- 3.5  $[(\text{CH}(\text{CMe}_2)_2(\text{NC}_6\text{F}_5)_2)\text{B}(\text{bipy})][2\cdot\text{Br}]$
- 3.6  $(\text{CH}(\text{CMe}_2)_2(\text{NC}_6\text{F}_5)_2)\text{AlMe}(\text{OTf})$
- 3.7  $(\text{CH}(\text{CMe}_2)_2(\text{NC}_6\text{F}_5)_2)\text{Al}(\text{OTf})_2$
- 3.8  $(\text{CH}(\text{CMe}_2)_2(\text{NC}_6\text{F}_5)_2)\text{Al}(\text{bipy})(\text{OTf})_2$
- 3.9  $[(\text{CH}(\text{CMe}_2)_2(\text{NC}_6\text{F}_5)_2)\text{Al}(\text{terpy})(\text{OTf})][\text{OTf}]$
- 3.10  $[(\text{CH}(\text{CMe}_2)_2(\text{NC}_6\text{F}_5)_2)\text{Al}(\text{tren})][2\cdot\text{OTf}]$
- 3.11  $(\text{CH}(\text{CMe}_2)_2(\text{NC}_6\text{F}_5)_2)\text{Ga}(\text{OTf})_2$
- 3.12  $(\text{CH}(\text{CMe}_2)_2(\text{NC}_6\text{F}_5)_2)\text{Ga}(\text{bipy})(\text{OTf})_2$
- 3.13  $[(\text{CH}(\text{CMe}_2)_2(\text{NC}_6\text{F}_5)_2)\text{Ga}(\text{terpy})(\text{OTf})][\text{OTf}]$
- 3.14  $[(\text{CH}(\text{CMe}_2)_2(\text{NC}_6\text{F}_5)_2)\text{Ga}(\text{tren})][2\cdot\text{OTf}]$
- 3.15  $((\text{CH}(\text{CMe}_2)_2(\text{NC}_6\text{F}_5)_2)\text{Al}(\text{OTf})(\text{OH}))_2$
- 3.16  $((\text{CH}(\text{CMe}_2)_2(\text{NC}_6\text{F}_5)_2)\text{Ga}(\text{OTf}))_2\text{O}$

# CHAPTER 1

## Synthetic Approaches to C<sub>6</sub>F<sub>5</sub>-Substituted $\beta$ -Diketimate Complexes of Boron, Aluminum, Gallium and Phosphorus

### INTRODUCTION

The introduction of  $\beta$ -diketimate ligands (Figure 1.1) into synthetic inorganic chemistry occurred in the mid- to late-1960's, at which time the synthetic, spectral, magnetic and structural features of several first row transition metal  $\beta$ -diketimate complexes were disclosed.<sup>1</sup> However, it was not until the mid-1990's that this type of ligand gained wide acceptance on the part of the inorganic chemistry community. In part the increased interest in  $\beta$ -diketimate ligands was driven by the search for replacements for the widely used cyclopentadienyl ligand class. However, other attractive features included the wide tunability of  $\beta$ -diketimates and the robust nature

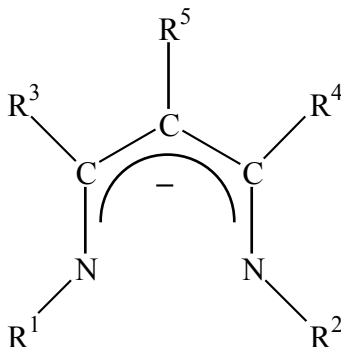


**Figure 1.1. General structure for a  $\beta$ -diketimate ligand.**

of the nitrogen-metal bonds. This led to their use for the support of catalytically active transition metal centers. For example, a  $\beta$ -diketiminato-supported zirconium complex was found to be an effective catalyst (with a methylaluminoxane, MAO, cocatalyst) for ethylene and propylene polymerization.<sup>2</sup> Since that time,  $\beta$ -diketiminato complexes have been reported for an increasingly large number of transition metal, lanthanide and main group elements.<sup>3</sup>

$\beta$ -diketiminates are uninegative ligands with the general structure shown in Figure 1.1. The substituents  $R^1$ ,  $R^2$ ,  $R^3$ ,  $R^4$  and  $R^5$  are typically H, alkyl or aryl groups. This type of ligand can also exhibit a wide variety of bonding modes such as  $\eta^5$  [NCCCN] (Figure 1.2a),<sup>4</sup>  $\eta^3$  [NCC] (Figure 1.2b),<sup>5</sup>  $\gamma$ -carbon (Figure 1.2c)<sup>3</sup> and N-CH<sub>2</sub> (as a result of C—H bond activation when  $R^3$  and  $R^4$  are methyl groups, Figure 1.2d).<sup>6</sup>

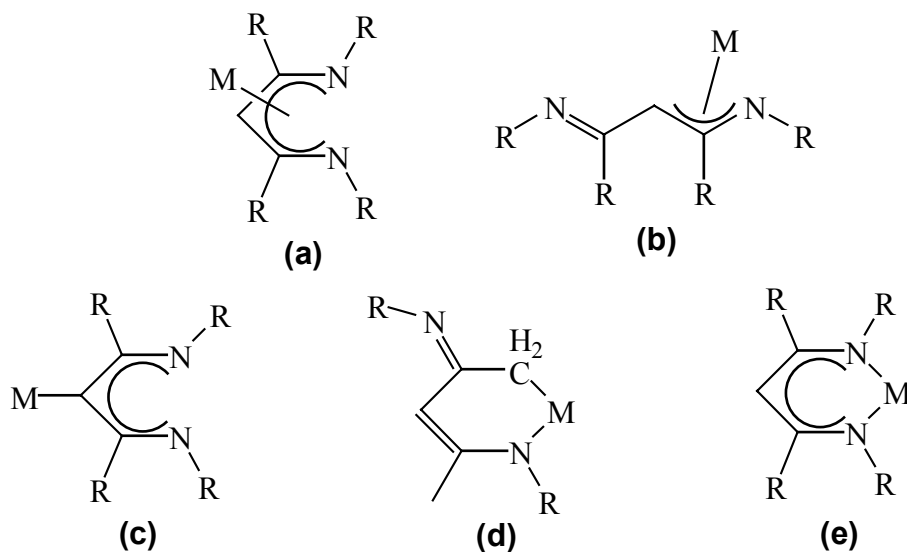
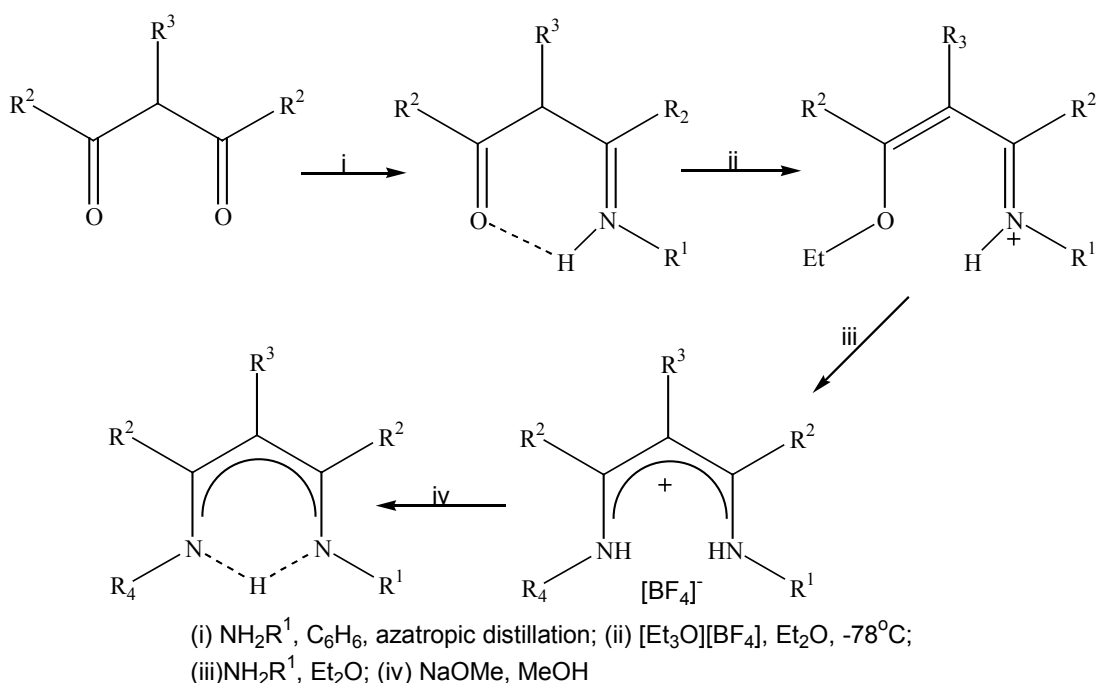


**Figure 1.2. Different binding modes of  $\beta$ -diketiminato ligands.**

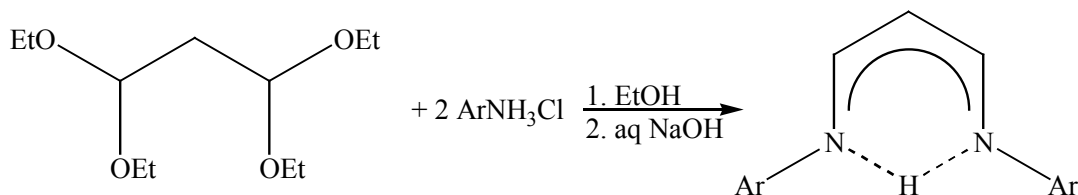
However, the most common mode of binding takes place *via* the two nitrogen atoms (the N,N' mode, Figure 1.2e).<sup>3</sup> Tuning of the R<sup>1</sup> and R<sup>2</sup> substituents has received the most attention because of their location on the nitrogen atoms maximizes the opportunity to influence both the steric and electronic properties of the ligand and the resulting complexes. Further ligand tunability arises because the R<sup>1</sup> and R<sup>2</sup> groups do not necessarily have to be identical. In fact several examples of such asymmetrically substituted  $\beta$ -diketiminates are known.<sup>7</sup>

Several procedures have been available for the synthesis of  $\beta$ -diketimate ligands, either as their conjugate acids ( $\beta$ -diketiminines) or as metal complexes. Most of the synthetic procedures involve the condensation reaction of a primary amine with



**Scheme 1.1. First reported synthesis of a  $\beta$ -diketimate ligand.**

either a  $\beta$ -diketone or 1,1,3,3-tetraethoxypropane. The first synthesis of a  $\beta$ -diketimine from a  $\beta$ -diketone *via* the condensation route was reported in late 1960's and is summarized in Scheme 1.1.<sup>1b</sup> Some care had to be exercised to avoid the reaction coming to a stop after the first condensation, thereby giving the enaminoketone (step (i) in Scheme 1.1). As shown in Scheme 1.2, 1,1,3,3-tetraalkoxypropane can also be employed as a convenient  $\beta$ -diketiminato precursor. The standard procedure involves treating this precursor with an aromatic amine hydrochloride in aqueous ethanol at 50 °C for 1 h, followed by storage at ambient temperature, crystallization of the  $\beta$ -diketimine hydrochloride, and release of the  $\beta$ -diketimine *via* reaction with aqueous sodium hydroxide.<sup>1d</sup>



**Scheme 1.2. Synthesis of a  $\beta$ -diketiminato ligand from tetraalkoxypropane.**

One of the approaches to the synthesis of  $\beta$ -diketiminato-supported metal complexes involves the reaction of a  $\alpha$ -hydrogen-free nitrile (RCN) or isonitrile (RNC) with a metal alkyl reagent ( $\text{M} \text{---} \text{CR}^1_2\text{R}$ ; typically M is lithium and  $\text{R}^1$  is preferentially a  $(\text{CH}_3)_3\text{Si}$  group). The mechanism of the nitrile reaction involves the insertion of the nitrile into metal-carbon bond (C—C coupling), followed by 1,3-migration of the  $\text{R}^1$  group from the carbon atom to the nitrogen atom.<sup>2</sup> The same insertion/migration steps are repeated for the second nitrile molecule. In the case of the isonitriles, the overall



process is the same a 1,2-migration occurs except that instead of 1,3-migration.<sup>8</sup> Some miscellaneous routes to metal  $\beta$ -diketiminate complexes include the reaction of  $\text{CoCl}_2$  with  $\text{LiNEt}_2$ ,<sup>1e,f</sup> the reaction of  $[\text{Pt}(\text{NH}_3)_6]\text{Cl}_4 \cdot \text{H}_2\text{O}$  with a  $\beta$ -diketone<sup>9</sup> and the reaction of  $\text{AlR}_3$  (R = methyl or ethyl) with a benzanilide.<sup>10</sup>

In 1997 the 2,6-diisopropylphenyl (Dipp) substituted  $\beta$ -diketimine, the conjugate acid of the corresponding  $\beta$ -diketiminate ( $\text{L}'^-$ , Figure 1.3a), was synthesized.<sup>11</sup> The availability of this ligand continues to have an enormous impact on synthetic inorganic chemistry. For example, this ligand has been used to stabilize a rare Zn-Zn bond<sup>12</sup> and a two-coordinate germanium(II) cation that does not exhibit any weak interactions with the counteranion.<sup>13</sup> Moreover, the  $\text{L}'^-$  ligand plays a spectator role in tin-, chromium- and zinc-based catalysts that are used for the polymerization of ethylene and lactide, and the copolymerization of cyclohexene and  $\text{CO}_2$ .<sup>14</sup> However, the biggest impact of the availability of this ligand has been evident in group 13 chemistry because of its ability to stabilize carbene analogues of aluminum ( $\text{L}'\text{Al}$ ),<sup>15</sup> gallium ( $\text{L}'\text{Ga}$ ),<sup>16</sup> indium ( $\text{L}'\text{In}$ )<sup>17</sup> and thallium ( $\text{L}'\text{Tl}$ )<sup>18</sup> as summarized in Figure 1.3b.

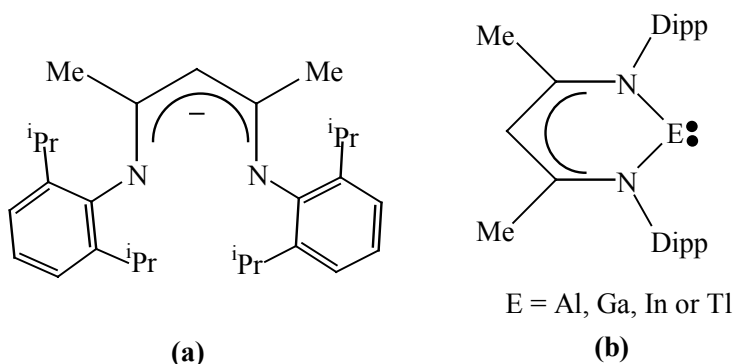


**Figure 1.3. (a) Structure of the Dipp-substituted  $\beta$ -diketiminate ligand. (b) General structure of the group 13 carbene analogues.**

The indium and thallium carbene analogues were obtained by treatment of the readily available M(I) halides (M = In and Tl) with the alkali metal  $\beta$ -diketiminate complexes. The gallium carbene analogue was synthesized *via* the reaction of “GaI”<sup>19</sup> with L’Li, and subsequent treatment with potassium metal to reduce any L’GaI<sub>2</sub> that had formed.<sup>16</sup> The synthesis of the aluminum analogue of a carbene complex was accomplished by the reduction of L’AlI<sub>2</sub> with potassium metal.<sup>15</sup> As of today a stable monomeric boron carbene analogue (a borylene) has not been reported in spite of the fact that the coordination chemistry of terminal borylenes has gained considerable momentum in recent years.<sup>20</sup> It is also worth noting that the first example of an anionic boron carbene (a boryl) has been synthesized very recently.<sup>21</sup> As expected, several Dipp-substituted  $\beta$ -diketiminate complexes are known in which the group 13 element is in the +3 oxidation state.<sup>3</sup>

It is generally recognized that the successful applications of the L’<sup>-</sup> ligand are due to its steric bulk and electron donating properties. As noted above, this combination of properties is responsible for the stability of group 13 carbene analogues. However, in order to study the  $\beta$ -diketiminate chemistry of electron-rich elements such as phosphorus, a  $\beta$ -diketiminate ligand with different steric and electronic properties was called for. In this context, the pentafluorophenyl-substituted  $\beta$ -diketiminate ligand ([CH(CMe<sub>2</sub>)<sub>2</sub>(NC<sub>6</sub>F<sub>5</sub>)<sub>2</sub>]<sup>-</sup>, L<sup>-</sup>, Figure 1.4)<sup>22</sup> seemed particularly attractive. For instance, it has been shown that benzene and hexafluorobenzene have opposite charge distributions<sup>23</sup> hence the L<sup>-</sup> ligand is predicted to possess very different electronic properties than the L’<sup>-</sup> ligand. Furthermore, the absence of the isopropyl groups on the

phenyl substituents of the  $L^-$  ligand would alleviate some of the steric encumbrance thus permitting the N,N'-chelation of larger main group fragments. Another attractive feature is that the chemistry of  $L^-$  has not been explored to any great extent. In fact, prior to this present work only two papers<sup>22,24</sup> had appeared in the literature and only one of these addressed the chemistry of a group 13 element, namely aluminum.<sup>24</sup>

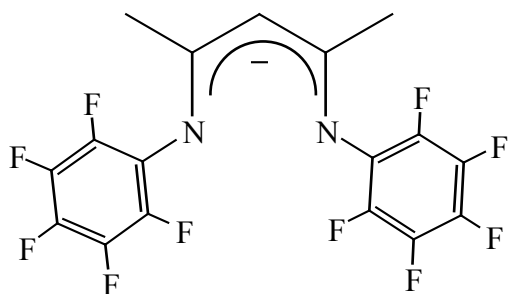


**Figure 1.4. Structure of the  $C_6F_5$ -substituted  $\beta$ -diketiminato ligand.**

In order to explore the chemistry of boron, aluminum, gallium and phosphorus complexes that employ  $L^-$  as the coordinating ligand, it was necessary to synthesize compounds with the general formula of  $LEX_2$  ( $E = B, Al, Ga$  or  $P$ ;  $X = Me, Cl, Br$  and  $I$ ). Very little information is available in the literature regarding  $\beta$ -diketiminato boron dihalide complexes. For example,  $\beta$ -diketiminato boron difluoride complexes in which the  $\beta$ -diketiminato ligands do not have the same structural formula as in Figure 1 but are actually di- and tripyrrylmethanes<sup>25a</sup> and dipyrromethanes,<sup>25b,c</sup> have been known since late 1960's and were found to possess interesting fluorescent properties. A few boron difluoride complexes supported by the more conventional  $\beta$ -diketiminato ligand structure shown in Figure 1 have been reported. The compound  $L^1BF_2$ <sup>26</sup> (Figure 1.5a) was prepared in low yield *via* the reaction of  $L^1H$  with  $BF_3(OEt_2)$  in the presence of

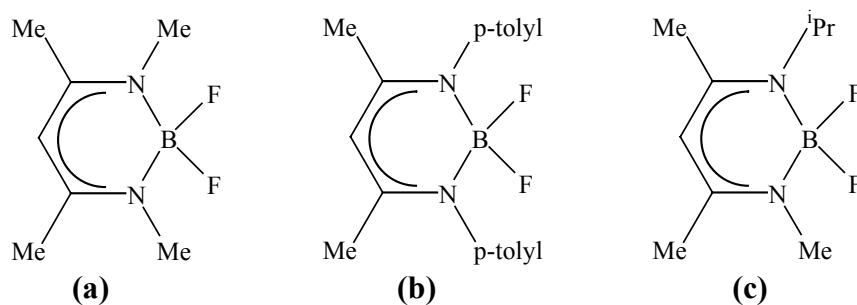
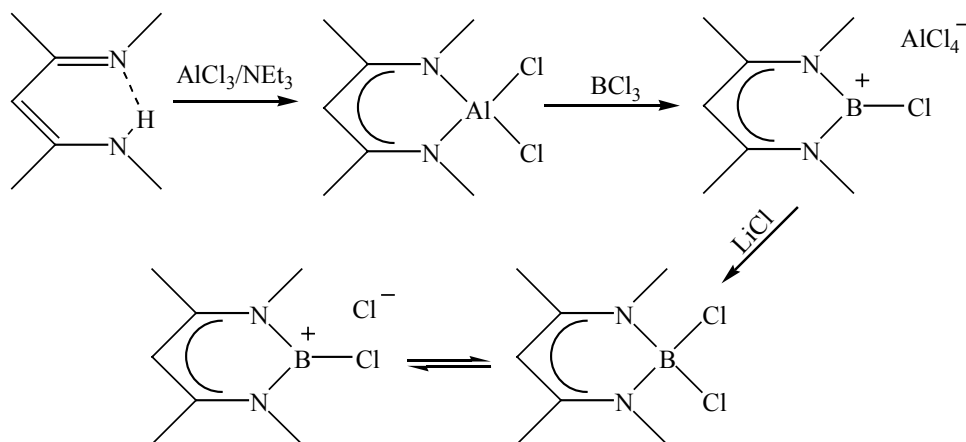


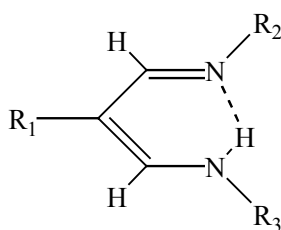
**Figure 1.5. Examples of  $\beta$ -diketiminato-supported boron difluoride complexes.**

triethylamine ( $\text{NEt}_3$ ) while  $\text{L}^{\text{II}}\text{BF}_2$ <sup>27</sup> (Figure 1.5b) was synthesized in moderate yield by treatment of  $\text{L}^{\text{II}}\text{Li}$  with  $\text{BF}_3(\text{OEt}_2)$ . The reaction of N-(isopropylidene)isopropylamine and  $^t\text{BuLi}$ , followed by the addition of N-methylacetonitrilium tetrafluoroborate, resulted in the formation of  $\text{L}^{\text{III}}\text{BF}_2$  (Figure 1.5c) in poor yield.<sup>7</sup> Furthermore,  $\text{L}^{\text{I}}\text{BCl}_2$ , the only example of a  $\beta$ -diketiminato boron dichloride complex, was synthesized in poor yield by the laborious sequence of reactions summarized in Scheme 1.3.<sup>28</sup> Moreover, it was claimed that  $\text{L}^{\text{I}}\text{BCl}_2$  is in equilibrium with  $[\text{L}^{\text{I}}\text{BCl}][\text{Cl}]$  (Scheme 1.3).



**Scheme 1.3. Synthesis of a  $\beta$ -diketiminato boron dichloride complex.**

Several examples of  $\beta$ -diketiminato phosphorus complexes are known. One such example features the [N,N']- and [ $\gamma$ ,N,N']-phosphanyl-substituted  $\beta$ -diketimine complexes that were synthesized *via* the reactions of malonodinitrile or phosphanylmalonodinitrile with two equivalents of a phosphine in the presence of two equivalents of [Cp<sub>2</sub>ZnClH]<sub>n</sub> (Figure 1.6a).<sup>29</sup> The other two examples of complexes of this type were prepared by treatment of Ph<sub>3-n</sub>PCl<sub>n</sub> (n = 1<sup>30a,b</sup> or 2<sup>31</sup>) with the lithium salt of a diisopropylphenyl-substituted  $\beta$ -diketiminato (L'Li). The resulting complex is shown in Figure 1.6b. Note that in both cases the phosphorus atom is bonded to the  $\gamma$ -carbon of the ligand backbone and that the hydrogen atom that was bound to the  $\gamma$ -carbon atom has undergone a migration to the one of the nitrogen atoms. One of the possible reasons for this type of phosphorus coordination is that both the phosphorous atom and the two nitrogen atoms are electron-rich moieties which disfavors N,N'-chelation on the part of the  $\beta$ -diketiminato ring. The other reason for the observed structural preference is that the bulky 2,6-diisopropylphenyl groups inhibit the approach of the Ph<sub>2</sub>P- and PhClP- moieties into the N,N' environment.<sup>30</sup> Moreover, in a <sup>31</sup>P NMR study of the reaction of L'Li with PCl<sub>3</sub> it was found that many unidentifiable products were formed.<sup>30b</sup> Thus, it became clear that the C<sub>6</sub>F<sub>5</sub>-substituted  $\beta$ -diketiminato ligand might be the most appropriate choice for N,N'-chelation of a phosphorus-based moiety, not only because of the diminished steric bulk compared to that of the L' ligand, but also because the electron withdrawing C<sub>6</sub>F<sub>5</sub> groups could reduce some of the electron density residing on the nitrogen atoms.

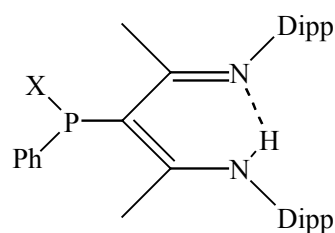


when  $R_1 = H$  then  $R_2 = P(N^iPr_2)_2$  and  $R_3 = PEt_2$  or  $PPh_2$

when  $R_1 = PPh_2$  then  $R_2 = R_3 = P(N^iPr_2)_2$  or  $Ph$

or  $R_2 = P(N^iPr_2)_2$  and  $R_3 = Me$

(a)



$X = Cl$  or  $Ph$

(b)

**Figure 1.6. (a) Phosphanyl-substituted  $\beta$ -diketiminato complexes (b) Dipp-substituted  $\beta$ -diketiminato ligand incorporating different phosphorus moieties.**

The syntheses and structural features of aluminum and gallium complexes supported by  $\beta$ -diketiminato ligands have received more emphasis than their boron and phosphorus analogues. For example, the Dipp-substituted  $\beta$ -diketiminato ligand ( $L'$ ) was employed for the preparation of several compounds with the general formula  $L'EX_2$ , where  $E = Al$  or  $Ga$  and  $X = Me, F, Cl$  or  $I$ .<sup>15,32,33</sup> The dibromo gallium derivative ( $L'GaBr_2$ ) is also known.<sup>33</sup> However, the analogous aluminum compound has not been reported. Mixed alkyl-halogen derivatives such as  $L'AlMeCl$ ,  $L'AlMeF$  and  $L'GaMeCl$  are also known.<sup>33</sup> Several other  $\beta$ -diketiminato ligands (e.g. Figure 1 where  $R^5 = H$ ,  $R^3 = R^4 = Me$  and  $R^1 = R^2 = Me$  ( $L^I$ ),  $iPr$  ( $L^{IV-}$ ),  $tBu$  ( $L^V$ ) or  $Ph$  ( $L^{VI-}$ )) have been used for the support of dichloro, dibromo and diiodo derivatives of aluminum and gallium.<sup>34,35,36</sup>

Several strategies have been used for the synthesis of aluminum and gallium  $\beta$ -diketiminato complexes. The dimethyl derivatives were synthesized in good yields by

treatment of the conjugate acid of a  $\beta$ -diketiminate ligand with the corresponding trimethylalane or trimethylgallane.<sup>15,32</sup> The compounds  $L'AlCl_2$ ,  $L'GaCl_2$  and  $L'GaBr_2$  were obtained in moderate to good yields *via* the reactions of  $L'Li\cdot OEt_2$  with the respective metal trihalides.<sup>32,33</sup> The diiodoalane  $L'AlI_2$  was prepared in good yield *via* the reaction of  $L'AlMe_2$  with molecular iodine,<sup>15</sup> while the analogous gallium diiodide was isolated in low yield from the reaction of “GaI” with  $L'Li\cdot OEt_2$ .<sup>32</sup> Interestingly, if the diethyl ether molecule was removed from the lithium salt of  $L'Li\cdot OEt_2$  prior to reaction with “GaI”, the gallium carbene  $L'Ga$  was obtained in low yields.<sup>16</sup> There are no reports in the literature of the reactions of  $L'Li$  (with or without the ether molecule) with aluminum or gallium triiodide. The  $L^I$  ligand (Figure 1,  $R^1 = R^2 = R^3 = R^4 = Me$  and  $R^5 = H$ ) has also been used for the support of aluminum dihalide moieties by treatment of the alane  $L^IAlH_2$  with  $Me_3NHX$  ( $X = Cl, Br$  or  $I$ ).<sup>36</sup> These reactions proceed in good yields. Use of the same synthetic procedure permitted the isolation of  $L^{VI}AlI_2$  ( $L^{VI}$ :  $R^1 = R^2 = Ph$ ,  $R^3 = R^4 = Me$  and  $R^5 = H$ ; see Figure 1) in good yield.<sup>35</sup> Moderate yields of  $L^IAlBr_2$ , and  $L^IAlI_2$  have also been obtained by the metathetical reactions of  $L^ILi$  with the corresponding aluminum trihalides.<sup>35</sup> Furthermore, the dichloro derivatives of aluminum and gallium supported by the  $L^I$ ,  $L^{IV}$  ( $R^1 = R^2 = iPr$ ,  $R^3 = R^4 = Me$  and  $R^5 = H$  from Figure 1) and  $L^V$  ( $R^1 = R^2 = tBu$ ,  $R^3 = R^4 = Me$  and  $R^5 = H$  from Figure 1) ligands have been synthesized in low yields *via* the reaction of the conjugate acid form of the ligands with  $ECl_3$  ( $E = Al$  or  $Ga$ ) in the presence of  $Et_3N$ .<sup>34</sup>

The current chapter is devoted to the synthesis and characterization of group 13 and phosphorus complexes supported by the  $[CH(CMe_2)_2(NC_6F_5)_2]^-$  ( $L^-$ ) ligand, namely

LBCl<sub>2</sub> (**1.6**), LBBBr<sub>2</sub> (**1.7**), LBI<sub>2</sub> (**1.8**), LAlMe<sub>2</sub> (**1.9**), LAlMeCl (**1.10**), LAlCl<sub>2</sub> (**1.11**), LAlI<sub>2</sub> (**1.12**), LGaMe<sub>2</sub> (**1.13**), LGaCl<sub>2</sub> (**1.14**), LGaI<sub>2</sub> (**1.15**), LPCl<sub>2</sub> (**1.16**)<sup>\*</sup> and LPClPh (**1.17**)<sup>\*</sup> (Figure 1.7). In particular, the main focus of the research is the development of a variety of synthetic pathways that can be used for the preparation of the complexes identified above. Special emphasis is placed on the synthesis of the boron derivatives because  $\beta$ -diketiminato boron dihalide complexes are relatively rare in comparison with their aluminum and gallium analogues. Six different synthetic methods have been investigated and these will be compared in terms of the purities and yields of the products. The first method is the methane elimination route, which involves the reaction of Me<sub>3-n</sub>ECln (E = Al or Ga; n = 0, 1 or 2) with CH(CMe<sub>2</sub>)<sub>2</sub>(NC<sub>6</sub>F<sub>5</sub>)(HNC<sub>6</sub>F<sub>5</sub>) (LH, **1.1**). The methane elimination route is not feasible for the synthesis of analogous boron and phosphorus because the electronegativity differences between carbon and boron, and carbon and phosphorus are not large enough to promote the elimination of

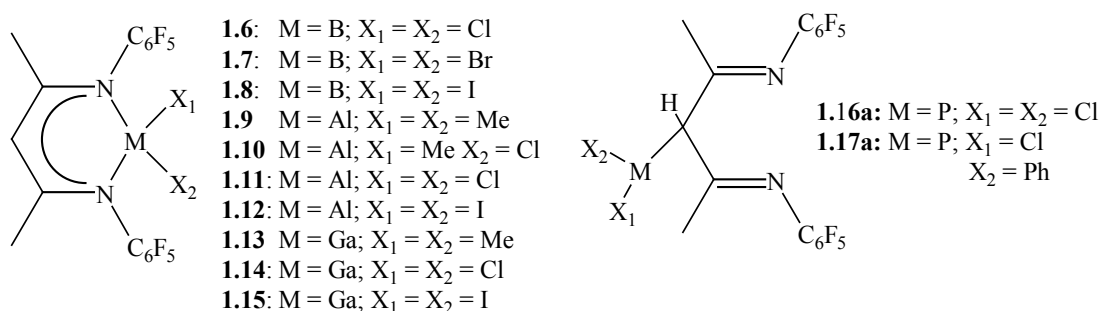


**Figure 1.7. General structure of the targeted compounds.**

<sup>\*</sup> The two phosphorus derivatives, **16** and **17**, form two different isomers when dissolved in solution. This behavior is discussed in Section 1.3.



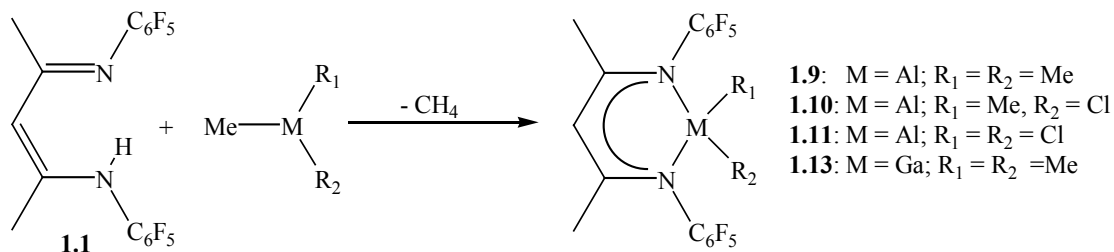
methane. The second method involves the reaction of LH (**1.1**) with various boron, aluminum, gallium and phosphorus halides in the presence of triethylamine. The reaction of the lithium salt of L<sup>-</sup>, (LLi·OEt<sub>2</sub>, **1.2**) with halide-based starting materials represents the third synthetic method, while the fourth and fifth synthetic methods are focused on the use of the heavier organometallic reagents LNa (**1.3**) and LSnCl (**1.4**), in place of **1.2**. The final method of preparation is focused on the reactions of [CH(CMe<sub>2</sub>)<sub>2</sub>(NC<sub>6</sub>F<sub>5</sub>)(Me<sub>3</sub>Si-NC<sub>6</sub>F<sub>5</sub>)] (LTMS, **1.5**) with the corresponding halide-containing starting materials.

Structural data were acquired for compounds **1.1**, **1.6**, **1.7**, **1.8**, **1.9**, **1.10**, **1.12**, **1.13**, **1.14**, **1.6a** and **1.17a** by the single-crystal X-ray diffraction experiments and their geometrical features and metrical parameters are compared with those of pertinent compounds from the literature.

## RESULTS AND DISCUSSION

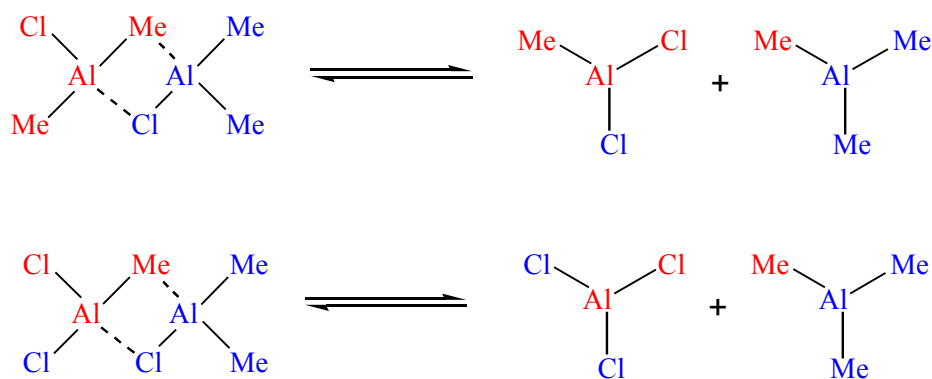
### Section 1.1. Methane Elimination Method

The overall methane elimination process is summarized in Scheme 1.4. The viability of this process depends critically on the protic character of the N-H hydrogen atom on the aminoimine (**1.1**) and the degree of negative charge buildup on the methyl group of the organometallic reagent, i.e. the polarity of the metal-carbon bond. Since the electronegativities of boron (2.0) and carbon (2.5) are close, the polarity of the B—C bonds is not sufficient to allow facile elimination of methane to take place. A similar comment applies to the attempts to prepare phosphorus compounds by this route (the electronegativity of phosphorus is 2.1). Thus, only selected aluminum and gallium derivatives (**1.9**, **1.10**, **1.11** and **1.13**) were synthesized using the methane elimination method. The general procedure involves the addition of the iminoamine (**1.1**) to equimolar quantities of Me<sub>3</sub>Al, Me<sub>2</sub>AlCl, MeAlCl<sub>2</sub> or Me<sub>3</sub>Ga at room temperature. After workup of the reaction mixtures, compounds **1.9**, **1.10**, **1.11** and **1.13** were isolated in virtually quantitative yields. Furthermore, examination of these products by multinuclear NMR spectroscopy revealed that no impurities were present. Although



**Scheme 1.4. General description of the methane elimination route.**

the methane elimination method could, in principle, be used for the synthesis of mixed ligand systems, such as  $\text{Me}_2\text{AlCl}$  and  $\text{MeAlCl}_2$ , problems could arise because of ligand scrambling of the reactants as illustrated in Scheme 1.5. In fact, it was found that significant quantities of **1.9** had accumulated in an attempted preparation of **1.10** with a six-month old sample of a 1.0 *M* solution of  $\text{Me}_2\text{AlCl}$  in hexane. This conclusion was based on low-resolution mass spectroscopic examination of the reaction mixture and X-ray crystallographic analysis of an isolated crystal. Due to the possibility of ligand scrambling,  $\text{MeAlCl}_2$  and  $\text{Me}_2\text{AlCl}$  were not used for subsequent syntheses because the complications could arise with respect to product analyses.

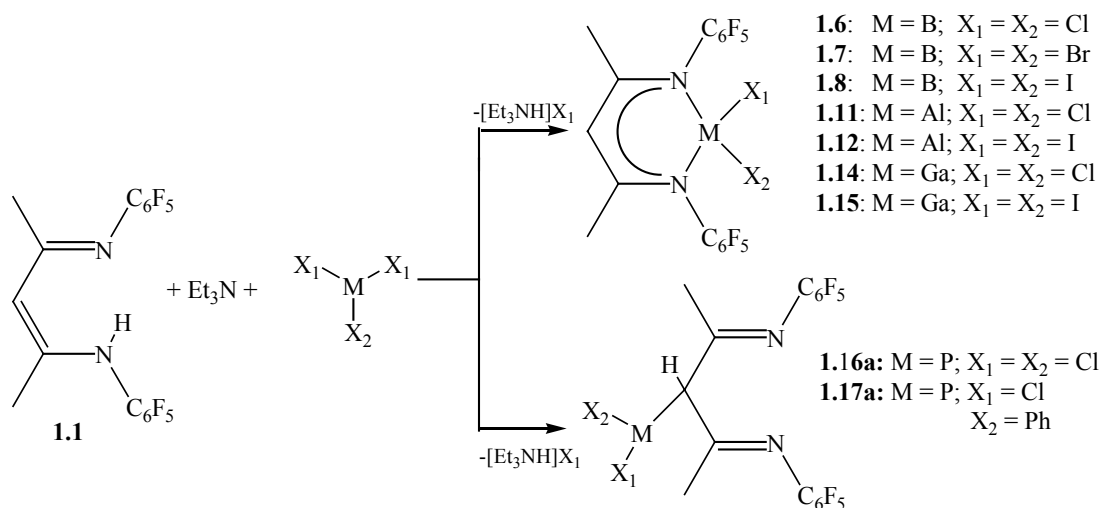


**Scheme 1.5. Possible ligand scrambling process for  $\text{Me}_2\text{AlCl}$ .**

## Section 1.2. Dehydrohalogenation Method

The concept behind the dehydrohalogenation method lies in the ability of the base  $\text{Et}_3\text{N}$  to abstract the N-H proton from the aminoimine (**1.1**) and a halide anion from the main group halide compound such as  $\text{BCl}_3$ ,  $\text{BBr}_3$ ,  $\text{AlI}_3$ ,  $\text{GaCl}_3$  or  $\text{PCl}_3$ . This method was investigated for the syntheses of compounds **1.6**, **1.7**, **1.8**, **1.11**, **1.12**, **1.14**, **1.15**, **1.16a** and **1.17a**. The general procedure, which is summarized in Scheme 1.6, involves the addition of the appropriate starting material ( $\text{BCl}_3$ ,  $\text{BBr}_3$ ,  $\text{BI}_3$ ,  $\text{AlCl}_3$ ,  $\text{AlI}_3$ ,  $\text{GaCl}_3$ ,  $\text{GaI}_3$ ,  $\text{PCl}_3$  or  $\text{PhPCl}_2$ ) to a toluene solution containing equimolar amounts of both the aminoimine and  $\text{Et}_3\text{N}$ . It should be noted that the desired final products from the group 13 and phosphorus-based reactions are different as depicted in Scheme 1.6.

Based on multinuclear NMR spectroscopic data, the dehydrohalogenation reactions involving  $\text{BCl}_3$  and  $\text{BBr}_3$  were found to result in the anticipated products **1.6** and **1.7**, respectively. However, in each case the desired product was contaminated with



Scheme 1.6. General description of the dehydrohalogenation method.

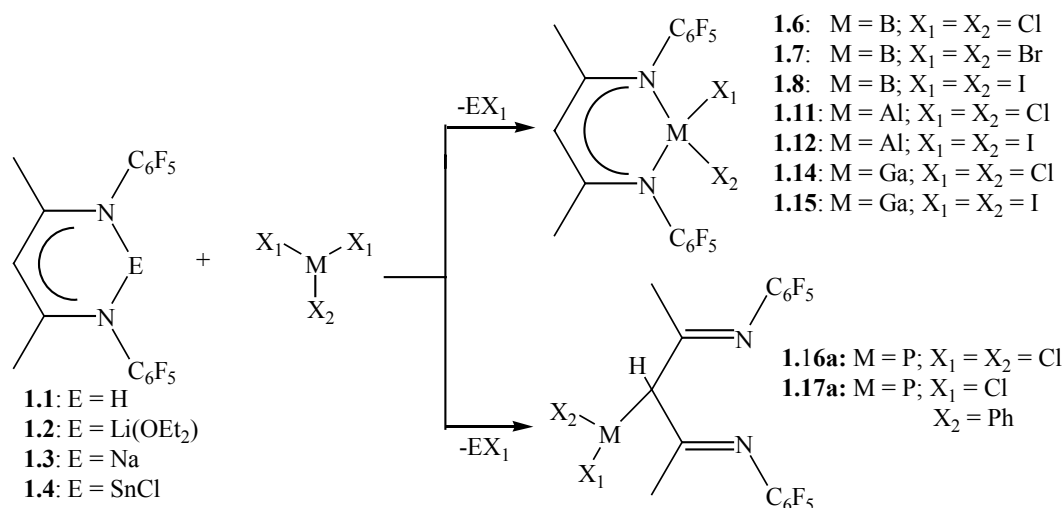
the Lewis acid-base complex  $\text{Et}_3\text{N}\cdot\text{BX}_3$  ( $\text{X} = \text{Cl}$  or  $\text{Br}$ ). Furthermore, based on  $^{11}\text{B}$  NMR spectroscopy, at least one unidentified boron-containing species was present in the product mixture. In the case of the  $\text{BI}_3$  reaction, multinuclear NMR spectroscopic examination of the resulting solid also revealed the presence of the desired product, along with traces of  $\text{Et}_3\text{N}\cdot\text{BI}_3$ .

The reactions involving the preparation of  $\beta$ -diketiminato-supported aluminum dihalides also resulted in the anticipated products **1.11** and **1.12**. However, as in the case of the boron analogues discussed above, contamination with the triethylamine-aluminum trihalide complex ( $\text{Et}_3\text{N}\cdot\text{AlX}_3$ ,  $\text{X} = \text{Cl}, \text{I}$ ) was detected by multinuclear NMR spectroscopy. The same observation was made in the case of the gallium complexes **1.14** and **1.15**. On the other hand, the dehydrohalogenation route failed for the two desired phosphorus compounds **1.16a** and **1.17a**. The identities of the various species in the product mixtures of the phosphorus-based reactions were not established.

In summary, the triethylamine-promoted dehydrohalogenation route is not a satisfactory synthetic method for either the group 13 or the group 15  $\beta$ -diketiminates of the intended types. The group 13 products were contaminated with  $\text{Et}_3\text{N}$  adducts of the  $\text{MX}_3$  starting materials and neither of the desired phosphorus compounds was detected in the respective product mixtures.

### Section 1.3. Salt Metathesis Methods

The driving force for the salt metathesis methods is the formation/elimination of a very thermodynamically stable byproduct such as LiCl, NaI or SnCl<sub>2</sub>. Three different  $\beta$ -diketiminate-supported metal-based reagents (**1.2**, **1.3** and **1.4**, Scheme 1.7) have been prepared and subsequently used for the attempted syntheses of the desired compounds **1.6**, **1.7**, **1.8**, **1.11**, **1.12**, **1.14**, **1.15**, **1.16a** and **1.17b**. The lithium-based  $\beta$ -diketiminate reagent **1.2** was prepared by treatment of the aminoimine (**1.1**) with MeLi. The purification of reagent **1.2** required recrystallization from hexane solution in the presence of diethyl ether. The sodium analogue **1.3** was prepared by the reaction of the aminoimine with NaNH<sub>2</sub> in a hexane/ether solvent mixture. However, during purification of this reagent, all of the diethyl ether solvent was removed from the resulting yellow solid by washing with hexane, followed by drying under reduced pressure. The tin-based reagent **1.4** was prepared by treatment of **1.3** with SnCl<sub>2</sub> in



**Scheme 1.7. General description of the salt elimination method.**

tetrahydrofuran solution. The general procedure for the syntheses of the targeted compounds **1.6**, **1.7**, **1.8**, **1.11**, **1.12**, **1.14** and **1.15** is summarized in Scheme 1.7 and involves the addition of a metal-based reagent (**1.2**, **1.3** or **1.4**) to a toluene solution containing an equimolar amount of BCl<sub>3</sub>, BBr<sub>3</sub>, BI<sub>3</sub>, AlCl<sub>3</sub>, AlI<sub>3</sub>, GaCl<sub>3</sub> or GaI<sub>3</sub> at -78 °C. The syntheses of desired phosphorus compounds **1.16a** and **1.17a** followed exactly the same procedure except that the solvent of choice was hexane.

The three different salt metathesis methods used for the syntheses of the β-diketiminato boron dihalides **1.6**, **1.7** and **1.8** were partially successful. For example, use of the lithium-based reagent **1.2** resulted in the formation of the desired products. However, based on multinuclear NMR spectroscopic analysis it was clear that the desired products represented only minor components in the overall product mixtures. The contaminants were not identified. Use of the sodium reagent **1.3** was more successful for the syntheses of the boron-containing derivatives **1.6**, **1.7** and **1.8**. Multinuclear NMR assay indicated that these β-diketiminates were produced in high purity. However, in a few instances the aminoimine **1.1** was detected as an impurity. Moreover, the yields of these products were not satisfactory as they ranged from poor to moderate. Use of the tin-containing reagent **1.4** for the small-scale syntheses of β-diketiminato boron dihalides was successful only in the case of **1.6** in terms of product purity and yield. The attempted synthesis of compound **1.7** by using the same tin-based reagent resulted in the formation of the desired product. However, samples of **1.7** were found to be contaminated with unidentified side-products. The reaction of **1.4** with BI<sub>3</sub>

resulted in the formation of an amorphous yellow/orange solid that is insoluble in the most common solvents. No further identification of this product was undertaken.

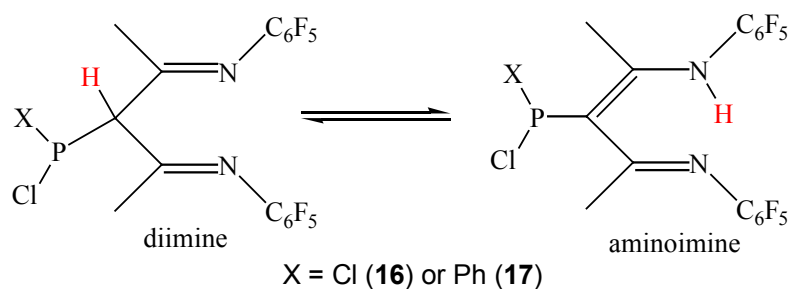
Somewhat better results were obtained in terms of the preparation of the  $\beta$ -diketiminato aluminum dihalides **1.11** and **1.12** by salt metathesis methods than in the case of the analogous boron derivatives. Of the three metallated  $\beta$ -diketimate reagents, the sodium-based reagent **1.3** was the best for the syntheses of the targeted aluminum compounds since the yields were moderate to high. On the other hand, only slightly inferior results were obtained when these aluminum  $\beta$ -diketimates were synthesized using the lithium and tin reagents **1.2** and **1.4**. Examination of the products by multinuclear NMR spectroscopy revealed some product contamination when the lithium-based reagent **1.2** was employed, while the tin-based reagent **1.4** was successful only for small-scale syntheses of compound **1.11**. The reaction of  $\text{AlI}_3$  with **1.3** resulted in the formation of an orange solid that was insoluble in most common solvents. No further identification of this amorphous material was undertaken.

In terms of product purity, the  $\beta$ -diketiminato gallium complexes **1.14** and **1.15** were best synthesized by treatment of the appropriate gallium trihalide with either the lithium- or sodium-based reagent, **1.2** or **1.3**. Somewhat superior yields were obtained if the sodium-based reagent was used. No impurities were detected in **1.14** and **1.15** by multinuclear NMR spectroscopy. As in the case of the analogous  $\beta$ -diketiminato boron and aluminum compounds, the use of the tin-based reagent was successful only for small-scale synthesis of compound **1.14**. Likewise, the reaction of  $\text{GaI}_3$  with the tin-



based reagent **1.4** resulted in the formation of a virtually insoluble, orange solid that was not further identified.

The salt metathesis methods employing either the lithium- or sodium-based reagents, **1.2** or **1.3**, were successful for the syntheses of the pure, crystalline  $\beta$ -diketiminato phosphorus compounds **1.16a** and **1.17a**. Slightly superior yields were obtained if the sodium reagent **1.3** was used. The critical variable in terms of optimizing the yields and purities of **1.16a** and **1.17a** was the reaction time. In fact, it was critical to filter the reaction mixture within 1 h of mixing the reactants in hexane solution. If allowed to stir for few hours the color of the reaction mixture changed from colorless to yellow. Monitoring of these reaction mixtures by multinuclear NMR spectroscopy revealed the growth of unidentified resonances, an observation that is consistent with decomposition of the desired products. It is also worth nothing that when the diimines **1.16a** and **1.17a** are dissolved in benzene or methylene chloride some conversion to the corresponding aminoimine forms **1.16b** or **1.17b** was observed (Scheme 1.8). Equilibrium between the isomeric diimine and aminoimine forms was



**Scheme 1.8. Equilibrium between diimine and aminoimine forms of phosphorus compounds.**

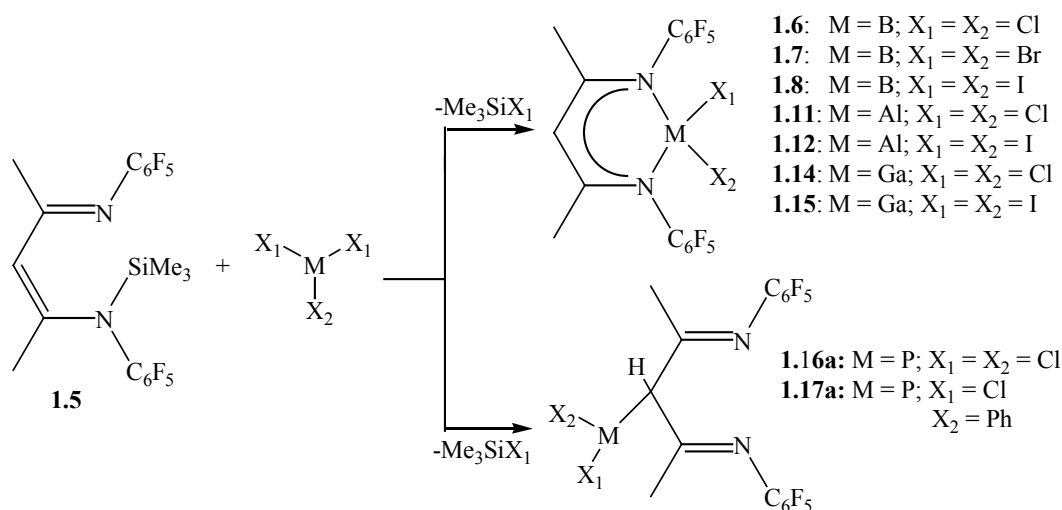
reached in approximately one day. At equilibrium the diimine and aminoimine forms were present in a mole ratio of  $\sim 2 : 3$ . Use of the tin reagent **1.4** for the syntheses of **1.16a** and **1.17a** was unsuccessful. NMR analysis revealed that neither of these compounds was present among the various products.

In summary, the salt metathesis method employing the lithium-based reagent **1.2** was successful only for the synthesis of the desired gallium compounds **1.14** and **1.15**, and phosphorus compounds **1.16a** and **1.17a**. The reason for the unsuccessful use of this method for the syntheses of the corresponding boron and aluminum compounds could be due to the presence of diethyl ether that was associated with the lithium-based reagents. In turn, the  $\text{Et}_2\text{O}$  molecules could form stable Lewis acid-base complexes of the type  $\text{Et}_2\text{O} \cdot \text{MX}_3$  (where  $\text{M} = \text{B}, \text{Al}$ ;  $\text{X} = \text{Cl}, \text{Br}, \text{I}$ ), which could interfere with desired reaction pathways. The use of the sodium-based reagent **1.3** was found to be successful for the syntheses of all of the targeted compounds. However, in a few instances impurities were detected during the synthesis of the boron  $\beta$ -diketiminates **1.6**, **1.7** and **1.8**. Furthermore, the yields of these compounds were not satisfactory. The tin-based reagent **1.4** can be employed only for small-scale syntheses of  $\beta$ -diketiminato boron, aluminum and gallium dihalides **1.6**, **1.11** and **1.14**. The reactions of iodo-substituted group 13 trihalides with the tin-based reagent **1.4** resulted in the formation of insoluble solids that were not identified. The attempted syntheses of the phosphorus-based compounds **1.16a** and **1.17a** by employing the tin-based route were also unsuccessful. One of the reasons why the tin-based reagent **1.4** was unsuitable for the intended metathesis reactions relates to the reduction potential of the  $\text{Sn(II)}$  moiety. One

example of the reductive behavior of Sn(II) relates to the reaction of  $\text{SnCl}_2$  with  $\text{PCl}_3$  to produce  $\text{SnCl}_4$  and “PCl” which, in turn, can be captured by diimine donor ligands.<sup>37</sup>

### Section 1.4. Trimethylsilyl Halide Elimination Method

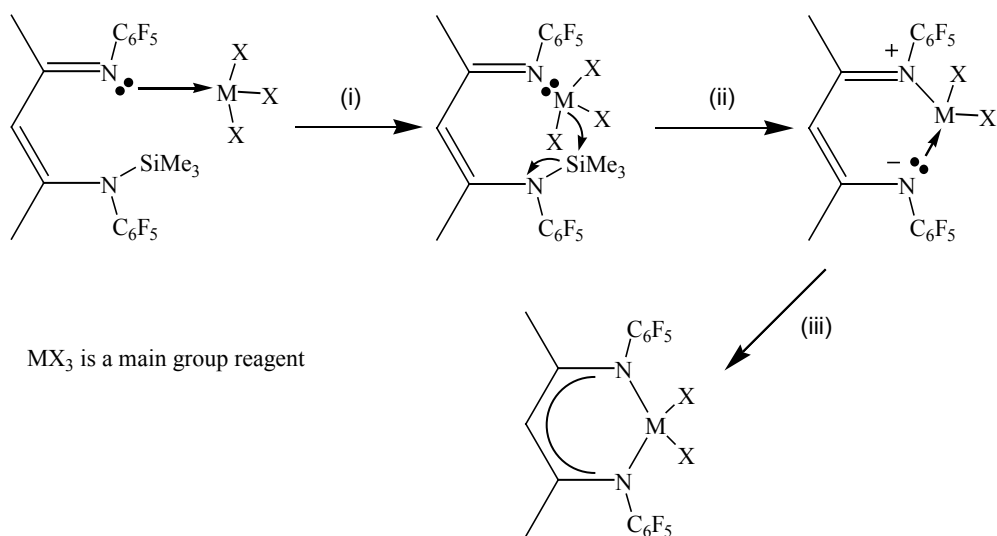
One of the reasons that the metathetical methods described in the previous sections are unsuccessful, or only partially successful, in terms of both product purity and yield is attributable to the highly reactive nature of the metal-based reagents even when these reactions were carried out at  $-78\text{ }^{\circ}\text{C}$ . The targeted boron compounds seemed particularly sensitive in this regard. It was therefore necessary to seek a milder reagent and this was achieved by replacement of the metal moieties with trimethylsilyl groups. In fact, trimethylsilyl halide elimination has already been shown to be a viable method for the synthesis of various amidinate-supported boron dihalides.<sup>38</sup> After exploring several different synthetic approaches, it was discovered that the best procedure for the preparation of the N-trimethylsilyl-substituted aminoimine **1.5** (Scheme 1.9) involves the reaction of the  $\beta$ -diketiminato sodium reagent **1.3** with  $\text{Me}_3\text{SiI}$ . It should be noted that this silyl-based reagent was prepared and used *in situ* because it is thermally sensitive and numerous attempts to isolate the pure compound



**Scheme 1.9.** General description of the trimethylsilyl halide elimination method.

were unsuccessful. The general procedure for the trimethylsilyl halide elimination method is summarized in Scheme 1.9 and involves the addition of the main group halide starting material ( $\text{BCl}_3$ ,  $\text{BBr}_3$ ,  $\text{BI}_3$ ,  $\text{AlCl}_3$ ,  $\text{AlI}_3$ ,  $\text{GaCl}_3$ ,  $\text{GaI}_3$ ,  $\text{PCl}_3$  or  $\text{PhPCl}_2$ ) to a freshly prepared toluene solution containing an equimolar amount of the silyl-based reagent.

The trimethylsilyl halide elimination method proved to be the most desirable synthetic route for the preparation of  $\beta$ -diketiminate boron dihalides **1.6**, **1.7** and **1.8**. Virtually quantitative yields of these compounds were obtained and examination of representative samples by multinuclear NMR revealed only traces of the toluene solvent. Very similar results were obtained in the reactions of the silyl-based reagent **1.5** with  $\text{AlI}_3$ ,  $\text{GaCl}_3$  and  $\text{GaI}_3$  to form the corresponding  $\beta$ -diketiminate-supported



**Scheme 1.10.** Possible reaction scheme for the formation of  $\beta$ -diketiminate-supported group 13 dihalide complexes by the reaction of the silyl-based reagent **1.5** with  $\text{MX}_3$ . (i) coordination of  $\text{MX}_3$  to the imine nitrogen; (ii) silane elimination; (iii) ring closure.

aluminum and gallium dihalides. However, there was no evidence of reaction when **1.5** was treated with  $\text{AlCl}_3$ ,  $\text{PCl}_3$  or  $\text{PhPCl}_2$ . The diminished reactivity of the phosphorus-based reagents in comparison with those of group 13 reagents (except for  $\text{AlCl}_3$ ) can be explained by proposing a plausible mechanistic scheme for the trimethylsilyl halide elimination process (Scheme 1.10) The initial step in the synthesis of the group 13 derivatives could involve coordination of  $\text{MX}_3$  to the imine nitrogen of the silyl reagent **1.5**, such a mechanistic assumption is based on earlier work from the Cowley group.<sup>39</sup> This initial step is then followed by the trimethylsilyl halide elimination and ring closure. In the case of the attempted reactions with  $\text{PCl}_3$  and  $\text{PhPCl}_2$ , the first step might not be possible because of the presence of lone pair-lone pair repulsion between the phosphorus and imino nitrogen lone pairs. In contrast, group 13 reagents are Lewis acidic and thus readily coordinate to the imino nitrogen center.

A possible explanation for the lack of reactivity of  $\text{AlCl}_3$  toward the silyl-based reagent **1.5** could relate to the strength of the Al—Cl bond. This particular bond (502 kJ/mol) is significantly stronger than all of the other group 13-halogen bonds involved in the trimethylsilyl halide elimination reactions (Table 1.1).<sup>40</sup> As a consequence, the trimethylsilyl halide elimination step (Scheme 1.10, step (ii)) does not take place in the case of the reaction of  $\text{AlCl}_3$  with **1.5**.

**Table 1.1. Bond dissociation energies in kJ/mol.**

	Cl	Br	I
B	427	390	361
Al	502	N/A	370
Ga	463	N/A	334

In summary, the trimethylsilyl halide elimination method produced better results in terms of product yields and purities than the other synthetic methods attempted previously. This was particularly so in the case of the targeted boron compounds **1.6**, **1.7** and **1.8**. Compounds **1.12**, **1.14** and **1.15** were also synthesized by this method. Somewhat surprisingly, the synthesis of the aluminum  $\beta$ -diketiminato **1.11** failed due to the strength of Al—Cl bond. Finally, the  $\beta$ -diketiminato phosphorus compounds **1.16** and **1.17** could not be synthesized by this method due to Lewis basic properties of the  $\text{PCl}_3$  and  $\text{PhPCl}_2$  starting materials.

### Section 1.5. Discussion of X-Ray Crystallographic Data

This section includes brief discussions of the main structural features of compounds **1.1**, **1.6**, **1.7**, **1.8**, **1.9**, **1.10**, **1.12**, **1.13**, **1.14**, **1.16a** and **1.17a**. More detailed summaries of the X-ray crystallographic data can be found in Chapter 4.

**(CH(CMe<sub>2</sub>)<sub>2</sub>(NC<sub>6</sub>F<sub>5</sub>)<sub>2</sub>)H (1, Figure 1.8)**<sup>41</sup>: Crystals of **1.1** were obtained by slow evaporation of a saturated hexane solution at room temperature. Overall, the crystal structure of **1.1** is very similar to those of (CH(CMe<sub>2</sub>)<sub>2</sub>(N-Dipp)<sub>2</sub>)H (L'H)<sup>42</sup> and (CH(CMe<sub>2</sub>)<sub>2</sub>(N-<sup>i</sup>Pr)<sub>2</sub>)H (L<sup>IV</sup>H).<sup>43</sup> All the bond distances in the C<sub>3</sub>N<sub>2</sub> fragment of **1.1** are identical as those observed in L'H and L<sup>IV</sup>H within experimental error. In terms of the nitrogen hydrogen atom position, **1.1** closely resembles L'H because this hydrogen is found closer to N(1) while in the case of L<sup>IV</sup>H the nitrogen hydrogen is positioned equidistantly between the two nitrogen atoms.

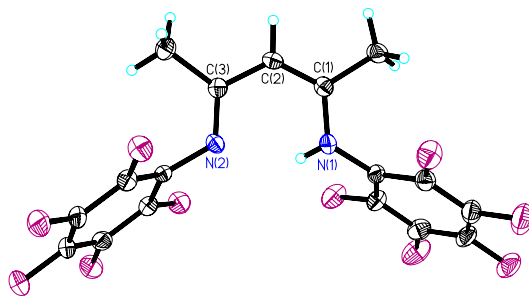


**Figure 1.8. Molecular structure of (CH(CMe<sub>2</sub>)<sub>2</sub>(NC<sub>6</sub>F<sub>5</sub>)<sub>2</sub>)H, **1.1**.**

**(CH(CMe<sub>2</sub>)<sub>2</sub>(NC<sub>6</sub>F<sub>5</sub>)<sub>2</sub>)BCl<sub>2</sub> (1.6, Figure 1.9)**: Crystals of **1.6** were obtained from a saturated toluene solution at – 20 °C. Only one β-diketiminato boron dichloride has been reported in the literature.<sup>28</sup> However, no X-ray structural data are available for this



compound. Structurally characterized compounds that most closely resemble **1.6** are amidinate-based boron dichloride derivatives of the type  $(R^1C(NR^2)_2)BCl_2$ , where the substituents  $R^1$  and  $R^2$  range from alkyl, aryl to amido.<sup>38</sup> These amidinate-based boron dichloride complexes have average B—N and B—Cl bond distances of 1.566(4) and 1.833(4) Å, respectively. By comparison, the average of the B—N and B—Cl bond distances in **6** are 1.529(2) and 1.882(3) Å, respectively. The shortening of the B—N bond and the elongation of the B—Cl bond in **1.6** compared with those observed for the amidinate-based complexes can be explained in terms of the N-B-N bite angle and the nature of the bonding between boron and nitrogen atoms. A four-coordinate boron center prefers a tetrahedral shape, (i.e.  $sp^3$  hybridization) with angles of (or close to)  $109.5^\circ$ . Also, the boron center in both the  $\beta$ -diketimate- and amidinate-based complexes forms one covalent and one donor-acceptor bond with the two nitrogen atoms. However, the two bonds become equivalent due to mixing of the resonance structures. Thus, due to the very acute bite angle (N-B-N) observed for the amidinate complexes (average of  $83.0(2)^\circ$ ), the orbital overlap between the boron and nitrogen atoms is not as good as in the case of **1.6** for which the bite angle is  $109.9(2)^\circ$ . In turn

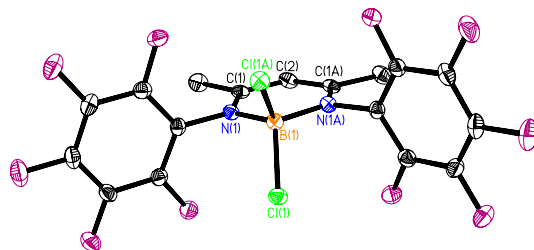


**Figure 1.9. Molecular structure of  $(CH(CMe_2)_2(NC_6F_5)_2)BCl_2$ , **1.6**. All hydrogen atoms have been omitted for clarity.**

this results in longer B—N bond distances for the amidinate complexes than those observed for **1.6**. Accordingly, the boron centers of the amidinate complexes are more Lewis acidic than the boron center of **1.6** which results in shortening of the B—Cl bonds in the case of the amidinate complexes. Furthermore, the boron center of **1.6** lies in the extended C<sub>3</sub>N<sub>2</sub> plane and the N—C (1.346(3) Å) and C—C (1.377(3) Å) bonds are similar to those observed for **1.7** and **1.8**. As in the case of many other similar  $\beta$ -diketiminato complexes delocalized  $\pi$ -bonding is found in the C<sub>3</sub>N<sub>2</sub> fragment.

**(CH(CMe<sub>2</sub>)<sub>2</sub>(NC<sub>6</sub>F<sub>5</sub>)<sub>2</sub>)BBr<sub>2</sub> (**1.7**, Figure 1.10):** Crystals of **1.7** were obtained from a saturated toluene solution at – 20 °C. There are no previous reports of any  $\beta$ -diketiminato-supported boron dibromide complexes. In fact, the closest type of structure that resembles **1.7** are those of the amidinate-based boron dibromide complexes.<sup>38</sup> For the same reasons as stated for **1.6**, the shortening of the average B—N (1.519(6) Å) bond distance and elongation of the average B—Br (2.054(5) Å) bond distance are observed for **1.7** when compared with those for the amidinate analogues (1.553(5) and 2.009(4) Å for the B—N and B—Br bond distances, respectively). The N—C (1.345(6) Å) and C—C (1.372(6) Å) bond distances are similar to those observed in **1.6** and **1.8** and, as in the case of many other similar  $\beta$ -diketiminato complexes, delocalized  $\pi$ -bonding is evident in the C<sub>3</sub>N<sub>2</sub> fragment. The N-B-N bond angle of **1.7** is 110.3(6)° and the boron center lies in the extended C<sub>3</sub>N<sub>2</sub> plane.

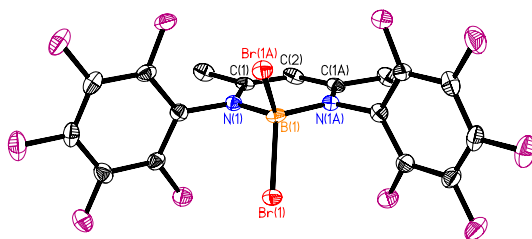


**Figure 1.10.** Molecular structure of  $(\text{CH}(\text{CMe}_2)_2(\text{NC}_6\text{F}_5)_2)\text{BBr}_2$ , **1.7**. All hydrogen atoms have been omitted for clarity.

$(\text{CH}(\text{CMe}_2)_2(\text{NC}_6\text{F}_5)_2)\text{BI}_2$  (**1.8**, Figure 1.11): Crystals of **1.8** were obtained from a saturated methylene chloride solution at  $-20\text{ }^\circ\text{C}$ . There are no previous reports of any  $\beta$ -diketiminato boron diiodide complexes. Furthermore, no amidinate analogues have been reported either. The B—N bond distances for **1.8** (1.523(4) and 1.533(4) Å) are not significantly different than those observed for **1.6** and **1.7**. The B—I bond lengths of 2.222(4) and 2.342(4) Å are comparable to those reported for the trimethylamine adduct of  $\text{BI}_3$ , for which the average B—I bond length is approximately 2.265(4) Å.<sup>44</sup> However, the two B—I bond distances for **1.8** are not identical, an observation that can be attributed to the puckering of the  $\text{C}_3\text{N}_2\text{B}$  ring. The puckering of this ring results from the steric interactions between the iodide substituents and  $\text{C}_6\text{F}_5$  rings, and can be expressed as the distance of the boron atom from the averaged extended  $\text{C}_3\text{N}_2$  plane. The boron center in **1.8** is approximately 0.484 Å from the  $\text{C}_3\text{N}_2$  plane. Interestingly, the B(1)—I(2) bond is almost perpendicular to the  $\text{C}_3\text{N}_2$  plane, an observation that could add to its elongation in comparison with the B(1)—I(1) bond. This bond distance discrepancy is also observed in the case of the 2,6-diisopropylphenyl-substituted  $\beta$ -

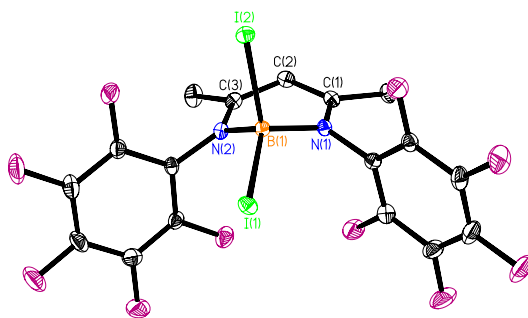


**Figure 1.11. Molecular structure of  $(\text{CH}(\text{CMe}_2)_2(\text{NC}_6\text{F}_5)_2)\text{BI}_2$ , **1.8**. All hydrogen atoms have been omitted for clarity.**

diketiminato aluminum diiodide, **1.12c**. The difference between the N-B-N angle for **1.8** ( $108.1(3)^\circ$ ) and those for **1.6** ( $109.9(2)^\circ$ ) and **1.7** ( $110.3(6)^\circ$ ) can also be attributed to the puckering of the  $\text{C}_3\text{N}_2\text{B}$  ring. Furthermore, the two N—C ( $1.337(5)$  and  $1.340(5)$  Å) and the two C—C ( $1.391(5)$  and  $1.388(5)$  Å) bond distances are similar in length to the ones observed in **1.6** and **1.7**. As in the case of many other similar  $\beta$ -diketiminato complexes, delocalized  $\pi$ -bonding is found in the  $\text{C}_3\text{N}_2$  fragment.

$(\text{CH}(\text{CMe}_2)_2(\text{NC}_6\text{F}_5)_2)\text{AlMe}_2$  (**1.9**, Figure 1.12)<sup>41</sup>: Crystals of **1.9** were obtained from a saturated toluene solution at  $-30^\circ\text{C}$ . Previously reported, structurally characterized ( $\beta$ -diketiminato) $\text{AlMe}_2$  compounds include  $[(\text{HC})(\text{CMe})_2(\text{N}(\text{p-tolyl}))_2]\text{AlMe}_2$ <sup>45</sup> (**1.9a**),  $[(\text{HC})(\text{CPh})_2(\text{N}(\text{p-ClC}_6\text{H}_4))_2]\text{AlMe}_2$ <sup>10</sup> (**1.9b**),  $[(\text{HC})(\text{CPh})_2(\text{N}(\text{SiMe}_3))_2]\text{AlMe}_2$ <sup>46</sup> (**1.9c**), and  $[(\text{HC})(\text{CMe})_2(\text{N}(2,6\text{-diisopropylphenyl}))_2]\text{AlMe}_2$ <sup>47</sup> (**1.9d**). The displacements of the aluminum center from the  $\text{C}_3\text{N}_2$  planes (the ring puckering) for **1.9a**, **1.9b**, **1.9c** and **1.9d** ( $0.313$ ,  $0.463$ ,  $0.999$  and  $0.729$  Å, respectively) are significantly larger than the same displacement for **1.9**, which is only  $0.073$  Å. The ring puckering has been attributed to the steric interactions between the N-substituents of a  $\beta$ -diketiminato

ligand and the metal substituents. This certainly holds true when comparing the structure of **1.9** with those of **1.9c** and **1.9d** since the trimethylsilyl and 2,6-diisopropylphenyl substituents are bulkier than the  $\text{C}_6\text{F}_5$  group. However, the sizable ring puckering observed for **1.9a** and **1.9b** compared with **1.9** may be due to crystal packing forces because the steric demands of the *p*-tolyl and *p*- $\text{ClC}_6\text{H}_4$  groups are comparable to those of the  $\text{C}_6\text{F}_5$  group. The averages of the two N—C (1.338(3) Å) and C—C (1.395(3) Å) bond distances are similar for all the structures discussed above and, as in the case of many other similar  $\beta$ -diketiminato complexes delocalized  $\pi$ -bonding is evident in the  $\text{C}_3\text{N}_2$  fragment. Additionally, the two Al—N (1.957(3) and 1.947(3) Å) and Al—C (1.9263(18) and 1.917(2) Å) bond lengths, and the N-Al-N bond angle for **1.9** ( $93.99(8)^\circ$ ) are comparable with the metric parameters for the other four structures regardless of the fact that a different degree of  $\text{C}_3\text{N}_2\text{Al}$  ring puckering is observed in each case.

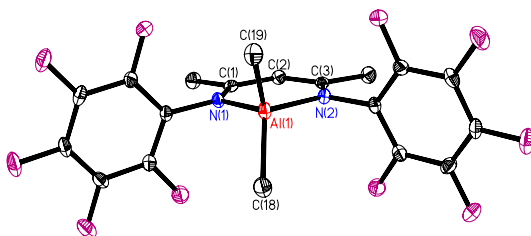


**Figure 1.12. Molecular structure of  $(\text{CH}(\text{CMe}_2)_2(\text{NC}_6\text{F}_5)_2)\text{AlMe}_2$ , **1.9**. All hydrogen atoms have been omitted for clarity.**

$(\text{CH}(\text{CMe}_2)_2(\text{NC}_6\text{F}_5)_2)\text{AlCl}_2$  (**1.11**, **Figure 1.13**)<sup>48</sup>: Crystals of **1.11** were obtained by vacuum sublimation. Previously reported, structurally characterized ( $\beta$ -diketiminato) $\text{AlCl}_2$  compounds include  $[(\text{HC})(\text{CMe})_2(\text{NMe})_2]\text{AlCl}_2$ <sup>34</sup> (**1.11a**),

$[(\text{HC})(\text{CMe})_2(\text{N}(\text{isopropyl}))_2]\text{AlCl}_2$ <sup>34</sup> (**1.11b**),  $[(\text{HC})(\text{CMe})_2(\text{N}(\text{p-tolyl}))_2]\text{AlCl}_2$ <sup>45</sup> (**1.11c**), and  $[(\text{HC})(\text{CMe})_2(\text{N}(2,6\text{-diisopropylphenyl}))_2]\text{AlCl}_2$ <sup>32</sup> (**1.11d**). The molecular structure of **1.11** bears a close resemblance to those of **1.11a** and **1.11c** with the respect to the  $\text{C}_3\text{N}_2\text{Al}$  ring. In all three structures the aluminum center is found to lie in the extended  $\text{C}_3\text{N}_2$  plane within experimental error. In the case of **1.11b** and **1.11d** the aluminum center is displaced by 0.321 and 0.525 Å, respectively, from the  $\text{C}_3\text{N}_2$  plane, an observation that can be attributed to the bulky nature of isopropyl and 2,6-diisopropylphenyl substituents. The average of the two N—C (1.348(6) Å) and C—C (1.389(7) Å) bond distances for **1.11** are similar for all structures discussed above and, as in the case of many other similar  $\beta$ -diketiminato complexes, delocalized  $\pi$ -bonding is evident in the  $\text{C}_3\text{N}_2$  fragment. Additionally, the two Al—N (1.866(4) and 1.872(4) Å) and Al—Cl (2.092(2) and 2.104(2) Å) bond distances are comparable in length to those of the other four structures. The most acute N-Al-N bond angle is observed for **1.11** (97.92(19)°) while in the case of **1.11a**, **1.11c** and **1.11d** these angles are 99.95(9)°, 99.41(12)° and 99.36(4)°, respectively. The largest N-Al-N bond angle is observed for **1.11b** (102.81(7)°).

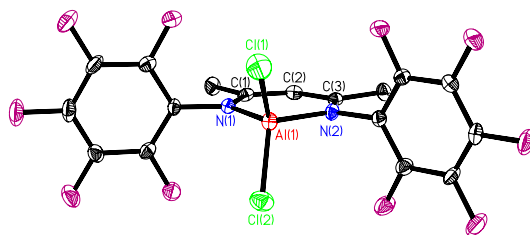


**Figure 1.13. Molecular structure of  $(\text{CH}(\text{CMe}_2)_2(\text{NC}_6\text{F}_5)_2)\text{AlCl}_2$ , **1.11**. All hydrogen atoms have been omitted for clarity.**

**(CH(CMe)<sub>2</sub>(NC<sub>6</sub>F<sub>5</sub>)<sub>2</sub>)AlI<sub>2</sub> (1.12, Figure 1.14):** Crystals of **1.12** were obtained by slow removal of solvent from a saturated toluene solution. Previously reported, structurally characterized (β-diketimate)AlI<sub>2</sub> compounds include [(HC)(CMe)<sub>2</sub>(NMe)<sub>2</sub>]AlI<sub>2</sub><sup>35</sup> (**1.12a**), [(HC)(CMe)<sub>2</sub>(N(isopropyl))<sub>2</sub>]AlI<sub>2</sub><sup>35</sup> (**1.12b**), and [(HC)(CMe)<sub>2</sub>(N(2,6-diisopropylphenyl))<sub>2</sub>]AlI<sub>2</sub><sup>32</sup> (**1.12c**). The displacement of the aluminum atom from the C<sub>3</sub>N<sub>2</sub> plane for **1.12**, **1.12a**, **1.12b** and **1.12c** (0.178, 0.246, 0.310 and 0.517 Å, respectively) is due to repulsive interactions between the iodide ligands on the aluminum center and the nitrogen substituents of the β-diketimate ligand. The steric influence of the iodide groups is even more evident when **1.11**, which possesses a planar C<sub>3</sub>N<sub>2</sub>Al ring, and **1.12** are compared because the only difference between **1.11** and **1.12** is the size of the halide ligands bonded to the aluminum atom. This steric influence of the iodide groups is also evident when **1.11a** and **1.11c** are compared with **1.12a** and **1.12b**. The averages of the two N—C (1.352(10) Å) and the two C—C (1.393(12) Å) bond distances in **1.12** are similar to those observed for the other three structures and, as in the case of many other similar β-diketimate complexes, delocalized π-bonding is found in the C<sub>3</sub>N<sub>2</sub> fragment. The two Al—N bond lengths for **1.12** (1.849(7) and 1.868(7) Å) are identical within experimental error, as are the Al—N bond lengths for **1.12a**, **1.12b** and **1.12c**. The Al—I bond lengths for **1.12** (2.499(3) and 2.517(3) Å) appear to be shorter than those observed in **1.12a** (2.522(6) and 2.554(5) Å), **1.12b** (2.547(2) and 2.549(2) Å) and **1.12c** (2.501(1) and 2.541(1) Å). However, the two Al—I bond distances for **1.12**, **1.12a** and **1.12b** are indistinguishable from each other within experimental error while in the case of **1.12c** the two Al—I

bonds are different in length. A similar observation was made in the case of **1.8**. Note also that the N-Al-N bond angle for **1.12** ( $98.0(3)^\circ$ ) is more acute than those for **1.12a** ( $100.6(3)^\circ$ ), **1.12b** ( $103.5(3)^\circ$ ) and **1.12c** ( $99.9(1)^\circ$ ).

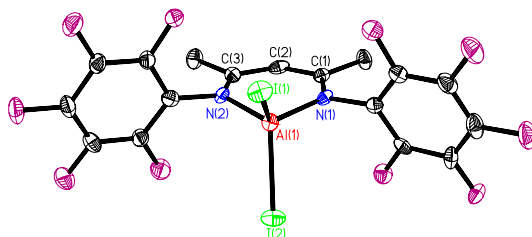


**Figure 1.14. Molecular structure of  $(\text{CH}(\text{CMe}_2)_2(\text{NC}_6\text{F}_5)_2)\text{AlI}_2$ , **1.12**. All hydrogen atoms have been omitted for clarity.**

$(\text{CH}(\text{CMe}_2)_2(\text{NC}_6\text{F}_5)_2)\text{GaMe}_2$  (**1.13**, **Figure 1.15**)<sup>41</sup>: Crystals of **1.13** were obtained from a saturated pentane solution at room temperature. Previously reported, structurally characterized  $(\beta\text{-diketiminate})\text{GaMe}_2$  compounds include  $[((\text{NC})\text{C})(\text{CMe})_2(\text{NH})_2]\text{GaMe}_2$ <sup>49</sup> (**1.13a**) and  $[(\text{HC})(\text{CMe})_2(\text{N}(2,6\text{-diisopropylphenyl}))_2]\text{GaMe}_2$ <sup>32</sup> (**1.13b**). The molecular structure of **1.13** bears a close resemblance to that of **1.13a** with the respect to the  $\text{C}_3\text{N}_2\text{Ga}$  ring geometry. In both structures the gallium atom is found to lie in the extended  $\text{C}_3\text{N}_2$  plane. In the structure of **1.13b** the gallium center is displaced  $0.760 \text{ \AA}$  from the  $\text{C}_3\text{N}_2$  plane, an observation that can be attributed to the bulky nature of 2,6-diisopropylphenyl substituents. The averages of the two N—C ( $1.332(5) \text{ \AA}$ ) and C—C ( $1.396(6) \text{ \AA}$ ) bond distances for **1.13** are similar to those observed for the other two structures and, as in the case of many other similar  $\beta\text{-diketiminate}$  complexes, delocalized  $\pi$ -bonding is found in the  $\text{C}_3\text{N}_2$  fragment. The two Ga—N ( $1.987(3)$  and



2.007(3) Å) bond lengths for **1.13** are different within experimental error. A similar situation prevails for **1.13b** (1.979(2) and 2.001(2) Å) but not for **1.13a** (1.957(2) and 1.969(2) Å). On the other hand, the two Ga—C bond distances (1.956(6) and 1.967(5) Å) in **1.13** are identical within experimental error as are the Ga—C bond lengths for **1.13a** (1.963(2) and 1.963(2) Å) and **1.13b** (1.970(2) and 1.979(2) Å). Finally, the value for the N—Al—N bond angle of **1.13** (92.49(13)°) falls between those observed for **1.13a** (90.95(9)°) and **1.13b** (93.92(7)°).

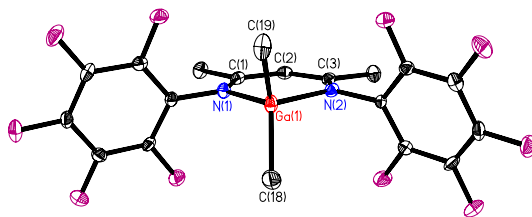


**Figure 1.15. Molecular structure of (CH(CMe<sub>2</sub>)<sub>2</sub>(NC<sub>6</sub>F<sub>5</sub>)<sub>2</sub>)GaMe<sub>2</sub>, **1.13**. All hydrogen atoms have been omitted for clarity.**

(CH(CMe<sub>2</sub>)<sub>2</sub>(NC<sub>6</sub>F<sub>5</sub>)<sub>2</sub>)GaCl<sub>2</sub> (**1.14**, Figure 1.16): Crystals of **1.14** were obtained from a saturated toluene solution at – 30 °C. Previously reported, structurally characterized (β-diketiminato)GaCl<sub>2</sub> compounds include [(HC)(CMe)<sub>2</sub>(NMe)<sub>2</sub>]GaCl<sub>2</sub><sup>34</sup> (**1.14a**), [(HC)(CMe)<sub>2</sub>(N(t-butyl))<sub>2</sub>]GaCl<sub>2</sub><sup>34</sup> (**1.14b**) and [(HC)(CMe)<sub>2</sub>(N(2,6-diisopropylphenyl))<sub>2</sub>]GaCl<sub>2</sub><sup>32</sup> (**1.14c**). The molecular structure of **1.14** bears a close resemblance to those of **1.14a** and **1.14b** with the respect to the geometry of C<sub>3</sub>N<sub>2</sub>Ga ring. In all three structures the gallium atom is found to lie in the extended C<sub>3</sub>N<sub>2</sub> plane within experimental error. In case of **1.14c** the gallium atom is displaced 0.508 Å from

said plane, an observation that can be attributed to the bulky nature of 2,6-diisopropylphenyl substituents. The averages of the two N—C (1.347(3) Å) and C—C bond lengths in **1.14** (1.390(3) Å) are similar to those observed in the other two gallium structures and, as in the case of many other similar  $\beta$ -diketiminate complexes, delocalized  $\pi$ -bonding is found in the  $C_3N_2$  fragment. The two Ga—N (1.9126(19) and 1.9062(19) Å) bond lengths for **1.14** are identical within experimental error and the Ga—N bond distances observed for **1.14b** (1.915(3) and 1.919(3) Å) and **1.14c** (1.926(3) and 1.906(3) Å) are similar, while those for **1.14a** (1.891(2) and 1.891(2) Å) are somewhat shorter. On the other hand, the two Ga—Cl bond distances (2.1502(8) and 2.1501(8) Å) for **14** are shorter than those found for **1.14a** (2.165(1) and 2.165(1) Å), **1.14b** (2.1924(19) and 2.1977(18) Å) and **1.14c** (2.228(1) and 2.218(1) Å), the last of which has the longest Ga—Cl bond lengths. With the exception of **1.14b**, which has the N-Ga-N bond angle of 106.98(8)°, those for **1.14** (99.02(8)°), **1.14a** (100.7(1)°) and **1.14c** (100.2(1)°) are very similar.

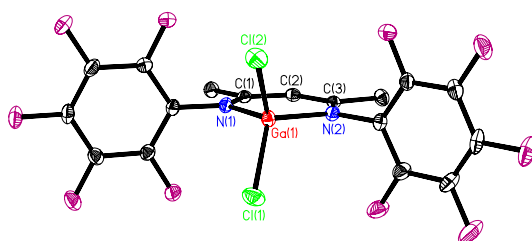


**Figure 1.16. Molecular structure of  $(CH(CMe_2)_2(NC_6F_5)_2)GaCl_2$ , **1.14**. All hydrogen atoms have been omitted for clarity.**

$(PCl_2)CH(CMe_2)_2(NC_6F_5)_2$  (**1.16a**, **Figure 1.17**): Crystals of **1.16a** were obtained during the removal of solvent from a pentane solution under reduced pressure. This

represents the first  $\beta$ -diketiminato phosphorus complex in which the two substituents on the phosphorus atom are exclusively halides. In the contrast to the structures of the  $\beta$ -diketiminato-supported boron, aluminum and gallium complexes discussed earlier, the phosphorus center is not N,N' chelated but instead binds to the  $\gamma$ -carbon atom of the  $\beta$ -diketiminato backbone. The previously reported  $\beta$ -diketiminato phosphorus compounds  $(\text{PhClP})\text{C}(\text{CMe}_2)_2(\text{N}(2,6\text{-diisopropylphenyl})(\text{HN}(2,6\text{-diisopropylphenyl}))^{31}$  (**1.17c**), and  $(\text{Ph}_2\text{P})\text{C}(\text{CMe}_2)_2(\text{N}(2,6\text{-diisopropylphenyl})(\text{HN}(2,6\text{-diisopropylphenyl}))^{30}$  (**1.17d**), exhibit the same bonding mode. However, the major structural difference between **1.16a**, **1.17c** and **1.17d** is that 1,3 hydrogen migration from the  $\gamma$ -carbon to one of the nitrogen atoms is observed for **1.17c** and **1.17d** which results in an aminoimine structure for these two complexes. In the case of **1.16a** this hydrogen is located on the  $\gamma$ -carbon atom resulting in a diimino structure. The difference between the aminoimine and diimine forms is also evident in the bond lengths. While **1.16a** has two short C—N

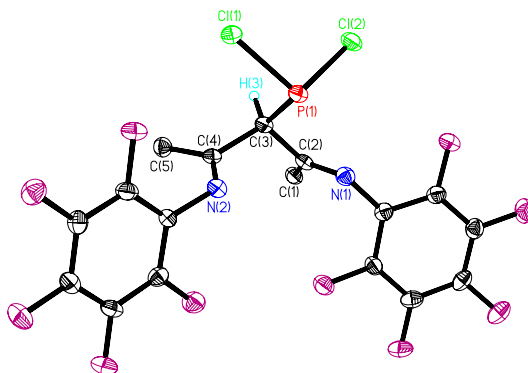


**Figure 1.17. Molecular structure of  $(\text{PCl}_2)\text{CH}(\text{CMe}_2)_2(\text{NC}_6\text{F}_5)_2$ , **1.16a**. All hydrogen atoms, except that on the  $\gamma$ -carbon, have been omitted for clarity.**

bonds (1.284(5) and 1.281(5) Å), compounds **1.17c** and **1.17d** have one short and one long N—C bond (1.397(7) and 1.488(7) Å for **1.17c** and 1.306(2) and 1.337(2) Å for **1.17d**). Furthermore, based on the X-ray crystal structure data for **1.17c** and **1.17d** there is evidence for  $\pi$ -type delocalization throughout the C<sub>3</sub>N<sub>2</sub>H ring. This is not the case for **1.16a**. The P—C( $\gamma$ ) bond distance for **1.16a** (1.864(5) Å) is longer than the analogous bond distances for **1.17c** (1.773(5) Å) and **1.17d** (1.8122(17) Å). The two P—Cl bond lengths for **1.16a** (2.0747(15) and 2.0675(15) Å) are shorter than that observed in **1.17c** (2.129(2) Å). The geometry around the phosphorus center is best described as pyramidal. One of the interesting aspects of this crystal structure relates to short P(1)⋯N(1) and P(1)⋯N(2) contacts of 2.690(4) and 2.894(4) Å, respectively (Figure 1.18). Both of these distances are appreciably shorter than the sum of van der Waals radii for P and N (3.40 Å). It is postulated that these two short contacts play a crucial role in the formation of the first N,N'-bonded chlorophophenium cation.<sup>52</sup>

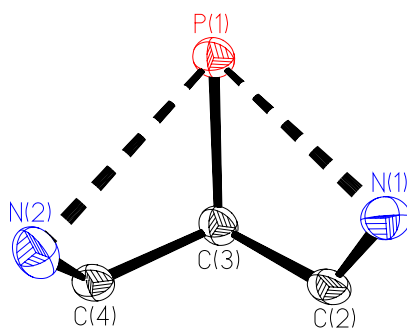


**Figure 1.18. View of the skeleton of 1.16a showing the short P⋯N contacts.**

(PhPCl)CH(CMe<sub>2</sub>)<sub>2</sub>(NC<sub>6</sub>F<sub>5</sub>)<sub>2</sub> (**1.17a**, Figure 1.19)<sup>50</sup>: Crystals of **1.17a** were obtained from a saturated hexane solution at − 30 °C. In terms of the substituents on the

phosphorus atom and its mode of binding, compound **1.17a** is analogous to **1.17c**. However, as in the case of **1.16a**, **1.17a** also exhibits a diimine form, which is different from the aminoimine form of **1.17c**, resulting in two short C—N bond distances (1.273(3) and 1.272(3) Å). The P—C( $\gamma$ ) distance of **1.17a** (1.876(3) Å) is longer than those observed for **1.17c** and **1.17d** but is identical to that observed for **1.16a** within experimental error. The P—Cl bond distance for **1.17a** (2.1196(12) Å) is longer than that observed for **1.16a** but very similar to the one observed for **1.17c**. The geometry around the phosphorus atom is best described as pyramidal. As in the case of **1.16a**, close P...N contacts are observed (2.633(9) and 3.054(10) Å). However, one contact is shorter and the other one is longer than the two close contacts observed for **1.16a**.

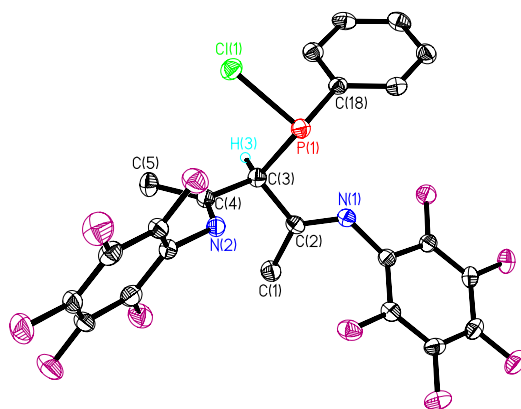


**Figure 1.19. Molecular structure of (PhPCl)CH(CMe<sub>2</sub>)<sub>2</sub>(NC<sub>6</sub>F<sub>5</sub>)<sub>2</sub>, **1.17a**. All hydrogen atoms, except that on the  $\gamma$ -carbon, have been omitted for clarity.**

## CONCLUSIONS

Six different synthetic methods have been explored in the synthesis of various  $\beta$ -diketiminato boron, aluminum, gallium and phosphorus compounds. The methane elimination route is the preferred method for several aluminum and gallium derivatives, specifically  $(\text{CH}(\text{CMe}_2)_2(\text{NC}_6\text{F}_5)_2)\text{AlMe}_2$  (**1.9**),  $(\text{CH}(\text{CMe}_2)_2(\text{NC}_6\text{F}_5)_2)\text{AlMeCl}$  (**1.10**),  $(\text{CH}(\text{CMe}_2)_2(\text{NC}_6\text{F}_5)_2)\text{AlCl}_2$  (**1.11**) and  $(\text{CH}(\text{CMe}_2)_2(\text{NC}_6\text{F}_5)_2)\text{GaMe}_2$  (**1.13**). However, it is important to note that fresh samples of starting materials are required on account of the possibility of ligand scrambling. The use of  $\text{Et}_3\text{N}$  for base-promoted dehydrohalogenation appeared to be an unreliable synthetic method for the synthesis of all of the desired group 13 derivatives. This is due to the facile formation of Lewis acid-base complexes of  $\text{Et}_3\text{N}$  with boron, aluminum and gallium trihalides. All attempts to prepare  $\beta$ -diketiminato-supported phosphorus compounds by this route resulted in mixtures of unidentified products. In terms of product purity, the salt elimination route using  $(\text{CH}(\text{CMe}_2)_2(\text{NC}_6\text{F}_5)_2)\text{Li}\cdot\text{OEt}_2$  ( $\text{LLi}\cdot\text{OEt}_2$ , **1.2**) gave excellent results for the syntheses of gallium and phosphorus compounds  $(\text{CH}(\text{CMe}_2)_2(\text{NC}_6\text{F}_5)_2)\text{GaCl}_2$  (**1.14**),  $(\text{CH}(\text{CMe}_2)_2(\text{NC}_6\text{F}_5)_2)\text{GaI}_2$  (**1.15**),  $(\text{PCl}_2)\text{CH}(\text{CMe}_2)_2(\text{NC}_6\text{F}_5)_2$  (**1.16a**) and  $(\text{PhPCl})\text{CH}(\text{CMe}_2)_2(\text{NC}_6\text{F}_5)_2$  (**1.17a**). The reason for the presence of impurities in the boron and aluminum derivatives prepared by this route appears to be due to the presence of diethyl ether, which is well known to form stable Lewis acid-base complexes with boron and aluminum trihalides. Replacement of the lithium reagent  $\text{LLi}\cdot\text{OEt}_2$  by  $(\text{CH}(\text{CMe}_2)_2(\text{NC}_6\text{F}_5)_2)\text{Na}$  ( $\text{LNa}$ , **1.3**), resulted in successful syntheses of the boron compounds  $(\text{CH}(\text{CMe}_2)_2(\text{NC}_6\text{F}_5)_2)\text{BCl}_2$  (**1.6**),  $(\text{CH}(\text{CMe}_2)_2(\text{NC}_6\text{F}_5)_2)\text{BBr}_2$

(**1.7**) and  $(\text{CH}(\text{CMe}_2)_2(\text{NC}_6\text{F}_5)_2)\text{BI}_2$  (**1.8**). However, the yields were low to moderate. The use of the  $\beta$ -diketiminato tin(II) chloride reagent,  $(\text{CH}(\text{CMe}_2)_2(\text{NC}_6\text{F}_5)_2)\text{SnCl}$  (**1.4**), is useful for the small-scale syntheses of **1.6**, **1.11** and **1.14**. The reactions of  $\text{BI}_3$ ,  $\text{AlI}_3$  and  $\text{GaI}_3$  with **1.4** resulted in insoluble solids, while the reactions with  $\text{PCl}_3$  and  $\text{PhPCl}_2$  yielded mixture of unidentifiable products. Finally, the silane elimination method provided the best results in terms of yields for the desired  $\beta$ -diketiminato-supported boron compounds **1.6**, **1.7** and **1.8**. Surprisingly,  $\text{AlCl}_3$  does not react with the silyl-based starting material  $\text{CH}(\text{CMe}_2)_2(\text{NC}_6\text{F}_5)(\text{Me}_3\text{Si-NC}_6\text{F}_5)$  (**1.5**) possibly due to the strength of the Al—Cl bond. The reason for the failure of the reactions involving  $\text{PCl}_3$  and  $\text{PhPCl}_2$  is presumably due to the Lewis basic nature of these reagents. It is also worth noting that the silyl-based  $\beta$ -diketiminato reagent **1.5** needs to be prepared fresh and used *in situ* since attempts to isolate free **1.5** resulted in approximately 30% decomposition.

Single-crystal X-ray diffraction studies of the  $\beta$ -diketiminato-supported group 13 compounds **1.6**, **1.7**, **1.8**, **1.9**, **1.10**, **1.12**, **1.13** and **1.14** revealed that in general the molecular structures of these compounds are very similar to those reported previously. Structural assay of compounds **1.16a** and **1.17a** revealed that these compounds adopt a diimine form which is isomeric with the aminoimine form that had been reported previously for  $\beta$ -diketiminato phosphorus compounds.

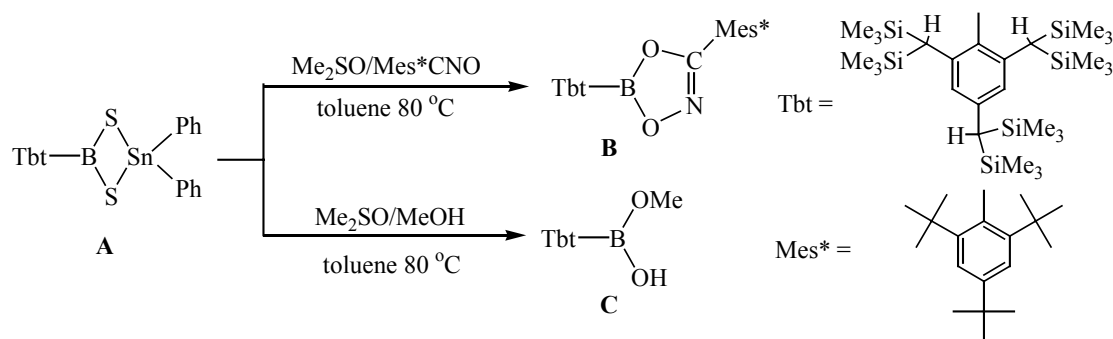
## CHAPTER 2

### Part I

## Synthesis and Characterization of a Coordinated Oxoborane. Lewis Acid Stabilization of a Boron-Oxygen Double Bond

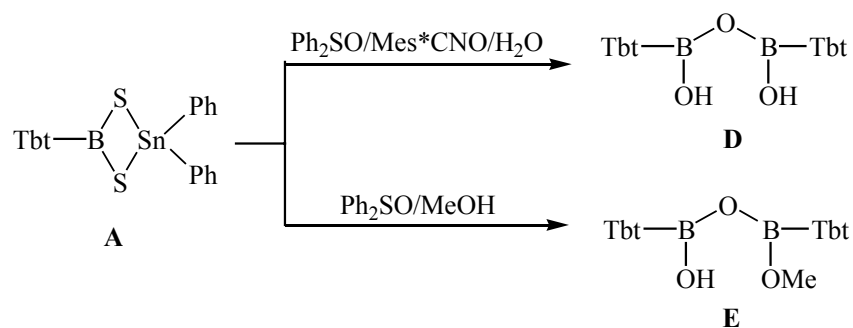
### INTRODUCTION

The isolation of a stable monomeric oxoborane ( $\text{RB}=\text{O}$ ) that features a formal double bond between boron and oxygen atoms, has proved to be elusive despite the use of kinetically stabilizing alkyl<sup>51</sup>, amido<sup>52</sup> or aryl<sup>53</sup> substituents. Convincing evidence has, however, been presented for the intermediacy of such species on the basis of variety of elegant trapping experiments. For example, Ozaki *et al.*<sup>53c</sup> oxidized a tin-containing four-membered boracycle (**A**) with dimethyl sulfoxide (DMSO) in the presence of the trapping agents  $\text{Mes}^*\text{CNO}$  and methanol thereby generating **B** and **C**, respectively (Scheme 2.1). The use of diphenyl sulfoxide (DPSO) as the oxidizing



**Scheme 2.1.** Oxidation of a four-membered boracycle by dimethyl sulfoxide (DMSO) and trapping of postulated  $\text{Tbt-B}=\text{O}$ .





**Scheme 2.2. Oxidation of a four-membered boracycle by diphenyl sulfoxide (DPSO) and trapping of postulated Tbt-B=O.**

agent, instead of DMSO, followed by trapping with Mes\*CNO/H<sub>2</sub>O or MeOH, resulted in the different trapping products **D** and **E**, respectively (Scheme 2.2). It was postulated that the intermediate in the DMSO oxidation experiments was the monomeric oxoborane Tbt-B=O stabilized by a DMSO molecule (Figure 2.1a). In the case of the DPSO oxidation the intermediate was postulated to be a dioxodiboretane (Figure 2.1b). Neither of these intermediates was isolated and their existence was postulated on the basis of <sup>11</sup>B NMR data.

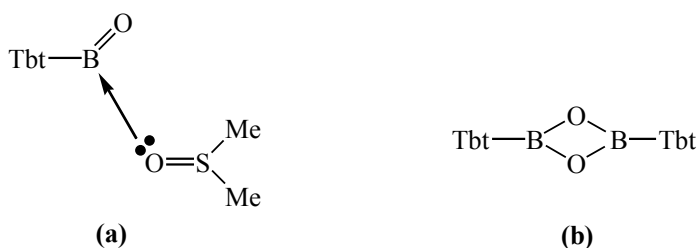
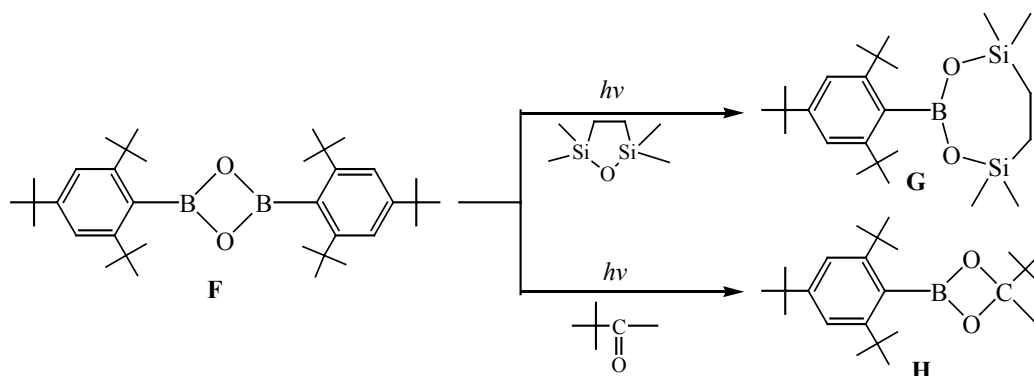


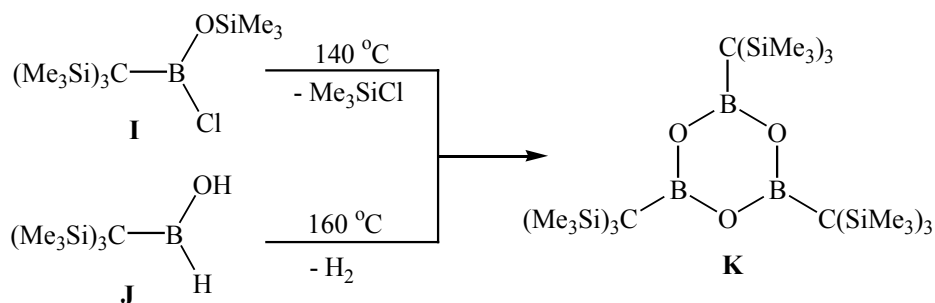
**Figure 2.1. Postulated intermediates in the oxidation of a four-membered boracycle with (a) dimethyl sulfoxide (b) diphenylsulfoxide.**

West *et al.*<sup>53a</sup> photolyzed dioxodiboretane **F** in the presence of the trapping agents disilaoxacyclopentane or *tert*-butylmethylketone and isolated the respective trapping products **G** and **H**, respectively (Scheme 2.3). It was postulated that the intermediate in this process was the monomeric oxoborane Mes\*-B=O. Irradiation of **F** in 3-methylpentane glass at – 196 °C resulted in a product which exhibited a weak UV absorption band at 314 nm. Although this product was attributed to a monomeric oxoborane it was never been fully characterized.



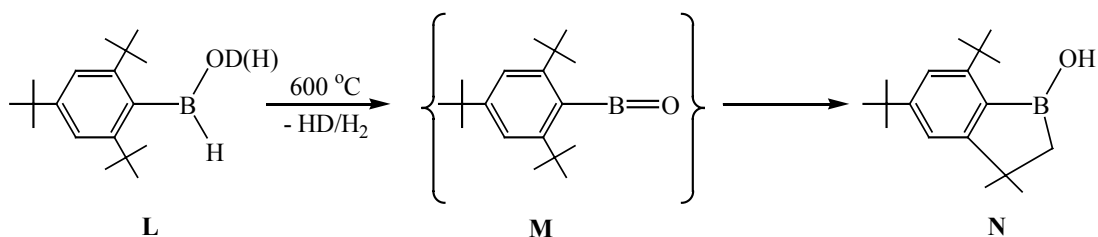
**Scheme 2.3. Photolysis of a dioxodiboretane in presence of trapping agents.**

Paetzold *et al.*<sup>51</sup> examined the gas-phase thermolysis of acyclic tris(trimethylsilyl)boranes (Me<sub>3</sub>Si)<sub>3</sub>-C-B(R<sup>1</sup>)(R<sup>2</sup>) ( **I**: R<sup>1</sup> = OSiMe<sub>3</sub>, R<sup>2</sup> = Cl; **J**: R<sup>1</sup> = OH, R<sup>2</sup> = H) and isolated the trimeric boroxane **K** which was fully characterized (Scheme 2.4). The reactive intermediate in these thermolyses was postulated to be the monomeric oxoborane, (Me<sub>3</sub>Si)<sub>3</sub>C-B=O.



**Scheme 2.4. Thermolysis of tris(trimethylsilyl)boranes.**

The most compelling evidence for the intermediacy of a monomeric oxoborane was provided by an experiment in which the deuterated boronic acid **L** was thermolyzed in the gas phase to give the bicyclic product **N** (Scheme 2.5).<sup>53b</sup> Of particular significance is the fact that thermolysis of the non-deuterated analogue of **L** also resulted in **N**. The first step in the thermolysis was thought to be the elimination of  $\text{H}_2$  or  $\text{HD}$  resulting in the generation of the monomeric oxoborane **M** as a reactive intermediate. In turn, it was postulated that **M** underwent insertion of the  $\text{B}=\text{O}$  moiety into a  $\text{C}-\text{H}$  bond of an *ortho*-*t*-Bu substituent.



**Scheme 2.5. Evidence for the existence of a monomeric oxoborane as a reactive intermediate.**

If the aforementioned experiments were carried out in the absence of trapping agents, the fate of the ephemeral monomeric oxoborane was oligomerization<sup>51,52,53a,c</sup> or insertion of the oxoborane oxygen atom into a C—H bond of the R ligand.<sup>3b</sup> To prevent the possibility of a C—H insertion reaction and minimize the opportunity for oligomerization, the C<sub>6</sub>F<sub>5</sub>-substituted  $\beta$ -diketiminate [CH(CMe)<sub>2</sub>(NC<sub>6</sub>F<sub>5</sub>)<sub>2</sub>]<sup>−</sup> (L<sup>−</sup>, Figure 2.2)<sup>22</sup> was selected as the supporting ligand. Part I of the present chapter is concerned with synthetic approaches to the monomeric oxoborane [CH(CMe)<sub>2</sub>(NC<sub>6</sub>F<sub>5</sub>)<sub>2</sub>]B=O.

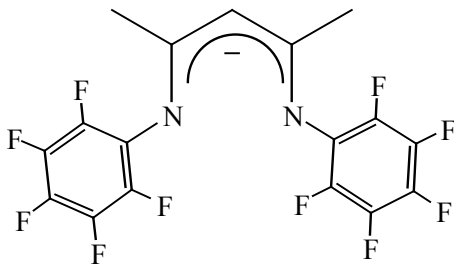


**Figure 2.2. Structure of the C<sub>6</sub>F<sub>5</sub>-substituted  $\beta$ -diketiminate ligand, L<sup>−</sup>.**

## RESULTS AND DISCUSSION

### Synthesis and Characterization of $[(\text{CH}(\text{CMe})_2(\text{NC}_6\text{F}_5)_2)\text{BCl}][\text{AlCl}_4]$ , **2.1**

Prior to the start of this project, the only viable synthetic pathway to  $\beta$ -diketiminato boron dihalides (other than the difluorides<sup>54</sup>) involved the exchange-autoionization reaction between a ( $\beta$ -diketiminato) $\text{AlCl}_2$  and  $\text{BCl}_3$  that was first reported by Kuhn *et al.*<sup>55</sup> Accordingly, the first syntheses of **2.1** were carried out by treatment of  $\text{LAlCl}_2$  (**1.11**) with  $\text{BCl}_3$ . However, when the synthesis of  $\text{LBCl}_2$  (**1.6**) became available (see Chapter 1), it was demonstrated that **2.1** could also be synthesized by a chloride abstraction reaction in which  $\text{AlCl}_3$  was added to an equimolar quantity of  $\text{LBCl}_2$  (**1.6**) in methylene chloride solution. The yields for both methods are essentially quantitative. The characteristic  $^{27}\text{Al}$  NMR peak for the  $[\text{AlCl}_4]^-$  anion was detected at  $\delta$  102.3<sup>56</sup> and the  $^{11}\text{B}$  chemical shift of  $\delta$  28.84 ppm is similar to the values of  $\delta$  23.05 and 32.16 ppm reported for  $[\text{L}''\text{BF}][\text{BF}_4]$  (**2.1a**) and  $[\text{L}''\text{BCl}][\text{AlCl}_4]$ , (**2.1b**), respectively, by Kuhn *et al.*<sup>55</sup> ( $\text{L}'' = [\text{CH}(\text{CMe})_2(\text{NMe})_2]$ ). The X-ray crystal structure of **2.1** (Figure 2.3) represents the first structural information for a  $\beta$ -diketiminato-supported haloborenium cation. However, AM1<sup>57</sup> calculations had been performed on **2.1b**<sup>55</sup> and the resulting values for the bond lengths and bond angles of the planar  $\text{C}_3\text{N}_2\text{B}$  ring are very similar to the averages of the corresponding bond lengths and angles for **2.1**. Furthermore, the computed B—Cl bond length of **2.1b** of 1.730 Å lies within experimental error of the average B—Cl bond for **2.1** (1.727(8) Å).

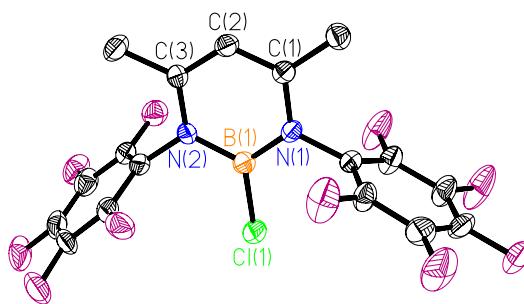


**Figure 2.3.** Molecular structure of  $[\text{LBCl}]^+$  cation of **2.1**. The  $[\text{AlCl}_4]^-$  anion and all hydrogen atoms have been omitted for clarity.

### Synthesis and Characterization of $[(\text{CH}(\text{CMe})_2(\text{NC}_6\text{F}_5)_2)\text{BPh}][\text{AlCl}_4]$ , **2.2**

Further support for the proposed formation of **2.1** *via* the exchange-autoionization reaction stems from the observation that  $\text{LAlCl}_2$  (**1.11**) reacts with  $\text{PhBCl}_2$  (Ph = phenyl) to form  $[\text{LBPh}][\text{AlCl}_4]$ , **2.2**, which has been structurally authenticated.<sup>48</sup> The characteristic peak for the  $[\text{AlCl}_4]^-$  anion was detected at  $\delta$  102.3 ppm.<sup>56</sup> However, the  $^{11}\text{B}$  chemical shift of  $\delta$  10.54 ppm for **2.2** is upfield shifted in comparison with the value of  $\delta$  33.50 ppm that was reported for the very similar boron cation  $[\text{L}'\text{BPh}][\text{Al}_2\text{Cl}_7]$ , **2a** ( $\text{L}' = [\text{CH}(\text{CMe})_2(\text{NAr})_2]^+$ ; Ar = 2,6-diisopropylphenyl).<sup>58</sup> The upfield shift of the  $^{11}\text{B}$  signal of **2.2** might be the result of weak coordination of  $\text{CD}_3\text{CN}$  solvent molecules to the cationic boron center. The molecular structures of **2.2** (Figure 2.4) and **2.2a** closely resemble each other. The average C—C (1.377(11) Å), C—N (1.361(10) Å) and N—B (1.441(9) Å) bond distances, and the B—C (1.531(15) Å) bond distance of **2.2** are identical to those for **2.2a** within experimental error. Furthermore, in both cases the  $\text{C}_3\text{N}_2\text{B}$  rings are planar (the sums of bond angles for the  $\text{C}_3\text{N}_2\text{B}$  rings of **2.2** and **2.2a** are  $719.6^\circ$  and  $716.8^\circ$ , respectively) and the boron atoms

adopt trigonal planar geometries (the sums of angles at boron is  $359.9^\circ$  for both **2.2** and **2.2a**). The only structural difference between **2.2** and **2.2a** is found in the orientation of the phenyl group relative to the  $C_3N_2B$  plane. For compound **2.2** the phenyl ring is perpendicular to the  $C_3N_2B$  plane ( $90^\circ$ ) while in the case of **2.2a** the phenyl ring is twisted by  $53.3^\circ$  with the respect to the  $C_3N_2B$  plane. This modest conformational difference can be attributed to the bulkier nature of the 2,6-diisopropylphenyl substituents of **2.2a** in comparison with that of the  $C_6F_5$  groups of **2.2**.

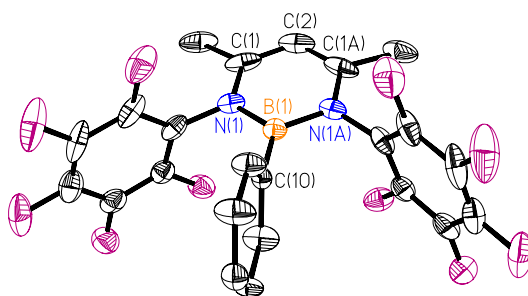


**Figure 2.4. Molecular structure of  $[LBPh]^+$  cation of **2.2**. The  $[AlCl_4]^-$  anion and all hydrogen atoms have been omitted for clarity.**

### Synthesis and Characterization of $(CH(CMe)_2(NC_6F_5)_2)B=O \rightarrow AlCl_3$ , **2.3**

Treatment of **2.1** with the stoichiometric quantity of  $H_2O$  in methylene chloride solution resulted in the formation of  $LB=O \rightarrow AlCl_3$ , the  $AlCl_3$  adduct of the targeted monomeric oxoborane  $LB=O$ . The  $^{11}B$  NMR signal of  $\delta$  40.1 ppm for **2.3** suggests a deshielded boron center in comparison with those of three-coordinate boron species.<sup>59</sup> This is probably due to the presence of the oxo group. The  $^{27}Al$  NMR chemical shift of  $\delta$  87.3 is typical of those reported for neutral four-coordinate aluminum complexes.<sup>59</sup> An X-ray crystallographic analysis of **2.3** confirmed both the spectroscopic indications

and the attachment of a molecule of  $\text{AlCl}_3$  to the oxygen atom of the oxoborane (Figure 2.5). The  $\text{C}_3\text{N}_2\text{B}$  ring of **2.3** is planar, as reflected by the fact that the sum of internal bond angles is  $719.9(1)^\circ$ . The average N—C ( $1.359(2)$  Å) and C—C ( $1.387(2)$  Å) bond distances are very similar to those determined for the boron cations **2.1**, **2.2** and **2.2a**. However, the B—N ( $1.472(2)$  and  $1.466(2)$  Å) bond lengths in **2.3** are slightly longer than those for **2.1**, **2.2** and **2.2a** ( $1.435(9)$ ,  $1.441(9)$  and  $1.440(9)$  Å, respectively). Such a trend is expected on the basis of the presence of a formal +1

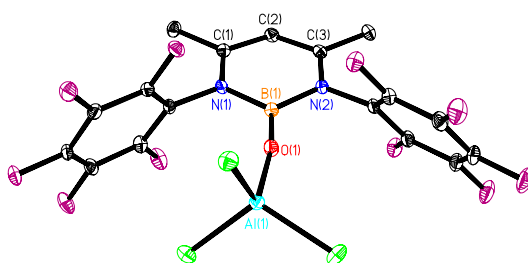


**Figure 2.5. Molecular structure of monomeric oxoborane  $\text{LB}=\text{O} \rightarrow \text{AlCl}_3$ , **2.3**. Hydrogen atoms have been omitted for clarity.**

charge on the boron center in the latter examples. The trigonal planar geometry at boron is indicated by the fact that the sum of bond angles at this center is  $360.0(1)^\circ$ . The B—O and O—Al bond lengths are  $1.304(2)$  and  $1.720(1)$  Å, respectively. It is difficult to make an assessment of the boron-oxygen bond order solely on the basis of length because examination of the Cambridge Crystallographic Data Base reveals that there is a pronounced dependence on the stereoelectronic characteristics of the other boron substituents. The B—O separations in singly bonded  $\text{N}_2\text{B—O}$  fragments (diaz- and triazaboroles) span the range of  $1.354(5) - 1.365(4)$  Å and are thus considerably longer than that in **2.3**. The B-O-Al angle in **2.3** ( $169.2(1)^\circ$ ) is comparable to the value of



163.76(2)° reported by Roesky *et al.*<sup>60</sup> for an interesting monoalumoxane  $L'''Al=O \cdot B(C_6F_5)_3$  ( $L''' = [HC(CMe)_2(NCH_2NEt_2)_2]^+$ ), which features a four-coordinate aluminum atom.

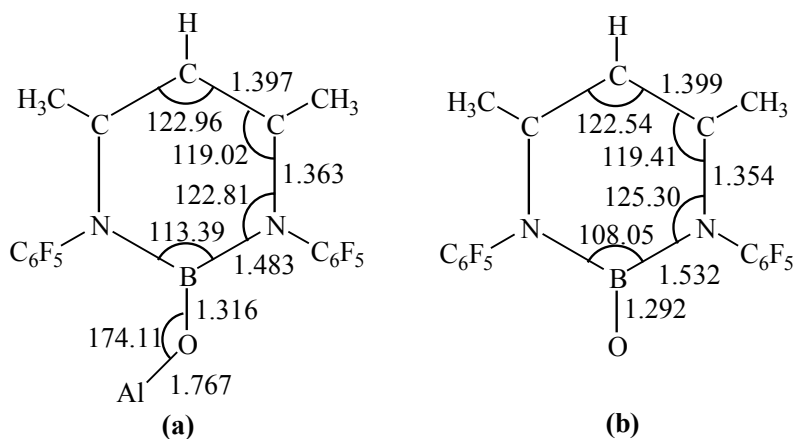


**Figure 2.6. Results of DFT calculations at the B3LYP level of theory and the 6-311+G(d) basis set for  $LB=O \rightarrow AlCl_3$ , **2.3a**, and  $LB=O$ , **2.3b**. Bond lengths and angles are expressed in Å and degrees, respectively.**

To gain additional insight into the electronic structure of **2.3** in general, and the nature of the boron-oxygen bond in particular, DFT calculations were carried out at the B3LYP level of theory<sup>61</sup> using the 6-311+G(d) basis set. The input coordinates for the geometry optimization were generated from the X-ray crystallographic data. The resulting structure (**2.3a**) is shown in Figure 2.6. Analogous calculations were performed on  $LB=O$  (**2.3b**) and the results are included Figure 2.6. Reference to Figure 2.6 and Tables 4.41 and 4.42 reveals that the computed metrical parameters for **2.3a** lie within 1% of the experimental values for **2.3**, with the exception of the O—Al distance and the B-O-Al angle for which the deviations are 2.8 and 2.9%, respectively. Regarding the latter deviation, the DFT calculations indicate that the B-O-Al angle

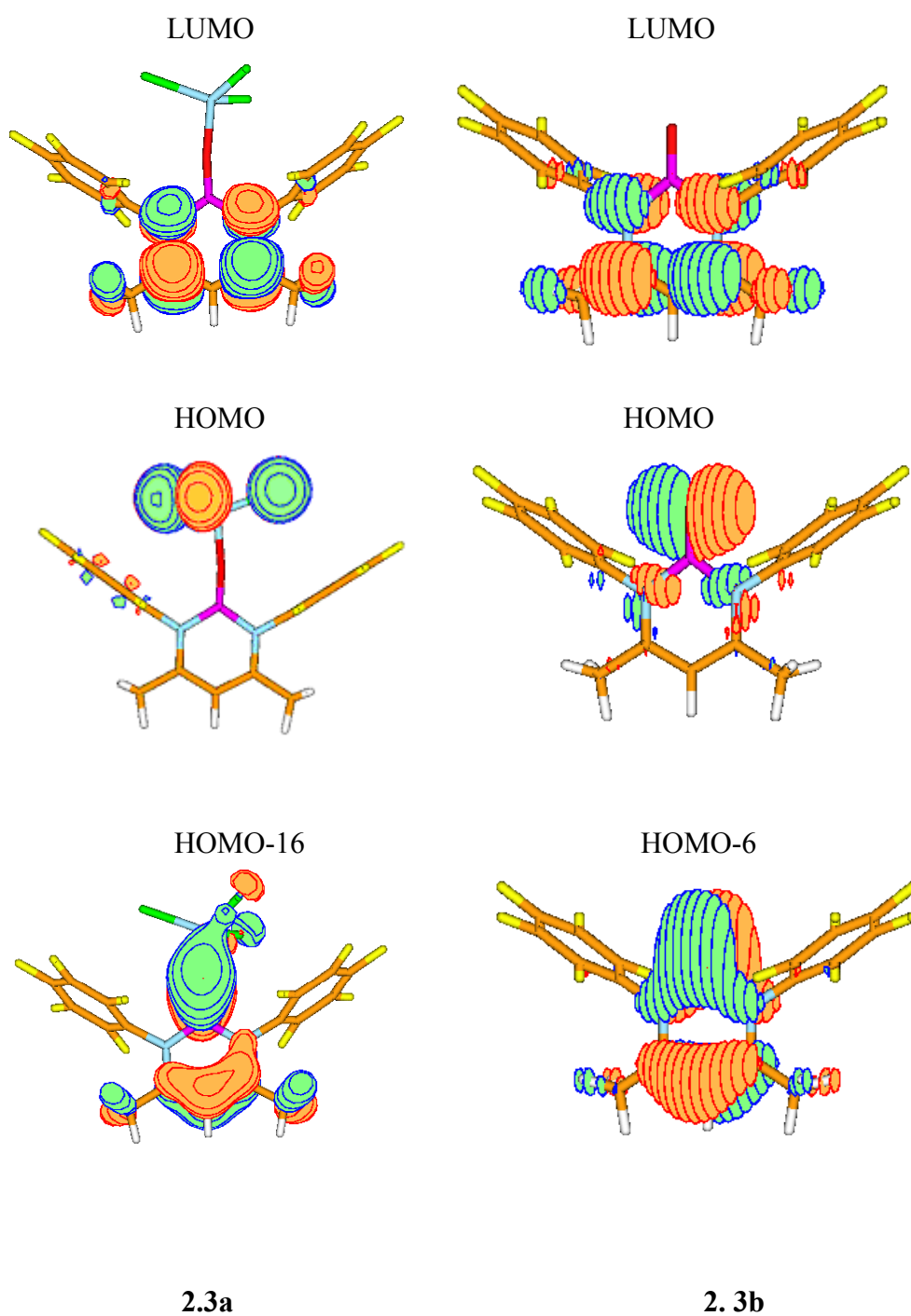


Figure 2.7. Selected MO's for  $\text{LB}=\text{O} \rightarrow \text{AlCl}_3$  (2.3a) and  $\text{LB}=\text{O}$  (2.3b).

deformation energy is small and that, for example, the difference in energy between a B-O-Al angles of 174.11° and one of 180.0° is only 0.72 kcal/mol. In terms of the C<sub>3</sub>N<sub>2</sub>B ring geometry, the major changes that take place when AlCl<sub>3</sub> is coordinated to the oxoborane **2.3b** are widening of the B-N-C angle and narrowing of the N-B-N angle. The C<sub>3</sub>N<sub>2</sub>B rings of **2.3a** and **2.3b** are both planar. The computed B—O distance for the free oxoborane **2.3b** is 1.292 Å, and the fact that this distance increased by only 1.9% upon coordination to AlCl<sub>3</sub> is suggestive of the retention of considerable double bond character in **2.3a**. For both **2.3a** and **2.3b**, the LUMO is  $\pi^*$  in nature (Figure 2.7). The HOMO of **2.3a** comprises the AlCl<sub>3</sub> chlorine lone pairs, while that of **2.3b** is principally oxygen lone pair in character. The HOMO-LUMO gaps for **2.3a** and **2.3b** are 83.38 and 91.18 kcal/mol, respectively. The B—O  $\pi$  bond in **2.3b** is evident in the HOMO-6 orbital (but note that there is also considerable participation by nitrogen 2p orbitals). In the case of **2.3a**, the  $\pi$  component of the B—O bond does not feature contributions from these nitrogen 2p orbitals. (Figure 2.7)

### Synthesis and Characterization of [CH(CMe)<sub>2</sub>(HNC<sub>6</sub>F<sub>5</sub>)<sub>2</sub>][AlCl<sub>4</sub>], **2.4**

When **2.1** was treated with excess H<sub>2</sub>O complete hydrolysis occurred, resulting in the formation of [LH<sub>2</sub>][AlCl<sub>4</sub>], **2.4**, as one of the products. The structure of **2.4** was determined by single crystal X-ray diffraction (Figure 2.8). The molecular structure of **2.4** resembles those of [L'H<sub>2</sub>][A], **2.4a**, (A = I<sup>-</sup>, AsCl<sub>4</sub><sup>-</sup> or SbCl<sub>4</sub><sup>-</sup>).<sup>62</sup> The cationic parts of both **2.4** and **2.4a** feature aryl substituents that are oriented in an essentially parallel fashion with respect to each other. The bond lengths and angles of the C<sub>5</sub>N<sub>2</sub> backbones

of **2.4** and **2.4a** are identical within experimental error. In both cases, delocalized  $\pi$ -bonding is evident along the N(1)-C(2)-C(3)-C(4)-N(2) chain. The ionic structure is preserved in solution as indicated by the detection of a  $^{27}\text{Al}$  NMR peak at  $\delta$  102.3 ppm which falls in the region characteristic of the presence of the  $[\text{AlCl}_4]^-$  anion.<sup>56</sup>

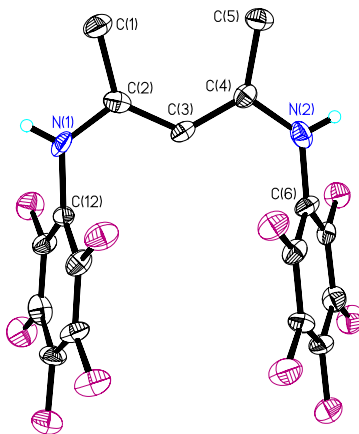
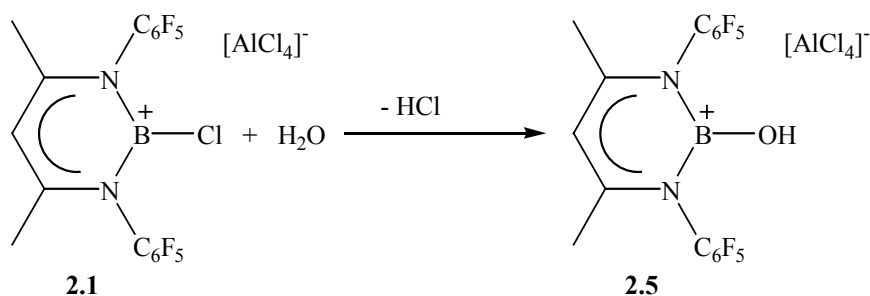


**Figure 2.8. Molecular structure of  $[\text{LH}_2][\text{AlCl}_4]$ , **2.4**. All hydrogen atoms, except those on the nitrogen atoms, and the  $[\text{AlCl}_4]^-$  anion have been omitted for clarity.**

### Synthesis and Characterization of $[\text{LB—OH}][\text{AlCl}_4]$ , **2.5**

On one of the occasions that **2.3** was prepared, a few crystals were isolated with a different morphology than that of **2.3**. Examination of a representative crystal by X-ray diffraction revealed its identity to be  $[\text{LBOH}][\text{AlCl}_4]$  (**2.5**, Figure 2.9). Unfortunately, numerous attempts to re-synthesize this compound failed. It is plausible, however, that **2.5** is an intermediate in the reaction of **2.1** with  $\text{H}_2\text{O}$  to produce **2.3**. As such, it represents the initial step in the hydrolysis of **2.1** in which a hydroxide group replaces the chloride anion (Scheme 2.6). The second step in the proposed sequence involves the elimination of  $\text{HCl}$  from **2.5** to form  $\text{LB=O} \rightarrow \text{AlCl}_3$  (**2.2**). The solid-state



**Scheme 2.6.** A possible reaction pathway in the synthesis of [LBOH][AlCl<sub>4</sub>], **2.5**.

structure of **2.5** consists of two very similar but independent ion pairs in which the average metrical parameters of the planar C<sub>3</sub>N<sub>2</sub>B rings are identical to those of **2.1** and **2.2** within experimental error. The average B—O bond length of 1.561(12) Å for **2.5** is approximately 20% longer than the B—O separation for **2.3**. A difference in B—O distances of this magnitude is anticipated because the formal B—O bond orders are two and one in **2.3** and **2.5**, respectively.

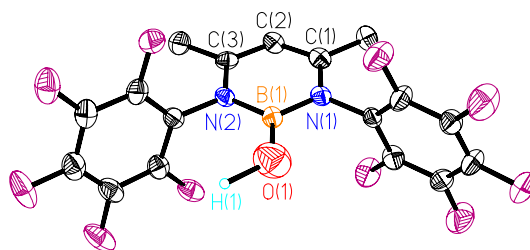


**Figure 2.9.** Molecular structure of [LB—OH]<sup>+</sup> cation of **2.5**. All hydrogen atoms, except that on the hydroxide group, have been omitted for clarity.

### Synthesis and Characterization of ((CH(CMe)<sub>2</sub>(NC<sub>6</sub>F<sub>5</sub>)<sub>2</sub>)BO)<sub>2</sub>, **2.6**

One of the ways to assess the importance of the Lewis acid AlCl<sub>3</sub> in the stabilization of the monomeric oxoborane complex **2.3** would be to attempt the synthesis of Lewis acid-free example. For this reason, the reaction of LBI<sub>2</sub> (**1.8**) with

Ag<sub>2</sub>O was explored. However, multinuclear NMR spectroscopic examination of the resulting reaction mixture did not show the presence of the desired Lewis acid-free monomeric oxoborane. Interestingly, however, the dimer of the targeted oxoborane (dioxodiboratene, **2.6**, Figure 2.10) was detected by high-resolution mass spectroscopy. Furthermore, the <sup>11</sup>B NMR spectrum of the product mixture exhibited distinct peaks at  $\delta$  0.06 and  $-1.85$  ppm. These <sup>11</sup>B chemical shifts differ significantly from that of **2.3** ( $\delta$  40.1 ppm). The peak at  $\delta$  0.06 represents the major component of the product mixture and it is believed to be due to the dioxodiboratene **2.6**. Unfortunately, it was not possible to isolate a sample of pure **2.6**. Note, however, that the proposed structure of **2.6** is very similar to that of the dimer (ArBO)<sub>2</sub> isolated by West *et al.*<sup>53a</sup> In conclusion, it is clear that the Lewis acid, AlCl<sub>3</sub>, plays a crucial role in stabilizing the monomeric oxoborane because all attempt to synthesize the unprotected monomeric oxoborane **2.3**, resulted in the formation of the dimeric form of the oxoborane **2.6** as one of the products.

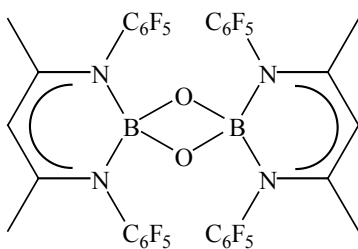


**Figure 2.10. Proposed structure of one of the products (2.6) of the reaction of LBI<sub>2</sub> with Ag<sub>2</sub>O.**

## CHAPTER 2

### Part II

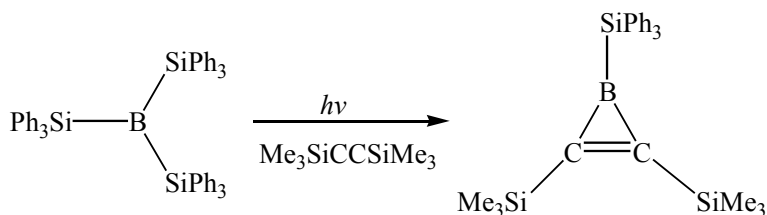
## A Single-Bonded Cationic Terminal Borylene Complex

### INTRODUCTION

One of the exciting recent aspects of synthetic organometallic chemistry relates to the quest for transition metal complexes that incorporate multiply bonded main group ligands. Interest in such species has been generated not only due to fundamental questions of structure and bonding, but also because of their potential roles as reagents and catalytic intermediates in important synthetic processes.<sup>63-66</sup> Even though the transition metal chemistry of the analogous carbon systems such as Fischer carbenes and Schrock-type alkylidenes<sup>63</sup> and their heavier congeners (e.g. silylenes (R<sub>2</sub>Si)<sup>15</sup>) have tended to dominate this area, the related chemistry of the group 13 analogues has begun to gain momentum in recent years.<sup>65,66</sup> In this context, the area of terminal borylene chemistry represents a small but important recent addition.

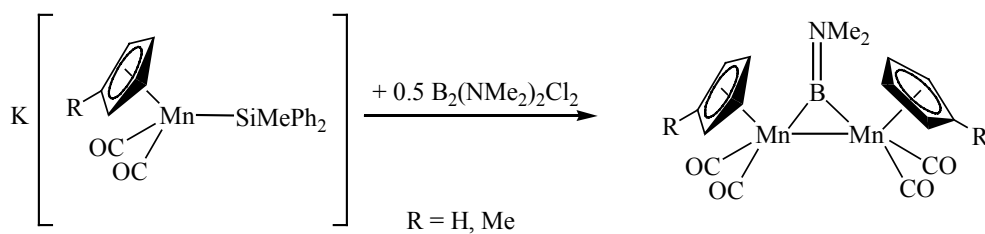
The first synthesis of a borylene compound was reported in 1967 by Timms<sup>67</sup> who generated fluoroborylene (BF) by the reaction of BF<sub>3</sub> with elemental boron at elevated temperatures (~ 2000 °C). Some 20 years later, West *et al.*<sup>68</sup> generated silylborylene (Ph<sub>3</sub>Si—B) by UV irradiation of (Ph<sub>3</sub>Si)<sub>3</sub>B in hydrocarbon matrices at – 196 °C. Both borylenes turned out to be very reactive species and their existence as reactive intermediates was deduced on the basis of various trapping experiments. For example, fluoroborylene was trapped by BF<sub>3</sub> to produce B<sub>2</sub>F<sub>4</sub><sup>67b</sup> while silylborylene

was trapped by bis(trimethylsilyl) acetylene to produce corresponding boracyclopropene (Scheme 2.7).<sup>68</sup>



**Scheme 2.7. Trapping of a reactive borylene.**

In 1990 reports of various fully characterized iridium complexes containing a metal-bound  $\text{BR}_2$  ligand were published, thus providing the first structural proof of a transition-metal-boryl complex.<sup>69</sup> These reports can be considered to represent the starting point of a new and thriving research area on transition-metal complexes of boron which includes borylene complexes. The first stable borylene complex, which features the boron ligand in a bridging position, was the unexpected product of the reaction of the diborane,  $\text{ClB}(\text{NMe}_2)\text{—B}(\text{NMe}_2)\text{Cl}$ , with  $\text{K}(\eta^5\text{-C}_5\text{H}_4\text{R})\text{Mn}(\text{CO})_2$ , where



**Scheme 2.8. Synthesis of the first bridging borylene complex.**

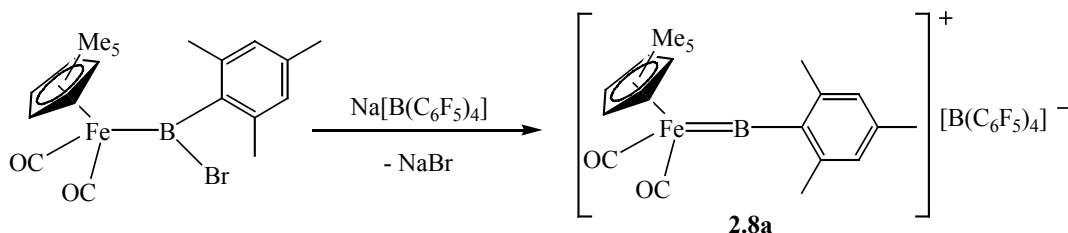




borylene complexes by the salt metathesis were unsuccessful. Subsequently, Brownschweig *et al.*<sup>71</sup> reported the photochemically induced transfer of a borylene ligand from one transition metal to another and Roper *et al.*<sup>65c</sup> synthesized amido-supported borylene complexes that are intramolecularly base stabilized at the boron center. One such compound was prepared by treatment of an osmium boryl complex with 8-aminoquinoline (Figure 2.11c).

The first terminal borylene complex without a stabilizing,  $\pi$ -donating boron substituent was reported by the Brownschweig group.<sup>65d</sup> As the consequence of using the tris(trimethylsilyl)silyl group ( $\text{Si}(\text{SiMe}_3)_3$ ) as the boron substituent (Figure 2.11d) the resulting terminal borylene complex was both coordinatively and electronically unsaturated. This complex underwent decomposition after a few hours at ambient temperatures both in solution and in the solid state. The thermal instability of this complex is due to the lack of ligand-to-boron  $\pi$  bonding since the steric bulk of the  $\text{Si}(\text{SiMe}_3)_3$  substituent is equal to or greater than that of the  $\text{N}(\text{SiMe}_3)_2$  substituent.

The common theme that relates the terminal borylene complexes discussed thus far is that they are all neutral. The first cationic terminal borylene complex **2.8a** (Scheme 2.9) was reported by Aldridge *et al.*<sup>72</sup> Compound **2.8a** was synthesized by



**Scheme 2.9. Synthesis of the first cation terminal borylene.**

halide abstraction from the precursor bromoboryl complex,  $(\eta^5\text{-C}_5\text{Me}_5)(\text{CO})_2\text{Fp}$   $\text{B}(\text{Br})\text{Mes}$  where  $\text{Mes} = 2,4,6\text{-trimethylphenyl}$ , which in turn was prepared by treatment of  $(\text{Mes})\text{BBR}_2$  with  $\text{K}[(\eta^5\text{-C}_5\text{Me}_5)\text{Fp}(\text{CO})_2]$ . The bond between the boron and iron atoms for **2.8a** was postulated to consist of a  $\text{B}\text{---}\text{Fe}$   $\sigma$ -bond and a  $\pi$  back bond from iron to boron resulting in an overall bond order of 2.<sup>72</sup> Subsequently, Aldridge *et al.*<sup>73</sup> prepared the diisopropylamido-supported cationic terminal borylene **2.8c** (Figure 2.12b) by an analogous procedure to that described for the synthesis of the mesityl-substituted derivative **2.8a**. Unfortunately, structural characterization of **2.8c** was not possible due to the oily nature of this product. However, replacement of the isopropyl groups of **2.8c** with cyclohexyl groups resulted in a crystalline product **2.8b** that proved to be suitable for X-ray crystallography (Figure 2.12a).<sup>74</sup> On the basis of the  $\text{F}\text{---}\text{B}$  distance, it was estimated that the order of this bond is between 1 and 2. The difference in bond order between **2.8a** and **2.8b** was attributed to the  $\pi$ -bonding competition at the boron center between the nitrogen lone pair and filled  $\text{Fe}(3d)$  in the case of **2.8b**.

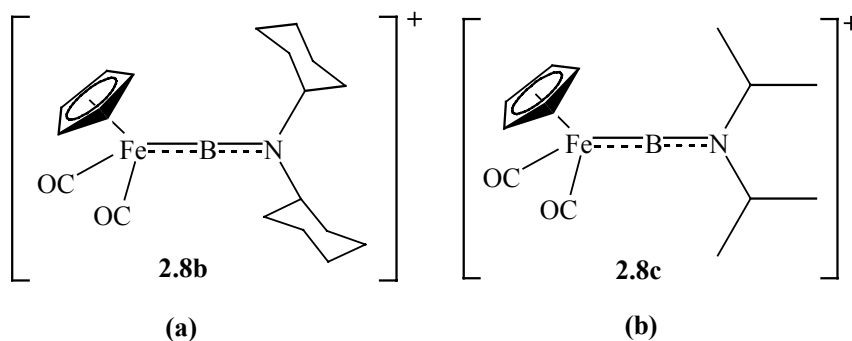


**Figure 2.12. Examples of (a) dicyclohexylamido (2.8b) and (b) diisopropylamido (2.8c) substituted cationic terminal borylene complexes. The corresponding anions are not shown.**

The objective of the second part of Chapter 2 was to attempt the synthesis of a cationic terminal borylene complex with bond order of 1. In order to accomplish this goal, it was recognized that it would be necessary to employ a strong  $\pi$ -donating substituent at the boron center. In this case, the  $\pi$ -type interaction in the F-B-N fragment would reside exclusively in the B-N region, thus eliminating the formation of a  $\pi$ -back bond from iron to boron. Based on extensive calculations performed on a wide variety of ligands<sup>75</sup>, the ligand that possesses the required  $\pi$ -donor ability is the pentamethylcyclopentadienide anion  $[\text{C}_5\text{Me}_5]^-$  ( $\text{Cp}^*$ ). Accordingly, this ligand was selected for the synthesis of the targeted cationic single-bonded borylene complex.

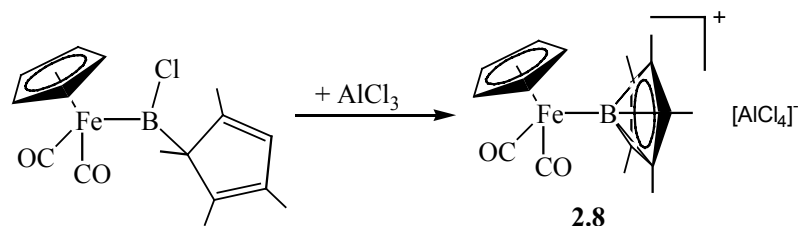
## RESULTS AND DISCUSSION

### Synthesis and Characterization of $(\eta^5\text{-C}_5\text{H}_5)\text{Fe}(\text{CO})_2\text{B}(\eta^1\text{-C}_5\text{Me}_5)\text{Cl}$ , **2.7**

The salt  $\text{K}[(\eta^5\text{-C}_5\text{H}_5)\text{Fe}(\text{CO})_2]^{76}$  was added to an equimolar quantity of  $(\eta^1\text{-C}_5\text{Me}_5)\text{BCl}_2^{77}$  in hexane solution at 25 °C and the reaction mixture was stirred overnight. Removal of the KCl by filtration, followed by solvent stripping, resulted in red, solid  $(\eta^5\text{-C}_5\text{H}_5)\text{Fe}(\text{CO})_2\text{B}(\eta^1\text{-C}_5\text{Me}_5)\text{Cl}$ , **2.7**. The  $^{11}\text{B}$  NMR signal for **2.7** was detected at  $\delta$  111.34 ppm which is downfield shifted compared to that of the starting material  $(\eta^1\text{-C}_5\text{Me}_5)\text{BCl}_2$  ( $^{11}\text{B}$  = 59.9 ppm). A change of chemical shift of this order of magnitude upon transition metal-boron bond formation has been observed previously.<sup>72-74</sup> Furthermore, the value for this  $^{11}\text{B}$  NMR shift suggests that the  $\text{C}_5\text{Me}_5$  ( $\text{Cp}^*$ ) moiety remains  $\eta^1$ -bonded to the boron atom. The unusual behavior of **2.7** in solvents such as methylene chloride limited the number of solvents that could be used to obtain X-ray suitable crystals of **2.7**. More details concerning this observation are discussed later in this section.

### Synthesis and Characterization of $[(\eta^5\text{-C}_5\text{H}_5)\text{Fe}(\text{CO})_2\text{B}(\eta^5\text{-C}_5\text{Me}_5)][\text{AlCl}_4]$ , **2.8**

When **2.7** was allowed to react with an equimolar amount of  $\text{AlCl}_3$  in methylene chloride solution at 25 °C, the  $^{11}\text{B}$  signal for **2.7** at  $\delta$  111.34 ppm was replaced by a new resonance at  $\delta$  -37.85 ppm and a sharp peak at  $\delta$  103.4 ppm was evident in the  $^{27}\text{Al}$  NMR spectrum, thus suggesting that the chloride abstraction reaction shown in Scheme 2.10 had taken place. Also, based on the  $^{11}\text{B}$  chemical shift value, it was implied that



**Scheme 2.10.** The synthesis of  $[(\eta^5\text{-C}_5\text{H}_5)\text{Fe}(\text{CO})_2(\text{B}(\eta^5\text{-C}_5\text{Me}_5))][\text{AlCl}_4]$ , **2.8**, by a halide abstraction reaction.

the Cp\* ring was  $\eta^5$ -bonded to the boron atom. Crystals suitable for X-ray diffraction analysis were obtained from a methylene chloride/hexane solution at room temperature.

The crystalline state of **2.8** consists of an assembly of discrete cations and anions (Figure 2.13a). As proposed based on the value of  $^{11}\text{B}$  chemical shift, the  $\text{C}_5\text{Me}_5$  group is bonded to the boron atom in an  $\eta^5$ -fashion. The average B—C bond distance is 1.799(4) Å and the X-B-Fe vector (X =  $\text{C}_5\text{Me}_5$  ring centroid) is essentially linear ( $177.86^\circ$ ). The most significant structural feature of the cation is that the B—Fe distance (1.977(3) Å) is 10.3% and 6.4 % longer than those for the cations  $[(\eta^5\text{-C}_5\text{Me}_5)(\text{CO})_2\text{FpBMe}_5]^+$ , **2.8a**<sup>72</sup>, and  $[(\eta^5\text{-C}_5\text{H}_5)(\text{CO})_2\text{FpB}(\text{NCy}_2)]^+$ , **2.8b**<sup>74</sup>, respectively (Mes = 2,4,6-trimethylphenyl and Cy = cyclohexyl), thus suggesting single bond character. Moreover, the B—Fe bond distance for **2.8** is very close to that determined for the neutral terminal borylene complex  $(\text{CO})_4\text{FeB}(\eta^5\text{-C}_5\text{Me}_5)$  (2.010(3) Å) which has been shown to possess a  $\text{B}\rightarrow\text{Fe}$  donor-acceptor bond of order 1.<sup>65a</sup>

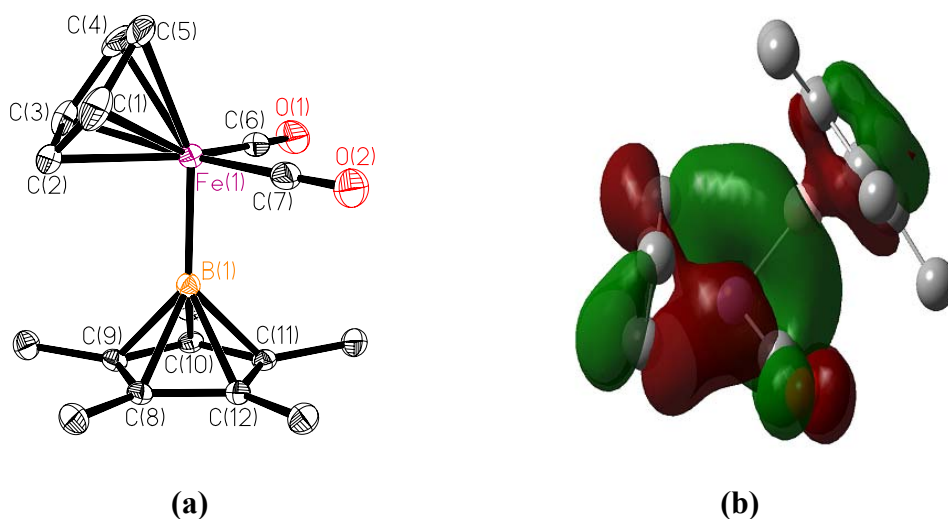


**Figure 2.13.** (a) Structure of the cation of **2.8** (the thermal ellipsoids are drawn at 30% probability and the hydrogen atoms and the anion have been omitted for clarity). (b) The HOMO-4 MO of  $[(\eta^5\text{-C}_5\text{H}_5)\text{Fe}(\text{CO})_2(\text{B}(\eta^5\text{-C}_5\text{Me}_5))]^+$  as calculated by the DFT method at the B3LYP level of theory showing the B—Fe  $\sigma$ -bond.

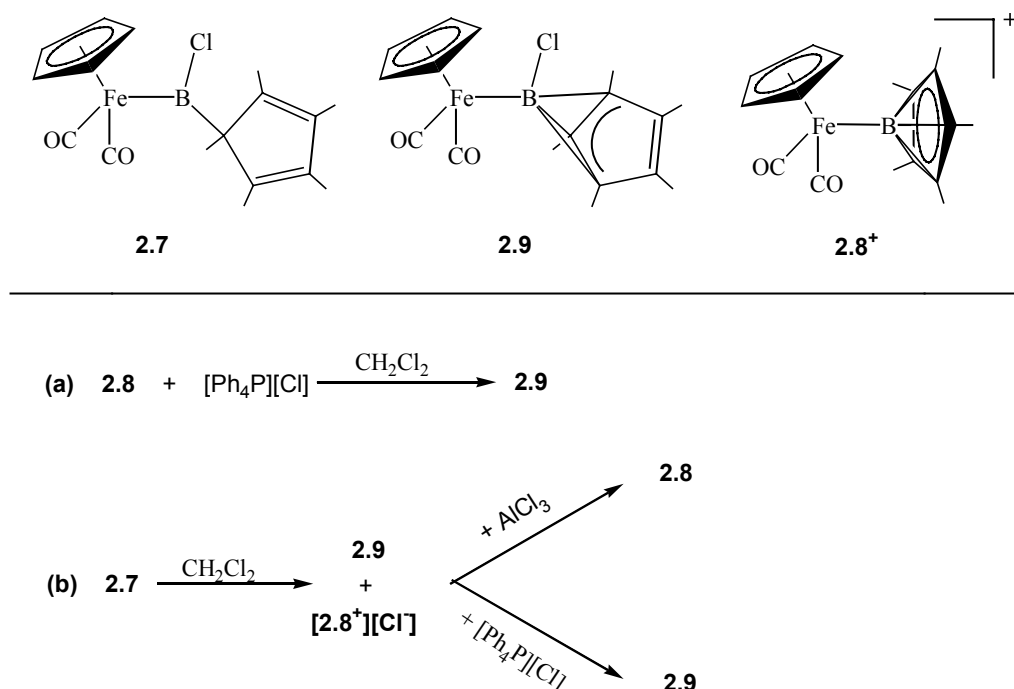
Significant differences are evident in the IR spectra of **2.8**, **2.8a** and **2.8b** in the CO stretching region. Thus, the CO stretching vibrations for **2.8** (2020 and 1962  $\text{cm}^{-1}$ ) appear at lower energy than those for **2.8a** (2055 and 2013  $\text{cm}^{-1}$ ) and **2.8b** (2071 and 2028  $\text{cm}^{-1}$ ), a trend which is consistent with less (or the absence of) Fe $\rightarrow$ B  $\pi$  back-bonding in the cation of **2.8**. Additionally, it is interesting to note that, while the CO stretching frequency for cations **2.8a** and **2.8b** are blue shifted with respect to those of their precursors  $(\eta^5\text{-C}_5\text{Me}_5)(\text{CO})_2\text{Fp}(\text{BMesBr})$  ( $\nu_{\text{CO}} = 2006, 1961 \text{ cm}^{-1}$ )<sup>72</sup> and  $(\eta^5\text{-C}_5\text{Me}_5)(\text{CO})_2\text{FpB}(\text{NCy}_2\text{Cl})$  ( $\nu_{\text{CO}} = 2000, 1939 \text{ cm}^{-1}$ )<sup>74</sup>, those of cation **2.8** are red shifted with respect of those to compound **2.7** ( $\nu_{\text{CO}} = 2052, 2000 \text{ cm}^{-1}$ ).

In order to gain additional insight into the electronic structure of the cation of **2.8**, a DFT calculation was carried out at the B3LYP level of theory.<sup>61</sup> The fractional

coordinates from the X-ray crystal structure were used as input data. The LANL2DZ basis set was used for the iron atom and the 6-31+G\* basis set was employed for the remaining elements. In general, there is a very good agreement between the theoretical and experimental values. For example, the computed B—Fe bond distance of 2.009 Å compares well with the experimental value of 1.978 Å. Likewise, there is a satisfactory accord between the computed X-B-Fe angle (178.16°) and that determined by experiment (177.86°). Based on a population analysis of the MO's, most of the covalent boron-iron bonding interaction is found in the HOMO-4 MO (Figure 2.13b) and is best described as a B→Fe donor-acceptor bond, the primary contributions to which arise from overlap of boron 2s and 2p<sub>z</sub> AO's with the iron 3d<sub>z<sup>2</sup></sub> AO (40.20, 16.38, 26.1%, respectively). An NBO analysis<sup>78</sup> indicates that the overall B—Fe bond order is one.

Aldrich *et al.*<sup>72</sup> showed that it was possible to regenerate the terminal borylene precursor of **2.8a**, (η<sup>5</sup>-C<sub>5</sub>Me<sub>5</sub>)(CO)<sub>2</sub>FpB(Mes)Br, by treatment of **2.8a** with the bromide anion source [Ph<sub>4</sub>P]Br in methylene chloride solution. Interestingly, however, the addition of the chloride source [Ph<sub>4</sub>P]Cl to **2.8** did not result in the formation of **2.7** but in the generation of a new species, **2.9**, with a <sup>11</sup>B chemical shift of δ 6.74 ppm (Scheme 2.11a). At this point it was postulated that this new compound could represent an intermediate in the synthesis of **2.8** from **2.7**. In this case, the C<sub>5</sub>Me<sub>5</sub> substituent is presumably bonded to boron in an η<sup>3</sup>-fashion and the B—Cl bond remains intact (Scheme 2.11). In an effort to gain more insight into the nature of **2.9** several other reactions were performed. One such reaction involved the dissolution of **2.7** in methylene chloride (Scheme 2.11b). A <sup>11</sup>B NMR study revealed that the peak for **2.7** at





**Scheme 2.11.** (a) addition of a chloride anion to **2.8** does not regenerate **2.7** but instead the intermediate **2.9** (b) dissolution of **2.7** in  $\text{CH}_2\text{Cl}_2$  results in a mixture of **2.9** and an analogue of **2.8**,  $[\text{2.8}^+][\text{Cl}]$ ; addition of  $[\text{Ph}_4\text{P}]\text{Cl}$  leads to **2.9** only while addition of  $\text{AlCl}_3$  produces **2.8**.

$\delta$  111.34 ppm disappeared completely after about 30 minutes and was replaced by two new peaks at  $\delta$  6.72 and  $-37.92$  ppm (Scheme 2.11a). The peak at  $\delta$   $-37.92$  ppm can be assigned to the cationic terminal borylene complex  $[\text{2.8}^+][\text{Cl}]$ , i.e. with a chloride rather than a  $\text{AlCl}_4^-$  counterion. This interpretation implies that compound **2.7** can autoionize, but not completely, to produce the cationic terminal borylene complex  $[\text{2.8}^+][\text{Cl}]$ . The peak at  $\delta$  6.72 ppm is identical to the one observed when **2.8** was treated with  $[\text{Ph}_4\text{P}]\text{Cl}$ . In turn, this provides additional evidence for the assignment of the  $\delta$  6.72 ppm resonance to **2.9**. Confirmatory evidence comes from treatment of a methylene chloride solution containing  $[\text{2.8}^+][\text{Cl}]$  and **2.9** with either  $\text{AlCl}_3$  or

[Ph<sub>4</sub>P]Cl (Scheme 2.9b). Following the addition of AlCl<sub>3</sub>, the peak at  $\delta$  6.72 ppm disappeared. However, the peak at  $\delta$  -37.92 ppm due to [2.8<sup>+</sup>][Cl<sup>-</sup>] changed slightly, which corresponds to the formation of 2.8. On the other hand, if [Ph<sub>4</sub>P]Cl was added to the [2.8<sup>+</sup>][Cl<sup>-</sup>]/2.9 mixture (Scheme 2.9b) the peak at  $\delta$ -37.92 ppm disappeared and the peak at  $\delta$ - 6.72 ppm was unchanged clearly indicating that this new compound 2.9 is an intermediate in the formation of 2.8 from 2.7 and that the C<sub>5</sub>Me<sub>5</sub> group is presumably bonded to boron in an  $\eta^3$ -fashion. In turn, this implies that the chloride anion does not dissociate from the boron center. Unfortunately, crystals of 2.9 suitable for the X-ray diffraction study were not obtained. Lastly, attempts were made to resynthesize 2.7 from 2.8 using [Ph<sub>4</sub>P]Cl as the chloride source. Non-polar solvents, such as hexanes or toluene, were employed because 2.7 does not autoionize in these solvents. Thus, mixtures of 2.8 and [Ph<sub>4</sub>P]Cl were made in both hexane and toluene. However, due to the ionic nature of both compounds 2.8 and [Ph<sub>4</sub>P]Cl no reaction was observed after the reaction mixtures had been allowed to stand for 7 days at ambient temperature.

## CONCLUSIONS

A stable Lewis acid-coordinated oxoborane  $(\text{CH}(\text{CMe})_2(\text{NC}_6\text{F}_5)_2)\text{B}=\text{O} \rightarrow \text{AlCl}_3$  ( $\text{LB}=\text{O} \rightarrow \text{AlCl}_3$ , **2.3**) that features a formal double bond between the boron and oxygen atoms has been synthesized and structurally characterized. DFT calculations indicate that the boron-oxygen functionality of compound **2.3** retains considerable double bond character despite the coordination of the Lewis acid  $\text{AlCl}_3$ . Furthermore, the importance of this stabilizing Lewis acid coordination was confirmed by the attempted synthesis of the monomeric oxoborane  $\text{LB}=\text{O}$  by the reaction of  $\text{LBI}_2$  with  $\text{Ag}_2\text{O}$ . This reaction resulted in the formation of dioxodiboretane  $[(\text{CH}(\text{CMe})_2(\text{NC}_6\text{F}_5)_2)\text{BO}]_2$  (**2.6**) which is the oxo-bridged dimer of the oxoborane monomer.

The pentamethylcyclopentadienyl substituent ( $\text{Cp}^*$ ) was the appropriate choice of the supporting ligand for the synthesis of a single-bonded terminal borylene complex. The structure of the resulting complex  $[(\eta^5\text{-C}_5\text{H}_5)\text{Fe}(\text{CO})_2\text{B}(\eta^5\text{-C}_5\text{Me}_5)][\text{AlCl}_4]$  (**2.8**) was established by single-crystal X-ray diffraction. It was also possible to detect, by multinuclear NMR experiments, an intermediate species  $[(\eta^5\text{-C}_5\text{H}_5)\text{Fe}(\text{CO})_2\text{B}(\eta^3\text{-C}_5\text{Me}_5)][\text{Cl}]$  (**2.9**) in the synthesis of **2.8** from  $(\eta^5\text{-C}_5\text{H}_5)\text{Fe}(\text{CO})_2\text{BCl}(\eta^5\text{-C}_5\text{Me}_5)$  (**2.7**). In this case, the  $\text{Cp}^*$  ring is bound to the boron center in an  $\eta^3$ -fashion. Furthermore, complex **2.8**, together with the complexes synthesized by the Aldrich group, demonstrate that the boron-metal bond order is sensitive to the electronic properties of the boron substituents and can vary from 1 to 2.

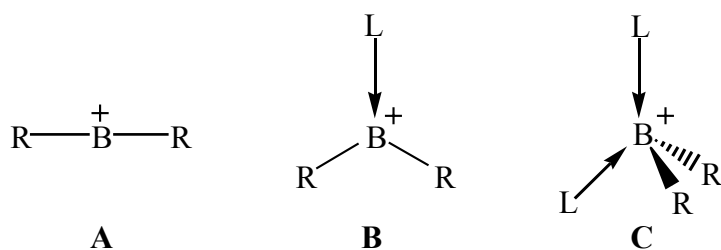
## CHAPTER 3

# Synthesis, Characterization, and Reactivity of $\beta$ -Diketiminato-Supported Boron, Aluminum and Gallium Bistriflate Complexes

### INTRODUCTION

The presence of six rather than a full complement of eight valence electrons at the central atom of neutral tricoordinate group 13 compounds ( $ER_3$ , E = group 13 element) results in the typical Lewis acidic behavior of these compounds. This property enables neutral tri-coordinate group 13 compounds to accommodate two additional valence electrons leading to the facile coordination of anionic and neutral bases. This characteristic acceptor property has spawned a wide variety of uses for boranes ranging from reagents for the synthesis of pharmaceuticals and other valuable products<sup>79</sup> to activators/initiators in catalytic polymerization processes.<sup>80</sup> In the realm of catalysis, the pentafluorophenyl-substituted borane  $B(C_6F_5)$ <sup>81</sup> and methylaluminoxane MAO<sup>82</sup> are employed as cocatalysts and activators for different types of polymerization reactions. In general, cationic group 13 compounds are expected to be significantly more potent acceptors than the corresponding neutral compounds, thus portending a new generation of catalysts and reagents with enhanced reactivity.

At the present time, three types of boron monocations have been identified (Figure 3.1). Cations **A**, **B** and **C** are typically referred to as borinium, borenium and boronium cations, respectively.<sup>83</sup> There are several synthetic methods that can be employed in the synthesis of different boron cations including B—X bond heterolysis,



R = uninegative ligand; L = neutral two-electron donor

**Figure 3.1. Coordination geometries of borinium (A), borenium (B) and boronium (C) monocations.**

(where X is a hydrogen or halide atom), protic and electrophilic attacks on B—N bonds, nucleophilic displacement, and metathesis reactions.<sup>83a</sup> As expected on the basis of their low coordination number and the fact that the boron atom has only four valence electrons, boronium cations are highly reactive and usually studied in the gas phase. However, a few borinium cations that employ stabilizing bulky amido (Figure 3.2a)<sup>84</sup> or phosphinimide (Figure 3.2b)<sup>85</sup> ligands are isolable at ambient temperature.

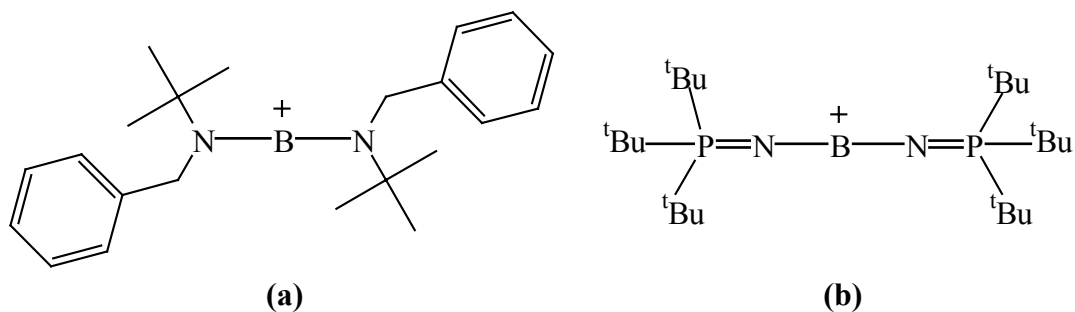


**Figure 3.2. Examples of borinium monocations that employ bulky (a) amido and (b) phosphinimide ligands. Corresponding anions have been omitted for clarity.**

Reports on borenium cations have been as elusive as their borinium counterparts because, prior to 1985, only three structurally authenticated examples of borenium cations had been reported and in each case a bulky auxiliary base capable of

electronic stabilization was required thus forming a five-membered nitrogen-based boracycle.<sup>86</sup> Subsequently Jutzi *et al.*<sup>87</sup> reported the synthesis of borenium cations *via* the reactions of dichloro( $\eta^1$ -pentamethylcyclopentadienyl)borane with the bulky nitrogen-based donors acridine and phenanthridine. The groups of Kuhn<sup>88</sup> and Cowley<sup>89</sup> have used  $\beta$ -diketiminato ligands for the support of several borenium cations (Figure 3.3a), while Manners *et al.*<sup>90</sup> showed that a halide could be abstracted from a boratophosphazene to yield a hybrid borazine-phosphazene cation (Figure 3.3b). Subsequently, Piers *et al.*<sup>91</sup> demonstrated that it is possible to use a non-nitrogen-based boracycle, together with a pyridine base, to stabilize a borenium cation (Figure 3.3c). Moreover, Fox *et al.*<sup>92</sup> reported a novel route to borenium cations by deboronation of an *ortho*-carborane with an iminotris(dimethylamino)phosphorane. Attempts to isolate crystals of the resulting protonated tris(imino)borane cation produced the first example of diborenium dication as a hydrolysis product (Scheme 3.1).

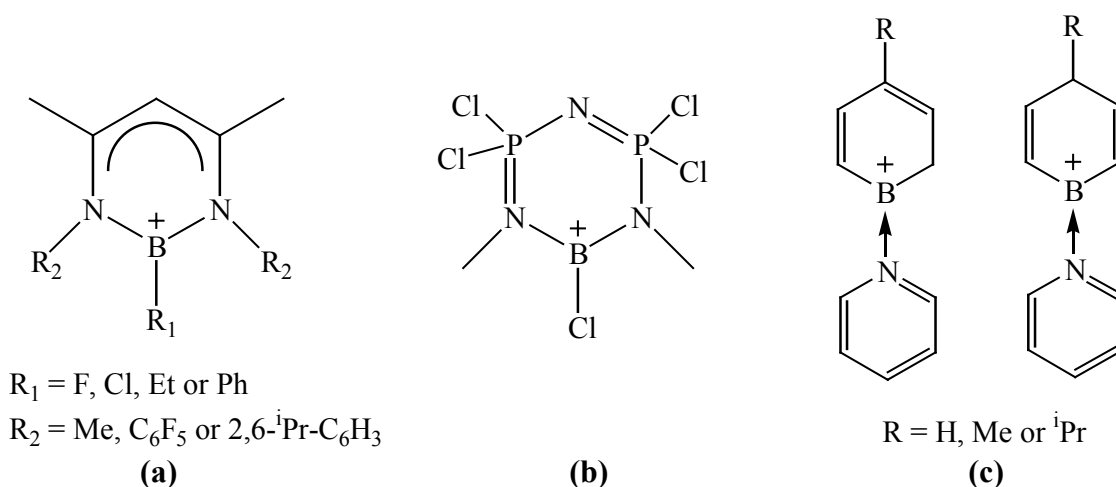
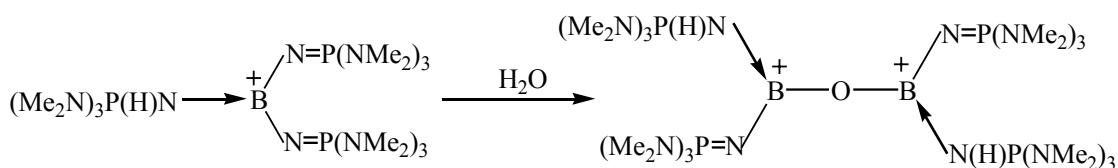


**Figure 3.3.** Examples of borenium monocations stabilized by (a)  $\beta$ -diketiminato ligands, (b) a phosphazene ligand and (c) non-nitrogen-based boracycle ligands. In each case, the corresponding anions have been omitted for clarity.



**Scheme 3.1.** Hydrolysis of a borenium cation led to the isolation of the first example of diboron dication. The corresponding anions have been omitted for clarity.

Overall, boronium cations have received the most attention because of their relative stability, which arises from the presence of a complete octet on boron and coordinative saturation at this center. In almost all cases, boronium cations feature two covalently bound ligands and two  $\sigma$ -donors that occupy the unfilled orbitals on the cationic boron center.<sup>83</sup> Due to the large number of reports on boronium cations,<sup>83</sup> the discussion will be confined to those examples which are of particular relevance to the present work. For example, Wagner *et al.*<sup>93</sup> prepared several ferrocene-based 2,2'-bipyridylboronium cations (Figure 3.4a) by nucleophilic displacement reactions in

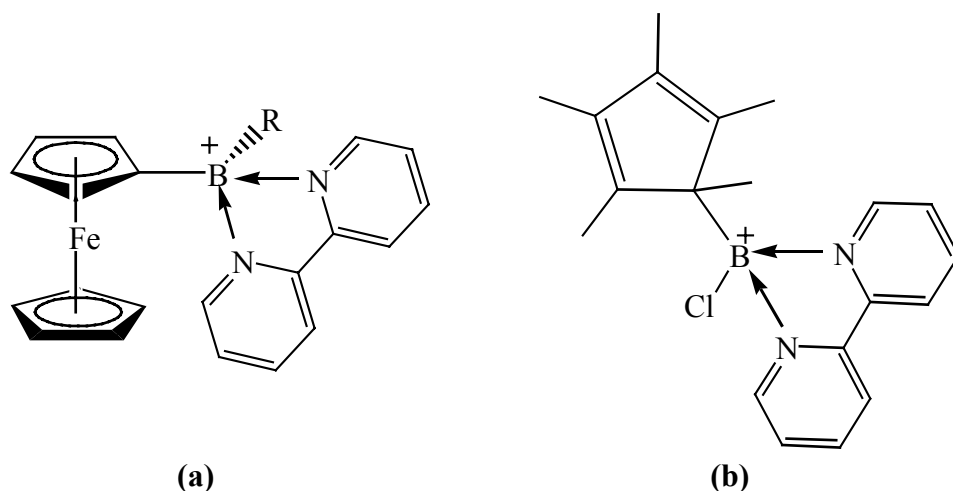


**Figure 3.4.** Examples of boronium cations that are stabilized by bipyridine molecule. Corresponding anions have been omitted for clarity.

which bipyridine was added to the corresponding ferrocenylborane precursors. Jutzi *et al.*<sup>87</sup> employed a similar approach for the synthesis of several  $\eta^1$ -pentamethylcyclopentadienyl-supported boronium cations (Figure 3.4b). However, these compounds were not crystallographically characterized. Finally, it is worth noting that even though boronium cations are coordinatively saturated, such cations can, however, be rendered catalytically active if one of the ancillary ligands is labile.<sup>94</sup>

The examples of structurally authenticated aluminum monocations are considerably more diverse than those of analogous boron because of the ability of aluminum to exhibit coordination numbers greater than four. A survey of the literature reveals that two-<sup>95</sup>, three-<sup>96</sup> and four-<sup>97</sup>, five-<sup>98</sup>, six-<sup>99</sup> and even seven-coordinate (Figure 3.5a)<sup>100</sup> aluminum monocations have been structurally characterized. Moreover, the dimerization of two three-coordinate monocations resulted in a novel dialuminum dication (Figure 3.5b), which was also structurally authenticated.<sup>101</sup>

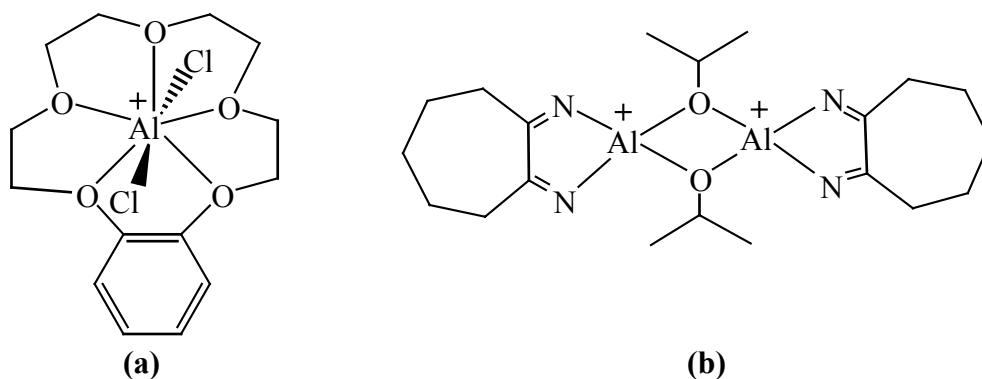


**Figure 3.5. Examples of (a) a seven-coordinate aluminum monocation and (b) an dialuminum dication. The corresponding anions have been omitted for clarity.**



Several synthetic methods have been employed for the synthesis of aluminum cations including halide displacement (nucleophilic displacement), halide or alkyl abstraction, halide elimination (metathesis) and redistribution reactions.<sup>102</sup> Due to their high electrophilicities, it is necessary to employ sterically demanding ligands in order to isolate two- and three-coordinate aluminum cations. The high electrophilicities of dialkylaluminum cations rendered them useful catalysts for Diels Alder reactions.<sup>103</sup> Four-coordinate aluminum cations that are capable of losing one ligand have been found to be active catalysts in the polymerization of ethylene.<sup>97</sup> Similarly, a six-coordinate aluminum cation with labile ligands has been shown to be an effective catalyst for the polymerization of oxarines.<sup>99</sup>

The literature examples of structurally characterized gallium monocations closely resemble those that have been reported for aluminum monocations. Thus, two-<sup>104</sup>, three-<sup>105</sup>, four-<sup>106</sup>, five-<sup>107</sup> and six-coordinate<sup>108</sup> gallium cations are known. As in the case of the corresponding aluminum cations, the two- and three-coordinate gallium cations require kinetic stabilization by bulky ligands<sup>104,105</sup> and the tetrahedral (four-coordinate) geometry is the one that is most commonly observed.<sup>102</sup> However, unlike aluminum, gallium is relatively stable in the +1 oxidation state<sup>109</sup> and, as a consequence, there are several examples of gallium(I) cations that have been isolated and structurally characterized. In one example, a gallium(I) cation is captured by a  $\pi$ -prismad ligand (Figure 3.6a),<sup>110</sup> while in another case the gallium(I) cation serves as a terminal ligand in a platinum-based complex (Figure 3.6b).<sup>111</sup> There is no information in the literature regarding the use of gallium cations as catalysts for polymerization or organic transformations.

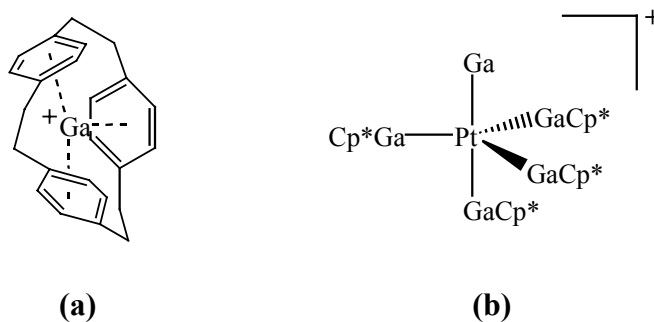


**Figure 3.6. Examples of gallium(I) cations. The corresponding anions omitted for clarity.**

One way to increase the electrophilic character of group 13 compounds, and hence enhance their catalytic properties, is to use labile anionic ligands. One such ligand is the trifluoromethanesulfonate ligand (triflate, OTf), which has been shown to exhibit lability in both transition metal and main group complexes.<sup>112</sup> Furthermore, many triflate-based compounds that incorporate alkali, alkali earth, d-block and group 13 elements have shown to be very good catalysts for several organic transformations. In the realm of boron, aluminum and gallium chemistry the triflate-based compounds have been intensely studied as replacements for more expensive transition metal catalysts. For example, triflate-based boron compounds have been shown to be useful for Friedel-Crafts alkylation, acylation and isomerization reactions<sup>113a</sup>, Morita-Baylis-Hilman-type reactions<sup>113b</sup>, and for the ring-opening polymerization of tetrahydrofuran.<sup>113c</sup> Likewise, aluminum tris(triflate), Al(OTf)<sub>3</sub>, has been employed as a catalyst for many important organic transformations including Friedel-Crafts alkylation, acylation and isomerization reactions<sup>113a</sup>, aminolysis of epoxides<sup>114a,b</sup>, intramolecular hydroalkoxylation of inactivated olefins<sup>114c</sup>, isomerisation/cyclization of

methallyloxy carboxylic acids<sup>114d</sup>, olefin epoxidation<sup>114e</sup> and ring opening of epoxides.<sup>114f</sup> Gallium tris(triflate), Ga(OTf)<sub>3</sub> has been used in a similar fashion as a catalyst for various organic reactions including Friedel-Crafts alkylation, acylation and isomerization<sup>113a,115a</sup>, the Beckmann rearrangement<sup>115b</sup>, the asymmetric Mukaiyama aldol reaction<sup>115c</sup> and the dehydration of aldoximes.<sup>115d</sup>

Despite the usefulness of boron, aluminum, and gallium tris-triflates, no structural information is available for these compounds. In fact, it is likely that the aluminum and gallium tris(triflate) complexes possess complex bridged structures.<sup>113a</sup> To shed more light on the catalytic mechanisms it seemed desirable to synthesize a family of well-characterized boron, aluminum and gallium triflates. In order to accomplish this goal it was decided to use a  $\beta$ -diketiminato as a supporting ligand. Accordingly, the work described in this chapter is focused on the synthesis of C<sub>6</sub>F<sub>5</sub>-substituted  $\beta$ -diketiminato<sup>22</sup>-supported boron, aluminum and gallium bis(triflate) complexes of the general formula (CH(CMe<sub>2</sub>)(NC<sub>6</sub>F<sub>5</sub>)<sub>2</sub>)E(OTf)<sub>2</sub> (LE(OTf)<sub>2</sub>, E = B, Al or Ga) and to explore the use such compounds both in the context of organic reactions and also as precursors for the synthesis of unprecedented group 13 dicationic species.

## RESULTS AND DISCUSSION

### Section 3.1. *Boron Triflates*

#### Synthesis and Characterization of $(\text{CH}(\text{CMe})_2(\text{NC}_6\text{F}_5)_2)\text{B}(\text{OTf})_2$ , **3.1**

Numerous reactions were carried out in order to determine the best possible reaction conditions for the synthesis of **3.1**. Thus, the three  $\beta$ -diketiminato boron dihalides  $\text{LBX}_2$  ( $\text{X} = \text{Cl}$  (**1.6**),  $\text{Br}$  (**1.7**) or  $\text{I}$  (**1.8**)) were allowed to react with the metal or silyl triflates  $\text{MOTf}$  ( $\text{M} = \text{Li}$ ,  $\text{K}$ ,  $\text{Ag}$  or  $\text{SiMe}_3$ ) in various stoichiometries in a variety of solvents that included toluene, methylene chloride and acetonitrile. The optimum conditions appeared to be the reaction of  $\text{LBCl}_2$  (**1.6**) with two equivalents of  $\text{AgOTf}$  in methylene chloride solution in the absence of light. In order to obtain crystals suitable for single-crystal X-ray diffraction experiments, it was necessary to recrystallize the crude product from a methylene chloride/hexane mixture (1:1). The X-ray crystal structure of **3.1** is illustrated in Figure 3.7. The bond lengths and angles of the  $\beta$ -diketiminato ring of **3.1** are very similar to those of **1.6**, **1.7** and **1.8** (Chapter 1). The displacement of the boron atom from the  $\text{C}_3\text{N}_2$  plane of **3.1** (0.423 Å) is very similar in magnitude to that observed for **1.8** (0.484 Å), a feature that can be attributed to repulsive interactions between the bulky triflate groups and the  $\text{C}_6\text{F}_5$  substituents on the  $\beta$ -diketiminato ligand. In terms of the range of boron-oxygen distances available from the Cambridge Structural Data Base, the  $\text{B}(1)\text{—O}(1)$  bond distance of 1.496(5) for **3.1** is close to the mean  $\text{B—O}$  value of 1.440 Å. However, the  $\text{B}(1)\text{—O}(4)$  bond distance (1.565(5) Å) is  $\sim 0.07$  Å longer than the  $\text{B}(1)\text{—O}(1)$  separation and thus suggestive of

incipient ionization toward the monocation  $[\text{LBOTf}]^+[\text{OTf}]^-$ . This was, however, not the case for the very similar boron bistriflate compound  $(\text{N}(\text{PCl}_2)_2(\text{NMe})_2)\text{B}(\text{OTf})_2$  (**3.1a**)<sup>90</sup> which features phosphazene backbone instead of a  $\beta$ -diketiminato framework. Here, the two B—O distances 1.530(8) and 1.505(8) Å are identical within experimental error. Interestingly, when  $\text{CD}_3\text{CN}$  is added to **3.1**, the  $^{11}\text{B}$  NMR resonance at  $\delta$  0.25 ppm decays and a new peak at  $\delta$  21.2 ppm emerges. Possibly, this is due to the  $\text{CD}_3\text{CN}$ -promoted extrusion of one of the triflate anions. Moreover, the addition of 4-dimethylaminopyridine (DMAP) to the methylene chloride solution of **3.1** resulted in the appearance of a new  $^{11}\text{B}$  signal at  $\delta$  2.90 ppm which is attributable to the formation of the DMAP-coordinated boron monocation  $([\text{LB}(\text{OTf})(\text{DMAP})]^+[\text{OTf}]^-)$ .

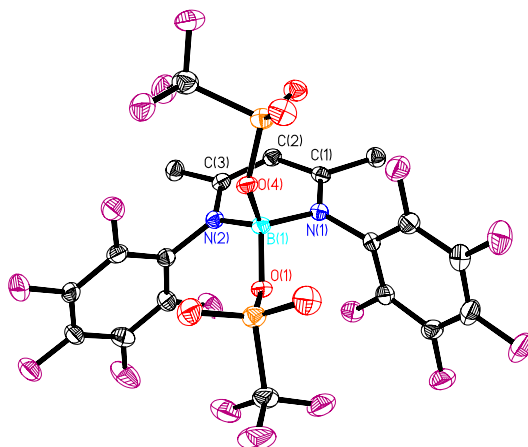


**Figure 3.7. Molecular structure of  $\text{LB}(\text{OTf})_2$ , **3.1**. Hydrogen atoms have been omitted for clarity.**

### Synthesis and Characterization of $[(\text{CH}(\text{CMe})_2(\text{NC}_6\text{F}_5)_2)\text{B}(\text{bipy})][2\cdot\text{OTf}]$ , **3.2**

It was evident from the molecular structure that **3.1** has a tendency to form a boron monocation. This view was supported by the changes in the NMR spectra that

took place when **3.1** was treated with the bases  $\text{CD}_3\text{CN}$  and DMAP. However, it was also clear that it would be necessary to employ a bidentate base to effect the removal of both triflate anions and thus generate a new type of boron cation, namely a boron dication. Accordingly, **3.1** was treated with an equimolar amounts of 2,2'-bipyridine (bipy) in methylene chloride solution at room temperature. This turned out to be the most appropriate method for the generation of the bistriflate salt of the desired boron dication **3.2**. The  $^{11}\text{B}$  NMR signal of  $\delta$  6.44 ppm falls in the spectral region that is typical for four-coordinate neutral boron species and boronium cations. However, for

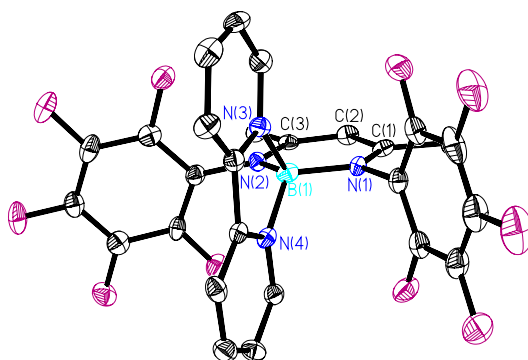


**Figure 3.8. Molecular structure of one of the two independent cations of [LB(bipy)][2-OTf], **3.2**. All hydrogen atoms and both triflate anions have been omitted for clarity.**

more definitive characterization, it was necessary to appeal to X-ray crystallography. There are two very similar, but independent, cation-anion pairs in the asymmetric unit, and the structure of one of the cations is illustrated in Figure 3.8. Overall, the X-ray crystallographic analysis confirms that **3.2** is the bis(triflate) salt of the boron dication  $[\text{LB}(\text{bipy})]^{2+}$ . The closest boron-triflate oxygen distance is 3.772 Å, which exceeds the

sum of van der Waals radii for B and O (3.5 Å).<sup>116</sup> As in the cases of the  $\beta$ -diketiminate-substituted monocations  $[\text{HC}(\text{CMe})_2(\text{NC}_6\text{F}_5)_2\text{BR}]^+$  (R = Cl (**2.1**); Ph (**2.2**)), the  $\text{BN}_2\text{C}_3$  ring is planar within experimental error. The average N—C (1.361(8) Å) and C—C (1.375(9) Å) bond distances for **3.2** are identical to those for **2.1** (1.364(8) and 1.390(9) Å, respectively) and **2.2** (1.361(10) and 1.377(11) Å, respectively) within experimental error. The bipy ligand is attached to the boron center in a bidentate fashion such that the bipy and  $\text{BN}_2\text{C}_3$  planes are approximately orthogonal. As a consequence of the tetrahedral boron geometry in **3.2**, the average B—N bond distance for the  $\text{BN}_2\text{C}_3$  ring (1.514(10) Å) is longer than that for the trigonal planar boron atom of **2.1** (1.435(9) Å) or **2.2** (1.441(9) Å). However, the average N—B—N bond angle for **3.2** (111.2(6)°) is comparable to those for **2.1** (116.6(6)°) and **2.2** (113.7(10)°). The average B—N (bipy) bond distance of 1.595(10) Å is shorter than that for the triflate salt of the 2,2'-bipyridylboronium monocation for which the average B—N(bipy) distance is 1.613(1) Å.<sup>117</sup>

Further insight into the electronic structure of the boron dication **3.2** was gained from DFT calculations that were carried out at the B3LYP level of theory<sup>61</sup> using the 6-31G\* basis set.<sup>122</sup> The input coordinates for the geometry optimization of the bipy-coordinated dication structure were generated from the X-ray crystallographic data. The calculated and observed metrical parameters agree with each other to within  $\pm 1.5\%$ . The HOMO is located primarily on the  $\text{C}_6\text{F}_5$  substituents and the  $\text{C}_3\text{N}_2\text{B}$  ring (Figure 3.9a). Regarding the latter, the ring  $\pi$ -character comprises  $\pi$ -allylic N—B—N and C—C—C fragments separated by a nodal plane that passes through the two N—C bonds. The

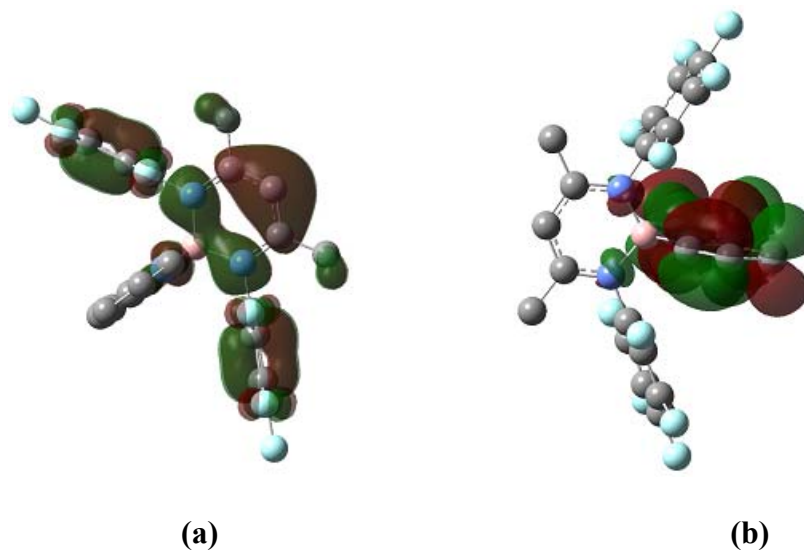


**Figure 3.9. (a) HOMO and (b) LUMO for 3.2.**

LUMO, which is of  $\pi^*$  character, is located primarily on the bipy rings (Figure 3.9b) and the HOMO–LUMO gap is 85.3 kcal/mol. The computed charge at the boron center is +1.3. This partial quenching of positive charge by a donor ligand is also a feature of borenium (**B**) and boronium (**C**) monocations.<sup>83</sup>

DFT calculations also provide an indication of the potentially high reactivity of the uncoordinated boron dication, **3.2a**. Thus, as illustrated in Figure 3.10, removal of the bipy ligand and generation of the free boron dication results in a structure in which one of the fluorine atoms of a  $\text{C}_6\text{F}_5$  group is attacked by the highly electron-deficient  $\text{B}^{2+}$  center. This interaction is accomplished by rotation of one of the  $\text{C}_6\text{F}_5$  rings such that it is approximately coplanar with the  $\text{BN}_2\text{C}_3$  ring. This conformation permits the formation of a  $\text{B}\cdots\text{F}\text{—C}$  interaction with  $\text{B}\cdots\text{F}$  and  $\text{C}\text{—F}$  distances of 1.507 and 1.536 Å, respectively. For comparison, the mean B–F and C–F bond distances from the Cambridge Structural Data Base are 1.362 and 1.335 Å, respectively. In turn, this



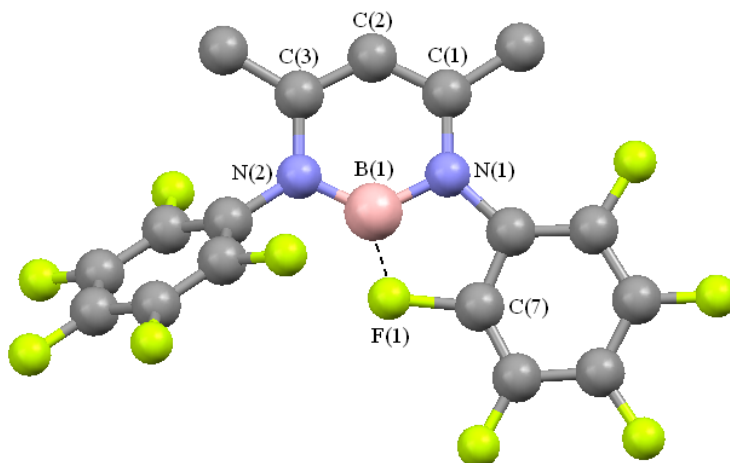


**Figure 3.10. Optimized structure of the free boron dication, 3.2a. Computed bond distances [Å] and angles [°]: B(1)-N(1) 1.418, B(1)-N(2) 1.393, B(1)-F(1) 1.507, F(1)-C(7) 1.536, N(1)-C(1) 1.401, N(2)-C(3) 1.404, C(1)-C(2) 1.402, C(2)-C(3) 1.404, N(1)-B(1)-N(2) 127.1, B(1)-N(1)-C(1) 116.9, N(1)-C(1)-C(2) 116.1, C(1)-C(2)-C(3) 126.5, C(2)-C(3)-N(2) 117.9, B(1)-N(2)-C(3) 115.4.**

B...F—C interaction has the effect of reducing the strongly electrophilic nature of the B<sup>2+</sup> center. From the standpoint of the  $\beta$ -diketiminato ring, the major changes that take place upon removal of the bipy ligand are  $\sim 0.1$  Å increases in the B(1)-N(1) and B(1)-N(2) bond distances and 15.5° and 4.2° increases in the N(1)-B(1)-N(2) and C(1)-C(2)-C(3) bond angles, respectively.

### **Synthesis and Characterization of [(CH(CMe)<sub>2</sub>(NC<sub>6</sub>F<sub>5</sub>)<sub>2</sub>)B(terpy)][2-OTf], 3.3.**

The reaction of **3.1** with 2,2':6',2''-terpyridine (terpy) was performed concurrently with the bipy reaction because, at that time, it was thought that the terpy ligand might be a better reagent for the removal of both triflate molecules from **3.1** due to its higher potential denticity. In fact, it was observed that both bipy and terpy were equally effective reagents for the synthesis of the desired boron dications **3.2** and **3.3**.

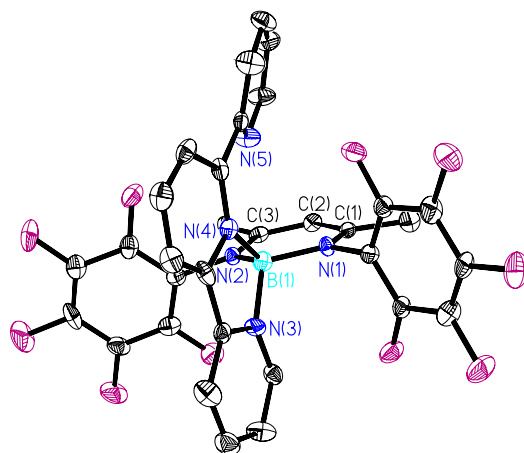


**Figure 3.11.** Molecular structure of one of the two independent units of [LB(terpy)][2·OTf], **3.3**. All hydrogen atoms and the two triflate anions have been omitted for clarity.

The X-ray crystallography analysis of the terpy-stabilized boron dication **3.3** (Figure 3.11) revealed that the structural features of this dication are very similar to those of **3.2**. The average N—C (1.368(16) Å), C—C (1.362(18) Å and B—N (1.151(18) Å) bond distances and the average N-B-N (111.5(11)°) bond angle for  $\beta$ -diketiminate ring of **3.3** are identical with those for **3.2** within experimental error. In the case of **3.3**, the terpy ligand uses only two of the three nitrogen atoms to bind to the boron center, leaving one arm of the terpy molecule unattached. This observation can be explained on the basis that, with rare exceptions<sup>118</sup>, boron complexes are restricted to being four-coordinate. As a result of the presence of an unattached arm of the terpy ligand, the average of the two B—N(terpy) bond distances of 1.579(18) and 1.648(18) Å are not identical which results in a more deshielded boron center. This deshielding of the boron center in **3.3** in comparison with **3.2**, in which the two B—N(bipy) bond distances are

identical, is manifested in the  $^{11}\text{B}$  NMR data for **3.3** and **3.2**. The  $^{11}\text{B}$  shifts for **3.2** and **3.3** are found at  $\delta$  6.44 and 7.43 ppm, respectively, which supports the idea that the boron center of **3.3** is more deshielded in comparison with that of **3.2**. This observation could also imply the terpy ligand of **3.3** is not as tightly bonded to boron as the bipy ligand of **3.2**.

**Synthesis and Characterization of  $[(\text{CH}(\text{CMe})_2(\text{NC}_6\text{F}_5)_2)\text{B}(\text{bipy})][2\cdot\text{X}]$ , X = I (**3.4**), Br (**3.5**).**

As pointed out in Section 1.5 of Chapter 1, the two B—I bond distances (2.222(4) and 2.342(2) Å) of the  $\text{LBI}_2$  molecule (**1.8**) are not identical. A similar observation was made in the case of **3.1** regarding the two B—O bond distances. It was therefore thought that **1.8** could be used for the synthesis of boron dication salt  $[\text{LB}(\text{bipy})][2\cdot\text{I}]$  (**3.4**) by treatment with bipy. The addition of bipy to a yellow methylene chloride solution containing an equimolar amount of  $\text{LBI}_2$  resulted in the immediate appearance of a red solid. Examination of the product by multinuclear NMR revealed that this red solid was indeed the boron dication **3.4**. The  $^{11}\text{B}$  shift of **3.4** ( $\delta$  6.52 ppm) is virtually identical to that of **3.2** ( $\delta$  6.44 ppm). In fact, the only significant difference between the NMR spectra of **3.2** and **3.4** is found in the bipy region of the  $^1\text{H}$  NMR spectra in which the peaks of **3.4** at  $\delta$  8.35, 8.87, 8.88 and 9.14 ppm are slightly shifted in comparison with the corresponding peaks of **3.2** at  $\delta$  8.33, 8.61, 8.83 and 9.32 ppm. These slight differences in the  $^1\text{H}$  NMR spectra of **3.2** and **3.4** could be due to differences in the anion-cation interactions. This hypothesis could also explain the red color of **3.4**, compared with the pale yellow color of **3.2**. It is plausible that charge

transfer from the iodide anions to the LUMO of **3.4** takes place and is responsible for the red color. As shown in Figure 3.9b, the LUMO of the boron dication is largely localized on the bipy ligand.

After it was realized that the  $\beta$ -diketiminato boron diiodide ( $\text{LBI}_2$ ) could be used to generate a boron dication, the reactions of  $\text{LBCl}_2$  (**1.6**) and  $\text{LBBr}_2$  (**1.7**) with bipy were also explored to determine whether or not the extrusion of two halide anions would occur. In the case of  $\text{LBCl}_2$  there was no  $^{11}\text{B}$  NMR evidence that reaction with bipy had taken place. On the other hand, the reaction of  $\text{LBBr}_2$  with bipy resulted in the formation of a yellow solid and examination of this product by multinuclear NMR revealed that dication  $[\text{LB}(\text{bipy})][2\cdot\text{Br}]$  (**3.5**) had formed. The salts **3.4** and **3.5** are considerably less soluble in the methylene chloride/acetonitrile mixed solvent than the analogous bistriflate salt **3.2**. As a consequence, it was not possible to obtain crystals of **3.4** and **3.5** suitable for X-ray diffraction studies.

### Section 3.2. *Aluminum Triflates*

#### **Synthesis and Characterization of $(\text{CH}(\text{CMe})_2(\text{NC}_6\text{F}_5)_2)\text{Al}(\text{OTf})(\text{Me})$ , **3.6**.**

The initial focus of  $\beta$ -diketiminato aluminum triflate work was the preparation of the monotriflate compound **3.6**. The only previously reported  $\beta$ -diketiminato aluminum monotriflate,  $(\text{CH}(\text{CMe})_2(\text{N-p-tolyl})_2)\text{Al}(\text{OTf})(\text{Me})$  (**3.6a**), was prepared by the addition of  $\text{AgOTf}$  to the aluminum dimethyl derivative,  $(\text{CH}(\text{CMe})_2(\text{N-p-tolyl})_2)\text{AlMe}_2$ .<sup>45</sup> This is a somewhat unusual reaction in which the silver cation of  $\text{AgOTf}$  is reduced to silver metal and the methyl group on the aluminum atom is

oxidized to ethane gas. The yield of this reaction was very low. It was realized that trimethylsilyl chloride elimination method might represent an improved route for the preparation of the desired  $\beta$ -diketiminato aluminum monotriflate complex  $(\text{CH}(\text{CMe})_2(\text{NC}_6\text{F}_5)_2)\text{Al}(\text{OTf})(\text{Me})$ , **3.6**. In fact, the reaction of  $\text{LAlMeCl}$  (**1.10**) with  $\text{Me}_3\text{SiOTf}$  was successful and resulted in a 62 % yield of crystalline **3.6**. The crystal structure of **3.6** is shown in Figure 3.12. In contrast to compound **3.6a**, the asymmetric unit of **3.6** consists of two independent molecules. In one of the independent molecules the aluminum atom lies in the extended  $\text{C}_3\text{N}_2$  plane within experimental error. In the other molecule, the aluminum atom is displaced by 0.385 Å from said plane. This displacement is somewhat greater than that reported for the molecular structure of **3.6a** (0.297 Å). The average C—N (1.324(10) Å), C—C (1.396(11) Å), Al—N (1.871(7) Å) and Al—C (1.933(8) Å) bond distances for **3.6** are identical with those found for **3.6a** within experimental error. However, the average Al—O bond length for **3.6** (1.819(6) Å) is shorter than that found for **3.6a** (1.873(4) Å). The length of the Al—O bonds

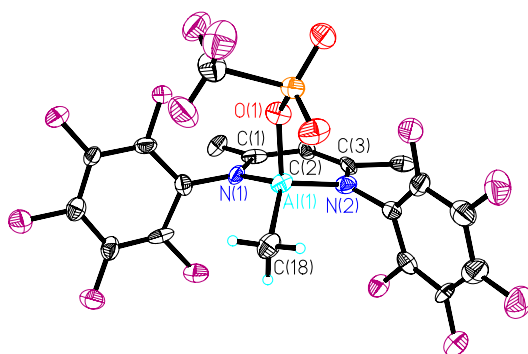


**Figure 3.12.** Molecular structure of one of the independent molecules of  $\text{LAl}(\text{OTf})\text{Me}$ , **3.6**. All hydrogen atoms, except those on the Al-*Me* group, have been omitted for clarity.

might be pertinent to the viability of triflate abstraction/displacement reactions in the sense that a triflate with a longer Al—O bond might be more easily displaced. However, since **3.6a** did not undergo triflate abstraction/displacement, it seemed unlikely that **3.6**, with a shorter Al—O bond distance, would undergo such a reaction. Accordingly, no triflate abstraction/displacement reactions were attempted with **3.6**.

### Synthesis and Characterization of $(\text{CH}(\text{CMe})_2(\text{NC}_6\text{F}_5)_2)\text{Al}(\text{OTf})_2$ , **3.7**.

Several approaches were explored in order to find the best possible reaction conditions for the synthesis of the  $\beta$ -diketiminato aluminum bistriflate **3.7**. The majority of these approaches involved the reactions of  $\text{LAlCl}_2$  (**1.11**) with varying amounts of the triflates  $\text{MOTf}$  ( $\text{M} = \text{Li}, \text{K}, \text{Ag}$  or  $\text{SiMe}_3$ ) in a variety of different solvents such as toluene, methylene chloride and acetonitrile. The reaction that produced **3.7** in the highest yield involved the addition of two equivalents of solid  $\text{AgOTf}$  to an acetonitrile solution of **1.11** in the absence of light. The resulting solid was identified on the basis of multinuclear NMR and high-resolution mass

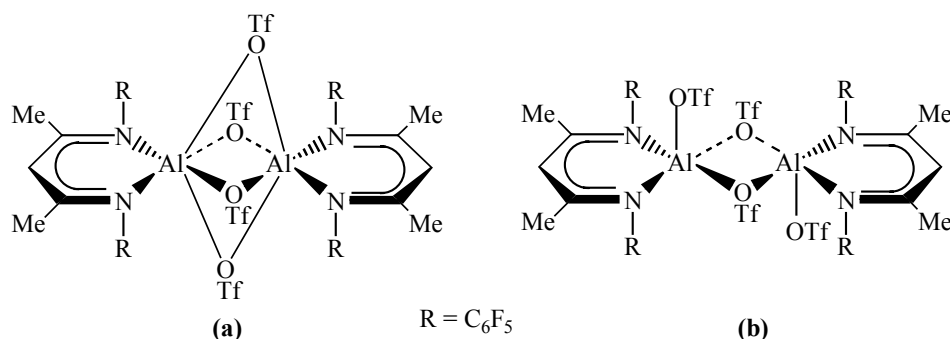
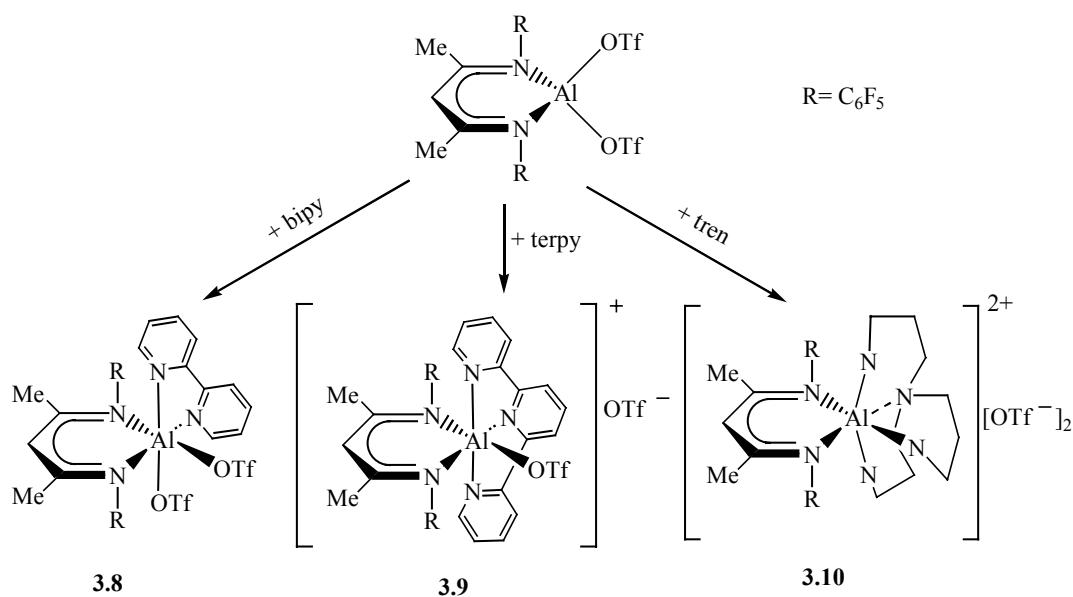


**Figure 3.13. Proposed structures for 3.7 (a) with all bridging triflates, (b) with bridging and terminal triflates.**

spectroscopy. Unfortunately, suitable crystals for X-ray diffraction analysis were not obtained. However, it is postulated that **3.7** exists as a dimer (Figure 3.13) since the analogous gallium derivative **3.11** was shown to possess such a dimeric structure by single crystal X-ray diffraction (Section 3.3, Figure 3.17). It is, however, not clear if all the triflate ligands are all bridging (Figure 3.12a) or whether there is a combination of bridging and terminal bonding modes for these ligands (Figure 3.12b).

**Syntheses and Characterizations of  $(\text{CH}(\text{CMe})_2(\text{NC}_6\text{F}_5)_2)\text{Al}(\text{bipy})(\text{OTf})_2$ , **3.8**,  $[(\text{CH}(\text{CMe})_2(\text{NC}_6\text{F}_5)_2)\text{Al}(\text{terpy})(\text{OTf})][\text{OTf}]$ , **3.9** and  $[(\text{CH}(\text{CMe})_2(\text{NC}_6\text{F}_5)_2)\text{Al}(\text{tren})][2\cdot\text{OTf}]$ , **3.9**.**

The reactivity of the aluminum bistriflate **3.7** toward three multidentate neutral Lewis bases 2,2'-bipyridine (bipy), 2,2':6',2''-terpyridine (terpy), and tris(2-aminoethyl)amine (tren) was investigated. A summary of the results of these reactions is presented Scheme 3.2. In contrast to the analogous reaction involving the boron bistriflate **3.1**, the reaction of **3.7** with bipy did not result in formation of a dication. In fact, the product of the aluminum bistriflate-bipy reaction (**3.8**) is a neutral coordination complex of the bipy ligand with the aluminum bistriflate. This complex features a six-coordinate aluminum center and both triflate ligands remain in the aluminum coordination sphere. Removal of one of the triflate ligands from the aluminum center was achieved by treatment of the aluminum bistriflate **3.7** with terpy. The product of this reaction (**3.9**) is best described as a six-coordinate aluminum monocation in which terpy functions as a tridentate ligand and one of the triflate ligands remains coordinated. It was evident from the previous two reactions involving the addition of bipy and terpy to **3.7** that the complete removal of both triflate groups would require coordination by a



**Scheme 3.2. Summary of the reactions of aluminum bistriflate **3.7** with the neutral Lewis bases bipy, terpy and tren.**

tetradentate Lewis base ligand. The tetradentate ligand that was chosen for this purpose was tris(2-aminoethyl)amine (tren). The reaction of **3.7** with tren produced the desired six-coordinate aluminum dication **3.10**. In this case, the tren ligand functions as a tetradentate ligand at the aluminum center and both triflate ligands have been extruded from the coordination sphere as triflate anions. It should be noted that **3.10** represents the first example of a new class of aluminum cation, namely an aluminum dication. Prior to this development only aluminum monocations and dialuminum dications had been reported.<sup>95-101</sup>

The molecular structures of **3.8**, **3.9** and **3.10** were determined by single-crystal X-ray diffraction experiments and are illustrated in Figure 3.14. The averages of the C—N (~ 1.39 Å) and C—C (~ 1.35 Å) bond distances for the C<sub>3</sub>N<sub>2</sub>Al rings of each of the three complexes are identical within experimental error. The average of the Al—N



bond lengths for the  $\beta$ -diketiminato aluminum rings ( $C_3N_2Al$ ) of **3.8** (1.982(2) Å) and **3.9** (1.974(4) Å) are shorter than that for **3.10** (2.008(5) Å). It should be noted that the two Al—N bond distances for the  $C_3N_2Al$  ring of **3.10** are unequal (1.962(5) and 2.054(4) Å). This discrepancy, and the elongation of the average Al—N bond distance for **3.10** in comparison with those of **3.8** and **3.9**, can be attributed to the degree of the displacement of the Al and  $\gamma$ -C atoms the from the N(1)C(1)C(3)N(2) ( $C_2N_2$ ) plane. The Al atom and the  $\gamma$ -C atom are positioned on the same side of the  $C_2N_2$  plane

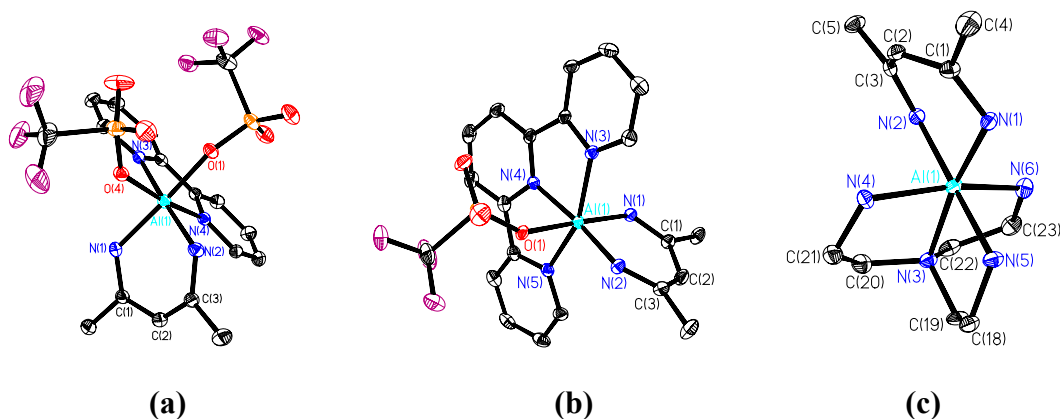


**Figure 3.14. Molecular structures of (a) 3.8, (b) 3.9 and (c) 3.10. In each case, the  $C_6F_5$ -groups and all hydrogen atoms have been omitted for clarity. The counteranions for 3.9 and 3.10 have also been omitted.**

resulting in boat conformations for the  $C_3N_2Al$  rings of **3.8**, **3.9** and **3.10**. The largest Al and  $\gamma$ -C atom displacements from the  $C_2N_2$  plane are found for **3.10** (0.836 and 0.224 Å, respectively), followed by those for **3.8** (0.483 and 0.130 Å, respectively) and the smallest such displacements being observed for **3.9** (0.312 and 0.061 Å, respectively). The magnitudes of the Al and  $\gamma$ -C atom displacements from the  $C_2N_2$  plane correlates well with the corresponding N-Al-N bond angles for **3.8** (90.24(10)°), **3.9** (92.19(15)°)

and **3.10** (88.18(18)°), in the sense that larger the displacement from the plane, the more acute the N-Al-N bond angle. The Al—O bond distances for the triflate ligands of **3.8** (1.902(2) and 1.941(2) Å) are not identical and the only Al—O bond distance for **3.9** (1.933(3) Å) is identical to that of the longer distance for **3.8** within experimental error. However, all of these Al—O bond distances for **3.8** and **3.9** are significantly longer than that for the aluminum monotriflate **3.6** (1.819(6) Å). Such a trend implies that the triflate complexes **3.8** and **3.9** are more reactive in comparison with **3.6** in terms of triflate anion displacement. The Al—N distances that are formed between the aluminum atoms and the neutral donor ligands bipy (**3.8**), terpy (**3.9**) and tren (**3.10**) are very similar, the average distance being approximately 2.05 Å. The only exceptions are the Al—N bond distances that involve the central nitrogen atoms of terpy (N(4)) and tren (N(3)) ligands for which the distances are 1.991(3) and 2.093(5) Å for **3.9** and **3.10**, respectively.

Multinuclear NMR studies of **3.8** and **3.9** revealed that the solution phase behavior is inconsistent with the X-ray crystallographic data. For example, the <sup>1</sup>H NMR spectrum for **3.8** revealed several different peaks for the methyl groups and three different peaks for the C(γ)—H proton of the β-diketiminate ligand backbone. This observation suggests that at least one triflate ligand has been extruded from the aluminum atom resulting in formation of the monocation species **3.8a** (Figure 3.15a). It is also possible that both triflate ligands have been extruded from the aluminum center resulting in the aluminum dication **3.8b** (Figure 3.15b), structural features of which would be analogous to those of the boron dication **3.2**. At the present time, it is not known if the coordination spheres of **3.8a** and **3.8b** contain any solvent molecules.

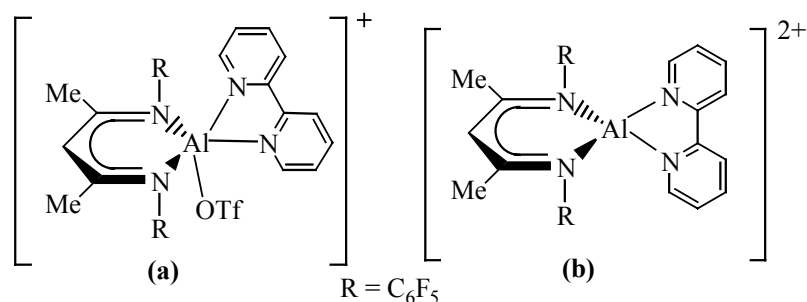


**Figure 3.15. Postulated solution phase structures for (a) 3.8a and (b) 3.8b.**

Furthermore, the solution phase  $^1H$  NMR spectra for **3.9** clearly exhibit two sets of peaks for each of the  $H-C(\gamma)$  and non-equivalent  $CH_3$  protons of the  $\beta$ -diketiminate backbone. It is postulated that the second set of peaks is due to the terpy-supported aluminum dication **3.9a** (Figure 3.16) that also includes a solvent molecule in its coordination sphere because the two  $CH_3$  groups of the  $\beta$ -diketiminate backbone are still chemically non-equivalent. It should be noted that the absence of additional peaks in the solution phase  $^{27}Al$  NMR spectra of both **3.8** and **3.9** does not necessarily imply that only one species is present in solution in each case because the  $^{27}Al$  signals for very low symmetry aluminum-containing species are often broadened to such extent that are unobservable. A case in point is the aluminum monotriflate **3.6**.

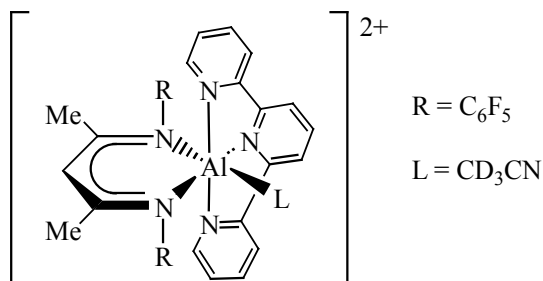


**Figure 3.16. Postulated solution phase structures for 3.9a.**

### Section 3.3. Gallium Triflates

#### Synthesis and Characterization of $(\text{CH}(\text{CMe})_2(\text{NC}_6\text{F}_5)_2)\text{Ga}(\text{OTf})_2$ , **3.11**.

The procedure employed for the synthesis of the  $\beta$ -diketiminato gallium bistriflate **3.11** is the same as that described for the synthesis of the aluminum analogue **3.7**. Solid AgOTf was added to an acetonitrile solution of  $\text{LGaCl}_2$  (**1.14**) at ambient temperature in the absence of light. The resulting white solid, which was obtained by workup of the reaction mixture, changed color to silver if it was left in the presence of light due to the light-induced decomposition of residual AgCl. Interestingly, this observation was not made in the case of the aluminum analogue **3.7**. The removal of residual solid AgCl from **3.11** was achieved by dissolution of the off-white solid in methylene chloride followed by a filtration. The yield of **3.11** was less than 50%. Fortunately, it was possible to use the AgCl-containing white solid **3.11** for subsequent reactions provided that light was excluded. In this way, the yields of products in subsequent reactions were superior to those realized by purification of **3.11**. The structure of **3.11** was determined by X-ray crystallography (Figure 3.17). In addition to the  $\beta$ -diketiminato ligand, each gallium atom of **3.11** is surrounded by three triflate ligands and an acetonitrile molecule. Of the three triflate ligands, one is bonded in a terminal fashion and the other two occupy bridging positions. The averages of the C—C (1.389(7) Å), C—N (1.351(6) Å) and Ga—N (1.961(4) Å) bond distances for the  $\beta$ -diketiminato gallium ( $\text{C}_3\text{N}_2\text{Ga}$ ) ring of **3.11** are very similar to those for  $\text{LGaMe}_2$  (**1.13**; 1.396(6), 1.332(5) and 1.997(5) Å, respectively) and  $\text{LGaCl}_2$  (**1.14**; 1.390(3), 1.347(3)

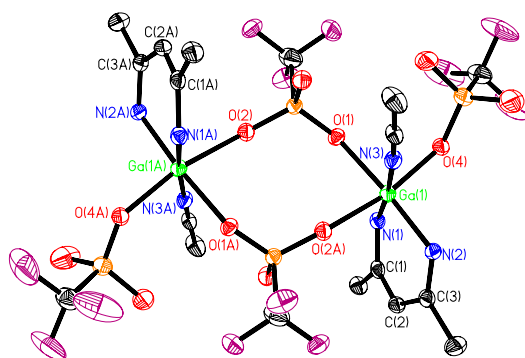
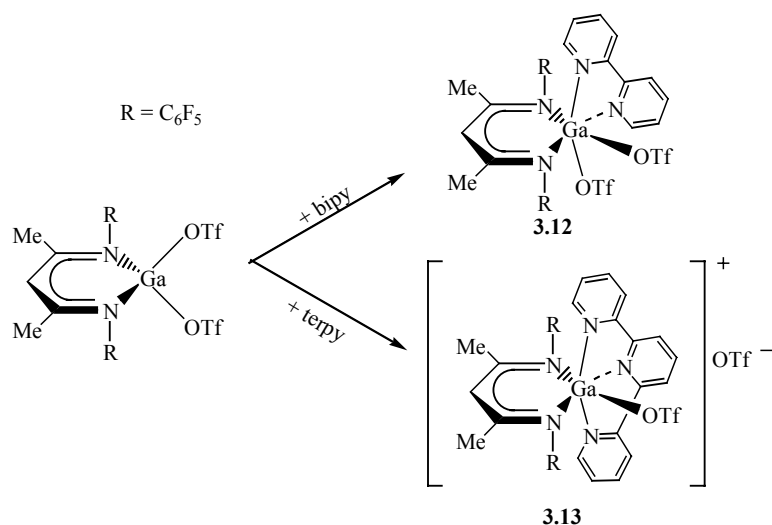


**Figure 3.17.** Molecular structure of **3.11**. The  $\text{C}_6\text{F}_5$  groups of the  $\beta$ -diketiminate ligands and all hydrogen molecules have been omitted for clarity.

and 1.910(2) Å, respectively). The N-Ga-N bond angle for **3.11** (92.88(14)°) is identical to that for **1.13** (92.49(13)°) within experimental error but more acute than the same angle for **3.14** (99.02(8)°). The  $\text{C}_3\text{N}_2\text{Ga}$  ring for **3.11** adopts a boat conformation in which the displacements of the gallium and C( $\gamma$ ) atoms from the  $\text{C}_2\text{N}_2$  plane are 0.590 and 0.103 Å, respectively. The other two structurally characterized gallium triflate compounds in the literature are [(2,6-(HNMe<sub>2</sub>)<sub>2</sub>-C<sub>6</sub>H<sub>3</sub>)GaH(OTf)<sub>2</sub>][OTf]<sup>119</sup> (**3.11a**) and (CH(CMe)<sub>2</sub>(2,6-(<sup>i</sup>Pr)<sub>2</sub>-C<sub>6</sub>H<sub>3</sub>N)<sub>2</sub>)Ga(OTf)(PPh<sub>2</sub>)<sup>120</sup> (**3.11b**). The Ga—O(terminal) bond distance for **3.11** of 1.964(3) Å is identical to the average Ga—O bond distances for both **3.11a** (1.950(9) Å) and **3.11b** (1.979(6) Å) within experimental error. On the other hand, the two Ga—O(bridging) bond distances for **3.11** of 2.069(3) and 2.101(3) Å are longer than the terminal one.

**Syntheses and Characterizations of  $(\text{CH}(\text{CMe})_2(\text{NC}_6\text{F}_5)_2)\text{Ga}(\text{bipy})(\text{OTf})_2$ , **3.12**,  $[(\text{CH}(\text{CMe})_2(\text{NC}_6\text{F}_5)_2)\text{Ga}(\text{terpy})(\text{OTf})][\text{OTf}]$ , **3.13**, and  $[(\text{CH}(\text{CMe})_2(\text{NC}_6\text{F}_5)_2)\text{Ga}(\text{tren})][2\cdot\text{OTf}]$ , **3.14**.**

Treatment of the  $\beta$ -diketiminato gallium bistriflate **3.11** with 2,2'-bipyridine (bipy) and 2,2':6',2''-terpyridine (terpy) resulted in the formation of **3.12** and **3.13**, respectively (Scheme 3.3). From the standpoint of the modes of coordination of the bipy and terpy ligands, compounds **3.12** and **3.13** are very similar to the aluminum complexes **3.8** and **3.9**. Single-crystal X-ray diffraction studies of **3.12** and **3.13** (Figure 3.18) revealed that both compounds feature six-coordinate gallium centers. Note, however, that compound **3.12** is a neutral species while compound **3.13** is a gallium monocation. The averages of the C—C and C—N bond distances for the  $\beta$ -diketiminato gallium ( $\text{C}_3\text{N}_2\text{Ga}$ ) rings of **3.12** (1.391(5) and 1.334(5) Å, respectively) and **3.13** (1.396(5) and 1.338(4) Å, respectively) are identical with those for **3.11** (1.389(7) and 1.351(6) Å, respectively) within experimental error. On the other hand,



**Scheme 3.3. Summary of the reactions of gallium bistriflate **3.11** with the neutral Lewis bases bipy and terpy.**

the average of the Ga—N bond length for the C<sub>3</sub>N<sub>2</sub>Ga rings of **3.12** (2.006(3) Å) and **3.13** (1.990(3) Å) are longer than that for **3.11** (1.961(4) Å). The average Ga—N(bipy) bond length of 2.073(3) Å for **3.12** is longer than the Ga(1)—N(4) bond length of 2.042(3) Å for **3.13** but shorter than the average of the other two Ga—N(terpy) bond lengths for **3.13** (2.107(3) Å). The displacements of the gallium atoms from the C<sub>2</sub>N<sub>2</sub> planes for **3.12** (0.459 Å) and **3.13** (0.304 Å) are less than that for **3.11** (0.590 Å). On the other hand, the N-Ga-N bond angle for **3.12** (91.64(12)°) is more acute than those for **3.11** (92.88(14)°) and **3.13** (93.68(11)°).

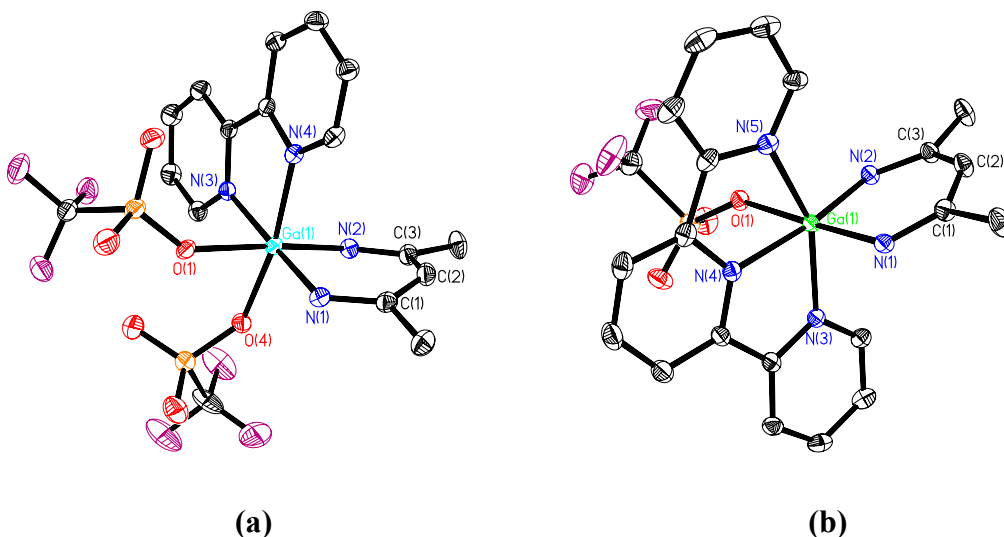


**Figure 3.18. Molecular structures of (a) 3.12 and (b) 3.13. In each case, the C<sub>6</sub>F<sub>5</sub>-groups and all hydrogen atoms have been omitted for clarity. The counteranion for 3.13 has also been omitted.**

Multinuclear NMR studies of **3.12** and **3.13** revealed that the solution phase behavior is inconsistent with the X-ray crystallographic data. For example, the <sup>1</sup>H and <sup>19</sup>F NMR spectra for **3.13** exhibit only one set of peaks for the H—C(γ)/CH<sub>3</sub> and CF<sub>3</sub>(OTF)/C<sub>6</sub>F<sub>5</sub> groups, respectively. Such an observation is indicative of the presence of only one species in the solution phase. It is proposed that this species is actually the

terpy-supported gallium dication **3.13a** that also includes a solvent molecule in its coordination sphere because the two CH<sub>3</sub> groups of the β-diketiminato backbone are chemically non-equivalent (Figure 3.19a). The H—C(γ)/CH<sub>3</sub> region of the <sup>1</sup>H NMR spectrum of **3.12** consists of multiple peaks, the appearance of which may be due to the presence of both the bipy-supported gallium monocation **3.12a** (Figure 3.19b) and the bipy-supported gallium dication **3.12b** (Figure 3.19c) formed by extrusion of one or both triflates from the aluminum coordination spheres, respectively. It is, however, not known if the solvent molecules are present in the coordination spheres of **3.12a** and **3.12b**.

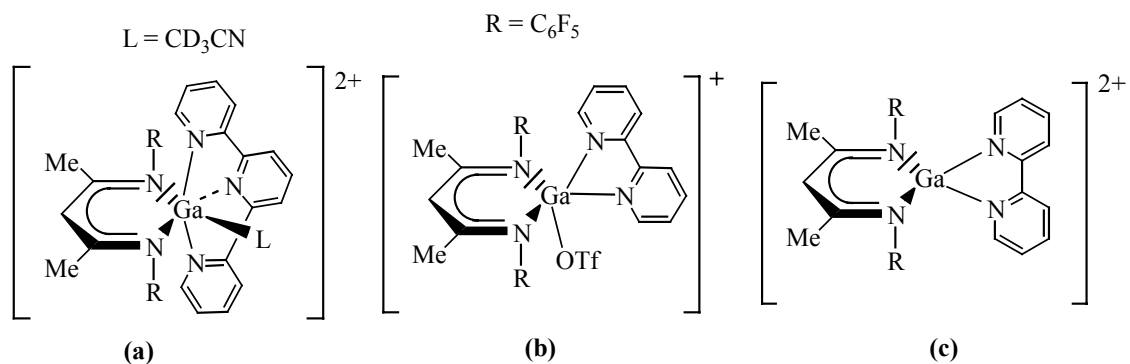
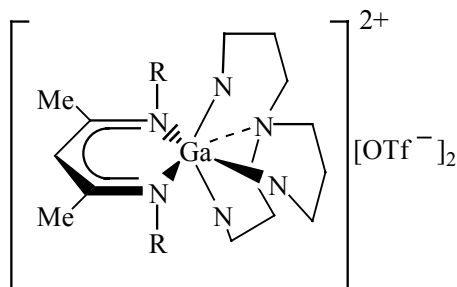


**Figure 3.19. Proposed solution phase structures for (a) 3.13a, (b) 3.12a and (c) 3.12b.**

The reaction of the gallium bistriflate **3.11** with tris(2-aminoethyl)amine (tren) did not result in a crystalline product hence it was not possible to acquire X-ray crystallographic data. However, examination of multinuclear NMR data obtained from the resulting solid revealed that compound **3.14** (Figure 3.20) had indeed been produced. For example, the N-H<sub>2</sub>, N-CH<sub>2</sub> and H<sub>2</sub>N-CH<sub>2</sub> peaks in the <sup>1</sup>H NMR spectrum for the free tren ligand are found at δ 1.40, 2.45 and 2.67 ppm, respectively, while in



the case of **3.14** they are found at  $\delta$  3.32, 2.60 and 2.85 ppm. The same peaks for the analogous aluminum dication **3.10** are found at  $\delta$  5.38, 2.74 and 2.97 ppm, respectively. Additionally, the  $^{13}\text{C}$  NMR chemical shifts of 39.71 and 54.68 ppm for the ethyl component of the bonded tren ligand for **3.14** are different than those for the free tren ligand (40.29 and 58.35 ppm). Note that similar concentrations for the  $^1\text{H}$  NMR samples of **3.10**, **3.14** and the free tren ligand were required because the  $^1\text{H}$  NMR shift of the N-*H2* peak was found to be concentration dependent in all three cases.

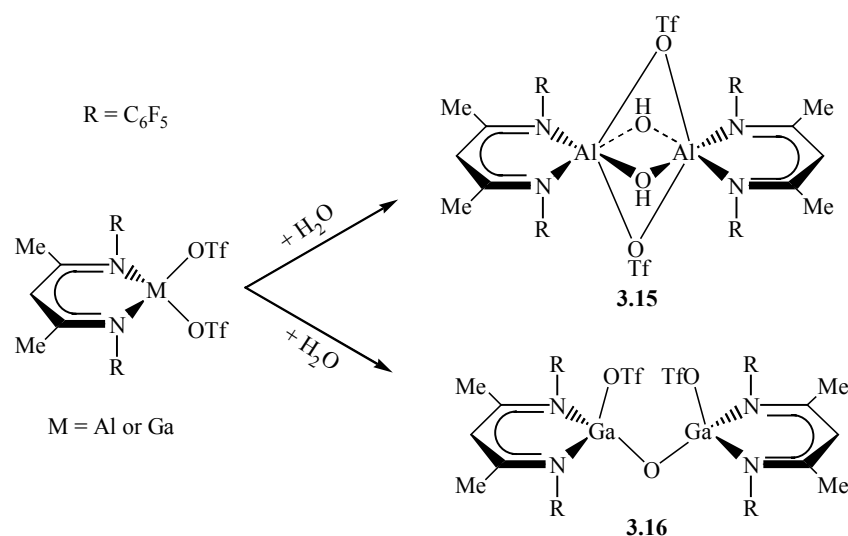


**3.14**

**Figure 3.20. Proposed structure for the  $\beta$ -diketiminato gallium dication supported by the tren ligand.**

### Section 3.4. *Hydrolysis products*

Manipulation of the aluminum and gallium bistriflate compounds **3.7** and **3.11** in methylene chloride solvents that contained unknown amounts of water resulted in the isolation of the hydrolysis products **3.15** and **3.16**, respectively (Scheme 3.4). A few crystals of **3.15** were isolated that had formed inside an NMR tube that contained a solution of **3.7** in  $\text{CD}_2\text{Cl}_2$ . Unfortunately, because of the small quantity of material, the characterization of **3.15** is based solely on a single-crystal X-ray diffraction experiment (Figure 3.20a). The dimer of **3.15** is held together by two bridging triflates and two bridging hydroxides. In this way each aluminum atom achieves a coordination number



**Scheme 3.4.** Hydrolysis products of the aluminum and gallium bistriflates, **3.15** and **3.16**.

of six. The average C—C (1.388(5) Å) and C—N (1.343(4) Å) bond distances for the two  $\beta$ -diketiminato aluminum rings of **3.15** are identical with those for **3.8** (1.389(4) and 1.345(3) Å, respectively), **3.9** (1.390(6) and 1.343(5) Å, respectively) and **3.10**

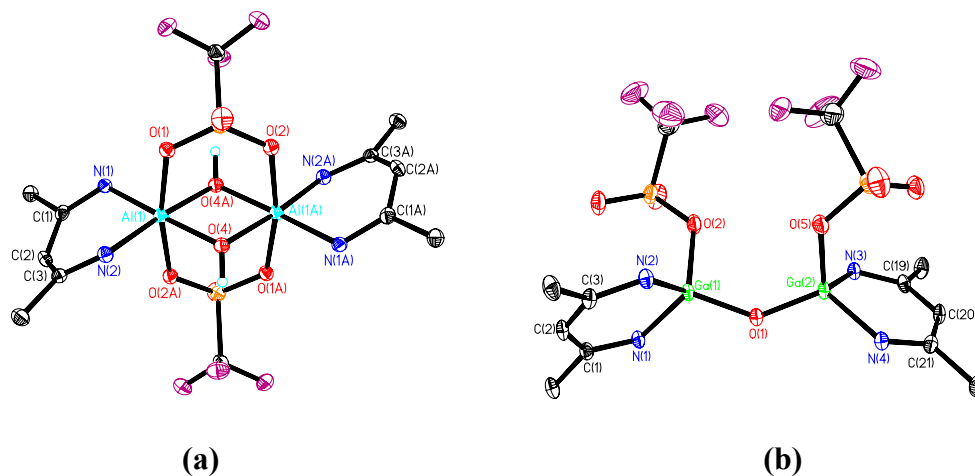


**Figure 3.21.** Molecular structures of (a) **3.15** and (b) **3.16**. The  $C_6F_5$  groups of the  $\beta$ -diketiminato ligands and all hydrogen atoms have been omitted for clarity.

(1.389(8) and 1.359(7) Å, respectively) within experimental error. However, the average Al—N bond length for **3.15** (1.932(3) Å) is shorter than those observed for **3.8** (1.982(2) Å), **3.9** (1.974(4) Å) and **3.10** (2.008(5) Å). The displacements of the aluminum and C( $\gamma$ ) atoms from the C<sub>2</sub>N<sub>2</sub> plane of **3.15** are 0.709 and 0.179 Å, respectively. This value for the aluminum atom displacement from the C<sub>2</sub>N<sub>2</sub> plane of **3.15** lies approximately between the values found for **3.8** (0.438 Å) and **3.10** (0.863 Å). On the other hand, the N-Al-N bond angle of 99.92(12)° for **3.15** is identical with that for **3.8** (90.24(10)°) within experimental error. The average bridging Al—O(triflate) bond length of 2.015(3) Å for **3.15** is significantly longer than the average terminal Al—O(triflate) bond lengths for **3.8** (1.923(2) Å) and **3.9** (1.933(3) Å), an observation which is anticipated on the basis of the nature of the triflate binding modes. As expected, the average bridging Al—O(hydroxide) bond length for **3.15** (1.870(4) Å) is considerably shorter than that for the bridging triflate ligands.

In an attempt to isolate and crystallize a sample of **3.11** using methylene chloride that contained unknown amount of water, a small crop of crystalline **3.16** was isolated (Figure 3.20b). An X-ray analysis of this gallium derivative **3.16** confirmed that, like aluminum analogue **3.15**, it is dimeric. However, in this case the bridging entity is a single oxo group. The averages of the C—C and C—N bond distances for both  $\beta$ -diketiminato gallium rings of **3.16** (1.387(5) and 1.350 Å, respectively) are identical with those for **3.11** (1.389(7) and 1.351(6) Å, respectively), **3.12** (1.391(5) and 1.334(5) Å, respectively) and **3.13** (1.396(5) and 1.338(4) Å, respectively). The shortening of the average Ga—N and Ga—O(triflate) bond distances for **3.16** (1.898(3) and 1.914(2) Å, respectively) in comparison with those for **3.11** (1.961(4) and 1.964(3)-

(terminal) Å, respectively), **3.12** (2.006(3) and 2.049(2) Å, respectively) and **3.13** (1.990(3) and 2.112(2) Å, respectively) is expected on the basis that the electrophilicity of the gallium atoms of these species since the four coordinate gallium centers of **3.16** are anticipated to be more electrophilic than the six-coordinate gallium centers of **3.11**, **3.12** and **3.13**. Further consequences of the shortening of the Ga—N bond lengths are widening of the average N-Ga-N bond angle and diminution of the average gallium atom displacement from the C<sub>2</sub>N<sub>2</sub> plane for **3.16** (99.46(11)° and 0.169 Å, respectively) in comparison with those for **3.11** (92.88(14)° and 0.590 Å, respectively), **3.12** (91.64(12)° and 0.459 Å, respectively) and **3.13** (93.68(11)° and 0.304 Å, respectively).

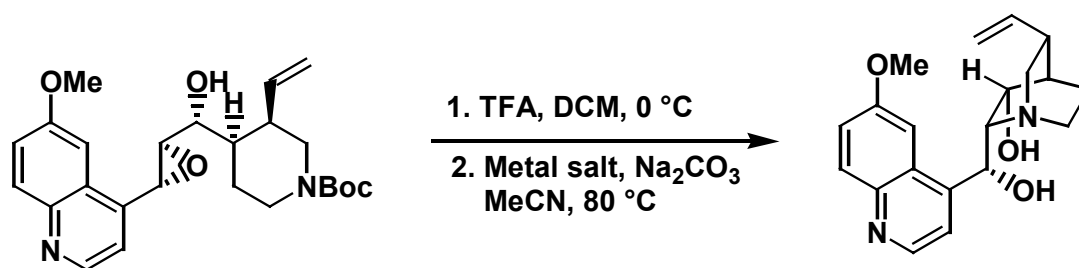
### Section 3.5. Organic Transformation\*

In order to access the [2.2.2] quinuclidine bicycle of the alkaloid natural product quinine, the cyclization a secondary amine on to a fairly sterically hindered epoxide is required (Figure 3.5). Following the standard deprotection of the *N*-Boc group to generate the free amine, it became clear the epoxide needed extra activation in order to react. Seemingly, the adjacent alcohol functionality can assist in additional coordination to a metal center to form a 5-membered chelate ring. Initially, titanium (IV) and lithium (I) Lewis acids were found to mediate this cyclization although the conversions were poor. Acetonitrile was solvent of choice in order to increase the solubility of the extremely polar amine. Sodium carbonate served as the base to deprotonate the crude amine and quench any excess acid that was present in the reaction mixture. The zinc

---

\* The synthetic work on the organic transformation was carried out by Pete Webber in the laboratory of Professor Michael J. Krische at the University of Texas at Austin.

triflate  $\text{Zn}(\text{OTf})_2$  was found to facilitate the cyclization although reaction times of 2 days at 80 °C were necessary for full conversion of the starting material. Interestingly, the aluminum bistriflate complex  $(\text{CH}(\text{CMe})_2(\text{NC}_6\text{F}_5)_2)\text{Al}(\text{OTf})_2$  (**3.7**) was found to facilitate the required cyclization in only 2 hours at 80 °C. Thus, although more experiments will be necessary, complex **3.7** represents a promising new reagent for effecting this type of cyclization reaction.



**Scheme 3.5. Amination of the epoxide.**

## CONCLUSIONS

The syntheses of the  $\beta$ -diketiminato boron, aluminum and gallium bistriflate complexes  $(\text{CH}(\text{CMe})_2(\text{NC}_6\text{F}_5)_2)\text{B}(\text{OTf})_2$  (**3.1**),  $(\text{CH}(\text{CMe})_2(\text{NC}_6\text{F}_5)_2)\text{Al}(\text{OTf})_2$  (**3.7**) and  $(\text{CH}(\text{CMe})_2(\text{NC}_6\text{F}_5)_2)\text{Ga}(\text{OTf})_2$  (**3.11**) were achieved by treatment of the corresponding dihalides with AgOTf. The structural characterizations of **3.1**, **3.11** and the two hydrolysis products  $[(\text{CH}(\text{CMe})_2(\text{NC}_6\text{F}_5)_2)\text{Al}(\text{OH})(\text{OTf})]_2$  (**3.15**) and  $[(\text{CH}(\text{CMe})_2(\text{NC}_6\text{F}_5)_2)\text{Ga}(\text{OTf})]_2\text{O}$  (**3.16**) were helpful in elucidating the structural complexity of these triflate-containing compounds. The reactivities of **3.1**, **3.7** and **3.11** with the neutral Lewis bases 2,2'-bipyridine (bipy), 2,2':6',2''-terpyridine (terpy) and tris(2-aminoethyl)amine (tren) were explored. The reactions of **3.1** with bipy and terpy resulted in the formation of the unprecedented  $\beta$ -diketiminato-supported boron dications  $[(\text{CH}(\text{CMe})_2(\text{NC}_6\text{F}_5)_2)\text{B}(\text{bipy})][2\cdot\text{OTf}]$  (**3.2**) and  $[(\text{CH}(\text{CMe})_2(\text{NC}_6\text{F}_5)_2)\text{B}(\text{terpy})][2\cdot\text{OTf}]$  (**3.3**). The analogous reactions of **3.7** with bipy and terpy resulted in the synthesis of the six-coordinate neutral and monocationic aluminum species  $(\text{CH}(\text{CMe})_2(\text{NC}_6\text{F}_5)_2)\text{Al}(\text{bipy})(\text{OTf})_2$  (**3.8**) and  $[(\text{CH}(\text{CMe})_2(\text{NC}_6\text{F}_5)_2)\text{Al}(\text{terpy})(\text{OTf})][\text{OTf}]$  (**3.9**), respectively. Comparable results were obtained when the gallium bistriflate **3.11** was treated with bipy and terpy. The resulting compounds  $(\text{CH}(\text{CMe})_2(\text{NC}_6\text{F}_5)_2)\text{Ga}(\text{bipy})(\text{OTf})_2$  (**3.12**) and  $[(\text{CH}(\text{CMe})_2(\text{NC}_6\text{F}_5)_2)\text{Ga}(\text{terpy})(\text{OTf})][\text{OTf}]$  (**3.13**) were characterized by single-crystal X-ray diffraction. Treatment of the aluminum bistriflate **3.7** with tren resulted in the synthesis of the first example of an aluminum dication,  $[(\text{CH}(\text{CMe})_2(\text{NC}_6\text{F}_5)_2)\text{Al}(\text{tren})][2\cdot\text{OTf}]$  (**3.10**), which was also structurally authenticated. Convincing multinuclear NMR evidence was found for the

formation of the gallium dication  $[(\text{CH}(\text{CMe})_2(\text{NC}_6\text{F}_5)_2)\text{Ga}(\text{tren})][2\cdot\text{OTf}]$ , which is the analogue of the aluminum dication **3.10**.

The potential use of the  $\beta$ -diketiminato boron, aluminum and gallium bistriflates **3.1**, **3.7** and **3.11** as catalysts was exemplified by an organic transformation involving the cyclization of a secondary amine on to a sterically hindered epoxide.

## CHAPTER 4

### Experimental

#### Section 4.1. *General Procedures*

All solvents were distilled over sodium benzophenone ketyl, except dichloromethane, which was distilled over  $\text{CaH}_2$ , and degassed prior to use. An M-Braun or VAC Vacuum Atmosphere argon-filled drybox was used for the manipulation of all solid reagents. All reactions were performed under dry, oxygen-free conditions using standard Schlenk or drybox techniques. To ensure the absence of water, all glassware was dried overnight in a 120 °C oven before use.

The reagents MeLi (1.6 M in diethyl ether),  $\text{NaNH}_2$ ,  $\text{SnCl}_2$ ,  $\text{Me}_3\text{SiCl}$ ,  $\text{Me}_3\text{SiI}$ ,  $\text{Et}_3\text{N}$ ,  $\text{BCl}_3$  (1 M in hexane),  $\text{BBr}_3$  (1 M in hexane),  $\text{BI}_3$ ,  $\text{PhBCl}_2$ ,  $\text{AlCl}_3$ ,  $\text{AlI}_3$ ,  $\text{GaCl}_3$ ,  $\text{GaI}_3$ ,  $\text{PCl}_3$ ,  $\text{PhPCl}_2$ ,  $\text{Ag}_2\text{O}$ ,  $\text{AgOTf}$ ,  $\text{Me}_3\text{SiOTf}$ ,  $\text{LiOTf}$ ,  $\text{KOTf}$ , 2,2'-bipyridine (bipy), 2,2':6',2''-terpyridine (terpy) and tris(2-aminoethyl)amine (tren) were purchased from a commercial source and used without further purification. The  $\text{C}_6\text{F}_5$ -substituted  $\beta$ -aminoimine<sup>22</sup> (**1.1**),  $\text{K}[\text{Fe}(\text{CO})_2(\eta^5\text{-C}_5\text{H}_5)]$ <sup>76</sup> and  $(\eta^1\text{-C}_5\text{Me}_5)\text{BCl}_2$ <sup>77</sup> were prepared according to the literature procedures.

#### Section 4.2. *Physical Measurements*

Low-resolution CI mass spectra were collected on a Finnigan MAT TSQ-700 machine; high-resolution mass spectra were measured on a VG Analytical ZAB-VE or Waters Micromass Autospec Ultima instrument. Low-resolution ESI mass spectra were



collected on a Finnigan MAT LCQ instrument; high-resolution mass spectra were measured on a Waters Micromass Q-TOF Premier instrument. Mass spectral samples were flame-sealed in glass capillaries to prevent exposure to oxygen. Unless otherwise noted, solution phase  $^1\text{H}$ ,  $^{11}\text{B}$ ,  $^{13}\text{C}$ ,  $^{19}\text{F}$ ,  $^{27}\text{Al}$ ,  $^{29}\text{Si}$  and  $^{31}\text{P}$  NMR spectra were recorded at 295 K on a Varian Inova-300 spectrometer ( $^1\text{H}$  300 MHz;  $^{11}\text{B}$  96 MHz;  $^{13}\text{C}$  75 MHz;  $^{19}\text{F}$  282 MHz;  $^{27}\text{Al}$  78 MHz;  $^{29}\text{Si}$  60 MHz;  $^{31}\text{P}$  282 MHz). NMR samples were flamed-sealed or recorded immediately following their removal from the drybox. Deuterodichloromethane, deuterobenzene and deuteroacetonitrile were obtained in sealed vials from a commercial source and used without further purification.  $^1\text{H}$  and  $^{13}\text{C}$  NMR spectra are reported relative to tetramethylsilane (0.00 ppm) and referenced to the solvent while  $^{29}\text{Si}$  NMR spectra are reported and referenced relative to tetramethylsilane (0.00 ppm).  $^{11}\text{B}$  NMR spectra are referenced and reported relative to  $\text{BF}_3\cdot\text{OEt}_2$  (0.00 ppm) while  $^{19}\text{F}$  NMR spectra are referenced and reported relative to  $\text{CFCl}_3$ . The  $^{27}\text{Al}$  NMR spectra are reported and referenced relative to  $\text{AlCl}_3$  in  $\text{D}_2\text{O}$  solution while  $^{31}\text{P}$  NMR spectra are referenced and reported relative to phosphoric acid (85%). Melting points were obtained on a Fisher-Johns apparatus after flame-sealing the samples in glass capillaries under argon; the reported values are uncorrected.

### **Section 4.3.** *X-Ray Crystallography*

Suitable single crystals were covered with a perfluorinated polyether oil to minimize exposure to oxygen. The X-ray data were collected on a Nonius Kappa CCD diffractometer equipped with an Oxford Cryostream liquid nitrogen-cooling stream. All structures were solved by direct methods and refined by full-matrix least squares on  $F^2$

using the Siemens SHELX PLUS 5.0 (PC) software package.<sup>121</sup> All non-hydrogen atoms were allowed anisotropic thermal motion. When possible, all hydrogen atoms were located via the model; however, it was occasionally necessary to place the hydrogen atoms in calculated positions (C—H 0.96 Å). The hydrogen atoms were refined using a rigid model and a general isotropic thermal parameter. The total number of reflections, collection ranges, and final R-values for each molecule are listed in the appropriate crystallographic data tables.

All samples were mounted on fine glass fibers using commercial silicon grease as an adhesive. All data collections were performed at 153(2) K using graphite-monochromated Mo-K $\alpha$  radiation ( $\lambda$  = 0.71073 Å). Correction applied for Lorentz-polarization in each case.

#### **Section 4.4. DFT calculations**

DFT calculations were carried out at the B3LYP level of theory<sup>61</sup> for compounds **2.3**, **2.3b**, **2.8**, **3.2** and **3.2a** using the Gaussian 03 suite of programs.<sup>122</sup> The 6-311+G\* basis set was used for **2.3** and **2.3b**. The LANL2DZ basis set was used for the iron atom and the 6-31+G\* basis set was employed for the remaining elements of compound **2.8** while the 6-31G basis set was used for **3.2** and **3.2a** to aid the computational efficiency. The geometries of **2.3**, **2.3b**, **2.8**, **3.2** and **3.2a** were fully optimized and their location as energy minima confirmed using vibrational frequency analysis. Graphical representations of calculated molecular orbitals of **2.3** and **2.3b** were obtained using MOLDEN<sup>123</sup> while in the case of **2.8**, **3.2** and **3.2a** the calculated molecular orbitals were obtained using the Gaussian 03 suite of programs.

#### Section 4.5. Experimental Procedures and Spectroscopic Data

**Preparation of  $(\text{CH}(\text{CMe}_2)_2(\text{NC}_6\text{F}_5)_2)\text{Li}\cdot\text{OEt}_2$ , **1.2**:** Solid **1.1** (0.74 g, 1.72 mmol) was dissolved in 30 mL of hexane and cooled down to 0 °C. A solution of 1.08 mL (1.73 mmol) of 1.6 M MeLi in Et<sub>2</sub>O was added dropwise and the reaction mixture was allowed to warm up to room temperature. Colorless crystals of **1.2** formed upon storage of the reaction mixture overnight at – 30 °C. The yield of **1.2** was essentially quantitative with melting point of 106 – 109 °C. MS (Cl<sup>+</sup>, CH<sub>4</sub>):  $m/z$  511 ([M+H]<sup>+</sup>). HRMS (Cl<sup>+</sup>, CH<sub>4</sub>): calcd for C<sub>21</sub>H<sub>18</sub>F<sub>10</sub>LiN<sub>2</sub>O,  $m/z$  511.1420; found, 511.1417. <sup>1</sup>H NMR (C<sub>6</sub>D<sub>6</sub>):  $\delta$  0.62 (t, 3H, CH<sub>3</sub> (Et<sub>2</sub>O)), 1.74 (s, 6H, CH<sub>3</sub>) 2.62 (q, 4H, CH<sub>2</sub> (Et<sub>2</sub>O)) 4.69 (s, 1H,  $\gamma$ -CH). <sup>19</sup>F NMR (C<sub>6</sub>D<sub>6</sub>):  $\delta$  -153.1 (d, *o*-F, 4F), -165.1 (t, *p*-F, 2F), -166.0 (m, *m*-F, 4F).

**Preparation of  $(\text{CH}(\text{CMe}_2)_2(\text{NC}_6\text{F}_5)_2)\text{Na}$ , **1.3**:** Solid **1.1** (4.00 g, 9.30 mmol) was dissolved in approximately 70 mL of a hexanes/ether (1:1) solvent mixture. 0.36 g (9.23 mmol) of NaNH<sub>2</sub> was added to the solution at room temperature and the reaction mixture was left to stir overnight. The mixed solvent was then removed under reduced pressure resulting in the formation of yellow solid, which was washed with three 10 mL portions of hexanes and dried under reduced pressure. The yield of **1.3** was 3.71 g (88.2 %) with decomposition point of ~ 166 °C. Due to the ionic nature of **1.3**, the  $m/z$  429 peak was the only one observed in the negative mode of the low resolution mass spectrum. The peak corresponds to L<sup>-</sup>. <sup>1</sup>H NMR (CD<sub>3</sub>CN):  $\delta$  1.83 (br, 6H, CH<sub>3</sub>), 4.58

(s, 1H,  $\gamma$ -CH).  $^{19}\text{F}$  NMR ( $\text{CD}_3\text{CN}$ ):  $\delta$  -155.51 (br, *o*-F, 4F), -169.03 (br, *m*-F, 4F), -172.48 (br, *p*-F, 2F).

**Preparation of  $(\text{CH}(\text{CMe}_2)_2(\text{NC}_6\text{F}_5)_2)\text{SnCl}$ , **1.4**:** Solid  $\text{SnCl}_2$  (0.419 g, 2.21 mmol) was transferred in approximately 70 mL of tetrahydrofuran (THF). 1.00 g (2.21 mmol) of **1.3** was added to the resulting solution at room temperature and the reaction mixture was left to stir overnight. The yellow solution was filtered through Celite® and the solvent and volatiles were removed under reduced pressure resulting in the formation of white solid. This solid was washed with three 10 mL portions of hexanes and dried under reduced pressure. The yield of **1.4** was 1.063 g (77.5 %) with decomposition point of  $\sim 197$  °C. MS ( $\text{Cl}^+$ ,  $\text{CH}_4$ ):  $m/z$  584 ( $\text{M}^+$ ). HRMS ( $\text{Cl}^+$ ,  $\text{CH}_4$ ): calcd for  $\text{C}_{17}\text{H}_7\text{ClN}_2\text{F}_{10}\text{Sn}$ ,  $m/z$  583.9160; found, 583.9164.  $^1\text{H}$  NMR ( $\text{CD}_2\text{Cl}_2$ ):  $\delta$  2.10 (s, 6H,  $\text{CH}_3$ ), 5.56 (s, 1H,  $\gamma$ -CH).  $^{19}\text{F}$  NMR ( $\text{CD}_2\text{Cl}_2$ ):  $\delta$  -144.76 (br, *o*-F, 2F), -148.21 (br, *o*-F, 2F), -157.64 (t, *p*-F, 2F,  $^3J = 21.4$  Hz), -162.11 (br, *m*-F, 4F).

**Preparation of  $\text{CH}(\text{CMe}_2)_2(\text{NC}_6\text{F}_5)(\text{Me}_3\text{Si-NC}_6\text{F}_5)$ , **1.5**:** Solid **1.3** (0.300 g, 0.664 mmol) and liquid  $\text{Me}_3\text{SiI}$  (0.133 g, 0.665 mmol) were mixed together in approximately 100 mL of toluene. The reaction mixture was left to stir for about 6 h after which it was filtered through Celite®. The reaction flask and the filter were washed with three 5 mL portions of toluene in order to ensure complete transfer of the product. At this point it was assumed that the yield was quantitative and this assumption proved to be correct as described in Section 1.4. Attempts to isolate neat **1.5** were unsuccessful because during

the process of solvent removal under reduced pressure about 30 % of the desired product was converted to the free ligand, **1.1**, on the basis of  $^1\text{H}$  NMR spectroscopy. The thermal instability of **1.5** was confirmed by a high temperature  $^1\text{H}$  NMR study in which, as the temperature was increased, the peak due to the  $\text{Me}_3\text{Si}$  moiety slowly decreased and disappeared completely at approximately 80 °C. The reason(s) and the exact decomposition pathway(s) are still not understood. As a result of the inability to isolate **1.5** in a pure form, it was used *in situ* in all subsequent reactions. It is also worth noting that other reactions were attempted in an effort to obtain pure **1.5**, such as the reaction of **1.2** with either  $\text{Me}_3\text{SiCl}$  or  $\text{Me}_3\text{SiI}$  and the reaction of **1.4** with  $\text{Me}_3\text{SiCl}$ . No reaction took place between **1.2** and  $\text{Me}_3\text{SiCl}$ , while the reaction of **1.2** with  $\text{Me}_3\text{SiI}$  took almost three days to reach completion. The reaction of **1.4** with  $\text{Me}_3\text{SiCl}$  resulted in complete conversion to **1.5** in the course of one day, thus the reaction of **1.4** with  $\text{Me}_3\text{SiI}$  is preferred route of obtaining **1.5** *in situ*. Even though neat **1.5** was not obtained, it was still possible to obtain pertinent spectroscopic data. On the basis of multinuclear NMR data, it was determined that the  $\text{Me}_3\text{Si}$  substituent is bound to only one nitrogen atom and if migration of the  $\text{Me}_3\text{Si}$  substituent between the two nitrogen atoms takes place then the process is slow on the NMR time scale. MS ( $\text{Cl}^+$ ,  $\text{CH}_4$ ):  $m/z$  503 ( $[\text{M}+\text{H}]^+$ ). HRMS ( $\text{Cl}^+$ ,  $\text{CH}_4$ ): calcd for  $\text{C}_{20}\text{H}_{17}\text{F}_{10}\text{N}_2\text{Si}$ ,  $m/z$  503.1001; found, 503.0997.  $^1\text{H}$  NMR ( $\text{C}_6\text{D}_6$ ):  $\delta$  -0.05 (s, 9H,  $(\text{CH}_3)_3\text{Si}$ ), 1.45 (s, 3H,  $\text{CH}_3$ ), 2.46 (s, 3H,  $\text{CH}_3$ ) 5.07 (s, 1H,  $\gamma\text{-CH}$ ).  $^{19}\text{F}$  NMR ( $\text{C}_6\text{D}_6$ ):  $\delta$  -146.94 (d, *o*-F, 2F,  $^3J = 23.5$  Hz) -154.10 (d, *o*-F, 2F,  $^3J = 23.5$  Hz), -155.43 (t, *p*-F, 1F,  $^3J = 22.6$  Hz), -161.20 (t, *p*-F, 2F,  $^3J =$

22.6 Hz), 162.33 (m, *m*-F, 2F) -164.829 (m, *m*-F, 2F),  $^{29}\text{Si}$  NMR ( $\text{C}_6\text{D}_6$ ):  $\delta$  12.41 (sharp, m).

**Preparation of  $(\text{CH}(\text{CMe}_2)_2(\text{NC}_6\text{F}_5)_2)\text{BCl}_2$ , **1.6**:** A solution of 0.66 mL of 1.0 *M*  $\text{BCl}_3$  in hexane was added to a freshly prepared solution of **1.5** (0.663 mmol) in 115 mL of toluene at ambient temperature. The reaction mixture was allowed to stir overnight, following which the solvent mixture and  $\text{Me}_3\text{SiCl}$  were removed under reduced pressure. Pale yellow solid **1.6** was isolated in virtually quantitative. Compound **1.6** starts decomposing at  $\sim 140$  °C. MS ( $\text{Cl}^-$ ,  $\text{CH}_4$ ):  $m/z$  509 ( $\text{M}^+$ ). HRMS ( $\text{Cl}^-$ ,  $\text{CH}_4$ ): calcd for  $\text{C}_{17}\text{H}_7\text{BN}_2\text{F}_{10}\text{Cl}_2$ ,  $m/z$  509.9920; found, 509.9918.  $^1\text{H}$  NMR ( $\text{CD}_2\text{Cl}_2$ ):  $\delta$  2.09 (s, 6H,  $\text{CH}_3$ ), 5.88 (s, 1H,  $\gamma\text{-CH}$ ).  $^{11}\text{B}$  NMR ( $\text{CD}_2\text{Cl}_2$ ):  $\delta$  4.82 (sharp, s).  $^{19}\text{F}$  NMR ( $\text{CD}_2\text{Cl}_2$ ):  $\delta$  -142.11 (d, *o*-F, 4F,  $^3J = 17.2$  Hz), -153.86 (t, *p*-F, 2F,  $^3J = 21.4$  Hz), -161.99 (m, *m*-F, 4F).

**Preparation of  $(\text{CH}(\text{CMe}_2)_2(\text{NC}_6\text{F}_5)_2)\text{BBr}_2$ , **1.7**:** The experimental procedure for the synthesis of **7** is exactly the same as in the case of compound **1.6**, in which 0.66 mL of 1.0 *M* solution of  $\text{BBr}_3$  in hexane was used instead of  $\text{BCl}_3$ . Pale yellow solid **1.7** was isolated in virtually quantitative yield. Compound **1.7** starts decomposing at about 100 °C and it becomes a dark brown solid at approximately 190 °C. MS ( $\text{Cl}^-$ ,  $\text{CH}_4$ ):  $m/z$  599 ( $[\text{M-H}]^+$ ). HRMS ( $\text{Cl}^-$ ,  $\text{CH}_4$ ): calcd for  $\text{C}_{17}\text{H}_7\text{BN}_2\text{F}_{10}\text{Br}_2$ ,  $m/z$  596.8831; found, 596.8832.  $^1\text{H}$  NMR ( $\text{CD}_2\text{Cl}_2$ ):  $\delta$  2.11 (s, 6H,  $\text{CH}_3$ ), 6.06 (s, 1H,  $\gamma\text{-CH}$ ).  $^{11}\text{B}$  NMR ( $\text{CD}_2\text{Cl}_2$ ):  $\delta$  -1.49 (sharp, s).  $^{19}\text{F}$  NMR ( $\text{CD}_2\text{Cl}_2$ ):  $\delta$  -141.04 (d, *o*-F, 4F,  $^3J = 17.2$  Hz), -153.49 (t, *p*-F, 2F,  $^3J = 21.4$  Hz), -161.71 (m, *m*-F, 4F).

**Preparation of (CH(CMe<sub>2</sub>)<sub>2</sub>(NC<sub>6</sub>F<sub>5</sub>)<sub>2</sub>)BI<sub>2</sub>, **1.8**:** A 20 mL toluene solution containing solution 0.259 g (0.663 mmol) of BI<sub>3</sub> was added to a freshly prepared solution of **1.5** (0.663 mmol) in 115 mL of toluene at ambient temperature. The reaction mixture was allowed to stir overnight, following which the solvent and Me<sub>3</sub>SiI were removed under reduced pressure. Yellow solid **1.8** was isolated in virtually quantitative yield. Compound **1.8** starts decomposing at about 70 °C. It turns into a deep red liquid at approximately 180 °C. MS (Cl<sup>-</sup>, CH<sub>4</sub>): *m/z* 693 ([M-H]<sup>-</sup>). HRMS (Cl<sup>-</sup>, CH<sub>4</sub>): calcd for C<sub>17</sub>H<sub>6</sub>BN<sub>2</sub>F<sub>10</sub>I<sub>2</sub>, *m/z* 692.8554; found, 692.8557. <sup>1</sup>H NMR (CD<sub>2</sub>Cl<sub>2</sub>): δ 2.15 (s, 6H, CH<sub>3</sub>), 6.38 (s, 1H, γ-CH). <sup>11</sup>B NMR (CD<sub>2</sub>Cl<sub>2</sub>): δ -22.07 (sharp, s). <sup>19</sup>F NMR (CD<sub>2</sub>Cl<sub>2</sub>): δ -139.94 (d, *o*-F, 4F, <sup>3</sup>J = 21.4 Hz), -153.05 (t, *p*-F, 2F, <sup>3</sup>J = 21.4 Hz), -161.24 (m, *m*-F, 4F).

**Preparation of (CH(CMe<sub>2</sub>)<sub>2</sub>(NC<sub>6</sub>F<sub>5</sub>)<sub>2</sub>)AlMe<sub>2</sub>, **1.9**:** A solution of 0.70 mL of 1.0 M Me<sub>3</sub>Al in hexane was added to a 30 mL toluene solution containing 0.300 g (0.700 mmol) of **1.1** at ambient temperature. The reaction mixture was allowed to stir overnight, following which the solvent mixture was removed under reduced pressure. White solid **1.9** was isolated in virtually quantitative yield with the melting point of 145-146 °C. MS (Cl<sup>+</sup>, CH<sub>4</sub>): *m/z* 487 ([M+H]<sup>+</sup>). HRMS (Cl<sup>+</sup>, CH<sub>4</sub>): calcd for C<sub>19</sub>H<sub>14</sub>AlN<sub>2</sub>F<sub>10</sub>, *m/z* 487.0813; found, 487.0820. <sup>1</sup>H NMR (C<sub>6</sub>D<sub>6</sub>): δ -0.49 (s, 6H, AlCH<sub>3</sub>), 1.27 (s, 6H, CH<sub>3</sub>), 4.74 (s, 1H, γ-CH). <sup>19</sup>F NMR (C<sub>6</sub>D<sub>6</sub>): δ -147 (d, *o*-F, 4F), -156 (t, *p*-F, 2F), -162 (m, *m*-F, 4F). <sup>27</sup>Al NMR (C<sub>6</sub>D<sub>6</sub>): δ 212 (br, s).

**Preparation of  $(\text{CH}(\text{CMe}_2)_2(\text{NC}_6\text{F}_5)_2)\text{AlMeCl}$ , **1.10**:** The experimental procedure for the synthesis of **1.10** is exactly the same as in the case of compound **1.9**, in which 0.70 mL of 1.0 M solution of  $\text{Me}_2\text{AlCl}$  in hexane was used instead of  $\text{Me}_3\text{Al}$ . White solid **1.10** was isolated in virtually quantitative yield. The spectroscopic data for **1.10** are in good agreement with the those published by Roesky *et al.*<sup>24</sup>

**Preparation of  $(\text{CH}(\text{CMe}_2)_2(\text{NC}_6\text{F}_5)_2)\text{AlCl}_2$ , **1.11**:** The experimental procedure for the synthesis of **1.11** is exactly the same as in the case of compound **1.9**, in which 0.70 mL of 1.0 M solution of  $\text{MeAlCl}_2$  in hexane was used instead of  $\text{Me}_3\text{Al}$ . Pale yellow solid **1.11** was isolated in virtually quantitative yield. Compound **1.11** can also be prepared by adding 0.300 g (0.633 mmol) of **3** to a 40 mL toluene solution containing 0.089 (0.663 mmol) g of  $\text{AlCl}_3$  at  $-78\text{ }^\circ\text{C}$ . After it was left to stir overnight, the reaction mixture was filtered through Celite®. Removal of the solvent resulted in 86 % yield of compound **1.11**. Compound **1.11** decomposes at  $\sim 212\text{ }^\circ\text{C}$ . MS ( $\text{Cl}^+$ ,  $\text{CH}_4$ ):  $m/z$  527 ( $[\text{M}+\text{H}]^+$ ). HRMS ( $\text{Cl}^+$ ,  $\text{CH}_4$ ): calcd for  $\text{C}_{17}\text{H}_7\text{AlN}_2\text{F}_{10}\text{Cl}_2$ ,  $m/z$  526.9720; found, 526.8731.  $^1\text{H}$  NMR ( $\text{CD}_2\text{Cl}_2$ ):  $\delta$  2.06 (s, 6H,  $\text{CH}_3$ ), 5.67 (s, 1H,  $\gamma\text{-CH}$ ).  $^{19}\text{F}$  NMR ( $\text{CD}_2\text{Cl}_2$ ):  $\delta$  -145.2 (d, *o*-F, 4F), -155.0 (t, *p*-F, 2F,  $^3J = 21.4\text{ Hz}$ ), -161.6 (m, *m*-F, 4F).  $^{27}\text{Al}$  NMR ( $\text{CD}_2\text{Cl}_2$ ):  $\delta$  98.6 (br, s).

**Preparation of  $(\text{CH}(\text{CMe}_2)_2(\text{NC}_6\text{F}_5)_2)\text{AlI}_2$ , **1.12**:** Solid **1.3** (0.300 g, 0.663 mmol) was added to a 40 mL toluene solution containing 0.270 g (0.663 mmol) of  $\text{AlI}_3$  at  $-78\text{ }^\circ\text{C}$ . After it was left to stir overnight, the reaction mixture was filtered through Celite®.



Removal of the solvent resulted in 87% of yellow solid **1.12**. Compound **1.12** can also be prepared in quantitative yield by the same reaction described for compound **1.8**, in which 0.270 g (0.633 mmol) of AlI<sub>3</sub> was used instead of BI<sub>3</sub>. The melting point of compound **1.12** is 174-177 °C. MS (CI<sup>+</sup>, CH<sub>4</sub>): *m/z* 711 ([M+H]<sup>+</sup>). HRMS (CI<sup>+</sup>, CH<sub>4</sub>): calcd for C<sub>17</sub>H<sub>7</sub>AlN<sub>2</sub>F<sub>10</sub>I<sub>2</sub>, *m/z* 710.8433; found, 710.9835. <sup>1</sup>H NMR (CD<sub>2</sub>Cl<sub>2</sub>): δ 2.09 (s, 6H, CH<sub>3</sub>), 5.78 (s, 1H, γ-CH). <sup>19</sup>F NMR (CD<sub>2</sub>Cl<sub>2</sub>): δ -142.34 (d, *o*-F, 4F, <sup>3</sup>J = 17.2 Hz), -154.63 (t, *p*-F, 2F, <sup>3</sup>J = 20.3 Hz), -161.32 (m, *m*-F, 4F). <sup>27</sup>Al NMR (CD<sub>2</sub>Cl<sub>2</sub>): δ 80.23 (br, s).

**Preparation of (CH(CMe<sub>2</sub>)<sub>2</sub>(NC<sub>6</sub>F<sub>5</sub>)<sub>2</sub>)GaMe<sub>2</sub>, 1.13:** Compound **1.13** was prepared by the same method described in the case of compound **9**, in which 0.080 g (0.700 mmol) of neat Me<sub>3</sub>Ga was used instead of Me<sub>3</sub>Al. This procedure results in virtually quantitative yield of white solid **1.13** with the melting point of 140-142 °C. MS (CI<sup>+</sup>, CH<sub>4</sub>): *m/z* 529 ([M+H]<sup>+</sup>). HRMS (CI<sup>+</sup>, CH<sub>4</sub>): calcd for C<sub>19</sub>H<sub>13</sub>AlN<sub>2</sub>F<sub>10</sub>, *m/z* 529.0253; found, 529.0266. <sup>1</sup>H NMR (C<sub>6</sub>D<sub>6</sub>): δ -0.17 (s, 6H, GaCH<sub>3</sub>), 1.32 (s, 6H, CH<sub>3</sub>), 4.70 (s, 1H, γ-CH). <sup>19</sup>F NMR (C<sub>6</sub>D<sub>6</sub>): δ -145 (d, *o*-F, 4F), -151 (t, *p*-F, 2F), -164 (m, *m*-F, 4F).

**Preparation of (CH(CMe<sub>2</sub>)<sub>2</sub>(NC<sub>6</sub>F<sub>5</sub>)<sub>2</sub>)GaCl<sub>2</sub>, 1.14:** The two experimental procedures for the synthesis of **1.11** can be used for the synthesis of **1.14**, in which 0.112 g (0.663 mmol) of GaCl<sub>3</sub> was used instead of AlI<sub>3</sub>. The trimethylsilyl halide elimination route resulted in quantitative yield of **14** while the salt metathesis produced compound **1.14** in 85% yield. Compound **1.14** is white solid with the melting point of 233-234 °C. MS

(Cl<sup>+</sup>, CH<sub>4</sub>): *m/z* 570 ([M+H]<sup>+</sup>). HRMS (Cl<sup>+</sup>, CH<sub>4</sub>): calcd for C<sub>17</sub>H<sub>7</sub>GaN<sub>2</sub>F<sub>10</sub>Cl<sub>2</sub>, *m/z* 567.9082; found, 567.9089; <sup>1</sup>H NMR (CD<sub>2</sub>Cl<sub>2</sub>): δ 2.11 (s, 6H, CH<sub>3</sub>), 5.63 (s, 1H, γ-CH). <sup>19</sup>F NMR (CD<sub>2</sub>Cl<sub>2</sub>): δ -145.42 (d, *o*-F, 4F, <sup>3</sup>J = 16.6 Hz), -154.88 (t, *p*-F, 2F, <sup>3</sup>J = 21.4 Hz), -161.43 (m, *m*-F, 4F).

**Preparation of (CH(CMe<sub>2</sub>)<sub>2</sub>(NC<sub>6</sub>F<sub>5</sub>)<sub>2</sub>)GaI<sub>2</sub>, 1.15:** The two experimental procedures for the synthesis of **1.14** can be used for the synthesis of **1.15**, in which 0.299 g (0.663 mmol) of GaI<sub>3</sub> was used instead of GaCl<sub>3</sub>. The silane elimination route resulted in quantitative yield of pale yellow solid **1.15** while the salt metathesis produced compound **1.15** in 83% yield. Compound **1.15** decomposes at ~ 180 °C. MS (Cl<sup>+</sup>, CH<sub>4</sub>): *m/z* 753 ([M+H]<sup>+</sup>). HRMS (Cl<sup>+</sup>, CH<sub>4</sub>): calcd for C<sub>17</sub>H<sub>7</sub>GaN<sub>2</sub>F<sub>10</sub>I<sub>2</sub>, *m/z* 752.7873; found, 752.7877. <sup>1</sup>H NMR (CD<sub>2</sub>Cl<sub>2</sub>): δ 1.94 (s, 6H, CH<sub>3</sub>), 5.61 (s, 1H, γ-CH). <sup>19</sup>F NMR (CD<sub>2</sub>Cl<sub>2</sub>): δ -139.30 (d, *o*-F, 4F, <sup>3</sup>J = 16.1 Hz), -151.43 (t, *p*-F, 2F, <sup>3</sup>J = 21.4 Hz), -157.92 (m, *m*-F, 4F).

**Preparation of (Cl<sub>2</sub>P)CH(CMe<sub>2</sub>)<sub>2</sub>(NC<sub>6</sub>F<sub>5</sub>)<sub>2</sub>, 1.16a:** Solid **1.3** (0.300 g, 0.663 mmol) was added to a 40 mL hexane solution containing 0.092 g (0.663 mmol) of PCl<sub>3</sub> at -78 °C. After it was left to stir for approximately 1 h, the reaction mixture was filtered through Celite®. Removal of the solvent resulted in 70% of white, crystalline **1.16a**. The melting point of compound **1.16a** is 128-130°C. MS (Cl<sup>+</sup>, CH<sub>4</sub>): *m/z* 531 ([M+H]<sup>+</sup>). HRMS (Cl<sup>+</sup>, CH<sub>4</sub>): calcd for C<sub>17</sub>H<sub>8</sub>PN<sub>2</sub>F<sub>10</sub>Cl<sub>2</sub>, *m/z* 530.9642; found, 530.9642. <sup>1</sup>H NMR (C<sub>6</sub>D<sub>6</sub>): δ 1.44 (d, 6H, CH<sub>3</sub>, <sup>4</sup>J<sub>P-H</sub> = 0.9 Hz), 4.04 (d, 1H, γ-CH, <sup>2</sup>J<sub>P-H</sub> = 4.5 Hz).

$^{19}\text{F}$  NMR ( $\text{C}_6\text{D}_6$ ):  $\delta$  -151.94 (m, *o*-F, 4F), -161.62 (t, *p*-F, 2F,  $^3J_{\text{F-F}} = 20.9$  Hz), -163.25 (m, *m*-F, 4F).  $^{31}\text{P}\{^1\text{H}\}$  NMR ( $\text{C}_6\text{D}_6$ ):  $\delta$  160.36 (s).

**Preparation of  $(\text{Cl}_2\text{P})\text{C}(\text{CMe}_2)_2(\text{NC}_6\text{F}_5)(\text{HNC}_6\text{F}_5)$ , **1.16b**:** Dissolution of 0.100 g (0.188 mmol) of **1.16a** in benzene or methylene chloride leads to the formation of **1.16b** as detected by multinuclear NMR. In solution compounds **1.16b** and **1.16a** exist in equilibrium in a 3:2 ratio. No attempts have been made to isolate neat **1.16b**. The melting point of **1.16b** is 128-130 °C. MS ( $\text{Cl}^+$ ,  $\text{CH}_4$ ):  $m/z$  531 ( $[\text{M}+\text{H}]^+$ ). HRMS ( $\text{Cl}^+$ ,  $\text{CH}_4$ ): calcd for  $\text{C}_{17}\text{H}_8\text{PN}_2\text{F}_{10}\text{Cl}_2$ ,  $m/z$  530.9642; found, 530.9642.  $^1\text{H}$  NMR ( $\text{C}_6\text{D}_6$ ):  $\delta$  2.11 (d, 6H,  $\text{CH}_3$ ,  $^4J_{\text{P-H}} = 3.9$  Hz), 14.17 (s, 1H, *NH*).  $^{19}\text{F}$  NMR ( $\text{C}_6\text{D}_6$ ):  $\delta$  -149.16 (m, *o*-F, 4F), -158.04 (t, *p*-F, 2F,  $^3J_{\text{F-F}} = 20.9$  Hz), -162.26 (m, *m*-F, 4F).  $^{31}\text{P}\{^1\text{H}\}$  NMR ( $\text{C}_6\text{D}_6$ ):  $\delta$  160.93.

**Preparation of  $(\text{PhClP})\text{CH}(\text{CMe}_2)_2(\text{NC}_6\text{F}_5)_2$ , **1.17a**:** The experimental procedure for the synthesis of **1.17a** is exactly the same as in the case of compound **1.16a**, in which 0.119 g (0.663 mmol) of  $\text{PhPCl}_2$  was used instead of  $\text{PCl}_3$ . The white crystalline **1.17a** was isolated in 17% yield. Compound **1.17a** melts 113-115 °C. MS ( $\text{Cl}^+$ ,  $\text{CH}_4$ ):  $m/z$  573 ( $\text{M}^+$ ). HRMS ( $\text{Cl}^+$ ,  $\text{CH}_4$ ): calcd for  $\text{C}_{23}\text{H}_{13}\text{PN}_2\text{F}_{10}\text{Cl}$ ,  $m/z$  573.0354; found, 573.0354.  $^1\text{H}$  NMR ( $\text{CD}_2\text{Cl}_2$ ):  $\delta$  1.80 (d, 3H,  $\text{CH}_3$ ,  $^4J_{\text{P-H}} = 1.0$  Hz), 2.19 (d, 3H,  $\text{CH}_3$ ,  $^4J_{\text{P-H}} = 1.0$  Hz), 4.61 (d, 1H,  $\gamma\text{-CH}$ ,  $^2J_{\text{P-H}} = 2.5$  Hz), 7.345 to 7.93 (m, 5H, aromatic).  $^{19}\text{F}$  NMR ( $\text{C}_6\text{D}_6$ ):  $\delta$  -152.30 (d, *o*-F, 2F,  $^2J_{\text{F-F}} = 19.7$  Hz), -152.63 (d, *o*-F, 2F,  $^2J_{\text{F-F}} = 19.7$  Hz), -161.88 (t, *p*-

F, 1F,  $^3J_{F-F} = 22.0$  Hz) -162.59 (t, *p*-F, 1F,  $^3J_{F-F} = 22.0$  Hz), -163.31 (m, *m*-F, 4F).  $^{31}\text{P}\{^1\text{H}\}$  NMR ( $\text{C}_6\text{D}_6$ ):  $\delta$  80.59 (s).

**Preparation of (PhClP)C(CMe<sub>2</sub>)<sub>2</sub>(NC<sub>6</sub>F<sub>5</sub>)(HNC<sub>6</sub>F<sub>5</sub>), **1.17b**:** Dissolution of 0.100g (0.175 mmol) of **1.17a** in benzene or methylene chloride solution results in the formation of **1.17b**. In solution compounds **1.17b** and **1.17a** exist in equilibrium in approximately 3:2 ratio. Attempts to isolate near **1.17b** have not been performed. The melting point of compound **1.17b** is 113-115 °C. MS ( $\text{Cl}^+$ ,  $\text{CH}_4$ ):  $m/z$  573 ( $\text{M}^+$ ). HRMS ( $\text{Cl}^+$ ,  $\text{CH}_4$ ): calcd for  $\text{C}_{23}\text{H}_{13}\text{PN}_2\text{F}_{10}\text{Cl}$ ,  $m/z$  573.0354; found, 573.0354.  $^1\text{H}$  NMR ( $\text{CD}_2\text{Cl}_2$ ):  $\delta$  2.16 (d, 6H,  $\text{CH}_3$ ,  $^4J_{\text{P-H}} = 1.0$  Hz) 7.34 to 7.94 (m, 5H, aromatic) 14.16 (s, 1H, NH).  $^{19}\text{F}$  NMR ( $\text{C}_6\text{D}_6$ ):  $\delta$  -149.47 (d, *o*-F, 4F,  $^2J_{F-F} = 17.8$  Hz) -158.84 (t, *p*-F, 1F,  $^3J_{F-F} = 23.1$  Hz) -162.57 (m, *m*-F, 4F).  $^{31}\text{P}\{^1\text{H}\}$  NMR ( $\text{C}_6\text{D}_6$ ):  $\delta$  88.32 (s).

### Preparation of [(CH(CMe)<sub>2</sub>(NC<sub>6</sub>F<sub>5</sub>)<sub>2</sub>)BCl][AlCl<sub>4</sub>], **2.1**

#### Method A

Boron trichloride (0.39 mL of a 1.0 *M* solution in hexane) was added dropwise to a solution of 0.186 g (0.353 mmol) of  $\text{LAlCl}_2$  (**1.11**) in 30 mL of pentane (or methylene chloride) at 25 °C and the reaction mixture was allowed to stir overnight at 25 °C. Removal of the solvent and excess  $\text{BCl}_3$  under reduced pressure afforded 0.216 g (94.9%) of white solid **2.1**.

### Method B

Aluminum trichloride (0.053 g, 0.397 mmol) was added to 30 mL of a methylene chloride solution of 0.200 g (0.391 mmol) of LBCl<sub>2</sub> (**1.6**) at 25 °C and the reaction mixture was allowed to stir overnight. Removal of the solvent under reduced pressure afforded an essentially quantitative yield of white solid **2.1**. Crystals obtained from a methylene chloride/hexane (1:1) solvent mixture at room temperature. The melting point of **2.1** is 195-198 °C. MS (Cl<sup>+</sup>, CH<sub>4</sub>): *m/z* 475 ([M-(AlCl<sub>4</sub>)]<sup>+</sup>). HRMS (Cl, CH<sub>4</sub>): calcd for C<sub>17</sub>H<sub>6</sub>BClF<sub>10</sub>N<sub>2</sub>, *m/z* 475.015971; found, 475.016373. <sup>1</sup>H NMR (300 MHz, CD<sub>2</sub>Cl<sub>2</sub>): δ 2.77 (s, 6H, Me), 7.66 (s, 1H, γ-CH). <sup>19</sup>F NMR (282 MHz, CD<sub>2</sub>Cl<sub>2</sub>): δ -145.46 (m, 4F, *o*-F), -146.17 (m, 2F, *p*-F), -156.897 (m, 4F, *m*-F). <sup>11</sup>B NMR (96 MHz, CD<sub>2</sub>Cl<sub>2</sub>): δ 28.84. <sup>27</sup>Al NMR (78 MHz, CD<sub>2</sub>Cl<sub>2</sub>): δ 102.34.

**Preparation of [(CH(CMe)<sub>2</sub>(NC<sub>6</sub>F<sub>5</sub>)<sub>2</sub>)BPh][AlCl<sub>4</sub>], **2.2**** The procedure used is the same as that described in *Method A* for the synthesis of **2.1** using 0.061 g (0.384 mmol) of PhBCl<sub>2</sub> and 0.200 g (0.380 mmol) of LAlCl<sub>2</sub>. An essentially quantitative yield of **2.2** was obtained. Colorless crystals of **2.2** were obtained from a CH<sub>2</sub>Cl<sub>2</sub>/hexane (1:1) mixture. Compound **2.2** decomposes at ~ 150 °C. MS (Cl<sup>+</sup>, CH<sub>4</sub>): *m/z* 517 ([M-(AlCl<sub>4</sub>)]<sup>+</sup>). HRMS (Cl, CH<sub>4</sub>): calcd for C<sub>23</sub>H<sub>13</sub>BF<sub>10</sub>N<sub>2</sub>, *m/z* 517.104844; found, 517.104966. <sup>1</sup>H NMR (300 MHz, CD<sub>3</sub>CN): δ 2.35 (s, 6H, Me), 6.660 (s, 1H, γ-CH), 7.12-7.28 (m, 5H, C<sub>6</sub>H<sub>5</sub>). <sup>19</sup>F NMR (282 MHz, CD<sub>3</sub>CN): δ -144.42 (m, 4F, *o*-F), -145.795 (m, 2F, *p*-F), -162.99 (m, 4F, *m*-F). <sup>11</sup>B NMR (96 MHz, CD<sub>3</sub>CN): δ 10.54. <sup>27</sup>Al NMR (78 MHz, CD<sub>2</sub>Cl<sub>2</sub>): δ 102.33.

**Preparation of  $(\text{CH}(\text{CMe})_2(\text{NC}_6\text{F}_5)_2)\text{B}=\text{O} \rightarrow \text{AlCl}_3$ , **2.3**.** Compound **2.1** (0.216 g, 0.335 mmol) was dissolved in 30 mL of  $\text{CH}_2\text{Cl}_2$  that contained an equimolar quantity of  $\text{H}_2\text{O}$ . The reaction mixture was layered with 20 mL of hexane, resulting in the formation of a small crop (~ 10% yield) of crystalline **2.3** (mp 160-161 °C). MS ( $\text{Cl}^+$ ,  $\text{CH}_4$ ):  $m/z$  457  $[\text{M}-(\text{AlCl}_3)]^+$ . HRMS (CI,  $\text{CH}_4$ ): calcd for  $\text{C}_{17}\text{H}_8\text{BF}_{10}\text{N}_2\text{O}$ ,  $m/z$  457.057001; found 457.058615.  $^1\text{H}$  NMR (300.14 MHz,  $\text{CD}_2\text{Cl}_2$ ):  $\delta$  2.49 (s, 6H, Me), 6.71 (s, 1H  $\gamma$ -CH).  $^{19}\text{F}$  NMR (282.39 MHz,  $\text{CD}_2\text{Cl}_2$ ):  $\delta$  -145.3 (m, 4F, *o*-F), -150.6 (t, 2F, *p*-F), -159.5 (m, 4F, *m*-F).  $^{11}\text{B}$  NMR (96.21 MHz,  $\text{CD}_2\text{Cl}_2$ ):  $\delta$  40.1.  $^{27}\text{Al}$  NMR (78.14 MHz,  $\text{CD}_2\text{Cl}_2$ ):  $\delta$  87.3.

**Preparation of  $[\text{CH}(\text{CMe})_2(\text{HNC}_6\text{F}_5)_2][\text{AlCl}_4]$ , **2.4**.** The procedure is the same as described for the synthesis of **2.3** using the same amount of **2.1**, and an excess of  $\text{H}_2\text{O}$ . Yield of crystalline **2.4** is approximately 0.034 g (15%). MS ( $\text{Cl}^+$ ,  $\text{CH}_4$ ):  $m/z$  431  $[\text{M}-(\text{AlCl}_4)]^+$ . HRMS (CI,  $\text{CH}_4$ ): calcd for  $\text{C}_{17}\text{H}_9\text{F}_{10}\text{N}_2$ ,  $m/z$  431.060606; found 431.061019.  $^1\text{H}$  NMR (300 MHz,  $\text{CD}_2\text{Cl}_2$ ):  $\delta$  2.86 (s, br, 6H, Me), 4.95 (s, br, 1H  $\gamma$ -CH), 5.83 (s, br, 2H, NH).  $^{19}\text{F}$  NMR (282 MHz,  $\text{CD}_2\text{Cl}_2$ ):  $\delta$  -143.83 (m, 4F, *o*-F), -150.54 (t, 2F, *p*-F), -160.10 (m, 4F, *m*-F).  $^{27}\text{Al}$  NMR (78 MHz,  $\text{CD}_2\text{Cl}_2$ ):  $\delta$  102.36.

**Preparation of  $[(\text{CH}(\text{CMe})_2(\text{NC}_6\text{F}_5)_2)\text{B}(\text{OH})][\text{AlCl}_4]$ , **2.5**.** On one occasion, during the synthesis of **2.3**, few crystals of **2.5** were isolated. Unfortunately, except for a single crystal X-ray diffraction study, no further characterization was possible.

**Preparation of ((CH(CMe)<sub>2</sub>(NC<sub>6</sub>F<sub>5</sub>)<sub>2</sub>)BO)<sub>2</sub>, 2.6.** Silver oxide (0.034 g, 0.014 mmol) was added to a 10 mL methylene chloride solution containing 0.100 g (0.014 mmol) of LBI<sub>2</sub> (**1.8**). The reaction mixture was allowed to stir overnight. After filtration through Celite®, the solvent volatiles were removed under reduced pressure yielding a pale yellow solid. Yield 0.053 g. One of the components of the resulting product mixture was identified as compound **2.6**. MS (CI<sup>+</sup>, CH<sub>4</sub>): *m/z* 913 ([M+H])<sup>+</sup>. HRMS (CI, CH<sub>4</sub>): calcd for C<sub>34</sub>H<sub>15</sub>B<sub>2</sub>F<sub>20</sub>N<sub>4</sub>O<sub>2</sub>, *m/z* 913.1062; found, 913.1069. <sup>1</sup>H NMR (300 MHz, CD<sub>2</sub>Cl<sub>2</sub>): δ 1.86 (s, 6H, Me), 5.32 (s, 1H, γ-CH). <sup>19</sup>F NMR (282 MHz, CD<sub>3</sub>CN): δ -144.53 (m, 4F, *o*-F), -159.02 (m, 2F, *p*-F), -164.86 (m, 4F, *m*-F). <sup>11</sup>B NMR (96 MHz, CD<sub>3</sub>CN): δ 0.06.

**Preparation of (η<sup>5</sup>-C<sub>5</sub>H<sub>5</sub>)Fe(CO)<sub>2</sub>B(η<sup>1</sup>-C<sub>5</sub>Me<sub>5</sub>)Cl, 2.7.** The salt K[Fe(CO)<sub>2</sub>(η<sup>5</sup>-C<sub>5</sub>H<sub>5</sub>)] (0.200 g, 0.926 mmol) was added to a 100 mL hexane solution containing 0.200 g (0.922 mmol) (η<sup>1</sup>-C<sub>5</sub>Me<sub>5</sub>)BCl<sub>2</sub> at 25 °C and the reaction mixture was stirred overnight. After filtration through Celite®, solvent and volatiles were removed under reduced pressure resulting in the formation of red, solid **2.7**. Compound **2.7** starts to decompose at ~ 70 °C. Yield 0.221 g (67%). MS (CI<sup>+</sup>, CH<sub>4</sub>): *m/z* 357 ([M-H]). HRMS (CI<sup>+</sup>, CH<sub>4</sub>): calcd for C<sub>17</sub>H<sub>19</sub>BClFeO<sub>2</sub>, *m/z* 357.0516; found, 357.0519. <sup>1</sup>H NMR (300 MHz, C<sub>6</sub>D<sub>6</sub>): δ 1.80 (s, 15H, C<sub>5</sub>Me<sub>5</sub>), 4.10 (s, 5H, C<sub>5</sub>H<sub>5</sub>). <sup>13</sup>C NMR (75 MHz, C<sub>6</sub>D<sub>6</sub>): δ 13.50 (s, C<sub>5</sub>Me<sub>5</sub>), 84.70 (s, C<sub>5</sub>H<sub>5</sub>) 126.25 (s, C<sub>5</sub>Me<sub>5</sub>), 214.04 (s, CO). <sup>11</sup>B NMR (96 MHz, C<sub>6</sub>D<sub>6</sub>): 111.34(s). IR (KBr disc) ν<sub>CO</sub> = 2000, 2052 cm<sup>-1</sup>.

**Preparation of  $[(\eta^5\text{-C}_5\text{H}_5)\text{Fe}(\text{CO})_2\text{B}(\eta^5\text{-C}_5\text{Me}_5)][\text{AlCl}_4]$ , **2.8**.** Aluminum trichloride (0.074 g, 0.558 mmol) was added to 30 mL of a methylene chloride solution containing 0.200 g (0.558 mmol) of **2.7** at 25 °C. The reaction mixture was allowed to stir overnight. Recrystallization from a  $\text{CH}_2\text{Cl}_2$ /hexane mixture resulted in the formation of a crop of pale yellow crystals. Yield 0.200 g (73%). Compound **2.8** decomposes at ~ 160 °C. MS ( $\text{Cl}^+$ ,  $\text{CH}_4$ ):  $m/z$  323 ( $[\text{M}-(\text{AlCl}_4)]^+$ ) HRMS ( $\text{Cl}^+$ ,  $\text{CH}_4$ ): calcd for  $\text{C}_{17}\text{H}_{20}\text{BFeO}_2$ ,  $m/z$  323.0906; found 323.0912.  $^1\text{H}$  NMR (300 MHz,  $\text{CD}_2\text{Cl}_2$ ):  $\delta$  2.21 (s, 15H,  $\text{C}_5\text{Me}_5$ ), 5.04 (s, 5H,  $\text{C}_5\text{H}_5$ ).  $^{13}\text{C}$  NMR (75 MHz,  $\text{CD}_2\text{Cl}_2$ ): 9.90 (s,  $\text{C}_5\text{Me}_5$ ), 83.59 (s,  $\text{C}_5\text{H}_5$ ), 115.5 ( $\text{C}_5\text{Me}_5$ ), 211.78 (s, CO).  $^{11}\text{B}$  NMR (96 MHz,  $\text{CD}_2\text{Cl}_2$ ):  $\delta$  -37.85 (s).  $^{27}\text{Al}$  NMR (78 MHz,  $\text{CD}_2\text{Cl}_2$ )  $\delta$  103.4 (s). IR (KBr disc)  $\nu_{\text{CO}}$  1962, 2020  $\text{cm}^{-1}$ .

**Preparation of  $(\text{CH}(\text{CMe})_2(\text{NC}_6\text{F}_5)_2)\text{B}(\text{OTf})_2$ , **3.1**.** Solid AgOTf (0.201 g, 0.782 mmol) was added to a solution of **1.6** (0.200 g, 0.391 mmol) in 30 mL of methylene chloride at ambient temperature. The reaction mixture was stirred overnight, following which it was filtered through Celite®. Removal of the solvent and volatiles under reduced pressure left pale yellow solid. Recrystallization of the crude product from a  $\text{CH}_2\text{Cl}_2$ /hexane (1:1) afforded colorless, crystalline **3.1** in 62% yield (0.179 g). The melting point of **3.1** is 194-197 °C. MS ( $\text{Cl}^+$ ,  $\text{CH}_4$ ):  $m/z$  738 ( $\text{M}^+$ ). HRMS ( $\text{Cl}^+$ ,  $\text{CH}_4$ ) calcd for  $\text{C}_{19}\text{H}_7\text{BF}_{16}\text{N}_2\text{O}_6\text{S}_2$ ,  $m/z$  737.9583; found, 737.9586;  $^1\text{H}$  NMR ( $\text{CD}_2\text{Cl}_2$ ):  $\delta$  2.21 (s, 6H,  $\text{CH}_3$ ), 6.18 (s, 1H,  $\gamma\text{-CH}$ ).  $^{11}\text{B}$  NMR ( $\text{CD}_2\text{Cl}_2$ ):  $\delta$  0.25 (sharp, s).  $^{19}\text{F}$  NMR ( $\text{CD}_2\text{Cl}_2$ ):  $\delta$  -78.33 (s, 6F, OTf), -144.01 (m, *o*-F, 4F), -151.54 (m, *p*-F, 2F), -161.13 (m, *m*-F, 4F).



**Preparation of [(CH(CMe)<sub>2</sub>(NC<sub>6</sub>F<sub>5</sub>)<sub>2</sub>)B(bipy)][2·OTf], **3.2**.** Solid 2,2'-bipyridine (0.011 g, 0.068 mmol) was added to a solution of **3.1** (0.050 g, 0.068 mmol) in 10 mL of methylene chloride at ambient temperature. After the reaction mixture had been stirred for 48 h, the resulting pale yellow precipitate was isolated by filtration. Crystals suitable for single-crystal X-ray diffraction study were obtained by recrystallization of this powder from a 50:45:5 methylene chloride/hexane/acetonitrile solvent mixture. Yield 0.051 g (84%). The melting point of **3.2** is 216-219 °C. MS (CI<sup>+</sup>, CH<sub>4</sub>): *m/z* 595 [M<sup>2+</sup>-H<sup>+</sup>]<sup>+</sup>. HRMS (CI<sup>+</sup>, CH<sub>4</sub>) calcd for C<sub>27</sub>H<sub>15</sub>BF<sub>10</sub>N<sub>4</sub>, *m/z* 596.1230; found, 596.1226; <sup>1</sup>H NMR (CD<sub>3</sub>CN): δ 2.32 (s, 6H, CH<sub>3</sub>), 6.66 (s, 1H, γ-CH), 8.33 (t, 2H, 5,5'-CH, <sup>3</sup>J<sub>HH</sub> = 6.9 Hz), 8.61 (d, 2H, 4,4'-CH, <sup>3</sup>J<sub>HH</sub> = 8.1 Hz), 8.83 (td, 2H, 3,3'-CH, <sup>3</sup>J<sub>HH</sub> = 8.1 Hz, <sup>5</sup>J<sub>HH</sub> = 1.3 Hz), 9.32 (m, br, 2H, 6,6'-CH); <sup>11</sup>B NMR (CD<sub>3</sub>CN): δ 6.44 (sharp, s). <sup>19</sup>F NMR (CD<sub>3</sub>CN): δ -79.73 (s, 6F, OTf), -143.55 (m, *o*-F, 4F), -151.05 (m, *p*-F, 2F), -159.36 (m, *m*-F, 4F).

**Preparation of [(CH(CMe)<sub>2</sub>(NC<sub>6</sub>F<sub>5</sub>)<sub>2</sub>)B(terpy)][2·OTf], **3.3**.** The procedure used is the same as that described for the synthesis of **3.2** using the same amount of **3.1**, and 0.015 (0.068 mmol) of 2,2':6',2''-terpyridine. The yield of pale yellow solid **3.3** was approximately 0.055 g (85%). Compound **3.3** decomposes at ~ 180 °C. MS (CI<sup>+</sup>, CH<sub>4</sub>): *m/z* 672 [M<sup>2+</sup>-H<sup>+</sup>]<sup>+</sup>. HRMS (CI<sup>+</sup>, CH<sub>4</sub>) calcd for C<sub>32</sub>H<sub>17</sub>BF<sub>10</sub>N<sub>5</sub>, *m/z* 672.1417; found, 672.1420; <sup>1</sup>H NMR (CD<sub>3</sub>CN): δ 2.17 (s, 6H, CH<sub>3</sub>), 6.45 (s, 1H, γ-CH), 7.72 (m, 1H, 6,4''-CH), 8.15-8.29 (m, 3H, 2,4'-2,5'-6,5''-CH), 8.61-8.65 (m, 2H, 3-,5-CH), 8.73-8.83 (m, 3H, 4-2,6'-6,6''-CH), 8.95-9.05 (m, 2H, 2,3'-6,3''-CH); <sup>11</sup>B NMR (CD<sub>3</sub>CN): δ 7.43

(sharp, s).  $^{19}\text{F}$  NMR ( $\text{CD}_3\text{CN}$ ):  $\delta$  -79.71 (s, 6F, OTf), -142.36 to -142.80 (m, *o*-F, 4F), -151.25 (t, *p*-F, 2F,  $^3J_{\text{FF}} = 21.4$  Hz), -159.04 to -159.78 (m, *m*-F, 4F).

**Preparation of  $[(\text{CH}(\text{CMe})_2(\text{NC}_6\text{F}_5)_2)\text{B}(\text{bipy})][2\text{-I}]$ , **3.4**.** The procedure used is the same as that described for the synthesis of **3.2** using 0.100 g (0.144 mmol) of **1.8** ( $\text{LBI}_2$ ) and 0.023 g (0.147 mmol) of 2,2'-bipyridine. The yield of red, solid **3.4** was 0.105 (86%). Compound **3.4** decomposes at  $\sim 250$  °C. MS ( $\text{Cl}^+$ ,  $\text{CH}_4$ ):  $m/z$  595 [ $\text{M}^{2+} - \text{H}^+$ ] $^+$ . HRMS ( $\text{Cl}^+$ ,  $\text{CH}_4$ ) calcd for  $\text{C}_{27}\text{H}_{15}\text{BF}_{10}\text{N}_4$ ,  $m/z$  596.1230; found, 596.1226;  $^1\text{H}$  NMR ( $\text{CD}_3\text{CN}$ ):  $\delta$  2.34 (s, 6H,  $\text{CH}_3$ ), 6.76 (s, 1H,  $\gamma\text{-CH}$ ), 8.35 (t, 2H, 5,5'-CH,  $^3J_{\text{HH}} = 6.8$  Hz), 8.87-8.88 (m, 4H, 3,3',4,4'-CH), 9.42 (m, br, 2H, 6,6'-CH);  $^{11}\text{B}$  NMR ( $\text{CD}_3\text{CN}$ ):  $\delta$  6.52 (sharp, s).  $^{19}\text{F}$  NMR ( $\text{CD}_3\text{CN}$ ):  $\delta$  -143.42 (m, *o*-F, 4F), -151.61 (m, *p*-F, 2F), -159.10 (m, *m*-F, 4F).

**Preparation of  $[(\text{CH}(\text{CMe})_2(\text{NC}_6\text{F}_5)_2)\text{B}(\text{bipy})][2\text{-Br}]$ , **3.5**.** The procedure used is the same as that described for the synthesis of **3.2** using 0.100 g (0.167 mmol) of **1.7** ( $\text{LBBr}_2$ ) and 0.026 g (0.167 mmol) of 2,2'-bipyridine. The yield of yellow, solid **3.5** was 0.107 (85%). Compound **3.5** decomposes at  $\sim 210$  °C. MS ( $\text{Cl}^+$ ,  $\text{CH}_4$ ):  $m/z$  595 [ $\text{M}^{2+} - \text{H}^+$ ] $^+$ . HRMS ( $\text{Cl}^+$ ,  $\text{CH}_4$ ) calcd for  $\text{C}_{27}\text{H}_{15}\text{BF}_{10}\text{N}_4$ ,  $m/z$  596.1230; found, 596.1226;  $^1\text{H}$  NMR ( $\text{CD}_3\text{CN}$ ):  $\delta$  2.35 (s, 6H,  $\text{CH}_3$ ), 6.81 (s, 1H,  $\gamma\text{-CH}$ ), 8.35 (t, 2H, 5,5'-CH,  $^3J_{\text{HH}} = 6.9$  Hz), 8.88 (td, 2H, 3,3'-CH,  $^3J_{\text{HH}} = 8.1$  Hz,  $^5J_{\text{HH}} = 1.2$  Hz), 9.22 (d, 2H, 4,4'-CH,  $^3J_{\text{HH}} = 8.1$  Hz), 9.46 (m, br, 2H, 6,6'-CH).  $^{11}\text{B}$  NMR ( $\text{CD}_3\text{CN}$ ):  $\delta$  6.55 (sharp, s).  $^{19}\text{F}$

NMR (CD<sub>3</sub>CN):  $\delta$  -143.51 (d, *o*-F, 4F,  $^3J_{\text{FF}} = 17.2$  Hz), -151.14 (t, *p*-F, 2F,  $^3J_{\text{FF}} = 21.7$  Hz), -159.38 (m, *m*-F, 4F).

**Preparation of (CH(CMe)<sub>2</sub>(NC<sub>6</sub>F<sub>5</sub>)<sub>2</sub>)Al(OTf)Me, 3.6.** Liquid Me<sub>3</sub>SiOTf (0.26 g, 1.170 mmol) was added to a 60 mL toluene solution containing 0.200 g (0.400 mmol) of LAlMeCl (**1.10**). The reaction mixture was stirred for 2 days at ambient temperature after which the solvent was reduced to approximately 25 mL and stored at -30 °C. Colorless crystals of **3.6** were isolated by filtration and obtained in 62% yield (0.15 g). The melting point of **3.6** is 145-146 °C. MS (Cl<sup>-</sup>, CH<sub>4</sub>):  $m/z$  620 [M]<sup>-</sup>. HRMS (Cl<sup>-</sup>, CH<sub>4</sub>) calcd for C<sub>19</sub>H<sub>10</sub>AlF<sub>13</sub>N<sub>2</sub>O<sub>3</sub>S,  $m/z$  620.0200; found, 620.0200; <sup>1</sup>H NMR (C<sub>6</sub>D<sub>6</sub>):  $\delta$  - 0.56 (s, 3H, Al-CH<sub>3</sub>), 1.22 (s, 6H, CH<sub>3</sub>), 4.76 (s, 1H,  $\gamma$ -CH). <sup>19</sup>F NMR (C<sub>6</sub>D<sub>6</sub>):  $\delta$  - 78.25 (s, 3F, OTF) -145.42 (d, *o*-F, 2F,  $^3J_{\text{FF}} = 17.8$  Hz) and -158.44 (d, *o*-F, 2F,  $^3J_{\text{FF}} = 24.0$  Hz), -153.49 (t, *p*-F, 2F,  $^3J_{\text{FF}} = 22.4$  Hz), -160.25 (m, *m*-F, 2F), - 160.89 (m, *m*-F, 2F).

**Preparation of (CH(CMe)<sub>2</sub>(NC<sub>6</sub>F<sub>5</sub>)<sub>2</sub>)Al(OTf)<sub>2</sub>, 3.7.** Solid AgOTf (0.680 g, 2.656 mmol) was added to a 40 mL acetonitrile solution containing 0.700 g (1.328 mmol) of **1.11** (LAlCl<sub>2</sub>) at ambient temperature in the absence of light. The solution mixture was left to stir for 2 days after which it was filtered through Celite® and solvent removed under reduced pressure resulting in 0.820 g (82%) of pale yellow solid **3.7**. The solid was used in subsequent reaction without further purification. The melting point of **3.7** is 93-96 °C. MS (Cl<sup>+</sup>, CH<sub>4</sub>):  $m/z$  755 [M+H]<sup>+</sup>. HRMS (Cl<sup>+</sup>, CH<sub>4</sub>) calcd for C<sub>19</sub>H<sub>8</sub>AlF<sub>16</sub>N<sub>2</sub>O<sub>6</sub>S<sub>2</sub>,  $m/z$  754.9384; found, 754.9389; <sup>1</sup>H NMR (CD<sub>3</sub>CN):  $\delta$  2.26 (s, 6H,

$\text{CH}_3$ ), 5.54 (s, 1H,  $\gamma\text{-CH}$ ).  $^{19}\text{F}$  NMR ( $\text{CD}_3\text{CN}$ ):  $\delta$  - 79.45 (s, 6F, OTf), - 145.68 to - 164.50 (m, 10F,  $\text{C}_6\text{F}_5$ ).  $^{27}\text{Al}$  NMR ( $\text{CD}_3\text{CN}$ ):  $\delta$  - 5.40.

**Preparation of  $(\text{CH}(\text{CMe})_2(\text{NC}_6\text{F}_5)_2)\text{Al}(\text{bipy})(\text{OTf})_2$ , **3.8**.** Solid 2,2'-bipyridine (0.021 g, 0.134 mmol) was added to a 10 mL methylene chloride solution containing 0.100 g (0.132 mmol) of **3.7**. The reaction mixture was left to stir overnight after which it was filtered. 10 mL of hexane was added to the resulting methylene chloride solution and the solvent mixture was left at ambient temperature to crystallize over the course of 2 days. Pale yellow crystalline solid **3.8** was collected. Yield 0.852 g (71%). Compound **3.8** decomposes at  $\sim 190^\circ\text{C}$ . MS ( $\text{Cl}^+$ ,  $\text{CH}_4$ ):  $m/z$  911  $[\text{M}+\text{H}]^+$ . HRMS ( $\text{Cl}^+$ ,  $\text{CH}_4$ ) calcd for  $\text{C}_{19}\text{H}_{16}\text{AlF}_{16}\text{N}_4\text{O}_6\text{S}_2$ ,  $m/z$  911.0071; found, 911.0064;  $^1\text{H}$  NMR ( $\text{CD}_3\text{CN}$ ):  $\delta$  1.62 to 2.74 (6H,  $\text{CH}_3$ ), 5.62, 5.64 and 5.65 (1H,  $\gamma\text{-CH}$ ), 7.03 to 9.30 (8H, bipy).  $^{19}\text{F}$  NMR ( $\text{CD}_3\text{CN}$ ):  $\delta$  -79.73 and - 80.56 (s, 6F, OTf), -143.98 to - 151.13 (m, *o*-F, 4F), -158.29 to - 161.04 (m, *p*-F, 2F), - 164.26 to - 164.78 (m, *m*-F, 4F).  $^{27}\text{Al}$  NMR ( $\text{CD}_3\text{CN}$ ):  $\delta$  13.09 (broad, s).

**Preparation of  $[(\text{CH}(\text{CMe})_2(\text{NC}_6\text{F}_5)_2)\text{Al}(\text{terpy})(\text{OTf})][\text{OTf}]$ , **3.9**.** Solid 2,2':6',2''-terpyridine (0.031 g, 0.133 mmol) was added to a 10 mL methylene chloride solution containing 0.100 g (0.132 mmol) of **3.7**. The reaction mixture was left to stir overnight after which it was filtered. 10 mL of hexane was added to the resulting methylene chloride solution and the solvent mixture was left at ambient temperature to crystallize over the course of 2 days. Pale yellow crystalline solid **3.9** was collected in 74% yield

(0.097 g). Compound **3.9** melts at 220-221 °C. MS ( $\text{Cl}^+$ ,  $\text{CH}_4$ ):  $m/z$  838  $[\text{M-OTf}]^+$ . HRMS ( $\text{Cl}^+$ ,  $\text{CH}_4$ ) calcd for  $\text{C}_{33}\text{H}_{18}\text{AlF}_{13}\text{N}_5\text{O}_3\text{S}$ ,  $m/z$  838.0738; found, 838.0732;  $^1\text{H}$  NMR ( $\text{CD}_3\text{CN}$ ):  $\delta$  1.65 and 1.67 (s, 3H,  $\text{CH}_3$ ), 2.25 and 2.26 (s, 3H,  $\text{CH}_3$ ), 5.84 and 5.85 (s, 1H,  $\gamma\text{-CH}$ ), 8.05 (m, 2H, 2,4'-6,4''-CH), 8.42 (m, 2H, 2,5'-6,5''-CH), 8.45 (m, 1H, 4-CH), 8.50 (m, 2H, 3-5-CH), 8.52 (m, 2H, 2,6'-6,6''-CH), 8.99 (m, 2H, 2,3'-6,3''-CH).  $^{19}\text{F}$  NMR ( $\text{CD}_3\text{CN}$ ):  $\delta$  -79.74 and - 80.68 (s, 6F, OTf), -144.64 and - 146.67 (d, *o*-F, 4F,  $^3J_{\text{FF}} = 16.9$  Hz), -154.74 and -158.40 (m, *p*-F, 2F), - 161.74 and - 163.04 (m, *m*-F, 4F).  $^{27}\text{Al}$  NMR ( $\text{CD}_3\text{CN}$ ):  $\delta$  17.72 (broad, s).

**Preparation of  $[(\text{CH}(\text{CMe})_2(\text{NC}_6\text{F}_5)_2)\text{Al}(\text{tren})][2\text{-OTf}]$ , **3.10**.** Liquid tris(2-aminoethyl)amine (0.020 g, 0.137 mmol) was added to 10 mL of an acetonitrile solution containing 0.100 g (0.132 mmol) of **3.7**. The reaction mixture was left to stir overnight. The solvent was removed under reduced pressure. The crude product was washed with three 1 mL portions of hexanes resulting in 0.092 g (77%) of pale green solid **3.10**. The crystals were obtained from a 1:1 methylene chloride/hexane solution at room temperature. Compound **3.10** decomposes at  $\sim 65$  °C. MS ( $\text{ES}^+$ ):  $m/z$  601  $[\text{M}^{2+}-\text{H}^+]^+$ . HRMS ( $\text{ESI}^+$ ) calcd for  $\text{C}_{23}\text{H}_{24}\text{AlF}_{10}\text{N}_6$ ,  $m/z$  601.1718; found, 601.1726.  $^1\text{H}$  NMR ( $\text{CD}_3\text{CN}$ ,  $[\text{M}] \cong 0.040$ ):  $\delta$  1.99 (s, 6H,  $\text{CH}_3$ ), 2.74 (t, 6H,  $\text{N-CH}_2$ ,  $^3J_{\text{HH}} = 5.4$  Hz), 2.97 (t, 6H,  $\text{H}_2\text{N-CH}_2$ ,  $^3J_{\text{HH}} = 5.7$  Hz), 5.34 (s, 1H,  $\gamma\text{-CH}$ ), 5.38 (s, br, 6H,  $\text{NH}_2$ ).  $^{13}\text{C}$  NMR ( $\text{CD}_3\text{CN}$ , saturated solution): 20.47 (s,  $\text{CH}_3$ ), 38.52 (s,  $\text{CH}_2\text{-NH}_2$ ), 52.25 (s,  $\text{N-CH}_2$ ), 98.74 (s,  $\text{H-C}(\gamma)$ ), 120.90 (q,  $\text{CF}_3$ ,  $^1J_{\text{CF}} = 319$  Hz), 137.04, 140.23 and 143.50 ( $\text{C}_6\text{F}_5$ ), 165.53 (s, C-N).  $^{19}\text{F}$  NMR ( $\text{CD}_3\text{CN}$ , saturated solution):  $\delta$  -79.65 (s, 6F, OTf), -151.72

(d, *o*-F, 4F,  $^3J_{\text{FF}} = 16.1$  Hz), - 163.64 (t, *p*-F, 2F,  $^3J_{\text{FF}} = 20.3$  Hz), - 166.02 (m, *m*-F, 4F).

$^{27}\text{Al}$  NMR ( $\text{CD}_3\text{CN}$ ): not observed.

**Preparation of  $(\text{CH}(\text{CMe})_2(\text{NC}_6\text{F}_5)_2)\text{Ga}(\text{OTf})_2$ , 3.11.** Solid AgOTf (0.685 g, 2.667 mmol) was added to a 40 mL acetonitrile solution containing 0.760 g (1.333 mmol) of LGaCl<sub>2</sub> (**1.14**) at ambient temperature in the absence of light. The solution mixture was left to stir for 2 days after which it was filtered through Celite® and solvent removed under reduced pressure resulting in 0.850 g of a white solid. The resulting solid contained AgCl impurities since it was sensitive to light. Removal of AgCl impurities was achieved by dissolution of the white solid in about 30 mL of methylene chloride followed by filtration and solvent removal under reduced pressure. Yield 0.52 g (49%). Crystals suitable for X-ray diffraction analysis were obtained from a methylene chloride/hexane (1:1) solution. However, the use of the AgCl-containing solid proved to produce higher overall yields in the subsequent reactions than if the purification was performed first. MS ( $\text{Cl}^+$ ,  $\text{CH}_4$ ):  $m/z$  798  $[\text{M}+\text{H}]^+$ . HRMS ( $\text{Cl}^+$ ,  $\text{CH}_4$ ) calcd for  $\text{C}_{19}\text{H}_8\text{GaF}_{16}\text{N}_2\text{O}_6\text{S}_2$ ,  $m/z$  796.8815; found, 796.8824.  $^1\text{H}$  NMR ( $\text{CD}_3\text{CN}$ ):  $\delta$  2.38 (s, 6H,  $\text{CH}_3$ ), 5.60 (s, 1H,  $\gamma\text{-CH}$ ).  $^{19}\text{F}$  NMR ( $\text{CD}_3\text{CN}$ ):  $\delta$  - 79.63 (s, 6F, OTf), (m, *o*-F, 4F), - 154.53 (m, *p*-F, 2F), -163.16 (m, *m*-F, 4F).

**Preparation of  $(\text{CH}(\text{CMe})_2(\text{NC}_6\text{F}_5)_2)\text{Ga}(\text{bipy})(\text{OTf})_2$ , 3.12.** The procedure used is the same as that described for the synthesis of **3.8** using 0.100 g (~ 0.125 mmol) of crude **3.11** and 0.020 g (0.128 mmol) of 2,2'-bipyridine and in the absence of light. The yield

of pale yellow solid **3.12** was 0.76g (63%). The crystals suitable for X-ray analysis were obtained from a methylene chloride/hexane (1:1) solvent mixture. Compound **3.12** decomposes at  $\sim 210$  °C. MS ( $\text{Cl}^+$ ,  $\text{CH}_4$ ):  $m/z$  953  $[\text{M}+\text{H}]^+$ . HRMS ( $\text{Cl}^+$ ,  $\text{CH}_4$ ) calcd for  $\text{C}_{29}\text{H}_{16}\text{GaF}_{16}\text{N}_4\text{O}_6\text{S}_2$ ,  $m/z$  952.9510; found, 952.9512;  $^1\text{H}$  NMR ( $\text{CD}_3\text{CN}$ ):  $\delta$  1.97 to 2.67 (6H,  $\text{CH}_3$ ), 5.70 to 6.62 (1H,  $\gamma\text{-CH}$ ), 7.31 to 9.13 (8H, bipy).  $^{19}\text{F}$  NMR ( $\text{CD}_3\text{CN}$ ):  $\delta$  -79.53 and -80.35 (s, 6F, OTf), -146.04 to -163.23 (10F,  $\text{C}_6\text{F}_5$ ).

**Preparation of  $[(\text{CH}(\text{CMe})_2(\text{NC}_6\text{F}_5)_2)\text{Ga}(\text{terpy})(\text{OTf})][\text{OTf}]$ , **3.13**.** The procedure used is the same as that described for the synthesis of **3.9** using 0.100 g ( $\sim 0.125$  mmol) of crude **3.11** and 0.030 g (0.128 mmol) 2,2':6',2''-terpyridine and in the absence of light. The yield of pale yellow solid **3.13** was 0.82g (63%). The crystals suitable for X-ray analysis were obtained from a methylene chloride/hexane (1:1) solvent mixture. The melting point of **3.13** is 219-221 °C. MS ( $\text{Cl}^+$ ,  $\text{CH}_4$ ):  $m/z$  880  $[\text{M}-\text{OTf}]^+$ . HRMS ( $\text{Cl}^+$ ,  $\text{CH}_4$ ) calcd for  $\text{C}_{33}\text{H}_{18}\text{GaF}_{13}\text{N}_5\text{O}_3\text{S}$ ,  $m/z$  880.0185; found, 880.0179.  $^1\text{H}$  NMR ( $\text{CD}_3\text{CN}$ ):  $\delta$  2.38 (s, 6H,  $\text{CH}_3$ ), 5.81 (s, 1H,  $\gamma\text{-CH}$ ), 8.16 (t, 2H, 2,4'-6,4''-CH,  $^3J_{\text{HH}} = 6.0$  Hz), 8.57 to 8.67 (m, 7H, 2,5'-6,5''-2,6'-6,6''-3-4-5-CH), 9.09 (d, 2H, 2,3'-6,3''-CH,  $^3J_{\text{HH}} = 5.4$  Hz).  $^{19}\text{F}$  NMR ( $\text{CD}_3\text{CN}$ ):  $\delta$  -80.15 (s, 6F, OTf), -146.70 (d, *o*-F, 4F,  $^3J_{\text{FF}} = 12.5$  Hz), -157.56 (m, *p*-F, 2F), -163.55 (m, *m*-F, 4F).

**Preparation of  $[(\text{CH}(\text{CMe})_2(\text{NC}_6\text{F}_5)_2)\text{Ga}(\text{tren})][2\text{-OTf}]$ , **3.14**.** Liquid tris(2-aminoethyl)amine (0.019 g, 0.130 mmol) was added to a 20 mL acetonitrile solution containing 0.100 g (0.125 mmol) of crude **3.11**. The reaction mixture was left to stir

overnight after which the solution was filtered and solvent removed under reduced pressure. The crude pale yellow solid was washed with three 2 mL portions of hexane resulting in 0.082 g (69%) of **3.14**. Compound **3.14** decomposes at  $\sim 100$  °C. The parent peak was not detected in the low-resolution mass spectrometry.  $^1\text{H}$  NMR ( $\text{CD}_3\text{CN}$ ,  $[\text{M}] \cong 0.034$ ):  $\delta$  2.27 (s, 6H,  $\text{CH}_3$ ), 2.60 (m, 6H,  $\text{N-CH}_2$ ), 2.85 (m, 6H,  $\text{H}_2\text{N-CH}_2$ ), 3.32 (s, br, 6H,  $\text{NH}_2$ ) 5.35 (s, 1H,  $\gamma\text{-CH}$ ),.  $^{13}\text{C}$  NMR ( $\text{CD}_3\text{CN}$ , saturated solution): 20.29 (s,  $\text{CH}_3$ ), 39.71 (s,  $\text{CH}_2\text{-NH}_2$ ), 54.68 (s,  $\text{N-CH}_2$ ), 98.58 (s,  $\text{H-C}(\gamma)$ ), 120.32 (m,  $\text{CF}_3$ ), 136.42, 139.91 and 143.35 ( $\text{C}_6\text{F}_5$ ), 165.36 (s,  $\text{C-N}$ ).  $^{19}\text{F}$  NMR ( $\text{CD}_3\text{CN}$ , saturated solution):  $\delta$  -79.87 (s, 6F, OTf), -151.83 (d, *o*-F, 4F,  $^3J_{\text{FF}} = 24.0$  Hz), - 163.81 (t, *p*-F, 2F,  $^3J_{\text{FF}} = 21.4$  Hz), - 166.18 (m, *m*-F, 4F).

**Preparation of  $[(\text{CH}(\text{CMe})_2(\text{NC}_6\text{F}_5)_2)\text{Al}(\text{OH})(\text{OTf})]_2$ , **3.15**.** On one occasion, few crystals of **3.15** formed inside an NMR tube in which **3.7** was dissolved in deuterated methylene chloride. Unfortunately, except for a single crystal X-ray diffraction study, no further characterization was possible.

**Preparation of  $[(\text{CH}(\text{CMe})_2(\text{NC}_6\text{F}_5)_2)\text{Ga}(\text{OTf})]_2\text{O}$ , **3.16**.** Solid AgOTf (0.901g, 3.506 mmol) was added to 40 mL of a acetonitrile solution containing 1.00 g (1.750 mmol) of  $\text{LGaCl}_2$  (**1.14**) in the absence of light. After 2 days the solution was filter and the resulting solid was extracted with 40 mL of methylene chloride that contained unknown amount of water. The resulting solution was stored at  $-30$  °C and a small crop of crystalline **3.16** formed (0.100g, 8.7 %). The melting point of **3.16** is 184-186 °C. MS



( $\text{Cl}^+$ ,  $\text{CH}_4$ ):  $m/z$  1314  $[\text{M}+\text{H}]^+$ . HRMS ( $\text{Cl}^+$ ,  $\text{CH}_4$ ) calcd for  $\text{C}_{36}\text{H}_{16}\text{Ga}_2\text{F}_{26}\text{N}_4\text{O}_7\text{S}_2$ ,  $m/z$  1311.8557; found, 1311.8558.  $^1\text{H}$  NMR ( $\text{CD}_3\text{CN}$ ):  $\delta$  1.93 and 2.11 (s, 12H,  $\text{CH}_3$ ), 5.83 (s, 2H,  $\gamma\text{-CH}$ ),  $^{19}\text{F}$  NMR ( $\text{CD}_3\text{CN}$ ):  $\delta$  -79.39 (s, 6F, OTf), - 146.92 and - 148.00 (m,  $o\text{-F}$ , 8F), -157.71 (m,  $p\text{-F}$ , 4F), - 163.75 and - 164.26 (m,  $m\text{-F}$ , 8F).

**Section 4.6.** *Figures and Tables of X-ray Crystallographic Data*

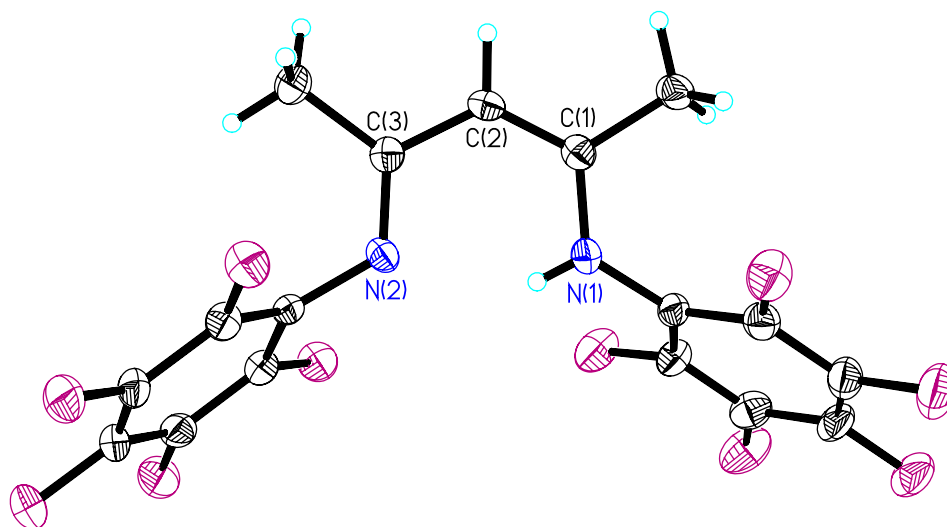


**Figure 4.1.** Molecular structure of CH(CMe<sub>2</sub>)<sub>2</sub>(NC<sub>6</sub>F<sub>5</sub>)(HNC<sub>6</sub>F<sub>5</sub>), 1.1, showing the atom number scheme for selected atoms. The thermal ellipsoids are shown at the 30 % probability level.

**Table 4.1. Crystal data and structure refinement for CH(CMe<sub>2</sub>)<sub>2</sub>(NC<sub>6</sub>F<sub>5</sub>) (HNC<sub>6</sub>F<sub>5</sub>), 1.1.**

Identification code	LH	
Empirical formula	C <sub>17</sub> H <sub>8</sub> F <sub>10</sub> N <sub>2</sub>	
Formula weight	430.25	
Temperature	153(2) K	
Wavelength	0.71069 Å	
Crystal system	triclinic	
Space group	P-1	
Unit cell dimensions	a = 7.212(5) Å	α = 98.129(5)°.
	b = 11.712(5) Å	β = 105.092(5)°.
	c = 12.704(5) Å	γ = 104.198(5)°.
Volume	980.0(9) Å <sup>3</sup>	
Z	2	
Density (calculated)	1.458 Mg/m <sup>3</sup>	
Absorption coefficient	0.154 mm <sup>-1</sup>	
F(000)	428	
Crystal size	0.15 x 0.10 x 0.10 mm <sup>3</sup>	
Theta range for data collection	1.70 to 27.48°.	
Index ranges	-7 ≤ h ≤ 9, -15 ≤ k ≤ 15, -16 ≤ l ≤ 14	
Reflections collected	7023	
Independent reflections	4443 [R(int) = 0.0398]	
Completeness to theta = 27.48°	98.7 %	
Absorption correction	Sphere	
Refinement method	Full-matrix least-squares on F <sup>2</sup>	
Data / restraints / parameters	4443 / 0 / 268	
Goodness-of-fit on F <sup>2</sup>	0.849	
Final R indices [I > 2σ(I)]	R1 = 0.0555, wR2 = 0.1307	
R indices (all data)	R1 = 0.1649, wR2 = 0.1582	
Largest diff. peak and hole	0.251 and -0.253 e.Å <sup>-3</sup>	

**Table 4.2. Selected bond lengths (Å) for CH(CMe<sub>2</sub>)<sub>2</sub>(NC<sub>6</sub>F<sub>5</sub>)(HNC<sub>6</sub>F<sub>5</sub>), 1.1.**

C(1)-C(2)	1.351(4)
C(2)-C(3)	1.430(4)
C(1)-N(1)	1.361(4)
C(3)-N(2)	1.313(4)

**Table 4.3. Selected bond angles (°) for CH(CMe<sub>2</sub>)<sub>2</sub>(NC<sub>6</sub>F<sub>5</sub>)(HNC<sub>6</sub>F<sub>5</sub>), 1.1.**

C(1)-C(2)-C(3)	126.7(3)
C(2)-C(1)-N(1)	121.5(3)
C(2)-C(3)-N(2)	119.0(3)

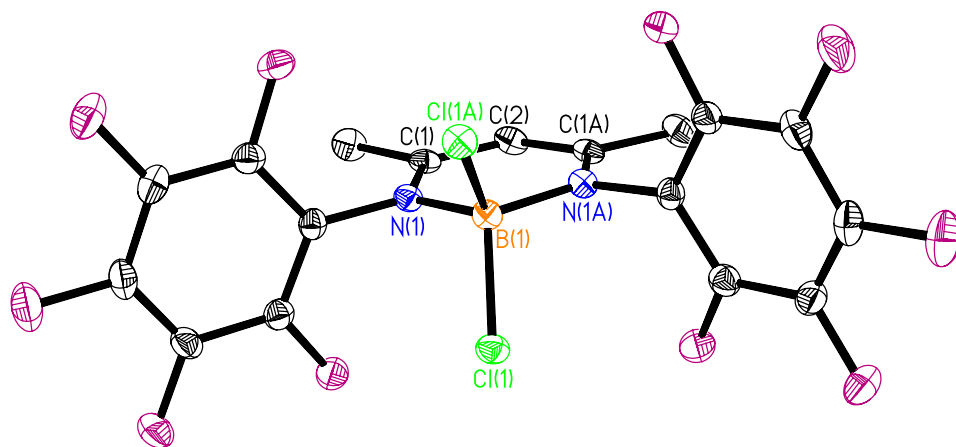


**Figure 4.2.** Molecular structure of  $(\text{CH}(\text{CMe}_2)_2(\text{NC}_6\text{F}_5)_2)\text{BCl}_2$ , 1.6, showing the atom number scheme for selected atoms. The thermal ellipsoids are shown at the 30 % probability level. All hydrogen atoms have been omitted for clarity.

**Table 4.4. Crystal data and structure refinement for (CH(CMe<sub>2</sub>)<sub>2</sub>(NC<sub>6</sub>F<sub>5</sub>)<sub>2</sub>)BCl<sub>2</sub>,****1.6.**

Identification code	LBCl2	
Empirical formula	C17 H7 B Cl2 F10 N2	
Formula weight	510.96	
Temperature	153(2) K	
Wavelength	0.71073 Å	
Crystal system	Orthorhombic	
Space group	Pbcn	
Unit cell dimensions	a = 21.996(4) Å	α = 90°.
	b = 7.2823(15) Å	β = 90°.
	c = 11.470(2) Å	γ = 90°.
Volume	1837.2(6) Å <sup>3</sup>	
Z	4	
Density (calculated)	1.847 Mg/m <sup>3</sup>	
Absorption coefficient	0.461 mm <sup>-1</sup>	
F(000)	1008	
Crystal size	0.03 x 0.03 x 0.03 mm <sup>3</sup>	
Theta range for data collection	2.95 to 27.49°.	
Index ranges	-28 ≤ h ≤ 28, -9 ≤ k ≤ 9, -14 ≤ l ≤ 14	
Reflections collected	3857	
Independent reflections	2104 [R(int) = 0.0273]	
Completeness to theta = 27.49°	99.7 %	
Absorption correction	Semi-empirical from equivalents	
Max. and min. transmission	0.986 and 0.986	
Refinement method	Full-matrix least-squares on F <sup>2</sup>	
Data / restraints / parameters	2104 / 6 / 147	
Goodness-of-fit on F <sup>2</sup>	1.049	
Final R indices [I > 2σ(I)]	R1 = 0.0388, wR2 = 0.0944	
R indices (all data)	R1 = 0.0710, wR2 = 0.1111	
Largest diff. peak and hole	0.318 and -0.273 e.Å <sup>-3</sup>	

**Table 4.5. Selected bond lengths (Å) for (CH(CMe<sub>2</sub>)<sub>2</sub>(NC<sub>6</sub>F<sub>5</sub>)<sub>2</sub>)BCl<sub>2</sub>, 1.6.**

C(1)-C(2)	1.377(3)
C(2)-C(1A)	1.377(3)
C(1)-N(1)	1.346(3)
C(1A)-N(1A)	1.346(3)
B(1)-N(1)	1.529(3)
B(1)-N(1A)	1.529(3)
B(1)-Cl(1)	1.882(2)
B(1)-Cl(1A)	1.882(2)

**Table 4.6 Selected bond angles (°) for (CH(CMe<sub>2</sub>)<sub>2</sub>(NC<sub>6</sub>F<sub>5</sub>)<sub>2</sub>)BCl<sub>2</sub>, 1.6.**

C(1)-C(2)-C(1A)	123.6(3)
C(2)-C(1)-N(1)	119.8(2)
C(2)-C(1A)-N(1A)	119.8(2)
C(1)-N(1)-B(1)	123.41(18)
C(1A)-N(1A)-B(1)	123.41(18)
N(1)-B(1)-N(1A)	109.9(2)
N(1)-B(1)-Cl(1)	110.37(6)
N(1)-B(1)-Cl(1A)	109.99(7)
N(1A)-B(1)-Cl(1)	109.99(7)
N(1A)-B(1)-Cl(1A)	110.37(6)
Cl(1)-B(1)-Cl(1A)	106.17(17)

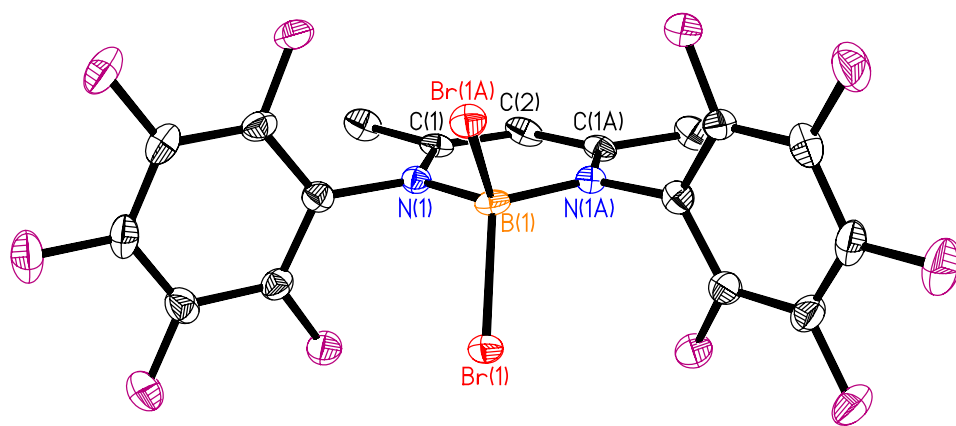


**Figure 4.3.** Molecular structure of  $(\text{CH}(\text{CMe}_2)_2(\text{NC}_6\text{F}_5)_2)\text{BBr}_2$ , 1.7, showing the atom number scheme for selected atoms. The thermal ellipsoids are shown at the 30 % probability level. All hydrogen atoms have been omitted for clarity.



**Table 4.7. Crystal data and structure refinement for (CH(CMe<sub>2</sub>)<sub>2</sub>(NC<sub>6</sub>F<sub>5</sub>)<sub>2</sub>)BBr<sub>2</sub>, 1.7.**

Identification code	LBBR2	
Empirical formula	C <sub>17</sub> H <sub>7</sub> B Br <sub>2</sub> F <sub>10</sub> N <sub>2</sub>	
Formula weight	599.88	
Temperature	153(2) K	
Wavelength	0.71069 Å	
Crystal system	Orthorhombic	
Space group	Pbna	
Unit cell dimensions	a = 7.457(5) Å	α = 90.000°.
	b = 11.566(5) Å	β = 90.000°.
	c = 22.002(5) Å	γ = 90.000°.
Volume	1897.6(16) Å <sup>3</sup>	
Z	4	
Density (calculated)	2.100 Mg/m <sup>3</sup>	
Absorption coefficient	4.376 mm <sup>-1</sup>	
F(000)	1152	
Crystal size	0.25 x 0.10 x 0.10 mm <sup>3</sup>	
Theta range for data collection	2.88 to 27.38°.	
Index ranges	-9 ≤ h ≤ 9, -14 ≤ k ≤ 14, -25 ≤ l ≤ 28	
Reflections collected	6513	
Independent reflections	2133 [R(int) = 0.0492]	
Completeness to theta = 27.38°	98.8 %	
Absorption correction	Semi-empirical from equivalents	
Max. and min. transmission	0.646 and 0.597	
Refinement method	Full-matrix least-squares on F <sup>2</sup>	
Data / restraints / parameters	2133 / 0 / 147	
Goodness-of-fit on F <sup>2</sup>	1.149	
Final R indices [I > 2σ(I)]	R1 = 0.0558, wR2 = 0.0990	
R indices (all data)	R1 = 0.0826, wR2 = 0.1068	
Largest diff. peak and hole	0.849 and -0.412 e.Å <sup>-3</sup>	

**Table 4.8. Selected bond lengths (Å) for (CH(CMe<sub>2</sub>)<sub>2</sub>(NC<sub>6</sub>F<sub>5</sub>)<sub>2</sub>)BBr<sub>2</sub>, 1.7.**

C(1)-C(2)	1.372(6)
C(2)-C(1A)	1.372(6)
C(1)-N(1)	1.345(6)
C(1A)-N(1A)	1.345(6)
B(1)-N(1)	1.519(6)
B(1)-N(1A)	1.519(6)
B(1)-Br(1)	2.054(5)
B(1)-Br(1A)	2.054(5)

**Table 4.9. Selected bond angles (°) for (CH(CMe<sub>2</sub>)<sub>2</sub>(NC<sub>6</sub>F<sub>5</sub>)<sub>2</sub>)BBr<sub>2</sub>, 1.7.**

C(1)-C(2)-C(1A)	123.6(7)
C(2)-C(1)-N(1)	119.4(5)
C(2)-C(1A)-N(1A)	119.4(5)
C(1)-N(1)-B(1)	123.2(5)
C(1A)-N(1A)-B(1)	123.2(5)
N(1)-B(1)-N(1A)	110.3(6)
N(1)-B(1)-Br(1)	110.54(16)
N(1)-B(1)-Br(1A)	110.20(16)
N(1A)-B(1)-Br(1)	110.20(16)
N(1A)-B(1)-Br(1A)	110.54(16)
Br(1)-B(1)-Br(1A)	104.9(4)

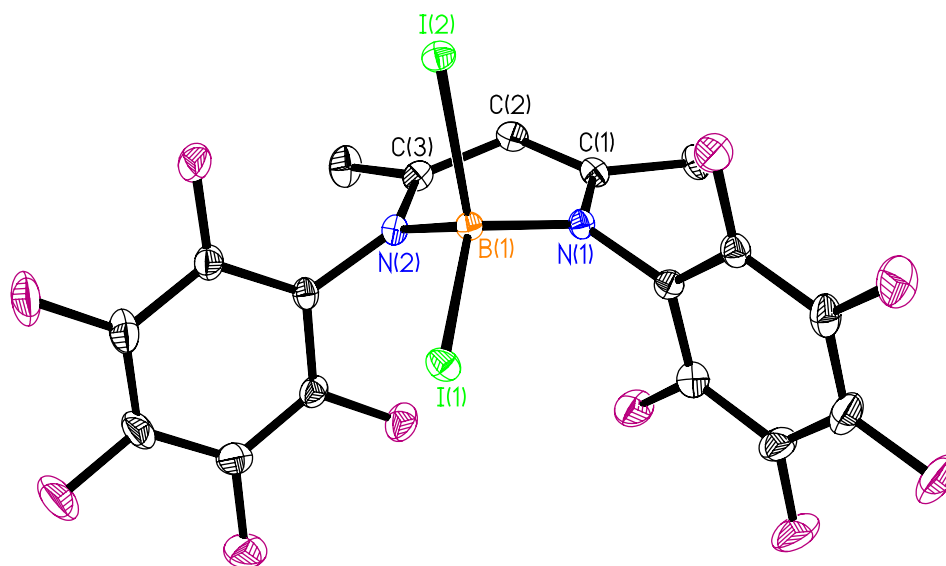


**Figure 4.4.** Molecular structure of  $(\text{CH}(\text{CMe}_2)_2(\text{NC}_6\text{F}_5)_2)\text{BI}_2$ , 1.8, showing the atom number scheme for selected atoms. The thermal ellipsoids are shown at the 30 % probability level. All hydrogen atoms have been omitted for clarity.

**Table 4.10. Crystal data and structure refinement for (CH(CMe<sub>2</sub>)<sub>2</sub>(NC<sub>6</sub>F<sub>5</sub>)<sub>2</sub>)BI<sub>2</sub>, 1.8.**

Identification code	LBI2	
Empirical formula	C17 H7 B F10 I2 N2	
Formula weight	693.86	
Temperature	153(2) K	
Wavelength	0.71069 Å	
Crystal system	Triclinic	
Space group	P-1	
Unit cell dimensions	a = 7.372(1) Å	a = 88.476(6)°.
	b = 11.711(2) Å	b = 87.593(6)°.
	c = 13.175(2) Å	g = 75.717(7)°.
Volume	1101.2(3) Å <sup>3</sup>	
Z	2	
Density (calculated)	2.093 Mg/m <sup>3</sup>	
Absorption coefficient	2.946 mm <sup>-1</sup>	
F(000)	648	
Crystal size	0.25 x 0.20 x 0.18 mm <sup>3</sup>	
Theta range for data collection	2.39 to 27.48°.	
Index ranges	-9<=h<=9, -14<=k<=15, -17<=l<=17	
Reflections collected	7532	
Independent reflections	5015 [R(int) = 0.0249]	
Completeness to theta = 27.48°	99.3 %	
Absorption correction	Semi-empirical from equivalents	
Max. and min. transmission	0.588 and 0.498	
Refinement method	Full-matrix least-squares on F <sup>2</sup>	
Data / restraints / parameters	5015 / 0 / 291	
Goodness-of-fit on F <sup>2</sup>	1.196	
Final R indices [I>2sigma(I)]	R1 = 0.0296, wR2 = 0.0946	
R indices (all data)	R1 = 0.0365, wR2 = 0.0978	
Largest diff. peak and hole	0.721 and -1.286 e.Å <sup>-3</sup>	

**Table 4.11. Selected bond lengths (Å) for (CH(CMe<sub>2</sub>)<sub>2</sub>(NC<sub>6</sub>F<sub>5</sub>)<sub>2</sub>)BI<sub>2</sub>, 1.8.**

C(1)-C(2)	1.391(5)
C(2)-C(3)	1.388(5)
C(1)-N(1)	1.337(5)
C(3)-N(2)	1.340(5)
B(1)-N(1)	1.533(4)
B(1)-N(2)	1.523(4)
B(1)-I(1)	2.222(4)
B(1)-I(2)	2.342(4)

**Table 4.12. Selected bond angles (°) for (CH(CMe<sub>2</sub>)<sub>2</sub>(NC<sub>6</sub>F<sub>5</sub>)<sub>2</sub>)BI<sub>2</sub>, 1.8.**

C(1)-C(2)-C(3)	120.5(4)
C(2)-C(1)-N(1)	119.8(3)
C(2)-C(3)-N(2)	119.3(3)
C(1)-N(1)-B(1)	118.3(3)
C(3)-N(2)-B(1)	118.5(3)
N(1)-B(1)-N(2)	108.1(3)
N(1)-B(1)-I(1)	112.6(2)
N(1)-B(1)-I(2)	107.9(2)
N(2)-B(1)-I(1)	113.0(2)
N(2)-B(1)-I(2)	107.0(2)
I(1)-B(1)-I(2)	108.04(15)

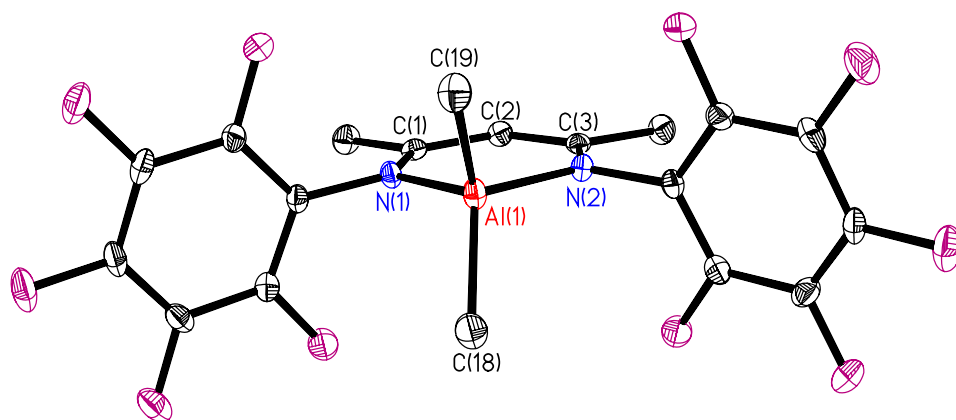


**Figure 4.5.** Molecular structure of  $(\text{CH}(\text{CMe}_2)_2(\text{NC}_6\text{F}_5)_2)\text{AlMe}_2$ , **1.9**, showing the atom number scheme for selected atoms. The thermal ellipsoids are shown at the 30 % probability level. All hydrogen atoms have been omitted for clarity.

**Table 4.13. Crystal data and structure refinement for (CH(CMe<sub>2</sub>)<sub>2</sub>(NC<sub>6</sub>F<sub>5</sub>)<sub>2</sub>)AlMe<sub>2</sub>, 1.9.**

Identification code	LAlMe2	
Empirical formula	C19 H13 Al Cl0 F10 N2	
Formula weight	486.29	
Temperature	153(2) K	
Wavelength	0.71069 Å	
Crystal system	Monoclinic	
Space group	P2 <sub>1</sub> /c	
Unit cell dimensions	a = 9.447(5) Å	α = 90.000(5)°.
	b = 24.498(5) Å	β = 95.396(5)°.
	c = 8.594(5) Å	γ = 90.000(5)°.
Volume	1980.1(16) Å <sup>3</sup>	
Z	4	
Density (calculated)	1.631 Mg/m <sup>3</sup>	
Absorption coefficient	0.204 mm <sup>-1</sup>	
F(000)	976	
Crystal size	0.20 x 0.17 x 0.15 mm <sup>3</sup>	
Theta range for data collection	2.90 to 27.44°.	
Index ranges	-12 ≤ h ≤ 9, -30 ≤ k ≤ 31, -11 ≤ l ≤ 10	
Reflections collected	11961	
Independent reflections	4484 [R(int) = 0.0512]	
Completeness to theta = 27.44°	99.2 %	
Absorption correction	None	
Max. and min. transmission	0.9700 and 0.9603	
Refinement method	Full-matrix least-squares on F <sup>2</sup>	
Data / restraints / parameters	4484 / 0 / 341	
Goodness-of-fit on F <sup>2</sup>	1.017	
Final R indices [I > 2σ(I)]	R1 = 0.0460, wR2 = 0.0881	
R indices (all data)	R1 = 0.1036, wR2 = 0.1058	
Largest diff. peak and hole	0.235 and -0.285 e.Å <sup>-3</sup>	

**Table 4.14. Selected bond lengths (Å) for (CH(CMe<sub>2</sub>)<sub>2</sub>(NC<sub>6</sub>F<sub>5</sub>)<sub>2</sub>)AlMe<sub>2</sub>, 1.9.**

C(1)-C(2)	1.395(3)
C(2)-C(3)	1.395(3)
C(1)-N(1)	1.333(3)
C(3)-N(2)	1.343(3)
Al(1)-N(1)	1.957(3)
Al(1)-N(2)	1.947(3)
Al(1)-C(18)	1.9263(18)
Al(1)-C(19)	1.917(2)

**Table 4.15. Selected bond angles (°) for (CH(CMe<sub>2</sub>)<sub>2</sub>(NC<sub>6</sub>F<sub>5</sub>)<sub>2</sub>)AlMe<sub>2</sub>, 1.9.**

C(1)-C(2)-C(3)	128.1(2)
C(2)-C(1)-N(1)	122.2(2)
C(2)-C(3)-N(2)	122.6(2)
C(1)-N(1)-Al(1)	126.75(15)
C(3)-N(2)-Al(1)	126.21(14)
N(1)-Al(1)-N(2)	93.99(8)
N(1)-Al(1)-C(18)	108.57(11)
N(1)-Al(1)-C(19)	110.37(11)
N(2)-Al(1)-C(18)	110.60(12)
N(2)-Al(1)-C(19)	111.56(11)
C(18)-Al(1)-C(19)	118.89(14)



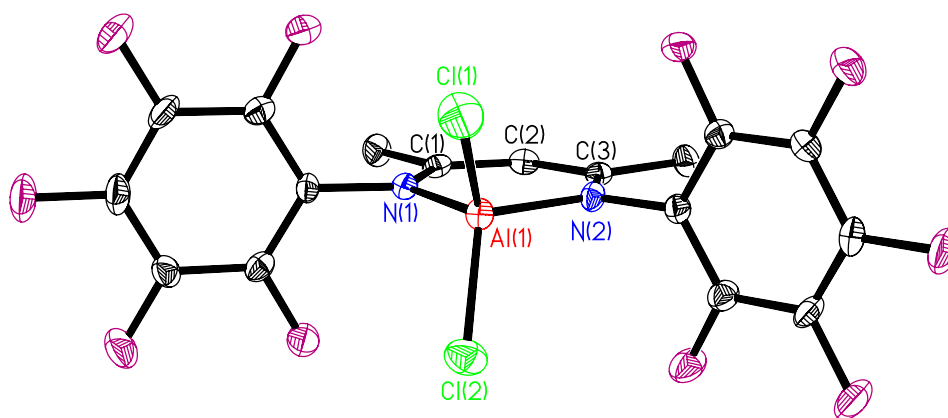


**Figure 4.6.** Molecular structure of  $(\text{CH}(\text{CMe}_2)_2(\text{NC}_6\text{F}_5)_2)\text{AlCl}_2$ , 1.11, showing the atom number scheme for selected atoms. The thermal ellipsoids are shown at the 30 % probability level. All hydrogen atoms have been omitted for clarity.

**Table 4.16. Crystal data and structure refinement for (CH(CMe<sub>2</sub>)<sub>2</sub>(NC<sub>6</sub>F<sub>5</sub>)<sub>2</sub>)AlCl<sub>2</sub>, 1.11.**

Identification code	LAlCl <sub>2</sub>	
Empirical formula	C <sub>17</sub> H <sub>7</sub> Al Cl <sub>2</sub> F <sub>10</sub> N <sub>2</sub>	
Formula weight	527.13	
Temperature	153(2) K	
Wavelength	0.71069 Å	
Crystal system	Monoclinic	
Space group	P2 <sub>1</sub> /c	
Unit cell dimensions	a = 11.224(5) Å	α = 90.000(5)°.
	b = 14.411(5) Å	β = 103.275(5)°.
	c = 12.659(5) Å	γ = 90.000(5)°.
Volume	1992.9(14) Å <sup>3</sup>	
Z	4	
Density (calculated)	1.757 Mg/m <sup>3</sup>	
Absorption coefficient	0.469 mm <sup>-1</sup>	
F(000)	1040	
Crystal size	0.31 x 0.25 x 0.17 mm <sup>3</sup>	
Theta range for data collection	3.10 to 27.48°.	
Index ranges	-14 ≤ h ≤ 14, -18 ≤ k ≤ 17, -16 ≤ l ≤ 16	
Reflections collected	7904	
Independent reflections	4525 [R(int) = 0.0800]	
Completeness to theta = 27.48°	99.0 %	
Absorption correction	None	
Max. and min. transmission	0.9244 and 0.8681	
Refinement method	Full-matrix least-squares on F <sup>2</sup>	
Data / restraints / parameters	4525 / 0 / 318	
Goodness-of-fit on F <sup>2</sup>	1.055	
Final R indices [I > 2σ(I)]	R <sub>1</sub> = 0.0779, wR <sub>2</sub> = 0.1590	
R indices (all data)	R <sub>1</sub> = 0.2094, wR <sub>2</sub> = 0.2099	
Extinction coefficient	0.0015(8)	
Largest diff. peak and hole	0.577 and -0.517 e.Å <sup>-3</sup>	

**Table 4.17. Selected bond lengths (Å) for (CH(CMe<sub>2</sub>)<sub>2</sub>(NC<sub>6</sub>F<sub>5</sub>)<sub>2</sub>)AlCl<sub>2</sub>, 1.11.**

C(1)-C(2)	1.379(7)
C(2)-C(3)	1.398(7)
C(1)-N(1)	1.352(6)
C(3)-N(2)	1.344(6)
Al(1)-N(1)	1.866(4)
Al(1)-N(2)	1.872(4)
Al(1)-Cl(1)	2.092(2)
Al(1)-Cl(2)	2.109(2)

**Table 4.18. Selected bond angles (°) for (CH(CMe<sub>2</sub>)<sub>2</sub>(NC<sub>6</sub>F<sub>5</sub>)<sub>2</sub>)AlCl<sub>2</sub>, 1.11.**

C(1)-C(2)-C(3)	130.1(5)
C(2)-C(1)-N(1)	122.0(5)
C(2)-C(3)-N(2)	120.8(5)
C(1)-N(1)-Al(1)	124.2(3)
C(3)-N(2)-Al(1)	125.1(3)
N(1)-Al(1)-N(2)	97.92(19)
N(1)-Al(1)-Cl(1)	112.48(15)
N(1)-Al(1)-Cl(2)	113.23(15)
N(2)-Al(1)-Cl(1)	111.88(15)
N(2)-Al(1)-Cl(2)	110.51(15)
Cl(1)-Al(1)-Cl(2)	110.32(10)

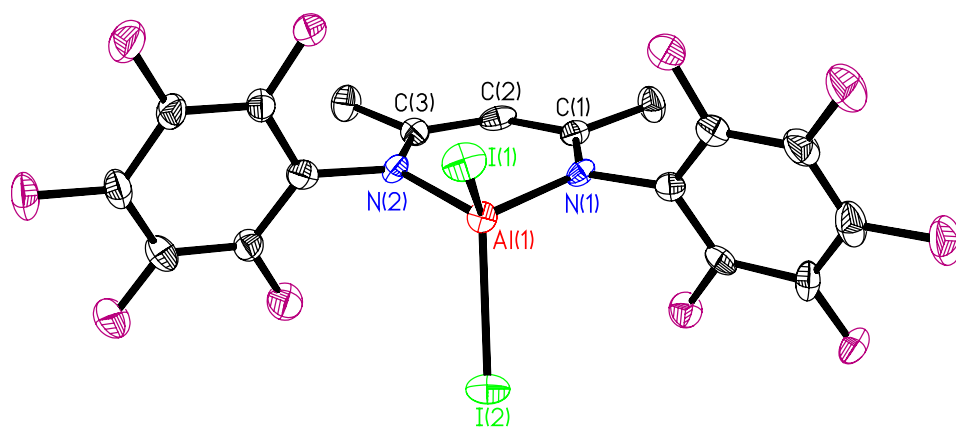


**Figure 4.7.** Molecular structure of  $(\text{CH}(\text{CMe}_2)_2(\text{NC}_6\text{F}_5)_2)\text{AlI}_2$ , **1.12**, showing the atom number scheme for selected atoms. The thermal ellipsoids are shown at the 30 % probability level. All hydrogen atoms have been omitted for clarity.

**Table 4.19. Crystal data and structure refinement for (CH(CMe<sub>2</sub>)<sub>2</sub>(NC<sub>6</sub>F<sub>5</sub>)<sub>2</sub>)AlI<sub>2</sub>, 1.12.**

Identification code	LAlI2	
Empirical formula	C17 H7 Al F10 I2 N2	
Formula weight	710.03	
Temperature	153(2) K	
Wavelength	0.71069 Å	
Crystal system	Monoclinic	
Space group	P2 <sub>1</sub> /n	
Unit cell dimensions	a = 7.077(5) Å	α = 90
	b = 24.719(5) Å	β = 97.352(5)°.
	c = 13.840(5) Å	γ = 90
Volume	2401(2) Å <sup>3</sup>	
Z	4	
Density (calculated)	1.964 Mg/m <sup>3</sup>	
Absorption coefficient	2.739 mm <sup>-1</sup>	
F(000)	1328	
Crystal size	0.20 x 0.16 x 0.12 mm <sup>3</sup>	
Theta range for data collection	2.22 to 25.50°.	
Index ranges	-8 ≤ h ≤ 8, -29 ≤ k ≤ 29, -15 ≤ l ≤ 16	
Reflections collected	18456	
Independent reflections	4463 [R(int) = 0.1408]	
Completeness to theta = 25.50°	99.8 %	
Absorption correction	None	
Max. and min. transmission	0.7346 and 0.6103	
Refinement method	Full-matrix least-squares on F <sup>2</sup>	
Data / restraints / parameters	4463 / 0 / 290	
Goodness-of-fit on F <sup>2</sup>	0.975	
Final R indices [I > 2σ(I)]	R1 = 0.0547, wR2 = 0.1290	
R indices (all data)	R1 = 0.1189, wR2 = 0.1474	
Extinction coefficient	0.0006(3)	
Largest diff. peak and hole	0.808 and -0.979 e.Å <sup>-3</sup>	

**Table 4.20. Selected bond lengths (Å) for (CH(CMe<sub>2</sub>)<sub>2</sub>(NC<sub>6</sub>F<sub>5</sub>)<sub>2</sub>)AlI<sub>2</sub>, 1.12.**

C(1)-C(2)	1.385(12)
C(2)-C(3)	1.401(12)
C(1)-N(1)	1.362(11)
C(3)-N(2)	1.341(10)
Al(1)-N(1)	1.849(7)
Al(1)-N(2)	1.868(7)
Al(1)-I(1)	2.499(3)
Al(1)-I(2)	2.517(3)

**Table 4.21. Selected bond angles (°) for (CH(CMe<sub>2</sub>)<sub>2</sub>(NC<sub>6</sub>F<sub>5</sub>)<sub>2</sub>)AlI<sub>2</sub>, 1.12.**

C(1)-C(2)-C(3)	128.3(8)
C(2)-C(1)-N(1)	121.8(8)
C(2)-C(3)-N(2)	122.5(8)
C(1)-N(1)-Al(1)	124.6(6)
C(3)-N(2)-Al(1)	124.0(6)
N(1)-Al(1)-N(2)	98.0(3)
N(1)-Al(1)-I(1)	114.8(2)
N(1)-Al(1)-I(2)	109.8(2)
N(2)-Al(1)-I(1)	112.1(2)
N(2)-Al(1)-I(2)	115.0(2)
I(1)-Al(1)-I(2)	107.12(10)

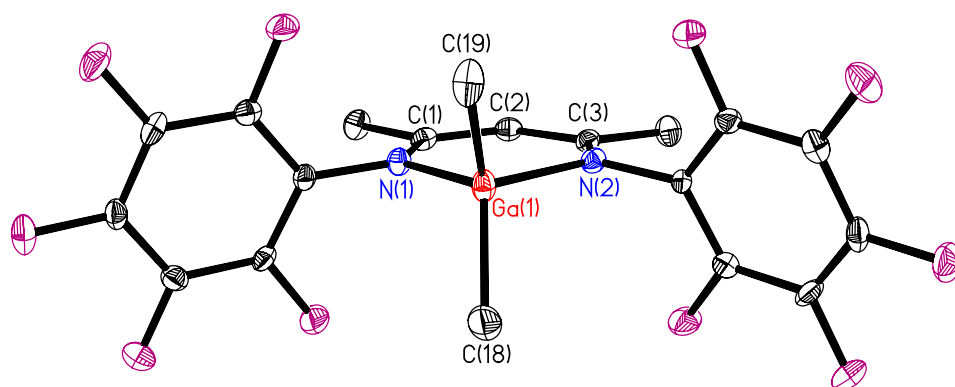


**Figure 4.8.** Molecular structure of  $(\text{CH}(\text{CMe}_2)_2(\text{NC}_6\text{F}_5)_2)\text{GaMe}_2$ , 1.13, showing the atom number scheme for selected atoms. The thermal ellipsoids are shown at the 30 % probability level. All hydrogen atoms have been omitted for clarity.

**Table 4.22. Crystal data and structure refinement for [CH(CMe<sub>2</sub>)<sub>2</sub>(NC<sub>6</sub>F<sub>5</sub>)<sub>2</sub>]GaMe<sub>2</sub>, 1.13**

Identification code	LGaMe2	
Empirical formula	C19 H13 F10 Ga N2	
Formula weight	529.03	
Temperature	153(2) K	
Wavelength	0.71069 Å	
Crystal system	Orthorhombic	
Space group	Pca2 <sub>1</sub>	
Unit cell dimensions	a = 25.347(5) Å	α = 90.000(5)°.
	b = 9.330(5) Å	β = 90.000(5)°.
	c = 8.323(5) Å	γ = 90.000(5)°.
Volume	1968.3(16) Å <sup>3</sup>	
Z	4	
Density (calculated)	1.785 Mg/m <sup>3</sup>	
Absorption coefficient	1.500 mm <sup>-1</sup>	
F(000)	1048	
Crystal size	0.21 x 0.16 x 0.14 mm <sup>3</sup>	
Theta range for data collection	2.93 to 26.50°.	
Index ranges	-31 ≤ h ≤ 31, -11 ≤ k ≤ 10, -10 ≤ l ≤ 10	
Reflections collected	7250	
Independent reflections	3845 [R(int) = 0.0334]	
Completeness to theta = 26.50°	99.7 %	
Absorption correction	None	
Max. and min. transmission	0.8175 and 0.7435	
Refinement method	Full-matrix least-squares on F <sup>2</sup>	
Data / restraints / parameters	3845 / 1 / 292	
Goodness-of-fit on F <sup>2</sup>	1.077	
Final R indices [I > 2σ(I)]	R1 = 0.0392, wR2 = 0.0785	
R indices (all data)	R1 = 0.0577, wR2 = 0.0847	
Absolute structure parameter	0.582(14)	
Extinction coefficient	0.0032(5)	
Largest diff. peak and hole	0.380 and -0.518 e.Å <sup>-3</sup>	



**Table 4.23. Selected bond lengths (Å) for (CH(CMe<sub>2</sub>)<sub>2</sub>(NC<sub>6</sub>F<sub>5</sub>)<sub>2</sub>)GaMe<sub>2</sub>, 1.13.**

C(1)-C(2)	1.381(6)
C(2)-C(3)	1.411(6)
C(1)-N(1)	1.334(5)
C(3)-N(2)	1.330(5)
Ga(1)-N(1)	1.987(3)
Ga(1)-N(2)	2.007(3)
Ga(1)-C(18)	1.956(6)
Ga(1)-C(19)	1.967(5)

**Table 4.24. Selected bond angles (°) for (CH(CMe<sub>2</sub>)<sub>2</sub>(NC<sub>6</sub>F<sub>5</sub>)<sub>2</sub>)GaMe<sub>2</sub>, 1.13.**

C(1)-C(2)-C(3)	129.8(4)
C(2)-C(1)-N(1)	123.1(3)
C(2)-C(3)-N(2)	122.3(4)
C(1)-N(1)-Ga(1)	126.1(3)
C(3)-N(2)-Ga(1)	126.0(3)
N(1)-Ga(1)-N(2)	92.49(13)
N(1)-Ga(1)-C(18)	109.13(18)
N(1)-Ga(1)-C(19)	109.43(17)
N(2)-Ga(1)-C(18)	106.73(18)
N(2)-Ga(1)-C(19)	110.66(18)
C(18)-Ga(1)-C(19)	123.9(2)

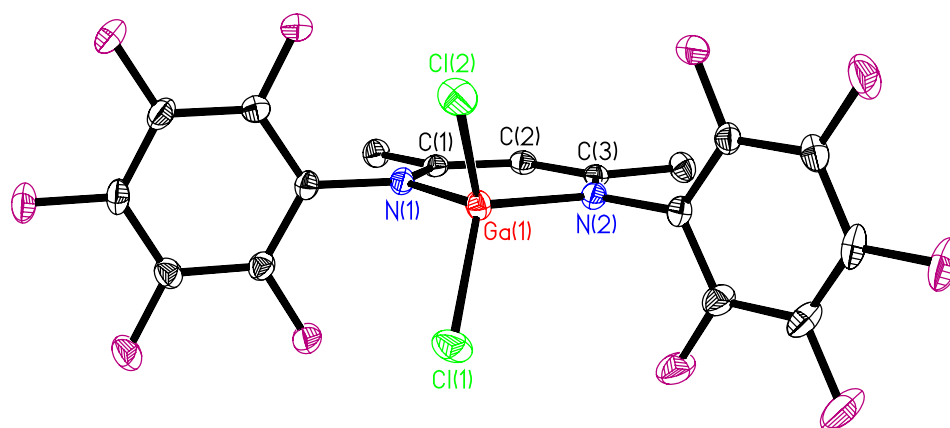


**Figure 4.9.** Molecular structure of  $(\text{CH}(\text{CMe}_2)_2(\text{NC}_6\text{F}_5)_2)\text{GaCl}_2$ , 1.14, showing the atom number scheme for selected atoms. The thermal ellipsoids are shown at the 30 % probability level. All hydrogen atoms have been omitted for clarity.

**Table 4.25. Crystal data and structure refinement for (CH(CMe<sub>2</sub>)<sub>2</sub>(NC<sub>6</sub>F<sub>5</sub>)<sub>2</sub>)GaCl<sub>2</sub>, 1.14.**

Identification code	LGaCl2	
Empirical formula	C17 H7 Cl2 F10 Ga N2	
Formula weight	569.87	
Temperature	153(2) K	
Wavelength	0.71069 Å	
Crystal system	Monoclinic	
Space group	P2 <sub>1</sub> /c	
Unit cell dimensions	a = 11.198(5) Å	a = 90.000°.
	b = 14.415(5) Å	b = 102.798(5)°.
	c = 12.683(5) Å	g = 90.000°.
Volume	1996.4(14) Å <sup>3</sup>	
Z	4	
Density (calculated)	1.896 Mg/m <sup>3</sup>	
Absorption coefficient	1.745 mm <sup>-1</sup>	
F(000)	1112	
Crystal size	0.25 x 0.20 x 0.20 mm <sup>3</sup>	
Theta range for data collection	2.17 to 27.44°.	
Index ranges	-14 ≤ h ≤ 14, -18 ≤ k ≤ 16, -16 ≤ l ≤ 16	
Reflections collected	8084	
Independent reflections	4537 [R(int) = 0.0266]	
Completeness to theta = 27.44°	99.6 %	
Absorption correction	Semi-empirical from equivalents	
Max. and min. transmission	0.705 and 0.664	
Refinement method	Full-matrix least-squares on F <sup>2</sup>	
Data / restraints / parameters	4537 / 0 / 291	
Goodness-of-fit on F <sup>2</sup>	1.031	
Final R indices [I > 2σ(I)]	R1 = 0.0348, wR2 = 0.0792	
R indices (all data)	R1 = 0.0569, wR2 = 0.0892	
Largest diff. peak and hole	0.602 and -0.455 e.Å <sup>-3</sup>	

**Table 4.26. Selected bond lengths (Å) for (CH(CMe<sub>2</sub>)<sub>2</sub>(NC<sub>6</sub>F<sub>5</sub>)<sub>2</sub>)GaCl<sub>2</sub>, 1.14.**

C(1)-C(2)	1.393(3)
C(2)-C(3)	1.387(3)
C(1)-N(1)	1.345(3)
C(3)-N(2)	1.349(3)
Ga(1)-N(1)	1.9126(19)
Ga(1)-N(2)	1.9062(19)
Ga(1)-Cl(1)	2.1502(8)
Ga(1)-Cl(2)	2.1201(8)

**Table 4.27. Selected bond angles (°) for (CH(CMe<sub>2</sub>)<sub>2</sub>(NC<sub>6</sub>F<sub>5</sub>)<sub>2</sub>)GaCl<sub>2</sub>, 1.14.**

C(1)-C(2)-C(3)	130.2(2)
C(2)-C(1)-N(1)	122.4(2)
C(2)-C(3)-N(2)	123.5(2)
C(1)-N(1)-Ga(1)	122.8(2)
C(3)-N(2)-Ga(1)	121.92(15)
N(1)-Ga(1)-N(2)	99.02(8)
N(1)-Ga(1)-Cl(1)	110.97(6)
N(1)-Ga(1)-Cl(2)	110.69(7)
N(2)-Ga(1)-Cl(1)	112.84(7)
N(2)-Ga(1)-Cl(2)	113.51(6)
Cl(1)-Ga(1)-Cl(2)	109.47(4)

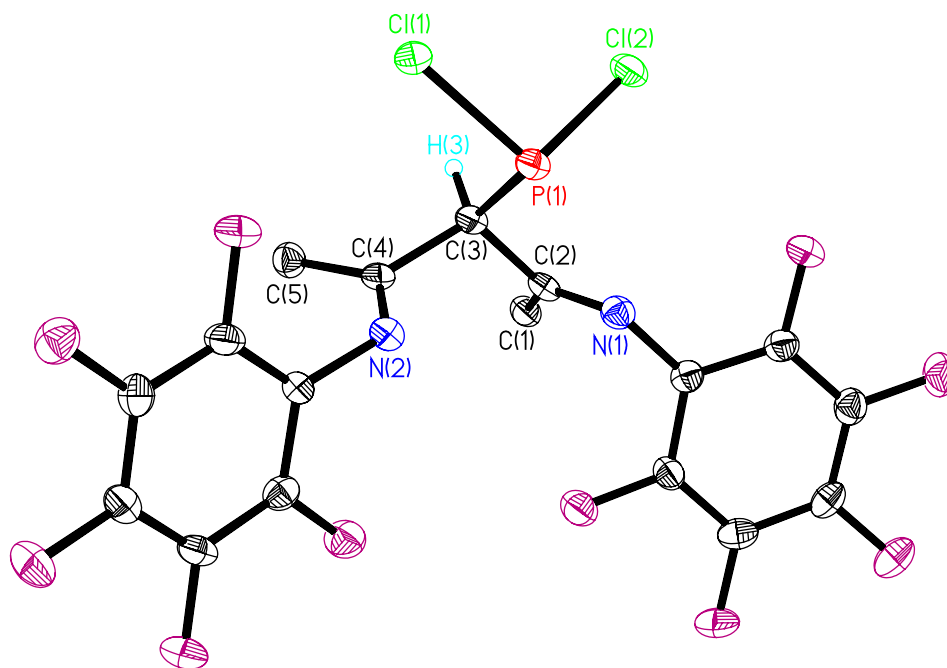


**Figure 4.10.** Molecular structure of  $(\text{Cl}_2\text{P})\text{CH}(\text{CMe}_2)_2(\text{NC}_6\text{F}_5)_2$ , 1.16a, showing the atom number scheme for selected atoms. The thermal ellipsoids are shown at the 30 % probability level. All hydrogen atoms, except that on the  $\gamma$ -carbon, have been omitted for clarity.

**Table 4.28. Crystal data and structure refinement for (Cl<sub>2</sub>P)CH(CMe<sub>2</sub>)<sub>2</sub>(NC<sub>6</sub>F<sub>5</sub>)<sub>2</sub>, 1.16a.**

Identification code	LPCl2	
Empirical formula	C17 H7 Cl2 F10 N2 P	
Formula weight	531.12	
Temperature	153(2) K	
Wavelength	0.71069 Å	
Crystal system	Orthorhombic	
Space group	Pna2 <sub>1</sub>	
Unit cell dimensions	a = 23.649(5) Å	α = 90.000(5)°.
	b = 6.050(5) Å	β = 90.000(5)°.
	c = 13.383(5) Å	γ = 90.000(5)°.
Volume	1914.8(18) Å <sup>3</sup>	
Z	4	
Density (calculated)	1.842 Mg/m <sup>3</sup>	
Absorption coefficient	0.526 mm <sup>-1</sup>	
F(000)	1048	
Crystal size	0.50 x 0.30 x 0.10 mm <sup>3</sup>	
Theta range for data collection	2.30 to 27.50°.	
Index ranges	-30 ≤ h ≤ 30, -7 ≤ k ≤ 7, -17 ≤ l ≤ 17	
Reflections collected	6534	
Independent reflections	3808 [R(int) = 0.0423]	
Completeness to theta = 27.50°	99.0 %	
Absorption correction	Semi-empirical from equivalents	
Max. and min. transmission	0.949 and 0.827	
Refinement method	Full-matrix least-squares on F <sup>2</sup>	
Data / restraints / parameters	3808 / 1 / 292	
Goodness-of-fit on F <sup>2</sup>	0.971	
Final R indices [I > 2σ(I)]	R1 = 0.0457, wR2 = 0.0865	
R indices (all data)	R1 = 0.0859, wR2 = 0.1001	
Absolute structure parameter	0.52(8)	
Largest diff. peak and hole	0.374 and -0.308 e.Å <sup>-3</sup>	

**Table 4.29. Selected bond lengths (Å) for (Cl<sub>2</sub>P)(CH(CMe<sub>2</sub>)<sub>2</sub>(NC<sub>6</sub>F<sub>5</sub>)<sub>2</sub>, 1.16a.**

C(1)-C(2)	1.495(6)
C(2)-C(3)	1.514(5)
C(3)-C(4)	1.532(5)
C(4)-C(5)	1.494(6)
C(2)-N(1)	1.281(5)
C(4)-N(2)	1.281(5)
C(3)-P(1)	1.854(5)
P(1)-Cl(1)	2.0747(15)
P(1)-Cl(2)	2.0675(15)

**Table 4.30. Selected bond angles (°) for (Cl<sub>2</sub>P)CH(CMe<sub>2</sub>)<sub>2</sub>(NC<sub>6</sub>F<sub>5</sub>)<sub>2</sub>, 1.16a.**

C(2)-C(3)-C(4)	115.5(3)
C(2)-C(3)-P(1)	107.3(3)
C(4)-C(3)-P(1)	107.0(3)
C(3)-P(1)-Cl(1)	96.01(14)
C(3)-P(1)-Cl(2)	96.67(14)
Cl(1)-P(1)-Cl(2)	99.70(7)

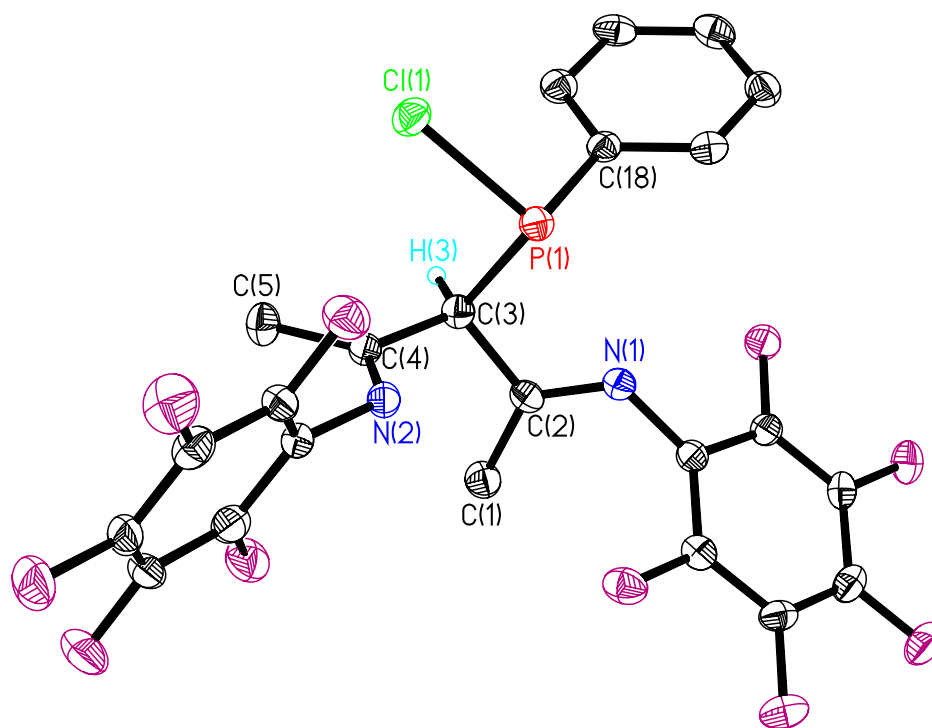


**Figure 4.11.** Molecular structure of (ClPhP)CH(CMe<sub>2</sub>)<sub>2</sub>(NC<sub>6</sub>F<sub>5</sub>)<sub>2</sub>, 1.17a, showing the atom number scheme for selected atoms. The thermal ellipsoids are shown at the 30 % probability level. All hydrogen atoms, except that on the  $\gamma$ -carbon, have been omitted for clarity.



**Table 4.31. Crystal data and structure refinement for (ClPhP)CH(CMe<sub>2</sub>)<sub>2</sub> (NC<sub>6</sub>F<sub>5</sub>)<sub>2</sub>, 1.17a.**

Identification code	LPhCl	
Empirical formula	C <sub>23</sub> H <sub>12</sub> Cl F <sub>10</sub> N <sub>2</sub> P	
Formula weight	572.77	
Temperature	153(2) K	
Wavelength	0.71069 Å	
Crystal system	Triclinic	
Space group	P-1	
Unit cell dimensions	a = 8.958(5) Å	α = 98.124(5)°.
	b = 11.590(5) Å	β = 93.164(5)°.
	c = 11.888(5) Å	γ = 109.558(5)°.
Volume	1144.4(9) Å <sup>3</sup>	
Z	2	
Density (calculated)	1.662 Mg/m <sup>3</sup>	
Absorption coefficient	0.335 mm <sup>-1</sup>	
F(000)	572	
Crystal size	0.20 x 0.17 x 0.15 mm <sup>3</sup>	
Theta range for data collection	2.34 to 27.50°.	
Index ranges	-11 ≤ h ≤ 8, -14 ≤ k ≤ 14, -15 ≤ l ≤ 15	
Reflections collected	7915	
Independent reflections	5207 [R(int) = 0.0354]	
Completeness to theta = 27.50°	99.1 %	
Absorption correction	Semi-empirical from equivalents	
Max. and min. transmission	0.951 and 0.935	
Refinement method	Full-matrix least-squares on F <sup>2</sup>	
Data / restraints / parameters	5207 / 0 / 336	
Goodness-of-fit on F <sup>2</sup>	0.984	
Final R indices [I > 2σ(I)]	R1 = 0.0490, wR2 = 0.1023	
R indices (all data)	R1 = 0.1267, wR2 = 0.1313	
Largest diff. peak and hole	0.278 and -0.334 e.Å <sup>-3</sup>	

**Table 4.32. Selected bond lengths (Å) for (ClPhP)CH(CMe<sub>2</sub>)<sub>2</sub>(NC<sub>6</sub>F<sub>5</sub>)<sub>2</sub>, 1.17a.**

C(1)-C(2)	1.493(6)
C(2)-C(3)	1.514(4)
C(3)-C(4)	1.413(4)
C(4)-C(5)	1.500(4)
C(2)-N(1)	1.273(3)
C(4)-N(2)	1.272(3)
C(3)-P(1)	1.876(3)
C(18)-P(1)	1.831(3)
P(1)-Cl(1)	2.1196(12)

**Table 4.33. Selected bond angles (°) for (ClPhP)CH(CMe<sub>2</sub>)<sub>2</sub>(NC<sub>6</sub>F<sub>5</sub>)<sub>2</sub>, 1.17a.**

C(2)-C(3)-C(4)	112.1(2)
C(2)-C(3)-P(1)	106.18(18)
C(4)-C(3)-P(1)	108.34(19)
C(3)-P(1)-C(18)	103.92(13)
C(3)-P(1)-Cl(1)	95.93(9)
C(18)-P(1)-Cl(1)	98.04(9)

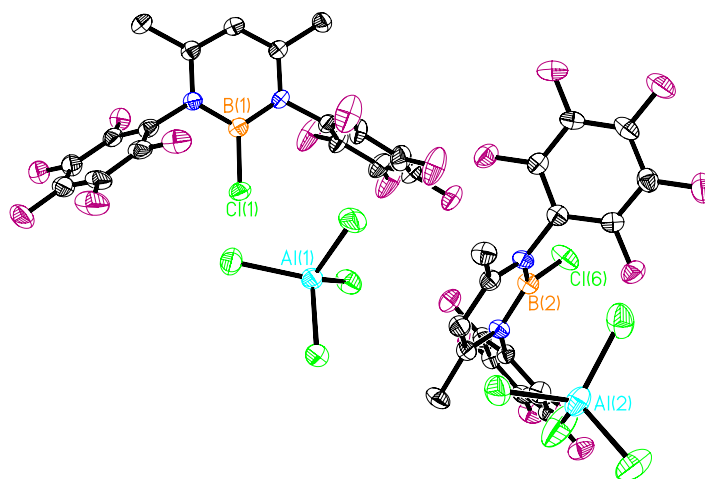


Figure 4.12. Molecular structure of  $[(\text{CH}(\text{CMe}_2)_2(\text{NC}_6\text{F}_5)_2)\text{BCl}][\text{AlCl}_4]$ , 2.1, showing the atom number scheme for selected atoms. The thermal ellipsoids are shown at the 30 % probability level. All hydrogen atoms have been omitted for clarity.

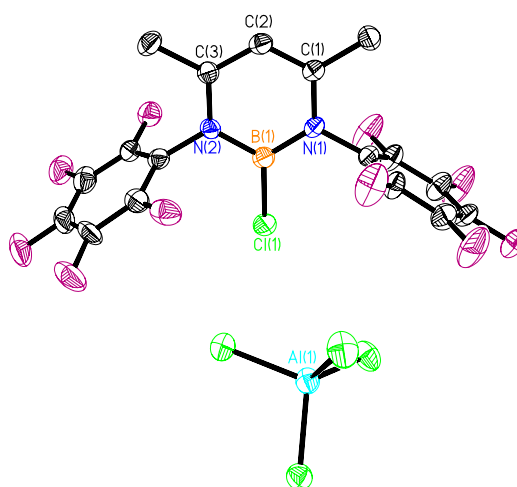


Figure 4.13. Molecular structure of one of the independent units of  $[(\text{CH}(\text{CMe}_2)_2(\text{NC}_6\text{F}_5)_2)\text{BCl}][\text{AlCl}_4]$ , 2.1, showing the atom number scheme for selected atoms. The thermal ellipsoids are shown at the 30 % probability level. All hydrogen atoms have been omitted for clarity.

**Table 4.34. Crystal data and structure refinement for [(CH(CMe<sub>2</sub>)<sub>2</sub>(NC<sub>6</sub>F<sub>5</sub>)<sub>2</sub>)BCl][AlCl<sub>4</sub>], 2.1.**

Identification code	[LBCl][AlCl <sub>4</sub> ]	
Empirical formula	C <sub>17</sub> H <sub>7</sub> Al B Cl <sub>5</sub> F <sub>10</sub> N <sub>2</sub>	
Formula weight	644.29	
Temperature	153(2) K	
Wavelength	0.71073 Å	
Crystal system	Triclinic	
Space group	P-1	
Unit cell dimensions	a = 12.270(3) Å	α = 89.71(3)°.
	b = 14.185(3) Å	β = 81.36(3)°.
	c = 14.556(3) Å	γ = 77.91(3)°.
Volume	2448.1(8) Å <sup>3</sup>	
Z	4	
Density (calculated)	1.748 Mg/m <sup>3</sup>	
Absorption coefficient	0.716 mm <sup>-1</sup>	
F(000)	1264	
Crystal size	0.20 x 0.20 x 0.10 mm <sup>3</sup>	
Theta range for data collection	1.42 to 26.02°.	
Index ranges	-14 ≤ h ≤ 15, -17 ≤ k ≤ 13, -17 ≤ l ≤ 15	
Reflections collected	13783	
Independent reflections	9534 [R(int) = 0.0472]	
Completeness to theta = 26.02°	98.9 %	
Absorption correction	None	
Max. and min. transmission	0.9319 and 0.8701	
Refinement method	Full-matrix least-squares on F <sup>2</sup>	
Data / restraints / parameters	9534 / 0 / 661	
Goodness-of-fit on F <sup>2</sup>	0.955	
Final R indices [I > 2σ(I)]	R <sub>1</sub> = 0.0626, wR <sub>2</sub> = 0.1534	
R indices (all data)	R <sub>1</sub> = 0.2047, wR <sub>2</sub> = 0.2371	
Largest diff. peak and hole	0.609 and -0.425 e.Å <sup>-3</sup>	

**Table 4.35. Selected bond lengths (Å) for [(CH(CMe<sub>2</sub>)<sub>2</sub>(NC<sub>6</sub>F<sub>5</sub>)<sub>2</sub>)BCl][AlCl<sub>4</sub>], 2.1.**

C(1)-C(2)	1.371(9)
C(2)-C(3)	1.392(9)
C(18)-C(19)	1.416(9)
C(19)-C(20)	1.383(9)
C(1)-N(1)	1.361(7)
C(3)-N(2)	1.366(7)
C(18)-N(3)	1.353(8)
C(20)-N(4)	1.377(8)
N(1)-B(1)	1.417(9)
N(2)-B(1)	1.442(9)
N(3)-B(2)	1.450(9)
N(4)-B(2)	1.432(9)
B(1)-Cl(1)	1.740(8)
B(2)-Cl(2)	1.714(8)

**Table 4.36. Selected bond angles (°) for [(CH(CMe<sub>2</sub>)<sub>2</sub>(NC<sub>6</sub>F<sub>5</sub>)<sub>2</sub>)BCl][AlCl<sub>4</sub>], 2.1.**

C(1)-C(2)-C(3)	123.7(6)
C(18)-C(19)-C(20)	121.1(6)
C(1)-N(1)-B(1)	121.4(5)
C(18)-N(3)-B(2)	122.0(5)
C(2)-C(1)-N(1)	118.7(6)
C(19)-C(18)-N(3)	119.3(6)
C(2)-C(3)-N(2)	117.6(6)
C(19)-C(20)-N(4)	119.6(5)
C(3)-N(2)-B(1)	121.2(6)
C(20)-N(4)-B(2)	121.8(5)
N(1)-B(1)-N(2)	117.2(6)
N(3)-B(2)-N(4)	115.9(6)
N(1)-B(1)-Cl(1)	122.2(5)
N(3)-B(2)-Cl(2)	122.2(5)
N(2)-B(1)-Cl(1)	120.7(6)
N(4)-B(2)-Cl(2)	121.9(5)

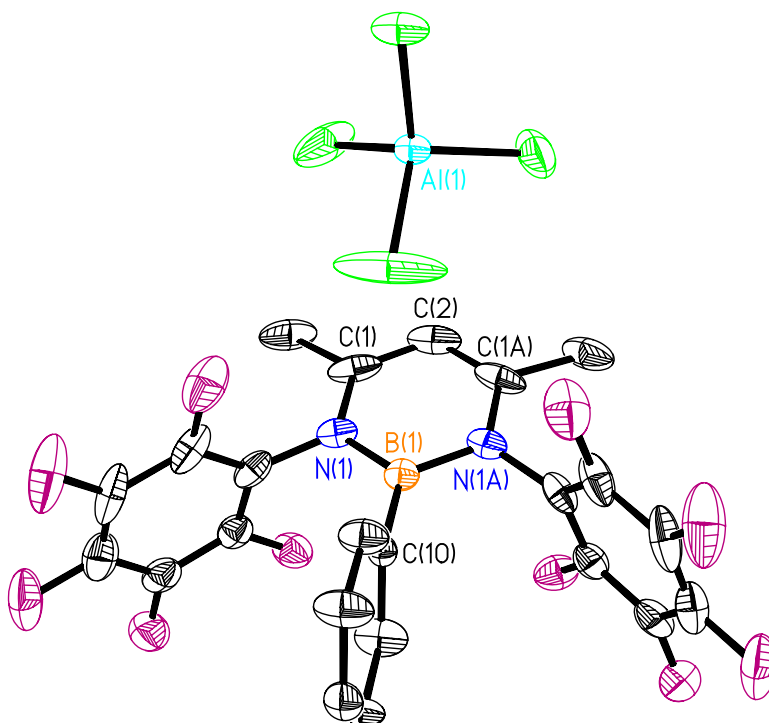


**Figure 4.14.** Molecular structure of  $[(\text{CH}(\text{CMe}_2)_2(\text{NC}_6\text{F}_5)_2)\text{BPh}][\text{AlCl}_4]$ , **2.2**, showing the atom number scheme for selected atoms. The thermal ellipsoids are shown at the 30 % probability level. All hydrogen atoms have been omitted for clarity.

**Table 4.37. Crystal data and structure refinement for [(CH(CMe<sub>2</sub>)<sub>2</sub>(NC<sub>6</sub>F<sub>5</sub>)<sub>2</sub>)BPh][AlCl<sub>4</sub>], 2.2.**

Identification code	[LBCl][AlCl <sub>4</sub> ]	
Empirical formula	C <sub>23</sub> H <sub>12</sub> Al B Cl <sub>4</sub> F <sub>10</sub> N <sub>2</sub>	
Formula weight	685.94	
Temperature	153(2) K	
Wavelength	0.71073 Å	
Crystal system	Orthorhombic	
Space group	Pnma	
Unit cell dimensions	a = 25.588(5) Å	α = 90°.
	b = 15.086(3) Å	β = 90°.
	c = 7.1553(14) Å	γ = 90°.
Volume	2762.1(9) Å <sup>3</sup>	
Z	4	
Density (calculated)	1.650 Mg/m <sup>3</sup>	
Absorption coefficient	0.547 mm <sup>-1</sup>	
F(000)	1360	
Crystal size	0.20 x 0.20 x 0.15 mm <sup>3</sup>	
Theta range for data collection	2.09 to 25.00°.	
Index ranges	-30 ≤ h ≤ 30, -17 ≤ k ≤ 17, -8 ≤ l ≤ 8	
Reflections collected	4596	
Independent reflections	2539 [R(int) = 0.1396]	
Completeness to theta = 25.00°	100.0 %	
Absorption correction	None	
Refinement method	Full-matrix least-squares on F <sup>2</sup>	
Data / restraints / parameters	2539 / 0 / 213	
Goodness-of-fit on F <sup>2</sup>	1.014	
Final R indices [I > 2σ(I)]	R1 = 0.0803, wR2 = 0.1864	
R indices (all data)	R1 = 0.2112, wR2 = 0.2491	
Extinction coefficient	0.0056(14)	
Largest diff. peak and hole	0.816 and -0.815 e.Å <sup>-3</sup>	

**Table 4.38. Selected bond lengths (Å) for [(CH(CMe<sub>2</sub>)<sub>2</sub>(NC<sub>6</sub>F<sub>5</sub>)<sub>2</sub>)BPh][AlCl<sub>4</sub>], 2.2.**

C(1)-C(2)	1.377(11)
C(1A)-C(2)	1.377(11)
C(1)-N(1)	1.361(10)
C(1A)-N(1A)	1.361(10)
N(1)-B(1)	1.441(9)
N(1A)-B(1)	1.441(9)
B(1)-C(10)	1.531(15)

**Table 4.39. Selected bond angles (°) for [(CH(CMe<sub>2</sub>)<sub>2</sub>(NC<sub>6</sub>F<sub>5</sub>)<sub>2</sub>)BPh][AlCl<sub>4</sub>], 2.2.**

C(1)-C(2)-C(1A)	120.3(12)
C(1)-N(1)-B(1)	122.5(8)
C(1A)-N(1A)-B(1)	122.5(8)
C(2)-C(1)-N(1)	120.3(10)
C(2)-C(1A)-N(1A)	120.3(10)
N(1)-B(1)-N(1A)	113.7(10)
N(1)-B(1)-C(10)	123.1(5)
N(1A)-B(1)-C(10)	123.1(5)



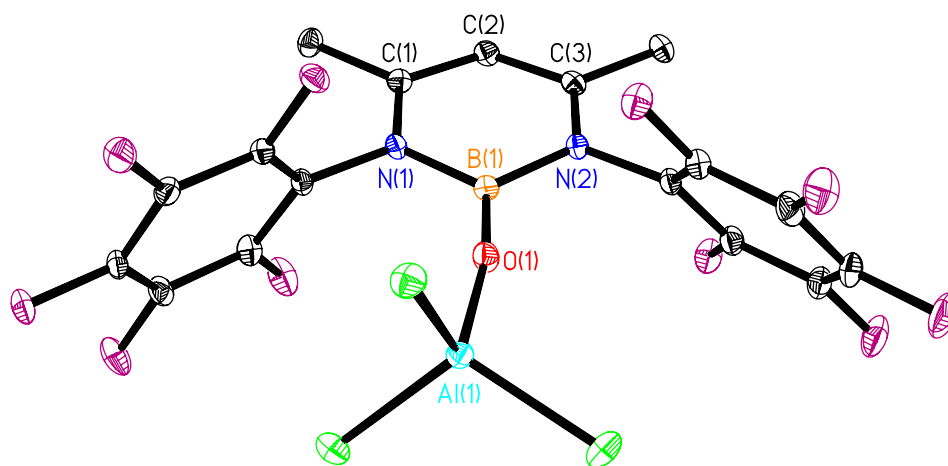


**Figure 4.15.** Molecular structure of  $(\text{CH}(\text{CMe}_2)_2(\text{NC}_6\text{F}_5)_2)\text{B}=\text{O} \rightarrow \text{AlCl}_3$ , **2.3**, showing the atom number scheme for selected atoms. The thermal ellipsoids are shown at the 30 % probability level. All hydrogen atoms have been omitted for clarity.

**Table 4.40. Crystal data and structure refinement for (CH(CMe<sub>2</sub>)<sub>2</sub>(NC<sub>6</sub>F<sub>5</sub>)<sub>2</sub>) B=O→AlCl<sub>3</sub>, 2.3.**

Identification code	LB=O→AlCl <sub>3</sub>	
Empirical formula	C <sub>17</sub> H <sub>7</sub> Al B Cl <sub>3</sub> F <sub>10</sub> N <sub>2</sub> O	
Formula weight	589.39	
Temperature	153(2) K	
Wavelength	0.71073 Å	
Crystal system	Orthorhombic	
Space group	P2 <sub>1</sub> 2 <sub>1</sub> 2 <sub>1</sub>	
Unit cell dimensions	a = 7.329 Å	α = 90°.
	b = 13.745 Å	β = 90°.
	c = 21.452 Å	γ = 90°.
Volume	2161.0 Å <sup>3</sup>	
Z	4	
Density (calculated)	1.812 Mg/m <sup>3</sup>	
Absorption coefficient	0.566 mm <sup>-1</sup>	
F(000)	1160	
Crystal size	0.30 x 0.30 x 0.30 mm <sup>3</sup>	
Theta range for data collection	2.41 to 27.48°.	
Index ranges	-9 ≤ h ≤ 9, -17 ≤ k ≤ 17, -27 ≤ l ≤ 27	
Reflections collected	4812	
Independent reflections	4812 [R(int) = 0.0000]	
Completeness to theta = 27.48°	99.5 %	
Absorption correction	None	
Max. and min. transmission	0.8486 and 0.8486	
Refinement method	Full-matrix least-squares on F <sup>2</sup>	
Data / restraints / parameters	4812 / 150 / 203	
Goodness-of-fit on F <sup>2</sup>	1.049	
Final R indices [I > 2σ(I)]	R1 = 0.1365, wR2 = 0.3333	
R indices (all data)	R1 = 0.1939, wR2 = 0.3769	
Absolute structure parameter	0.4(4)	
Largest diff. peak and hole	1.978 and -1.154 e.Å <sup>-3</sup>	

**Table 4.41. Selected bond lengths (Å) for (CH(CMe<sub>2</sub>)<sub>2</sub>(NC<sub>6</sub>F<sub>5</sub>)<sub>2</sub>)B=O→AlCl<sub>3</sub>, 2.3.**

C(1)-C(2)	1.387(2)
C(2)-C(3)	1.388(2)
C(1)-N(1)	1.361(2)
C(3)-N(2)	1.356(2)
N(1)-B(1)	1.472(2)
N(2)-B(1)	1.466(2)
B(1)-O(1)	1.304(2)
O(1)-Al(1)	1.720(1)

**Table 4.42. Selected bond angles (°) for (CH(CMe<sub>2</sub>)<sub>2</sub>(NC<sub>6</sub>F<sub>5</sub>)<sub>2</sub>)B=O→AlCl<sub>3</sub>, 2.3.**

C(1)-C(2)-C(3)	123.2(1)
C(1)-N(1)-B(1)	122.1(5)
C(2)-C(1)-N(1)	119.1(1)
C(2)-C(3)-N(2)	118.5(1)
C(3)-N(2)-B(1)	123.9(2)
N(1)-B(1)-N(2)	119.9(1)
N(1)-B(1)-O(1)	122.8(1)
N(2)-B(1)-O(1)	123.2(2)
B(1)-O(1)-Al(1)	169.2(1)

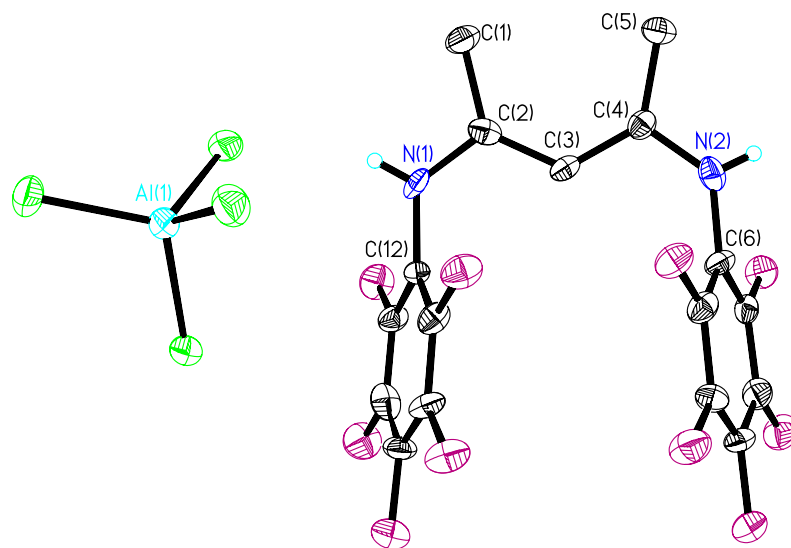


**Figure 4.16.** Molecular structure of  $[\text{CH}(\text{CMe}_2)_2(\text{HNC}_6\text{F}_5)_2][\text{AlCl}_4]$ , **2.4**, showing the atom number scheme for selected atoms. The thermal ellipsoids are shown at the 30 % probability level. All hydrogen atoms, except those on the nitrogen atoms, have been omitted for clarity.

**Table 4.43. Crystal data and structure refinement for [CH(CMe<sub>2</sub>)<sub>2</sub>(HNC<sub>6</sub>F<sub>5</sub>)<sub>2</sub>][AlCl<sub>4</sub>], 2.4.**

Identification code	[LH <sub>2</sub> ][AlCl <sub>4</sub> ]	
Empirical formula	C <sub>17</sub> H <sub>9</sub> Al Cl <sub>4</sub> F <sub>10</sub> N <sub>2</sub>	
Formula weight	600.04	
Temperature	153(2) K	
Wavelength	0.71069 Å	
Crystal system	Monoclinic	
Space group	P2 <sub>1</sub> /c	
Unit cell dimensions	a = 9.772(5) Å	α = 90.000(5)°.
	b = 19.786(5) Å	β = 93.110(5)°.
	c = 11.833(5) Å	γ = 90.000(5)°.
Volume	2284.5(16) Å <sup>3</sup>	
Z	4	
Density (calculated)	1.745 Mg/m <sup>3</sup>	
Absorption coefficient	0.647 mm <sup>-1</sup>	
F(000)	1184	
Crystal size	0.30 x 0.20 x 0.05 mm <sup>3</sup>	
Theta range for data collection	2.93 to 27.50°.	
Index ranges	-12 ≤ h ≤ 12, -25 ≤ k ≤ 23, -15 ≤ l ≤ 15	
Reflections collected	9541	
Independent reflections	5138 [R(int) = 0.1610]	
Completeness to theta = 27.50°	97.8 %	
Absorption correction	None	
Refinement method	Full-matrix least-squares on F <sup>2</sup>	
Data / restraints / parameters	5138 / 0 / 318	
Goodness-of-fit on F <sup>2</sup>	1.030	
Final R indices [I > 2σ(I)]	R <sub>1</sub> = 0.1037, wR <sub>2</sub> = 0.1289	
R indices (all data)	R <sub>1</sub> = 0.2884, wR <sub>2</sub> = 0.1741	
Extinction coefficient	0.0053(6)	
Largest diff. peak and hole	0.415 and -0.454 e.Å <sup>-3</sup>	

**Table 4.44. Selected bond lengths (Å) for [CH(CMe<sub>2</sub>)<sub>2</sub>(HNC<sub>6</sub>F<sub>5</sub>)<sub>2</sub>][AlCl<sub>4</sub>], 2.4.**

C(1)-C(2)	1.494(10)
C(2)-C(3)	1.389(10)
C(3)-C(4)	1.382(10)
C(4)-C(5)	1.486(9)
C(2)-N(1)	1.354(9)
C(4)-N(2)	1.341(10)

**Table 4.45. Selected bond angles (°) for [CH(CMe<sub>2</sub>)<sub>2</sub>(HNC<sub>6</sub>F<sub>5</sub>)<sub>2</sub>] [AlCl<sub>4</sub>], 2.4.**

C(1)-C(2)-C(3)	128.3(7)
C(2)-C(3)-C(4)	125.8(7)
C(3)-C(4)-C(5)	129.4(7)
C(1)-C(2)-N(1)	113.3(7)
C(3)-C(2)-N(1)	118.5(7)
C(3)-C(4)-N(2)	115.5(7)
C(5)-C(4)-N(2)	115.0(7)

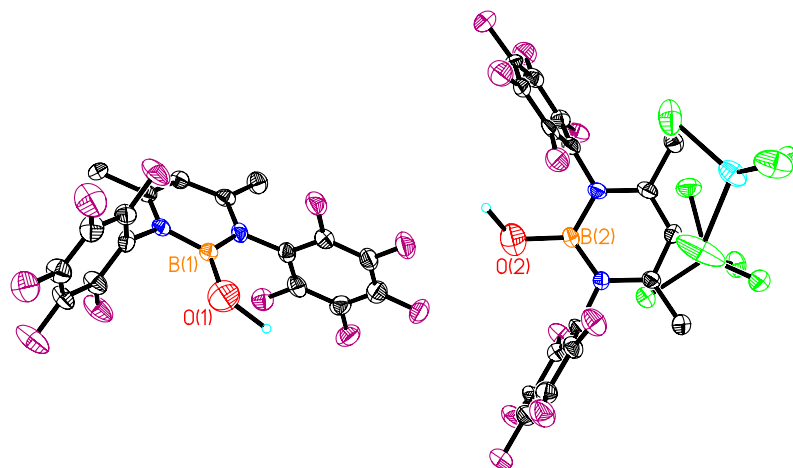


Figure 4.17. Molecular structure of  $[(\text{CH}(\text{CMe}_2)_2(\text{NC}_6\text{F}_5)_2)\text{B}(\text{OH})][\text{AlCl}_4]$ , 2.5, showing the atom number scheme for selected atoms. The thermal ellipsoids are shown at the 30 % probability level. All hydrogen atoms, except those on the oxygen atoms, have been omitted for clarity.

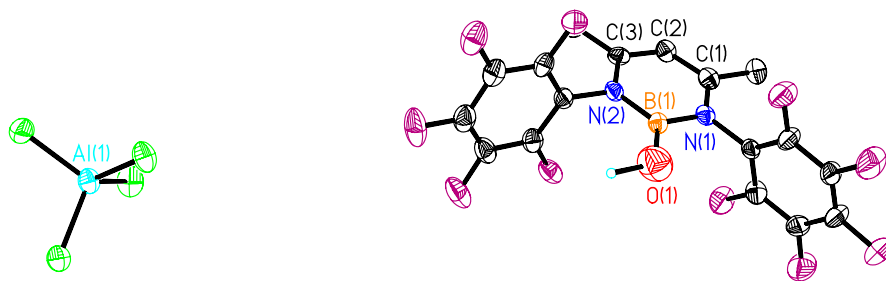


Figure 4.18. Molecular structure of one of the independent units of  $[(\text{CH}(\text{CMe}_2)_2(\text{NC}_6\text{F}_5)_2)\text{B}(\text{OH})][\text{AlCl}_4]$ , 2.5, showing the atom number scheme for selected atoms. The thermal ellipsoids are shown at the 30 % probability level. All hydrogen atoms, except that on the oxygen atom, have been omitted for clarity.

**Table 4.46. Crystal data and structure refinement for [(CH(CMe<sub>2</sub>)<sub>2</sub>(NC<sub>6</sub>F<sub>5</sub>)<sub>2</sub>)B(OH)][AlCl<sub>4</sub>], 2.5.**

Identification code	[LB(OH)][AlCl <sub>4</sub> ]	
Empirical formula	C <sub>17</sub> H <sub>8</sub> Al B Cl <sub>4</sub> F <sub>10</sub> N <sub>2</sub> O	
Formula weight	625.85	
Temperature	153(2) K	
Wavelength	0.71073 Å	
Crystal system	Triclinic	
Space group	P-1	
Unit cell dimensions	a = 12.076(2) Å	α = 89.67(3)°.
	b = 14.249(3) Å	β = 81.47(3)°.
	c = 14.700(3) Å	γ = 78.54(3)°.
Volume	2451.0(8) Å <sup>3</sup>	
Z	5	
Density (calculated)	1.696 Mg/m <sup>3</sup>	
Absorption coefficient	0.610 mm <sup>-1</sup>	
F(000)	1232	
Crystal size	0.18 x 0.18 x 0.15 mm <sup>3</sup>	
Theta range for data collection	3.00 to 27.59°.	
Index ranges	-14 ≤ h ≤ 15, -18 ≤ k ≤ 17, -19 ≤ l ≤ 18	
Reflections collected	18786	
Independent reflections	10777 [R(int) = 0.1871]	
Completeness to theta = 27.59°	94.8 %	
Absorption correction	None	
Max. and min. transmission	0.9141 and 0.8982	
Refinement method	Full-matrix least-squares on F <sup>2</sup>	
Data / restraints / parameters	10777 / 0 / 669	
Goodness-of-fit on F <sup>2</sup>	0.894	
Final R indices [I > 2σ(I)]	R <sub>1</sub> = 0.0803, wR <sub>2</sub> = 0.1376	
R indices (all data)	R <sub>1</sub> = 0.3452, wR <sub>2</sub> = 0.2101	
Largest diff. peak and hole	0.329 and -0.404 e.Å <sup>-3</sup>	



**Table 4.47. Selected bond lengths (Å) for [(CH(CMe<sub>2</sub>)<sub>2</sub>(NC<sub>6</sub>F<sub>5</sub>)<sub>2</sub>)B(OH)][AlCl<sub>4</sub>], 2.5.**

C(1)-C(2)	1.379(11)
C(2)-C(3)	1.383(10)
C(18)-C(19)	1.374(11)
C(19)-C(20)	1.390(11)
C(1)-N(1)	1.359(9)
C(3)-N(2)	1.379(9)
C(18)-N(3)	1.362(9)
C(20)-N(4)	1.358(9)
N(1)-B(1)	1.453(11)
N(2)-B(1)	1.456(11)
N(3)-B(2)	1.462(11)
N(4)-B(2)	1.436(11)
B(1)-O(1)	1.557(12)
B(2)-O(2)	1.566(12)

**Table 4.48. Selected bond angles (°) for [(CH(CMe<sub>2</sub>)<sub>2</sub>(NC<sub>6</sub>F<sub>5</sub>)<sub>2</sub>)B(OH)][AlCl<sub>4</sub>], 2.5.**

C(1)-C(2)-C(3)	123.7(9)
C(18)-C(19)-C(20)	124.2(9)
C(1)-N(1)-B(1)	123.0(7)
C(18)-N(3)-B(2)	120.6(7)
C(2)-C(1)-N(1)	118.6(8)
C(19)-C(18)-N(3)	119.1(8)
C(2)-C(3)-N(2)	117.6(8)
C(19)-C(20)-N(4)	116.7(8)
C(3)-N(2)-B(1)	123.2(7)
C(20)-N(4)-B(2)	123.5(7)
N(1)-B(1)-N(2)	113.6(8)
N(3)-B(2)-N(4)	115.3(7)
N(1)-B(1)-O(1)	122.9(8)
N(3)-B(2)-O(2)	122.1(8)
N(2)-B(1)-O(1)	123.5(8)
N(4)-B(2)-O(2)	122.4(8)

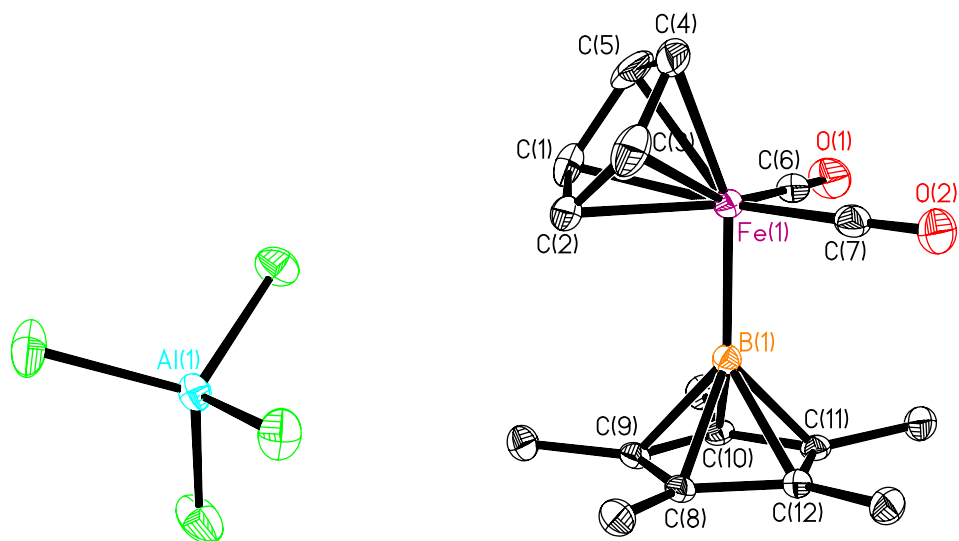


Figure 4.19. Molecular structure of  $[(\eta^5\text{-C}_5\text{H}_5)\text{Fe}(\text{CO})_2\text{B}(\eta^5\text{-C}_5\text{Me}_5)][\text{AlCl}_4]$ , 2.8, showing the atom number scheme for selected atoms. The thermal ellipsoids are shown at the 30 % probability level. All hydrogen atoms have been omitted for clarity.

**Table 4.49. Crystal data and structure refinement for  $[(\eta^5\text{-C}_5\text{H}_5)\text{Fe}(\text{CO})_2\text{B}(\eta^5\text{-C}_5\text{Me}_5)][\text{AlCl}_4]$ , 2.8.**

Identification code	[FpBCp*][AlCl <sub>4</sub> ]	
Empirical formula	C <sub>17</sub> H <sub>20</sub> Al B Cl <sub>4</sub> Fe O <sub>2</sub>	
Formula weight	491.77	
Temperature	153(2) K	
Wavelength	0.71073 Å	
Crystal system	Monoclinic	
Space group	P2 <sub>1</sub> /n	
Unit cell dimensions	a = 11.227(2) Å	α = 90°.
	b = 15.692(3) Å	β = 91.24(3)°.
	c = 12.337(3) Å	γ = 90°.
Volume	2173.0(8) Å <sup>3</sup>	
Z	4	
Density (calculated)	1.503 Mg/m <sup>3</sup>	
Absorption coefficient	1.235 mm <sup>-1</sup>	
F(000)	1000	
Crystal size	0.15 x 0.08 x 0.08 mm <sup>3</sup>	
Theta range for data collection	2.10 to 27.50°.	
Index ranges	-11 ≤ h ≤ 14, -19 ≤ k ≤ 20, -14 ≤ l ≤ 16	
Reflections collected	13965	
Independent reflections	4966 [R(int) = 0.0595]	
Completeness to theta = 27.50°	99.6 %	
Absorption correction	Semi-empirical from equivalents	
Max. and min. transmission	0.9076 and 0.8364	
Refinement method	Full-matrix least-squares on F <sup>2</sup>	
Data / restraints / parameters	4966 / 0 / 240	
Goodness-of-fit on F <sup>2</sup>	1.024	
Final R indices [I > 2σ(I)]	R <sub>1</sub> = 0.0435, wR <sub>2</sub> = 0.0843	
R indices (all data)	R <sub>1</sub> = 0.0909, wR <sub>2</sub> = 0.0979	
Largest diff. peak and hole	0.391 and -0.404 e.Å <sup>-3</sup>	

**Table 4.50. Selected bond lengths (Å) for  $[(\eta^5\text{-C}_5\text{H}_5)\text{Fe}(\text{CO})_2\text{B}(\eta^5\text{-C}_5\text{Me}_5)][\text{AlCl}_4]$ , 2.8.**

Fe(1)-B(1)	1.977(3)
B(1)-C(8)	1.794(4)
B(1)-C(9)	1.792(4)
B(1)-C(10)	1.803(4)
B(1)-C(11)	1.803(4)
B(1)-C(12)	1.801(4)
B(1)-X	1.326
Fe(1)-C(6)	1.754(3)
Fe(1)-C(7)	1.760(4)
Fe(1)-X	1.719
C(6)-O(1)	1.149(3)
C(7)-O(2)	1.145(4)

**Table 4.51. Selected bond angles (°) for  $[(\eta^5\text{-C}_5\text{H}_5)\text{Fe}(\text{CO})_2\text{B}(\eta^5\text{-C}_5\text{Me}_5)][\text{AlCl}_4]$ , 2.8.**

Fe(1)-B(1)-X	177.86
B(1)-Fe(1)-X	123.63
C(6)-Fe(1)-C(7)	96.25(13)

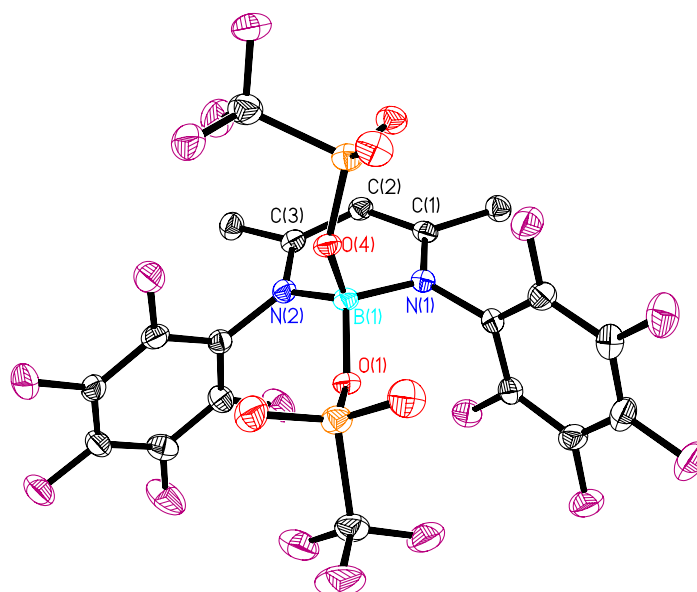


**Figure 4.20.** Molecular structure of  $(\text{CH}(\text{CMe}_2)_2(\text{NC}_6\text{F}_5)_2)\text{B}(\text{OTf})_2$ , **3.1**, showing the atom number scheme for selected atoms. The thermal ellipsoids are shown at the 30 % probability level. All hydrogen atoms have been omitted for clarity.

**Table 4.52. Crystal data and structure refinement for (CH(CMe<sub>2</sub>)<sub>2</sub>(NC<sub>6</sub>F<sub>5</sub>)<sub>2</sub>)B(OTf)<sub>2</sub>, 3.1.**

Identification code	LB(OTf) <sub>2</sub>	
Empirical formula	C <sub>19</sub> H <sub>7</sub> B F <sub>16</sub> N <sub>2</sub> O <sub>6</sub> S <sub>2</sub>	
Formula weight	738.20	
Temperature	153(2) K	
Wavelength	0.71073 Å	
Crystal system	Monoclinic	
Space group	P2 <sub>1</sub> /c	
Unit cell dimensions	a = 7.7912(16) Å	α = 90°.
	b = 13.764(3) Å	β = 96.00(3)°.
	c = 24.388(5) Å	γ = 90°.
Volume	2601.0(9) Å <sup>3</sup>	
Z	4	
Density (calculated)	1.885 Mg/m <sup>3</sup>	
Absorption coefficient	0.362 mm <sup>-1</sup>	
F(000)	1456	
Crystal size	0.25 x 0.20 x 0.20 mm <sup>3</sup>	
Theta range for data collection	2.92 to 27.50°.	
Index ranges	-10 ≤ h ≤ 10, -17 ≤ k ≤ 17, -31 ≤ l ≤ 30	
Reflections collected	20703	
Independent reflections	5946 [R(int) = 0.1272]	
Completeness to theta = 27.50°	99.6 %	
Absorption correction	None	
Max. and min. transmission	0.9312 and 0.9150	
Refinement method	Full-matrix least-squares on F <sup>2</sup>	
Data / restraints / parameters	5946 / 0 / 417	
Goodness-of-fit on F <sup>2</sup>	0.972	
Final R indices [I > 2σ(I)]	R1 = 0.0575, wR2 = 0.1136	
R indices (all data)	R1 = 0.1668, wR2 = 0.1504	
Largest diff. peak and hole	0.383 and -0.432 e.Å <sup>-3</sup>	

**Table 4.53. Selected bond lengths (Å) for (CH(CMe<sub>2</sub>)<sub>2</sub>(NC<sub>6</sub>F<sub>5</sub>)<sub>2</sub>)B(OTf)<sub>2</sub>, 3.1.**

C(1)-C(2)	1.370(5)
C(2)-C(3)	1.376(5)
C(1)-N(1)	1.344(4)
C(3)-N(2)	1.358(4)
B(1)-N(1)	1.508(5)
B(1)-N(2)	1.492(5)
B(1)-O(1)	1.496(5)
B(1)-O(4)	1.565(5)

**Table 4.54. Selected bond angles (°) for (CH(CMe<sub>2</sub>)<sub>2</sub>(NC<sub>6</sub>F<sub>5</sub>)<sub>2</sub>)B(OTf)<sub>2</sub>, 3.1.**

C(1)-C(2)-C(3)	122.7(3)
C(2)-C(1)-N(1)	119.5(3)
C(2)-C(3)-N(2)	118.9(3)
C(1)-N(1)-B(1)	119.7(3)
C(3)-N(2)-B(1)	119.9(3)
N(1)-B(1)-N(2)	110.3(3)
N(1)-B(1)-O(1)	109.2(3)
N(1)-B(1)-O(4)	112.2(3)
N(2)-B(1)-O(1)	109.4(3)
N(2)-B(1)-O(4)	111.0(3)
O(1)-B(1)-O(4)	104.5(3)

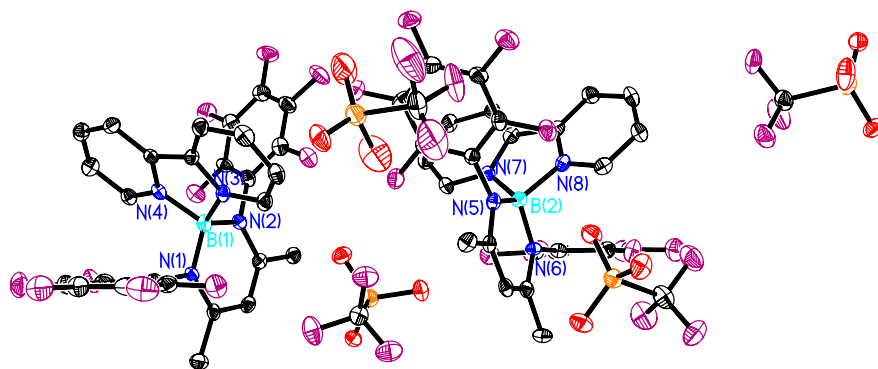


Figure 4.21. Molecular structure of  $[(\text{CH}(\text{CMe}_2)_2(\text{NC}_6\text{F}_5)_2)\text{B}(\text{bipy})][2\cdot\text{OTf}]$ , 3.2, showing the atom number scheme for selected atoms. The thermal ellipsoids are shown at the 30 % probability level. All hydrogen atoms have been omitted for clarity.

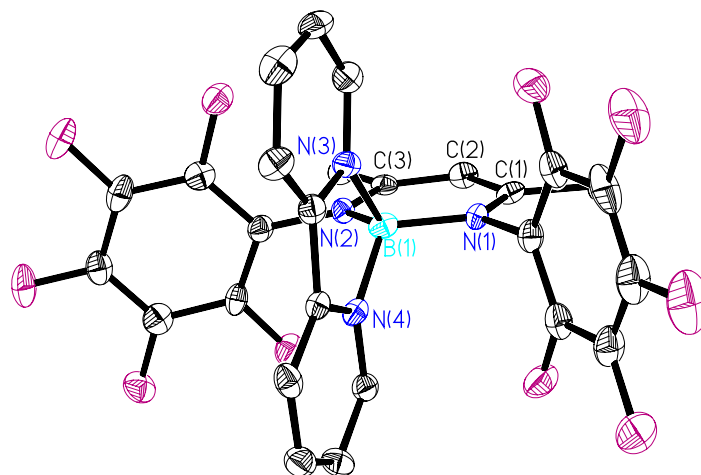


Figure 4.22. Molecular structure of one of the two independent units of  $[(\text{CH}(\text{CMe}_2)_2(\text{NC}_6\text{F}_5)_2)\text{B}(\text{bipy})][2\cdot\text{OTf}]$ , 3.2, showing the atom number scheme for selected atoms. The thermal ellipsoids are shown at the 30 % probability level. All hydrogen atoms and the two triflate anions have been omitted for clarity.



**Table 4.55. Crystal data and structure refinement for [CH(CMe<sub>2</sub>)<sub>2</sub>(NC<sub>6</sub>F<sub>5</sub>)<sub>2</sub>B(bipy)][2·OTf], 3.2.**

Identification code	[LB(bipy)][2·OTf]	
Empirical formula	C <sub>29</sub> H <sub>15</sub> B F <sub>16</sub> N <sub>4</sub> O <sub>6</sub> S <sub>2</sub>	
Formula weight	894.38	
Temperature	153(2) K	
Wavelength	0.71073 Å	
Crystal system	Triclinic	
Space group	P-1	
Unit cell dimensions	a = 12.756(3) Å	α = 98.15(3)°.
	b = 15.622(3) Å	β = 109.09(3)°.
	c = 18.567(4) Å	γ = 93.92(3)°.
Volume	3435.0(12) Å <sup>3</sup>	
Z	4	
Density (calculated)	1.729 Mg/m <sup>3</sup>	
Absorption coefficient	0.292 mm <sup>-1</sup>	
F(000)	1784	
Crystal size	0.15 x 0.15 x 0.15 mm <sup>3</sup>	
Theta range for data collection	1.18 to 27.46°.	
Index ranges	-15 ≤ h ≤ 16, -20 ≤ k ≤ 17, -24 ≤ l ≤ 20	
Reflections collected	22139	
Independent reflections	15349 [R(int) = 0.0790]	
Completeness to theta = 27.46°	97.6 %	
Absorption correction	None	
Max. and min. transmission	0.9575 and 0.9575	
Refinement method	Full-matrix least-squares on F <sup>2</sup>	
Data / restraints / parameters	15349 / 0 / 1035	
Goodness-of-fit on F <sup>2</sup>	0.941	
Final R indices [I > 2σ(I)]	R <sub>1</sub> = 0.0777, wR <sub>2</sub> = 0.1781	
R indices (all data)	R <sub>1</sub> = 0.2818, wR <sub>2</sub> = 0.2904	
Largest diff. peak and hole	1.400 and -0.493 e.Å <sup>-3</sup>	

**Table 4.56. Selected bond lengths (Å) for [(CH(CMe<sub>2</sub>)<sub>2</sub>(NC<sub>6</sub>F<sub>5</sub>)<sub>2</sub>)B(bipy)][2·OTf], 3.2.**

C(1)-C(2)	1.373(9)	C(30)-C(31)	1.382(9)
C(2)-C(3)	1.366(9)	C(31)-C(32)	1.379(9)
C(1)-N(1)	1.366(8)	C(30)-N(5)	1.360(8)
C(3)-N(2)	1.362(8)	C(32)-N(6)	1.357(8)
N(1)-B(1)	1.511(10)	N(5)-B(2)	1.519(9)
N(2)-B(1)	1.512(9)	N(6)-B(2)	1.512(9)
N(3)-B(1)	1.605(10)	N(7)-B(2)	1.598(10)
N(4)-B(1)	1.578(10)	N(8)-B(2)	1.600(10)

**Table 4.57. Selected bond angles (°) for [(CH(CMe<sub>2</sub>)<sub>2</sub>(NC<sub>6</sub>F<sub>5</sub>)<sub>2</sub>)B(bipy)][2·OTf], 3.2.**

C(1)-C(2)-C(3)	122.3(6)	C(30)-C(31)-C(32)	123.4(7)
C(2)-C(1)-N(1)	120.6(6)	C(31)-C(30)-N(5)	119.5(6)
C(2)-C(3)-N(2)	121.2(6)	C(31)-C(32)-N(6)	119.8(6)
C(1)-N(1)-B(1)	122.0(5)	C(30)-N(5)-B(2)	123.0(5)
C(3)-N(2)-B(1)	121.7(6)	C(32)-N(6)-B(2)	123.2(5)
N(1)-B(1)-N(2)	111.6(6)	N(5)-B(2)-N(6)	110.9(6)
N(1)-B(1)-N(3)	110.0(6)	N(5)-B(2)-N(7)	112.9(6)
N(1)-B(1)-N(4)	112.7(6)	N(5)-B(2)-N(8)	112.8(6)
N(2)-B(1)-N(3)	112.7(6)	N(6)-B(2)-N(7)	112.0(6)
N(2)-B(1)-N(4)	113.4(6)	N(6)-B(2)-N(8)	116.6(6)
N(3)-B(1)-N(4)	95.5(5)	N(7)-B(2)-N(8)	95.9(5)

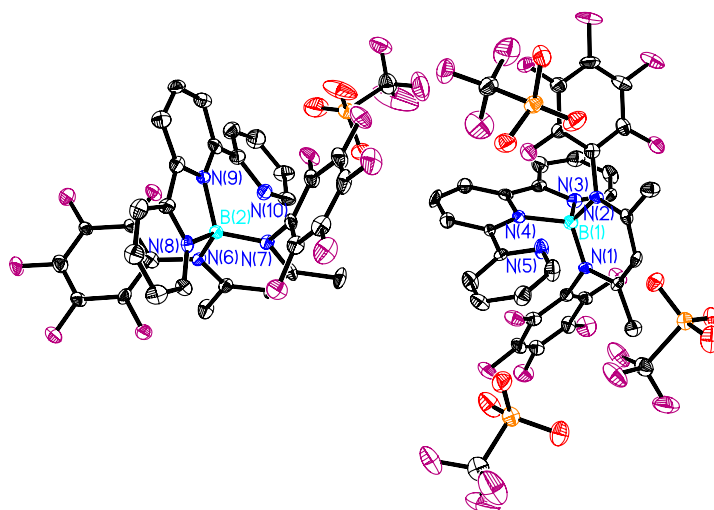


**Figure 4.23.** Molecular structure of  $[(\text{CH}(\text{CMe}_2)_2(\text{NC}_6\text{F}_5)_2)\text{B}(\text{terpy})][2\cdot\text{OTf}]$ , **3.3**, showing the atom number scheme for selected atoms. The thermal ellipsoids are shown at the 30 % probability level. All hydrogen atoms have been omitted for clarity.

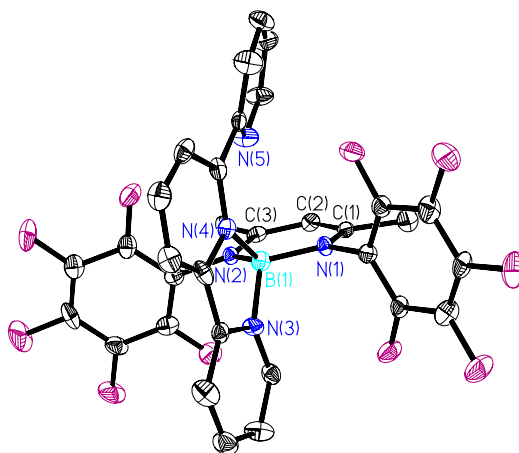


**Figure 4.24.** Molecular structure of one of the two independent units of  $[(\text{CH}(\text{CMe}_2)_2(\text{NC}_6\text{F}_5)_2)\text{B}(\text{terpy})][2\cdot\text{OTf}]$ , **3.3**, showing the atom number scheme for selected atoms. The thermal ellipsoids are shown at the 30 % probability level. All hydrogen atoms and the two triflate anions have been omitted for clarity.

**Table 4.58. Crystal data and structure refinement for [CH(CMe<sub>2</sub>)<sub>2</sub>(NC<sub>6</sub>F<sub>5</sub>)<sub>2</sub>)B(terpy)][2·OTf], 3.3.**

Identification code	[LB(terpy)][2·OTf]	
Empirical formula	C <sub>34</sub> H <sub>18</sub> B F <sub>16</sub> N <sub>5</sub> O <sub>6</sub> S <sub>2</sub>	
Formula weight	704.26	
Temperature	153(2) K	
Wavelength	0.71073 Å	
Crystal system	Triclinic	
Space group	P-1	
Unit cell dimensions	a = 12.479(3) Å	α = 96.88(3)°.
	b = 17.648(4) Å	β = 98.89(3)°.
	c = 18.995(4) Å	γ = 91.36(3)°.
Volume	4099.4(14) Å <sup>3</sup>	
Z	6	
Density (calculated)	1.712 Mg/m <sup>3</sup>	
Absorption coefficient	0.386 mm <sup>-1</sup>	
F(000)	2112	
Crystal size	0.20 x 0.15 x 0.15 mm <sup>3</sup>	
Theta range for data collection	1.09 to 27.50°.	
Index ranges	-16 ≤ h ≤ 16, -22 ≤ k ≤ 22, -19 ≤ l ≤ 24	
Reflections collected	27051	
Independent reflections	18411 [R(int) = 0.0733]	
Completeness to theta = 27.50°	97.7 %	
Absorption correction	None	
Refinement method	Full-matrix least-squares on F <sup>2</sup>	
Data / restraints / parameters	18411 / 0 / 1193	
Goodness-of-fit on F <sup>2</sup>	1.033	
Final R indices [I > 2σ(I)]	R1 = 0.1676, wR2 = 0.4570	
R indices (all data)	R1 = 0.2762, wR2 = 0.5143	
Extinction coefficient	0.0170(18)	
Largest diff. peak and hole	1.167 and -0.716 e.Å <sup>-3</sup>	

**Table 4.59. Selected bond lengths (Å) for [(CH(CMe<sub>2</sub>)<sub>2</sub>(NC<sub>6</sub>F<sub>5</sub>)<sub>2</sub>)B(terpy)][[2·OTf], 3.3.**

C(1)-C(2)	1.367(17)	C(33)-C(34)	1.362(16)
C(2)-C(3)	1.356(18)	C(34)-C(35)	1.364(16)
C(1)-N(1)	1.344(15)	C(33)-N(6)	1.370(15)
C(3)-N(2)	1.372(16)	C(35)-N(7)	1.385(16)
N(1)-B(1)	1.531(18)	N(6)-B(2)	1.502(16)
N(2)-B(1)	1.498(18)	N(7)-B(2)	1.529(16)
N(3)-B(1)	1.584(18)	N(8)-B(2)	1.571(17)
N(4)-B(1)	1.656(18)	N(9)-B(2)	1.640(17)

**Table 4.60. Selected bond angles (°) for [(CH(CMe<sub>2</sub>)<sub>2</sub>(NC<sub>6</sub>F<sub>5</sub>)<sub>2</sub>)B(terpy)][[2·OTf], 3.3.**

C(1)-C(2)-C(3)	123.4(11)	C(33)-C(34)-C(35)	124.5(11)
C(2)-C(1)-N(1)	120.1(11)	C(34)-C(33)-N(6)	119.5(11)
C(2)-C(3)-N(2)	120.7(11)	C(34)-C(35)-N(7)	119.8(10)
C(1)-N(1)-B(1)	122.2(10)	C(33)-N(6)-B(2)	123.2(10)
C(3)-N(2)-B(1)	121.4(10)	C(35)-N(7)-B(2)	121.4(9)
N(1)-B(1)-N(2)	111.5(11)	N(6)-B(2)-N(7)	111.5(10)
N(1)-B(1)-N(3)	110.3(11)	N(6)-B(2)-N(8)	110.4(11)
N(1)-B(1)-N(4)	114.1(10)	N(6)-B(2)-N(9)	115.6(10)
N(2)-B(1)-N(3)	109.0(11)	N(7)-B(2)-N(8)	108.1(10)
N(2)-B(1)-N(4)	115.4(11)	N(7)-B(2)-N(9)	113.9(9)
N(3)-B(1)-N(4)	95.2(10)	N(8)-B(2)-N(9)	96.1(9)

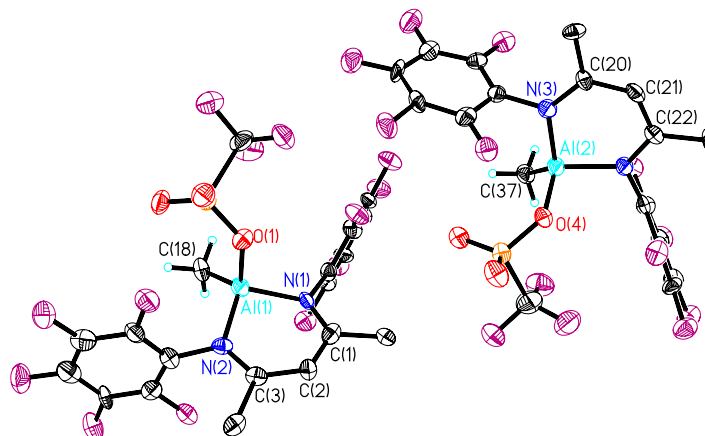


Figure 4.25. Molecular structure of  $(\text{CH}(\text{CMe}_2)_2(\text{NC}_6\text{F}_5)_2)\text{Al}(\text{OTf})\text{Me}$ , 3.6, showing the atom number scheme for selected atoms. The thermal ellipsoids are shown at the 30 % probability level. All hydrogen atoms except those on the Al-Me group have been omitted for clarity.

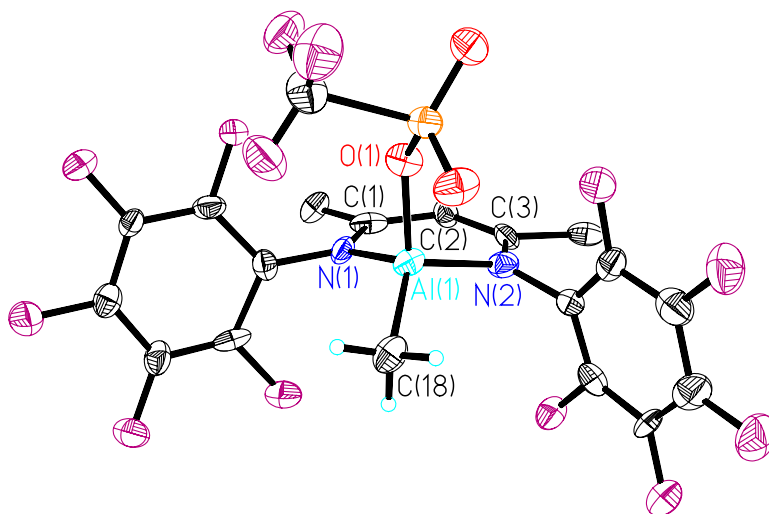


Figure 4.26. Molecular structure of one of the two independent units of  $(\text{CH}(\text{CMe}_2)_2(\text{NC}_6\text{F}_5)_2)\text{Al}(\text{OTf})\text{Me}$ , 3.6, showing the atom number scheme for selected atoms. The thermal ellipsoids are shown at the 30 % probability level. All hydrogen atoms, except those on the Al-Me group, have been omitted for clarity.

**Table 4.61. Crystal data and structure refinement for (CH(CMe<sub>2</sub>)<sub>2</sub>(NC<sub>6</sub>F<sub>5</sub>)<sub>2</sub>) Al(OTf)Me, 3.6.**

Identification code	LAl(OTf)Me	
Empirical formula	C <sub>38</sub> H <sub>20</sub> Al <sub>2</sub> F <sub>26</sub> N <sub>4</sub> O <sub>6</sub> S <sub>2</sub>	
Formula weight	1240.66	
Temperature	153(2) K	
Wavelength	0.71069 Å	
Crystal system	Triclinic	
Space group	P-1	
Unit cell dimensions	a = 11.207(5) Å	α = 62.228(5)°.
	b = 16.174(5) Å	β = 80.765(5)°.
	c = 16.617(5) Å	γ = 88.074(5)°.
Volume	2627.6(16) Å <sup>3</sup>	
Z	2	
Density (calculated)	1.568 Mg/m <sup>3</sup>	
Absorption coefficient	0.273 mm <sup>-1</sup>	
F(000)	1232	
Crystal size	0.20 x 0.15 x 0.20 mm <sup>3</sup>	
Theta range for data collection	1.40 to 27.35°.	
Index ranges	-13 ≤ h ≤ 14, -20 ≤ k ≤ 15, -21 ≤ l ≤ 21	
Reflections collected	16895	
Independent reflections	10473 [R(int) = 0.1146]	
Completeness to theta = 27.35°	88.1 %	
Absorption correction	None	
Refinement method	Full-matrix least-squares on F <sup>2</sup>	
Data / restraints / parameters	10473 / 432 / 709	
Goodness-of-fit on F <sup>2</sup>	0.752	
Final R indices [I > 2σ(I)]	R1 = 0.0843, wR2 = 0.1815	
R indices (all data)	R1 = 0.3061, wR2 = 0.2370	
Largest diff. peak and hole	0.373 and -0.391 e.Å <sup>-3</sup>	

**Table 4.62. Selected bond lengths (Å) for (CH(CMe<sub>2</sub>)<sub>2</sub>(NC<sub>6</sub>F<sub>5</sub>)<sub>2</sub>)Al(OTf)Me, 3.6.**

C(1)-C(2)	1.396(11)	C(20)-C(21)	1.400(10)
C(2)-C(3)	1.382(10)	C(21)-C(22)	1.408(10)
C(1)-N(1)	1.330(10)	C(20)-N(3)	1.337(9)
C(3)-N(2)	1.333(9)	C(22)-N(4)	1.306(9)
N(1)-Al(1)	1.859(7)	N(3)-Al(2)	1.876(7)
N(2)-Al(1)	1.876(7)	N(4)-Al(2)	1.874(7)
O(1)-Al(1)	1.825(6)	O(4)-Al(2)	1.813(6)
C(18)-Al(1)	1.934(8)	C(37)-Al(2)	1.933(8)

**Table 4.63. Selected bond angles (°) for (CH(CMe<sub>2</sub>)<sub>2</sub>(NC<sub>6</sub>F<sub>5</sub>)<sub>2</sub>)Al(OTf)Me, 3.6.**

C(1)-C(2)-C(3)	125.8(8)	C(20)-C(21)-C(22)	129.0(7)
C(2)-C(1)-N(1)	123.5(8)	C(21)-C(20)-N(3)	122.1(8)
C(2)-C(3)-N(2)	123.9(8)	C(21)-C(22)-N(4)	120.4(8)
C(1)-N(1)-Al(1)	123.1(6)	C(20)-N(3)-Al(2)	124.6(6)
C(3)-N(2)-Al(1)	122.8(6)	C(22)-N(4)-Al(2)	127.3(6)
N(1)-Al(1)-N(2)	96.7(3)	N(3)-Al(2)-N(4)	96.6(3)
N(1)-Al(1)-O(1)	100.8(3)	N(3)-Al(2)-O(1)	101.1(3)
N(1)-Al(1)-C(18)	120.4(4)	N(3)-Al(2)-C(37)	119.3(3)
N(2)-Al(1)-O(1)	105.7(3)	N(4)-Al(2)-O(1)	107.1(3)
N(2)-Al(1)-C(18)	116.4(3)	N(4)-Al(2)-C(37)	118.7(3)
O(1)-Al(1)-C(18)	114.2(3)	O(1)-Al(2)-C(37)	111.6(3)



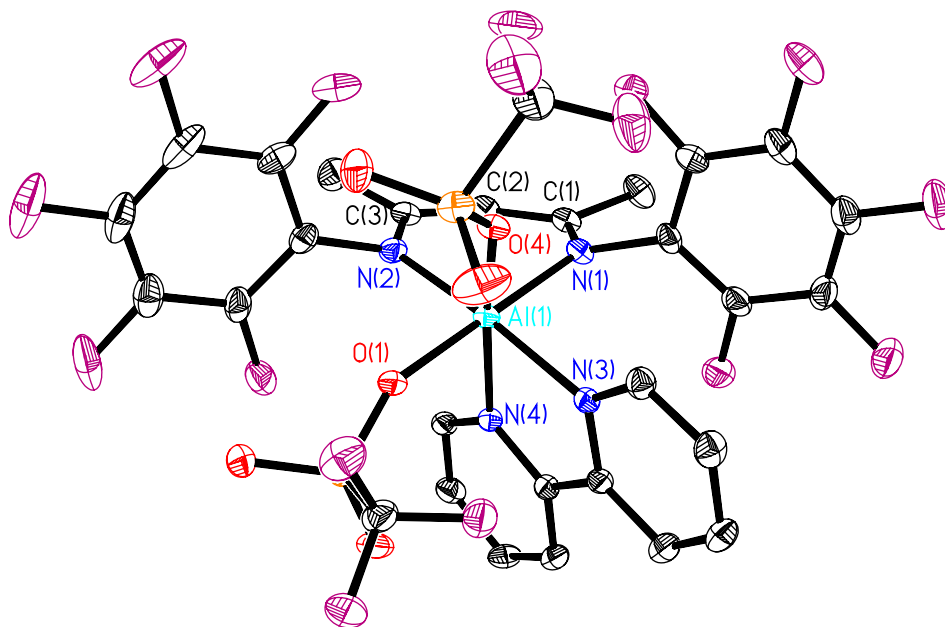


**Figure 4.27.** Molecular structure of  $(\text{CH}(\text{CMe}_2)_2(\text{NC}_6\text{F}_5)_2)\text{Al}(\text{OTf})_2(\text{bipy})$ , **3.8**, showing the atom number scheme for selected atoms. The thermal ellipsoids are shown at the 30 % probability level. All hydrogen atoms have been omitted for clarity.

**Table 4.64. Crystal data and structure refinement for (CH(CMe<sub>2</sub>)<sub>2</sub>(NC<sub>6</sub>F<sub>5</sub>)<sub>2</sub>)Al(OTf)<sub>2</sub>(bipy), 3.8.**

Identification code	LAl(OTf) <sub>2</sub> (bipy)	
Empirical formula	C <sub>29</sub> H <sub>15</sub> Al F <sub>16</sub> N <sub>4</sub> O <sub>6</sub> S <sub>2</sub>	
Formula weight	910.57	
Temperature	153(2) K	
Wavelength	0.71069 Å	
Crystal system	Monoclinic	
Space group	C2/c	
Unit cell dimensions	a = 34.635(5) Å	a = 90.000°.
	b = 12.688(5) Å	b = 103.128(5)°.
	c = 17.564(5) Å	g = 90.000°.
Volume	7517(4) Å <sup>3</sup>	
Z	8	
Density (calculated)	1.609 Mg/m <sup>3</sup>	
Absorption coefficient	0.291 mm <sup>-1</sup>	
F(000)	3632	
Crystal size	0.18 x 0.17 x 0.15 mm <sup>3</sup>	
Theta range for data collection	1.71 to 27.50°.	
Index ranges	-44 ≤ h ≤ 44, -14 ≤ k ≤ 16, -22 ≤ l ≤ 22	
Reflections collected	14331	
Independent reflections	8618 [R(int) = 0.0364]	
Completeness to theta = 27.50°	99.8 %	
Absorption correction	Semi-empirical from equivalents	
Max. and min. transmission	0.9577 and 0.9495	
Refinement method	Full-matrix least-squares on F <sup>2</sup>	
Data / restraints / parameters	8618 / 0 / 527	
Goodness-of-fit on F <sup>2</sup>	1.005	
Final R indices [I > 2σ(I)]	R1 = 0.0530, wR2 = 0.1362	
R indices (all data)	R1 = 0.0961, wR2 = 0.1518	
Extinction coefficient	0.00026(10)	
Largest diff. peak and hole	0.421 and -0.398 e.Å <sup>-3</sup>	

**Table 4.65. Selected bond lengths (Å) for (CH(CMe<sub>2</sub>)<sub>2</sub>(NC<sub>6</sub>F<sub>5</sub>)<sub>2</sub>)Al(OTf)<sub>2</sub>(bipy), 3.8.**

C(1)-C(2)	1.389(4)	C(2)-C(3)	1.389(4)
C(1)-N(1)	1.341(3)	C(3)-N(2)	1.348(2)
N(1)-Al(1)	1.989(2)	N(2)-Al(1)	1.975(2)
N(4)-Al(1)	2.047(2)	O(4)-Al(1)	1.902(2)
N(3)-Al(1)	2.053(2)	O(1)-Al(1)	1.941(2)

**Table 4.66. Selected bond angles (°) for (CH(CMe<sub>2</sub>)<sub>2</sub>(NC<sub>6</sub>F<sub>5</sub>)<sub>2</sub>)Al(OTf)<sub>2</sub>(bipy), 3.8.**

C(1)-C(2)-C(3)	127.3(3)	C(2)-C(1)-N(1)	122.6(3)
C(2)-C(3)-N(2)	122.3(3)	C(1)-N(1)-Al(1)	124.4(2)
C(3)-N(2)-Al(1)	125.5(2)	N(1)-Al(1)-N(2)	90.24(10)
N(1)-Al(1)-N(4)	91.78(9)	N(1)-Al(1)-O(4)	91.06(9)
N(1)-Al(1)-N(3)	90.53(9)	N(2)-Al(1)-N(4)	94.87(9)
N(2)-Al(1)-O(4)	94.33(9)	N(2)-Al(1)-O(1)	91.44(9)
N(4)-Al(1)-N(3)	79.07(9)	N(4)-Al(1)-O(1)	90.02(8)
O(4)-Al(1)-N(3)	91.69(8)	O(4)-Al(1)-O(1)	86.87(8)
N(3)-Al(1)-O(1)	88.00(8)		

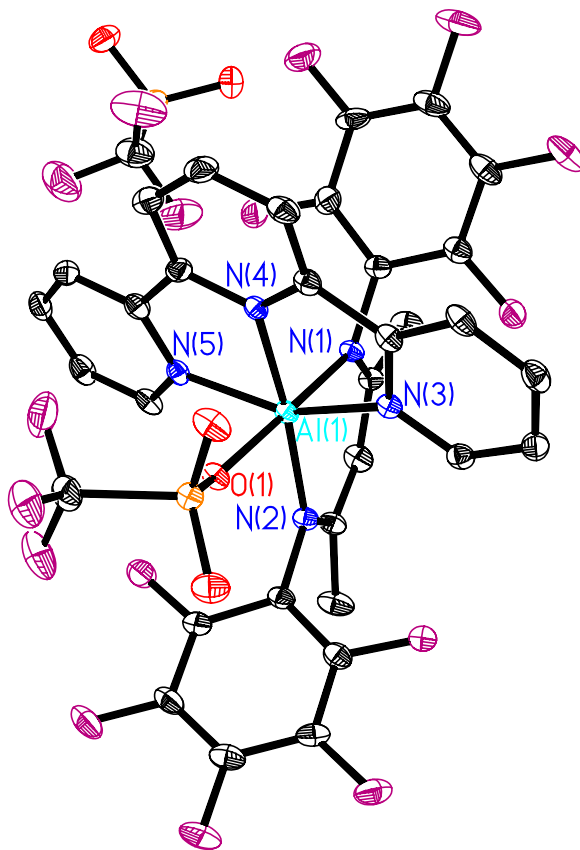


Figure 4.28. Molecular structure of  $[(\text{CH}(\text{CMe}_2)_2(\text{NC}_6\text{F}_5)_2)\text{Al}(\text{OTf})(\text{terpy})][\text{OTf}]$ , 3.9, showing the atom number scheme for selected atoms. The thermal ellipsoids are shown at the 30 % probability level. All hydrogen atoms and the solvent molecules have been omitted for clarity.

**Table 4.67. Crystal data and structure refinement for [(CH(CMe<sub>2</sub>)<sub>2</sub>(NC<sub>6</sub>F<sub>5</sub>)<sub>2</sub>)Al(OTf)(terpy)][OTf], 3.9.**

Identification code	[LAl(OTf)(terpy)][OTf]	
Empirical formula	C <sub>37</sub> H <sub>24</sub> Al Cl <sub>6</sub> F <sub>16</sub> N <sub>5</sub> O <sub>6</sub> S <sub>2</sub>	
Formula weight	1242.41	
Temperature	153(2) K	
Wavelength	0.71069 Å	
Crystal system	Monoclinic	
Space group	P2 <sub>1</sub> /c	
Unit cell dimensions	a = 19.758(5) Å	α = 90.000(5)°.
	b = 13.678(5) Å	β = 113.289(5)°.
	c = 19.512(5) Å	γ = 90.000(5)°.
Volume	4843(2) Å <sup>3</sup>	
Z	4	
Density (calculated)	1.704 Mg/m <sup>3</sup>	
Absorption coefficient	0.571 mm <sup>-1</sup>	
F(000)	2480	
Crystal size	0.20 x 0.15 x 0.13 mm <sup>3</sup>	
Theta range for data collection	2.10 to 27.50°.	
Index ranges	-25 ≤ h ≤ 25, -17 ≤ k ≤ 15, -25 ≤ l ≤ 25	
Reflections collected	19427	
Independent reflections	10976 [R(int) = 0.0720]	
Completeness to theta = 27.50°	98.7 %	
Absorption correction	None	
Max. and min. transmission	0.9294 and 0.8943	
Refinement method	Full-matrix least-squares on F <sup>2</sup>	
Data / restraints / parameters	10976 / 0 / 653	
Goodness-of-fit on F <sup>2</sup>	1.033	
Final R indices [I > 2σ(I)]	R1 = 0.0670, wR2 = 0.1692	
R indices (all data)	R1 = 0.1678, wR2 = 0.2118	
Largest diff. peak and hole	0.797 and -0.816 e.Å <sup>-3</sup>	

**Table 4.68. Selected bond lengths (Å) for [(CH(CMe<sub>2</sub>)<sub>2</sub>(NC<sub>6</sub>F<sub>5</sub>)<sub>2</sub>)Al(OTf)(terpy)] [OTf], 3.9.**

C(1)-C(2)	1.400(6)	C(2)-C(3)	1.380(6)
C(1)-N(1)	1.328(5)	C(3)-N(2)	1.357(5)
N(1)-Al(1)	1.975(4)	N(2)-Al(1)	1.967(4)
N(3)-Al(1)	2.056(3)	N(5)-Al(1)	2.060(3)
N(4)-Al(1)	1.991(3)	O(1)-Al(1)	1.933(3)

**Table 4.69. Selected bond angles (°) for [(CH(CMe<sub>2</sub>)<sub>2</sub>(NC<sub>6</sub>F<sub>5</sub>)<sub>2</sub>)Al(OTf)(terpy)] [OTf], 3.9.**

C(1)-C(2)-C(3)	128.5(4)	C(2)-C(1)-N(1)	122.1(4)
C(2)-C(3)-N(2)	123.4(4)	C(1)-N(1)-Al(1)	126.2(4)
C(3)-N(2)-Al(1)	124.6(3)	N(1)-Al(1)-N(2)	92.19(15)
N(1)-Al(1)-N(3)	90.18(14)	N(1)-Al(1)-N(5)	90.42(14)
N(1)-Al(1)-N(4)	95.43(14)	N(2)-Al(1)-N(3)	102.62(14)
N(2)-Al(1)-N(5)	102.62(14)	N(2)-Al(1)-O(1)	86.99(14)
N(3)-Al(1)-N(4)	78.10(14)	N(3)-Al(1)-O(1)	91.85(13)
N(5)-Al(1)-N(4)	77.67(14)	N(5)-Al(1)-O(1)	87.89(13)
N(4)-Al(1)-O(1)	85.37(13)		

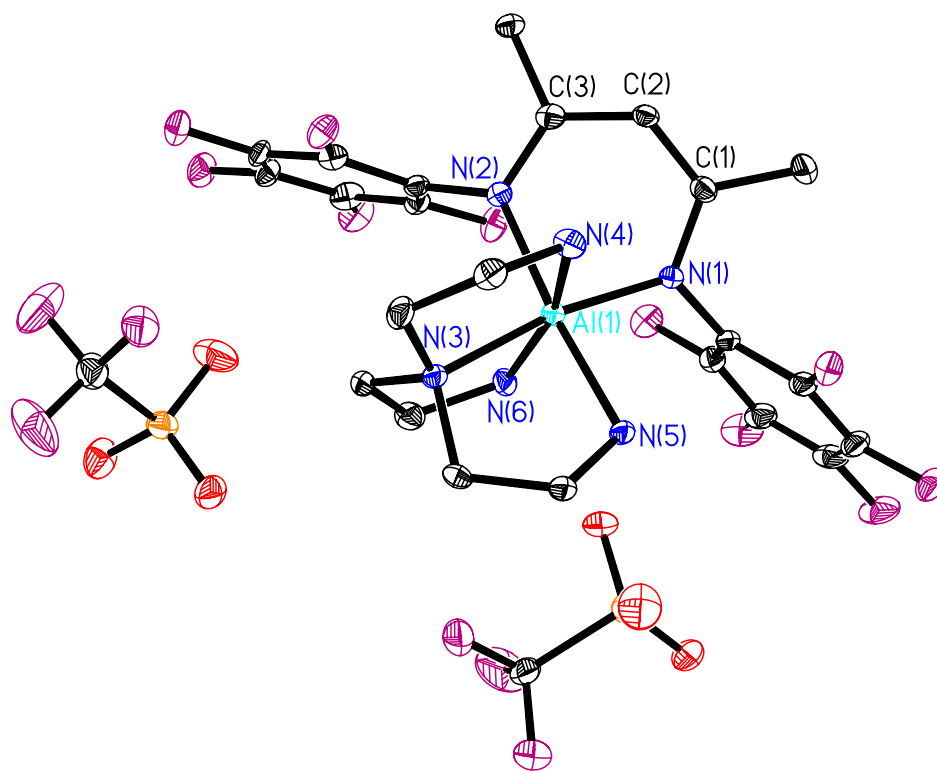


**Figure 4.29.** Molecular structure of  $[(\text{CH}(\text{CMe}_2)_2(\text{NC}_6\text{F}_5)_2)\text{Al}(\text{tren})][2\cdot\text{OTf}]$ , **3.10**, showing the atom number scheme for selected atoms. The thermal ellipsoids are shown at the 30 % probability level. All hydrogen atoms have been omitted for clarity.

**Table 4.70. Crystal data and structure refinement for [(CH(CMe<sub>2</sub>)<sub>2</sub>(NC<sub>6</sub>F<sub>5</sub>)<sub>2</sub>)Al(tren)][2·OTf], 3.10.**

Identification code	[LAl(tren)][2·OTf]	
Empirical formula	C <sub>27</sub> H <sub>23</sub> Al Cl <sub>4</sub> F <sub>16</sub> N <sub>6</sub> O <sub>6</sub> S <sub>2</sub>	
Formula weight	1064.41	
Temperature	153(2) K	
Wavelength	0.71073 Å	
Crystal system	Monoclinic	
Space group	P2 <sub>1</sub> /c	
Unit cell dimensions	a = 11.195(2) Å	α = 90°.
	b = 21.287(4) Å	β = 100.34(3)°.
	c = 17.378(4) Å	γ = 90°.
Volume	4073.9(14) Å <sup>3</sup>	
Z	4	
Density (calculated)	1.735 Mg/m <sup>3</sup>	
Absorption coefficient	0.537 mm <sup>-1</sup>	
F(000)	2128	
Crystal size	0.20 x 0.20 x 0.15 mm <sup>3</sup>	
Theta range for data collection	1.53 to 27.00°.	
Index ranges	-14 ≤ h ≤ 14, -27 ≤ k ≤ 24, -22 ≤ l ≤ 22	
Reflections collected	14891	
Independent reflections	8853 [R(int) = 0.0696]	
Completeness to theta = 27.00°	99.4 %	
Absorption correction	None	
Max. and min. transmission	0.9238 and 0.9002	
Refinement method	Full-matrix least-squares on F <sup>2</sup>	
Data / restraints / parameters	8853 / 0 / 558	
Goodness-of-fit on F <sup>2</sup>	1.021	
Final R indices [I > 2σ(I)]	R <sub>1</sub> = 0.0763, wR <sub>2</sub> = 0.1971	
R indices (all data)	R <sub>1</sub> = 0.1778, wR <sub>2</sub> = 0.2668	
Largest diff. peak and hole	0.981 and -0.897 e.Å <sup>-3</sup>	



**Table 4.71. Selected bond lengths (Å) for [(CH(CMe<sub>2</sub>)<sub>2</sub>(NC<sub>6</sub>F<sub>5</sub>)<sub>2</sub>)Al(tren)] [2·OTf], 3.10.**

C(1)-C(2)	1.372(7)	C(2)-C(3)	1.405(8)
C(1)-N(1)	1.365(7)	C(3)-N(2)	1.354(7)
N(1)-Al(1)	1.962(5)	N(2)-Al(1)	2.054(4)
N(4)-Al(1)	2.053(5)	N(6)-Al(1)	2.037(5)
N(5)-Al(1)	2.086(4)	N(3)-Al(1)	2.093(5)

**Table 4.72. Selected bond angles (°) for [(CH(CMe<sub>2</sub>)<sub>2</sub>(NC<sub>6</sub>F<sub>5</sub>)<sub>2</sub>)Al(tren)] [2·OTf], 3.10.**

C(1)-C(2)-C(3)	125.2(5)	C(2)-C(1)-N(1)	121.7(5)
C(2)-C(3)-N(2)	122.8(5)	C(1)-N(1)-Al(1)	120.1(3)
C(3)-N(2)-Al(1)	118.1(4)	N(1)-Al(1)-N(2)	88.18(18)
N(1)-Al(1)-N(4)	97.39(19)	N(1)-Al(1)-N(6)	98.02(19)
N(1)-Al(1)-N(5)	87.65(18)	N(2)-Al(1)-N(4)	88.04(19)
N(2)-Al(1)-N(6)	90.41(19)	N(2)-Al(1)-N(3)	102.00(18)
N(4)-Al(1)-N(5)	89.35(19)	N(4)-Al(1)-N(3)	83.88(19)
N(6)-Al(1)-N(5)	93.32(19)	N(6)-Al(1)-N(3)	81.31(19)
N(5)-Al(1)-N(3)	82.23(18)		

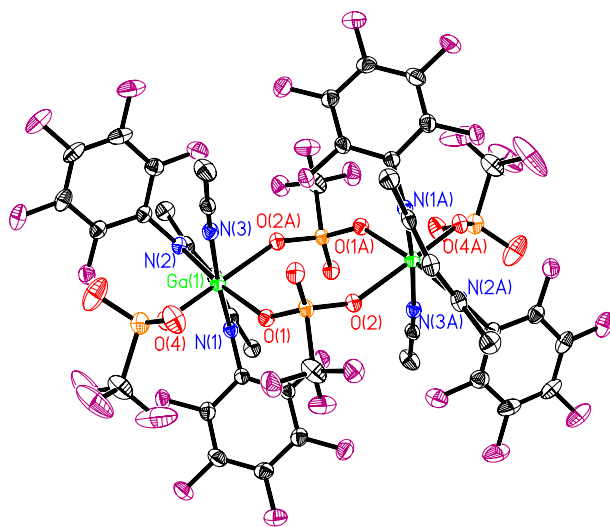


Figure 4.30. Molecular structure of  $((\text{CH}(\text{CMe}_2)_2(\text{NC}_6\text{F}_5)_2)\text{Ga}(\text{OTf})_2(\text{CH}_3\text{CN}))_2$ , 3.11, showing the atom number scheme for selected atoms. The thermal ellipsoids are shown at the 30 % probability level. All hydrogen atoms have been omitted for clarity.

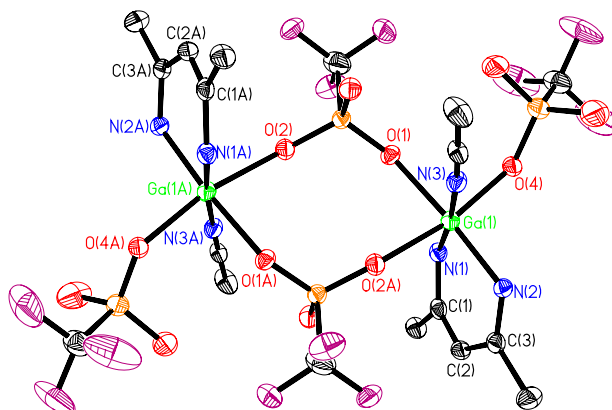


Figure 4.31. Molecular structure of  $((\text{CH}(\text{CMe}_2)_2(\text{NC}_6\text{F}_5)_2)\text{Ga}(\text{OTf})_2(\text{CH}_3\text{CN}))_2$ , 3.11, showing the atom number scheme for selected atoms. The thermal ellipsoids are shown at the 30 % probability level. All hydrogen atoms and the  $\text{C}_6\text{F}_5$ -substituents have been omitted for clarity.

**Table 4.73. Crystal data and structure refinement for ((CH(CMe<sub>2</sub>)<sub>2</sub>(NC<sub>6</sub>F<sub>5</sub>)<sub>2</sub>)Ga(OTf)<sub>2</sub>(CH<sub>3</sub>CN))<sub>2</sub>, 3.11.**

Identification code	[LGa(OTf) <sub>2</sub> (CH <sub>3</sub> CN)] <sub>2</sub>	
Empirical formula	C <sub>42</sub> H <sub>20</sub> F <sub>32</sub> Ga <sub>2</sub> N <sub>6</sub> O <sub>12</sub> S <sub>4</sub>	
Formula weight	1676.32	
Temperature	153(2) K	
Wavelength	0.71073 Å	
Crystal system	Monoclinic	
Space group	P2 <sub>1</sub> /c	
Unit cell dimensions	a = 12.725(3) Å	α = 90°.
	b = 11.572(2) Å	β = 102.61(3)°.
	c = 19.975(4) Å	γ = 90°.
Volume	2870.6(10) Å <sup>3</sup>	
Z	2	
Density (calculated)	1.939 Mg/m <sup>3</sup>	
Absorption coefficient	1.253 mm <sup>-1</sup>	
F(000)	1648	
Crystal size	0.20 x 0.18 x 0.15 mm <sup>3</sup>	
Theta range for data collection	2.09 to 27.46°.	
Index ranges	-16 ≤ h ≤ 16, -14 ≤ k ≤ 11, -25 ≤ l ≤ 25	
Reflections collected	11208	
Independent reflections	6540 [R(int) = 0.0391]	
Completeness to theta = 27.46°	99.8 %	
Absorption correction	Semi-empirical from equivalents	
Max. and min. transmission	0.8344 and 0.7877	
Refinement method	Full-matrix least-squares on F <sup>2</sup>	
Data / restraints / parameters	6540 / 18 / 439	
Goodness-of-fit on F <sup>2</sup>	1.036	
Final R indices [I > 2σ(I)]	R1 = 0.0581, wR2 = 0.1452	
R indices (all data)	R1 = 0.1057, wR2 = 0.1790	
Largest diff. peak and hole	1.241 and -0.940 e.Å <sup>-3</sup>	

**Table 4.74. Selected bond lengths (Å) for ((CH(CMe<sub>2</sub>)<sub>2</sub>(NC<sub>6</sub>F<sub>5</sub>)<sub>2</sub>)Ga(OTf)<sub>2</sub>(CH<sub>3</sub>CN))<sub>2</sub>, 3.11.**

C(1)-C(2)	1.384(7)	C(2)-C(3)	1.394(7)
C(1)-N(1)	1.358(6)	C(3)-N(2)	1.344(6)
N(1)-Ga(1)	1.954(4)	N(2)-Ga(1)	1.969(3)
O(2A)-Ga(1)	2.101(3)	O(4)-Ga(1)	1.964(3)
O(1)-Ga(1)	2.069(3)	N(3)-Ga(1)	2.047(4)

**Table 4.75. Selected bond angles (°) for ((CH(CMe<sub>2</sub>)<sub>2</sub>(NC<sub>6</sub>F<sub>5</sub>)<sub>2</sub>)Ga(OTf)<sub>2</sub>(CH<sub>3</sub>CN))<sub>2</sub>, 3.11.**

C(1)-C(2)-C(3)	128.1(4)	C(2)-C(1)-N(1)	123.6(4)
C(2)-C(3)-N(2)	122.0(4)	C(1)-N(1)-Ga(1)	120.7(3)
C(3)-N(2)-Ga(1)	122.3(3)	N(1)-Ga(1)-N(2)	92.88(14)
N(1)-Ga(1)-O(2A)	94.78(13)	N(1)-Ga(1)-O(4)	94.56(14)
N(1)-Ga(1)-O(1)	90.29(13)	N(2)-Ga(1)-O(2A)	89.83(14)
N(2)-Ga(1)-O(4)	98.07(14)	N(2)-Ga(1)-N(3)	90.60(15)
O(2A)-Ga(1)-O(1)	84.29(12)	O(2A)-Ga(1)-N(3)	82.02(14)
O(4)-Ga(1)-O(1)	87.28(12)	O(4)-Ga(1)-N(3)	88.12(14)
O(1)-Ga(1)-N(3)	85.93(13)		

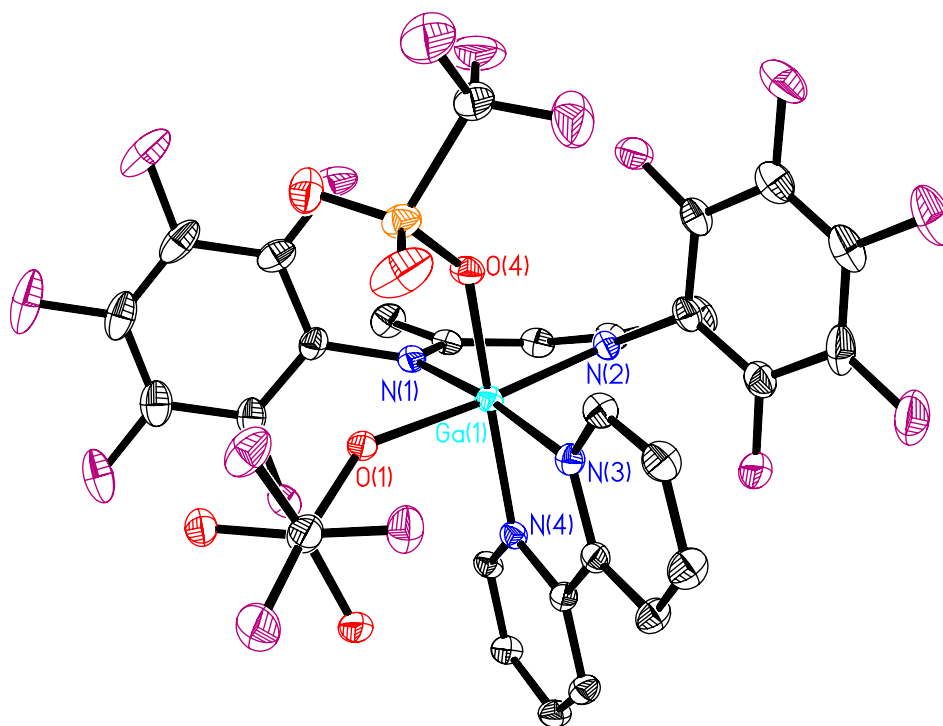


**Figure 4.32.** Molecular structure of  $(\text{CH}(\text{CMe}_2)_2(\text{NC}_6\text{F}_5)_2)\text{Ga}(\text{OTf})_2(\text{bipy})$ , **3.12**, showing the atom number scheme for selected atoms. The thermal ellipsoids are shown at the 30 % probability level. All hydrogen atoms have been omitted for clarity.

**Table 4.76. Crystal data and structure refinement for (CH(CMe<sub>2</sub>)<sub>2</sub>(NC<sub>6</sub>F<sub>5</sub>)<sub>2</sub>)Ga(OTf)<sub>2</sub>(bipy), 3.12.**

Identification code	LGa(OTf) <sub>2</sub> (bipy)	
Empirical formula	C <sub>29</sub> H <sub>15</sub> F <sub>16</sub> Ga N <sub>4</sub> O <sub>6</sub> S <sub>2</sub>	
Formula weight	953.29	
Temperature	153(2) K	
Wavelength	0.71069 Å	
Crystal system	Monoclinic	
Space group	C2/c	
Unit cell dimensions	a = 34.912(5) Å	a = 90°.
	b = 12.692(5) Å	b = 102.752(5)°.
	c = 17.375(5) Å	g = 90°.
Volume	7509(4) Å <sup>3</sup>	
Z	8	
Density (calculated)	1.686 Mg/m <sup>3</sup>	
Absorption coefficient	0.970 mm <sup>-1</sup>	
F(000)	3776	
Crystal size	0.18 x 0.15 x 0.15 mm <sup>3</sup>	
Theta range for data collection	1.71 to 27.47°.	
Index ranges	-44 ≤ h ≤ 44, -16 ≤ k ≤ 15, -22 ≤ l ≤ 22	
Reflections collected	14699	
Independent reflections	8555 [R(int) = 0.0363]	
Completeness to theta = 27.47°	99.4 %	
Absorption correction	Semi-empirical from equivalents	
Max. and min. transmission	0.8682 and 0.8448	
Refinement method	Full-matrix least-squares on F <sup>2</sup>	
Data / restraints / parameters	8555 / 0 / 525	
Goodness-of-fit on F <sup>2</sup>	1.029	
Final R indices [I > 2σ(I)]	R1 = 0.0525, wR2 = 0.1438	
R indices (all data)	R1 = 0.0894, wR2 = 0.1571	
Largest diff. peak and hole	0.698 and -0.559 e.Å <sup>-3</sup>	

**Table 4.77. Selected bond lengths (Å) for (CH(CMe<sub>2</sub>)<sub>2</sub>(NC<sub>6</sub>F<sub>5</sub>)<sub>2</sub>)Ga(OTf)<sub>2</sub>(bipy), 3.12.**

C(1)-C(2)	1.389(5)	C(2)-C(3)	1.393(5)
C(1)-N(1)	1.336(5)	C(3)-N(2)	1.331(5)
N(1)-Ga(1)	1.999(3)	N(2)-Ga(1)	2.012(3)
N(4)-Ga(1)	2.069(3)	O(4)-Ga(1)	2.014(2)
O(1)-Ga(1)	2.085(2)	N(3)-Ga(1)	2.077(3)

**Table 4.78. Selected bond angles (°) for (CH(CMe<sub>2</sub>)<sub>2</sub>(NC<sub>6</sub>F<sub>5</sub>)<sub>2</sub>)Ga(OTf)<sub>2</sub>(bipy), 3.12.**

C(1)-C(2)-C(3)	128.6(4)	C(2)-C(1)-N(1)	123.0(3)
C(2)-C(3)-N(2)	122.6(3)	C(1)-N(1)-Ga(1)	123.8(2)
C(3)-N(2)-Ga(1)	123.2(2)	N(1)-Ga(1)-N(2)	91.64(12)
N(1)-Ga(1)-N(4)	96.26(11)	N(1)-Ga(1)-O(4)	93.02(11)
N(1)-Ga(1)-O(1)	90.40(11)	N(2)-Ga(1)-N(4)	94.29(11)
N(2)-Ga(1)-O(4)	90.36(10)	N(2)-Ga(1)-N(3)	92.56(12)
N(4)-Ga(1)-O(1)	90.88(10)	N(4)-Ga(1)-N(3)	78.99(11)
O(4)-Ga(1)-O(1)	84.12(9)	O(4)-Ga(1)-N(3)	91.40(10)
O(1)-Ga(1)-N(3)	85.85(10)		

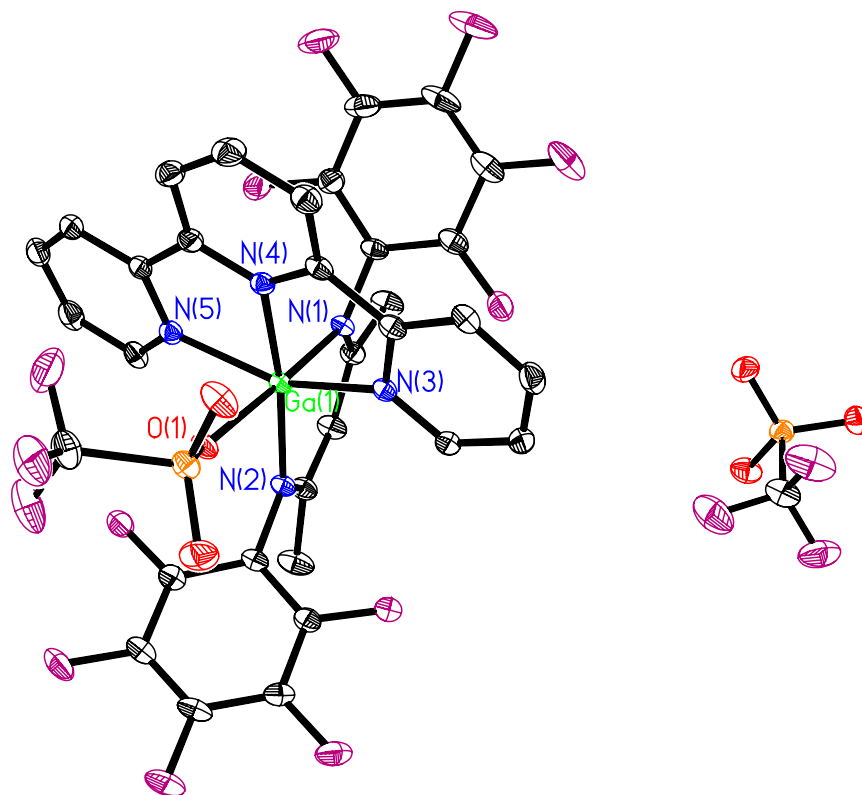


Figure 4.33. Molecular structure of  $[(\text{CH}(\text{CMe}_2)_2(\text{NC}_6\text{F}_5)_2)\text{Ga}(\text{OTf})(\text{terpy})][\text{OTf}]$ , 3.13, showing the atom number scheme for selected atoms. The thermal ellipsoids are shown at the 30 % probability level. All hydrogen atoms and the solvent molecules have been omitted for clarity.



**Table 4.79. Crystal data and structure refinement for [(CH(CMe<sub>2</sub>)<sub>2</sub>(NC<sub>6</sub>F<sub>5</sub>)<sub>2</sub>)Ga(OTf)(terpy)][OTf], 3.13.**

Identification code	[LGa(OTf)(terpy)][OTf]	
Empirical formula	C <sub>37</sub> H <sub>24</sub> Cl <sub>6</sub> F <sub>16</sub> Ga N <sub>5</sub> O <sub>6</sub> S <sub>2</sub>	
Formula weight	1285.15	
Temperature	153(2) K	
Wavelength	0.71073 Å	
Crystal system	Monoclinic	
Space group	P2 <sub>1</sub> /c	
Unit cell dimensions	a = 19.726(4) Å	a = 90°.
	b = 13.672(3) Å	b = 113.17(3)°.
	c = 19.629(4) Å	g = 90°.
Volume	4867(2) Å <sup>3</sup>	
Z	4	
Density (calculated)	1.754 Mg/m <sup>3</sup>	
Absorption coefficient	1.092 mm <sup>-1</sup>	
F(000)	2552	
Crystal size	0.18 x 0.13 x 0.10 mm <sup>3</sup>	
Theta range for data collection	2.25 to 27.50°.	
Index ranges	-25 ≤ h ≤ 25, -17 ≤ k ≤ 16, -25 ≤ l ≤ 25	
Reflections collected	19931	
Independent reflections	11098 [R(int) = 0.0341]	
Completeness to theta = 27.50°	99.2 %	
Absorption correction	Semi-empirical from equivalents	
Max. and min. transmission	0.8986 and 0.8276	
Refinement method	Full-matrix least-squares on F <sup>2</sup>	
Data / restraints / parameters	11098 / 0 / 660	
Goodness-of-fit on F <sup>2</sup>	1.048	
Final R indices [I > 2σ(I)]	R1 = 0.0520, wR2 = 0.1368	
R indices (all data)	R1 = 0.0843, wR2 = 0.1620	
Largest diff. peak and hole	0.918 and -0.734 e.Å <sup>-3</sup>	

**Table 4.80. Selected bond lengths (Å) for [(CH(CMe<sub>2</sub>)<sub>2</sub>(NC<sub>6</sub>F<sub>5</sub>)<sub>2</sub>)Ga(OTf)(terpy)] [OTf], 3.13.**

C(1)-C(2)	1.408(5)	C(2)-C(3)	1.384(5)
C(1)-N(1)	1.329(4)	C(3)-N(2)	1.356(4)
N(1)-Ga(1)	1.997(3)	N(2)-Ga(1)	1.983(3)
N(3)-Ga(1)	2.101(3)	N(5)-Ga(1)	2.112(3)
N(4)-Ga(1)	2.042(3)	O(1)-Ga(1)	2.112(2)

**Table 4.81. Selected bond angles (°) for [(CH(CMe<sub>2</sub>)<sub>2</sub>(NC<sub>6</sub>F<sub>5</sub>)<sub>2</sub>)Ga(OTf)(terpy)] [OTf], 3.13.**

C(1)-C(2)-C(3)	129.1(3)	C(2)-C(1)-N(1)	122.9(3)
C(2)-C(3)-N(2)	124.2(3)	C(1)-N(1)-Ga(1)	124.4(2)
C(3)-N(2)-Ga(1)	123.2(2)	N(1)-Ga(1)-N(2)	93.68(11)
N(1)-Ga(1)-N(3)	91.63(10)	N(1)-Ga(1)-N(5)	92.15(11)
N(1)-Ga(1)-N(4)	97.33(11)	N(2)-Ga(1)-N(3)	103.50(11)
N(2)-Ga(1)-N(5)	101.95(11)	N(2)-Ga(1)-O(1)	86.28(10)
N(3)-Ga(1)-N(4)	77.03(11)	N(3)-Ga(1)-O(1)	90.90(10)
N(5)-Ga(1)-N(4)	76.94(11)	N(5)-Ga(1)-O(1)	85.33(10)
N(4)-Ga(1)-O(1)	82.69(10)		

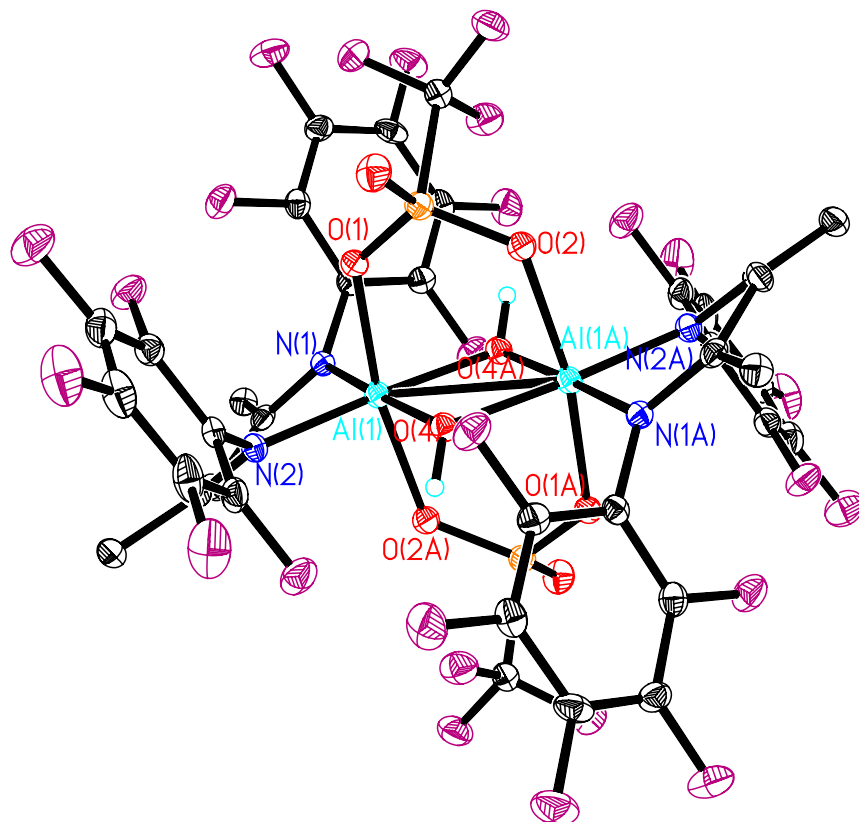


**Figure 4.34.** Molecular structure of  $((\text{CH}(\text{CMe}_2)_2(\text{NC}_6\text{F}_5)_2)\text{Al}(\text{OTf})(\text{OH}))_2$ , **3.15**, showing the atom number scheme for selected atoms. The thermal ellipsoids are shown at the 30 % probability level. All hydrogen atoms have been omitted for clarity.

**Table 4.82. Crystal data and structure refinement for ((CH(CMe<sub>2</sub>)<sub>2</sub>(NC<sub>6</sub>F<sub>5</sub>)<sub>2</sub>)Al(OTf)(OH))<sub>2</sub>, 3.15.**

Identification code	LAl(OTf)(OH)	
Empirical formula	C <sub>18</sub> H <sub>8</sub> Al F <sub>13</sub> N <sub>2</sub> O <sub>4</sub> S	
Formula weight	622.30	
Temperature	153(2) K	
Wavelength	0.71069 Å	
Crystal system	Monoclinic	
Space group	P2 <sub>1</sub> /n	
Unit cell dimensions	a = 11.430(5) Å	α = 90.000(5)°.
	b = 12.434(5) Å	β = 107.823(5)°.
	c = 15.903(5) Å	γ = 90.000(5)°.
Volume	2151.7(14) Å <sup>3</sup>	
Z	4	
Density (calculated)	1.921 Mg/m <sup>3</sup>	
Absorption coefficient	0.337 mm <sup>-1</sup>	
F(000)	1232	
Crystal size	0.16 x 0.10 x 0.15 mm <sup>3</sup>	
Theta range for data collection	1.94 to 27.47°.	
Index ranges	-14 ≤ h ≤ 14, -15 ≤ k ≤ 16, -20 ≤ l ≤ 20	
Reflections collected	9164	
Independent reflections	4924 [R(int) = 0.0422]	
Completeness to theta = 27.47°	99.9 %	
Absorption correction	None	
Refinement method	Full-matrix least-squares on F <sup>2</sup>	
Data / restraints / parameters	4924 / 0 / 359	
Goodness-of-fit on F <sup>2</sup>	1.094	
Final R indices [I > 2σ(I)]	R <sub>1</sub> = 0.0590, wR <sub>2</sub> = 0.1369	
R indices (all data)	R <sub>1</sub> = 0.1121, wR <sub>2</sub> = 0.1789	
Extinction coefficient	0.023(2)	
Largest diff. peak and hole	0.846 and -0.859 e.Å <sup>-3</sup>	

**Table 4.83. Selected bond lengths (Å) for ((CH(CMe<sub>2</sub>)<sub>2</sub>(NC<sub>6</sub>F<sub>5</sub>)<sub>2</sub>)Al(OTf)(OH))<sub>2</sub>, 3.15.**

C(1)-C(2)	1.397(5)	C(2)-C(3)	1.380(5)
C(1)-N(1)	1.337(4)	C(3)-N(2)	1.349(4)
N(1)-Al(1)	1.929(3)	N(2)-Al(1)	1.933(3)
O(1)-Al(1)	2.001(3)	O(2A)-Al(1)	2.030(3)
O(4A)-Al(1)	1.870(4)	O(4)-Al(1)	1.870(3)

**Table 4.84. Selected bond angles (°) for ((CH(CMe<sub>2</sub>)<sub>2</sub>(NC<sub>6</sub>F<sub>5</sub>)<sub>2</sub>)Al(OTf)(OH))<sub>2</sub>, 3.15.**

C(1)-C(2)-C(3)	125.5(3)	C(2)-C(1)-N(1)	121.4(3)
C(2)-C(3)-N(2)	121.8(3)	C(1)-N(1)-Al(1)	122.5(2)
C(3)-N(2)-Al(1)	122.0(2)	N(1)-Al(1)-N(2)	89.92(12)
N(1)-Al(1)-O(1)	95.41(11)	N(1)-Al(1)-O(2A)	92.18(11)
N(1)-Al(1)-O(4A)	95.48(11)	N(2)-Al(1)-O(1)	93.94(11)
N(2)-Al(1)-O(2A)	94.10(12)	N(2)-Al(1)-O(4)	93.67(11)
O(1)-Al(1)-O(4A)	86.64(11)	O(1)-Al(1)-O(4)	85.64(11)
O(2A)-Al(1)-O(4A)	84.63(11)	O(2A)-Al(1)-O(4)	86.28(10)
O(4A)-Al(1)-O(4)	80.90(11)	Al(1)-O(4)-Al(1A)	99.10(11)

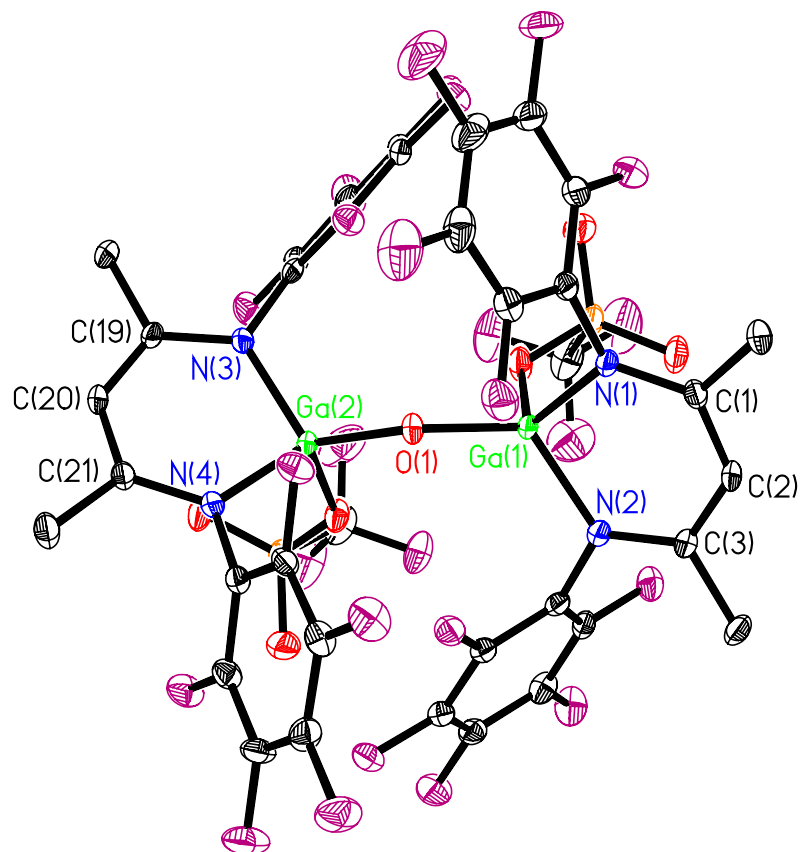


**Figure 4.35.** Molecular structure of  $((\text{CH}(\text{CMe}_2)_2(\text{NC}_6\text{F}_5)_2)\text{Ga}(\text{OTf}))_2\text{O}$ , **3.16**, showing the atom number scheme for selected atoms. The thermal ellipsoids are shown at the 30 % probability level. All hydrogen atoms have been omitted for clarity.

**Table 4.85. Crystal data and structure refinement for ((CH(CMe<sub>2</sub>)<sub>2</sub>(NC<sub>6</sub>F<sub>5</sub>)<sub>2</sub>)Ga(OTf))<sub>2</sub>O, 3.16.**

Identification code	(LGa(OTf)) <sub>2</sub> O	
Empirical formula	C <sub>37</sub> H <sub>16</sub> Cl <sub>2</sub> F <sub>26</sub> Ga <sub>2</sub> N <sub>4</sub> O <sub>7</sub> S <sub>2</sub>	
Formula weight	1397.00	
Temperature	153(2) K	
Wavelength	0.71073 Å	
Crystal system	Orthorhombic	
Space group	Pbca	
Unit cell dimensions	a = 20.787(4) Å	α = 90°.
	b = 20.376(4) Å	β = 90°.
	c = 23.060(5) Å	γ = 90°.
Volume	9767(3) Å <sup>3</sup>	
Z	8	
Density (calculated)	1.900 Mg/m <sup>3</sup>	
Absorption coefficient	1.450 mm <sup>-1</sup>	
F(000)	5472	
Crystal size	0.15 x 0.12 x 0.10 mm <sup>3</sup>	
Theta range for data collection	2.19 to 27.48°.	
Index ranges	-26 ≤ h ≤ 26, -26 ≤ k ≤ 26, -29 ≤ l ≤ 29	
Reflections collected	21365	
Independent reflections	11179 [R(int) = 0.0470]	
Completeness to theta = 27.48°	99.9 %	
Absorption correction	Semi-empirical from equivalents	
Max. and min. transmission	0.8686 and 0.8119	
Refinement method	Full-matrix least-squares on F <sup>2</sup>	
Data / restraints / parameters	11179 / 0 / 725	
Goodness-of-fit on F <sup>2</sup>	0.968	
Final R indices [I > 2σ(I)]	R1 = 0.0416, wR2 = 0.1026	
R indices (all data)	R1 = 0.0867, wR2 = 0.1331	
Largest diff. peak and hole	0.666 and -0.879 e.Å <sup>-3</sup>	

**Table 4.86. Selected bond lengths (Å) for ((CH(CMe<sub>2</sub>)<sub>2</sub>(NC<sub>6</sub>F<sub>5</sub>)<sub>2</sub>)Ga(OTf))<sub>2</sub>O, 3.16.**

C(1)-C(2)	1.386(5)	C(19)-C(20)	1.385(5)
C(2)-C(3)	1.396(5)	C(20)-C(21)	1.381(5)
C(1)-N(1)	1.345(4)	C(19)-N(3)	1.351(4)
C(3)-N(2)	1.351(4)	C(21)-N(4)	1.353(4)
N(1)-Ga(1)	1.896(2)	N(3)-Ga(2)	1.901(3)
N(2)-Ga(1)	1.904(3)	N(4)-Ga(2)	1.900(3)
O(1)-Ga(1)	1.750(2)	O(1)-Ga(2)	1.754(2)
O(2)-Ga(1)	1.915(2)	O(5)-Ga(2)	1.913(2)

**Table 4.87. Selected bond angles (°) for ((CH(CMe<sub>2</sub>)<sub>2</sub>(NC<sub>6</sub>F<sub>5</sub>)<sub>2</sub>)Ga(OTf))<sub>2</sub>O, 3.16.**

C(1)-C(2)-C(3)	129.8(3)	C(19)-C(20)-C(21)	129.4(3)
C(2)-C(1)-N(1)	122.9(3)	C(20)-C(19)-N(3)	123.9(3)
C(2)-C(3)-N(2)	122.8(3)	C(20)-C(21)-N(4)	123.3(3)
C(1)-N(1)-Ga(1)	122.3(2)	C(19)-N(3)-Ga(2)	120.8(2)
C(3)-N(2)-Ga(1)	121.8(2)	C(21)-N(4)-Ga(2)	121.4(2)
N(1)-Ga(1)-N(2)	99.32(11)	N(3)-Ga(2)-N(4)	99.59(11)
N(1)-Ga(1)-O(1)	112.06(10)	N(3)-Ga(2)-O(1)	119.11(11)
N(1)-Ga(1)-O(2)	111.40(11)	N(3)-Ga(2)-O(5)	110.42(11)
N(2)-Ga(1)-O(1)	123.68(11)	N(4)-Ga(2)-O(1)	115.09(10)
N(2)-Ga(1)-O(2)	108.00(11)	N(4)-Ga(2)-O(5)	108.48(11)
O(1)-Ga(1)-O(2)	102.43(10)	O(1)-Ga(2)-O(5)	103.97(10)
Ga(1)-O(1)-Ga(2)	137.63(13)		



## References

1. (a) Holm, R. H.; Everett, G. W.; Chakravorty, A. *Prog. Inorg. Chem.* **1966**, 7, 83. (b) McGeachin, S. G. *Can. J. Chem.* **1968**, 46, 1903. (c) Dorman, L. C. *Tetrahedron Lett.* **1966**, 4, 459. (d) Barry, W. J.; Finar, I.; Mooney, E. F. *Spectrochim. Acta* **1965**, 21, 1095. (e) Bonnett, R.; Bradley, D. C.; Fisher, K. J. *Chem. Commun.* **1968**, 886. (f) Bonnett, R.; Bradley, D. C.; Fisher, K. J.; Rendall, I. F. *J. Chem. Soc. (A)* **1971**, 1622. (g) Parks, J. E.; Holm, R. H. *Inorg. Chem.* **1968**, 7, 1408. (h) Richards, C. P.; Webb, G. A. *J. Inorg. Nucl. Chem.* **1969**, 31, 3459. (i) Tsybina, N. M.; Vinokurov, V. G.; Protopopova, T. V.; Skoldinov, A. P. *J. Gen. Chem., USSR* **1966**, 36, 1383. (j) Cotton, F. A.; DeBoer, B. G.; Pipal, J. R. *Inorg. Chem.* **1970**, 9, 783. (k) Elder, M.; Penfold, B. R.; *J. Chem. Soc. (A)* **1969**, 2556. (l) Honeybourne, C. L.; Webb, G. A. *Mol. Phys.* **1969**, 17, 17. (m) Honeybourne, C. L.; Webb, G. A. *Chem. Phys. Lett.* **1968**, 2, 426.
2. Hitchcock, P. B.; Lappert, M. F.; Lui, D.-S. *J. Chem. Soc., Chem. Commun.* **1994**, 2637.
3. For an excellent review, see: Bourget-Merle, L.; Lappert, M. F.; Severn, J. R. *Chem. Rev.* **2002**, 102, 3031.
4. Fahim, M.; Taylor, N. J.; Xin, S.; Collins, S. *Organometallics*, **1998**, 17, 1315.
5. Harder, S. *Angew. Chem. Int. Ed.* **2003**, 42, 3430.
6. Lesikar, L. A.; Richards, A. F. *J. Organomet. Chem.* **2006**, 691, 4250.
7. Park, K.-H.; Marshall, W. J. *J. Org. Chem.* **2005**, 70, 2075.
8. (a) Hitchcock, P. B.; Lappert, M. F.; Layh, M. *Chem Commun.* **1998**, 201. (b) Hitchcock, P. B.; Lappert, M. F.; Layh, M. *J. Chem. Soc. Dalton Trans.* **2001**, 2409.
9. Evans, I. P.; Everett, G. W.; Sargeson, A. M. *J. Am. Chem. Soc.* **1976**, 98, 8041.
10. Huang, Y.-L.; Huang, B.-H.; Ko, B.-T.; Lin, C.-C. *J. Chem. Soc. Dalton Trans.* **2001**, 1359.
11. Feldman, J.; McLain, S. J.; Parthasarathy, A.; Marshall, W. J.; Calabrese, C. J.; Arthur, S. D. *Organometallics*, **1997**, 16, 1514.
12. Wang, Y.; Quillian, B.; Wei, P.; Wang, H.; Yang, X.-J.; Xie, Y.; King, B. R.; Scheyer, P. v. R.; Schaefer, III, F. H.; Robinson, G. H. *J. Am. Chem. Soc.* **2005**, 127, 11944.
13. Stender, M.; Phillips, A. D.; Power, P. P. *Inorg. Chem.* **2001**, 40, 5314.
14. (a) Gibson, V. C.; Maddox, P. J.; Newton, C.; Redshaw, C.; Solan, G.; White, A. J. P.; Williams, D. J. *Chem. Commun.* **1998**, 1651. (b) Chamberlain, B. M.; Cheng, M.; Moore, D. R.; Ovitt, T. M.; Lobkovsky, E. B.; Coates, G. W. *J. Am. Chem. Soc.* **2001**, 123, 3229. (c) Dove, A. P.; Gibson, V. C.; Marshall, E. L.; White, A. J. P.; Williams, D. J. *Chem. Commun.* **2001**, 283.
15. Cui, C.; Roesky, H. W.; Schmidt, H.-G.; Noltemeyer, M.; Hao, H.; Cimpoesu, F. *Angew. Chem. Int. Ed.* **2000**, 39, 4274.
16. Hardman, N. J.; Eichler, B. E.; Power, P. P.; *Chem. Commun.* **2000**, 1991.

17. Hill, M. S.; Hitchcock, P. B. *Chem. Commun.* **2004**, 1818.
18. Cheng, Y.; Hitchcock, P. B.; Lappert, M. F.; Zhou, M. *Chem. Commun.* **2005**, 752.
19. Green, M. H. L.; Mountford, P.; Smout, G. J.; Speel, S. R. *Polyhedron*, **1990**, 9, 2763.
20. For a recent review see: Braunschewig, H.; Kollann, C.; Rais, D. *Angew. Chem. Int. Ed.* **2006**, 45, 5254.
21. Segawa, Y.; Yamashita, M.; Nozaki, K. *Science*, **2006**, 314, 112.
22. Panda, A.; Stender, M.; Wright, R. J.; Olmstead, M. M.; Klavins, P.; Power, P. *P. Inorg. Chem.* **2002**, 41, 3909.
23. (a) Davis, D. W.; Shirley, D. A.; Thomas, T. D. *J. Am. Chem. Soc.* **1972**, 94, 6565. (b) Coates, G. W.; Dunn, A. R.; Henling, L. M.; Dougherty, D. A.; Grubbs, R. H. *Angew. Chem. Int. Ed. Engl.* **1997**, 36, 248.
24. Yang, Z.; Zhu, H.; Ma, X.; Chai, J.; Roesky, H. W.; He, C.; Magull, J.; Schmidt, H.-G.; Noltemeyer, M. *Inorg. Chem.* **2006**, 45, 1823.
25. (a) Treibs, A.; Kreutzer, F.-H. *Liebigs Ann. Chem.* **1968**, 2405. (b) Chen, J.; Burghart, A.; Derecskei-Kovacs, A.; Burgess, K. *J. Org. Chem.* **2000**, 65, 2900. (c) Beer, G.; Niederal, C.; Gimme, S.; Daub, J. *Angew. Chem. Int. Ed.* **2000**, 39, 3252.
26. Kuhn, N.; Kuhn, A.; Speis, M.; Bläser, D.; Boese, R. *Chem. Ber.* **1990**, 123, 1301.
27. Qian, B.; Baek, S. W.; Smith, M. R. *Polyhedron* **1999**, 18, 2405.
28. Kuhn, N.; Kuhn, A.; Lewandowski, J.; Speis, M. *Chem. Ber.* **1991**, 124, 2197.
29. Maraval, A.; Owsianik, K.; Arquier, D.; Igau, A.; Coppel Y.; Donnadieu, B.; Zablocka, M.; Majoral, J.-P. *Eur. J. Inorg. Chem.* **2003**, 960.
30. (a) Ragogna, P. J.; Burford, N.; D'eon, M.; McDonald, R. *Chem. Commun.* **2003**, 1052. (b) Burford, N.; D'eon, M.; Ragogna, P.; McDonald, R.; Ferguson, M. J. *Inorg. Chem.* **2004**, 43, 734.
31. Hitchcock, P. B.; Lappert, M. F.; Nycz, J. E. *Chem. Commun.* **2003**, 1142.
32. Stender, M.; Eichler, B. E.; Hardaman, N. J.; Power, P. P.; Prust, J.; Noltemeyer, M.; Roesky, H. W. *Inorg. Chem.* **2001**, 40, 2794.
33. Singh, S.; Ahn, H.-J.; Stasch, A.; Jancik, V.; Roesky, H. W.; Pal, A.; Biadene, M.; Herbst-Irmer, R.; Noltemeyer, M.; Schmidt, H.-G. *Inorg. Chem.* **2006**, 45, 1853.
34. Kuhn, N.; Fahl, J.; Fuchs, S.; Steimann, M.; Henkel, G.; Maulitz, A. H. *Z. Anorg. Allg. Chem.* **1999**, 625, 2108.
35. Kuhn, N.; Fuchs, S.; Steimann, M. *Z. Anorg. Allg. Chem.* **2002**, 628, 458.
36. Fuchs, S.; Steimann, M.; Kuhn, N. *Phosphorus, Sulfur, Silicon and the Related Elements* **2001**, 168-169, 573.
37. Reeske, G.; Hoberg, C. R.; Hill, N. J.; Cowley, A. H. *J. Am. Chem. Soc.* **2006**, 128, 2800.
38. (a) Hill, N. J.; Findlater, M.; Cowley, A. H. *Dalton Trans.* **2005**, 3229. (b) Findlater, M.; Hill, N. J.; Cowley, A. H. *Polyhedron* **2006**, 25, 983.
39. Hill, N. J.; Moore, J. A.; Findlater, M.; Cowley, A. H. *Chem. Commun.* **2005**, 5462.

40. Lide, R. D. ed., CRC Handbook of Chemistry and Physics, *Internet Version 2007*, (87<sup>th</sup> Edition), <<http://www.hbcpnetbase.com>>, Taylor and Francis, Boca Raton, FL, 2007.
41. Vidovic, D.; Jones, J. N.; Moore, J. A.; Cowley, A. H. *Z. Anorg. Allg. Chem.* **2005**, *631*, 2888.
42. Stender, M.; Wright R. J.; Eichler B. E.; Prust, J.; Olmstead, M. M.; Roesky, H. W. Power, P. P. *J. Chem. Soc. Dalton Trans.* **2001**, 3465.
43. Brownstein, S.; Gabe, E. J.; Prasad, L. *Can. J. Chem.* **1983**, *61*, 1410.
44. Clippard, P. H.; Hanson, J. C.; Taylor, R. C. *J. Cryst. Mol. Struct.* **1971**, *1*, 363.
45. Qian, B.; Ward, D. L.; Smith, M. R. *Organometallics* **1998**, *17*, 3070.
46. Coslédan, F.; Hitchcock, P. B.; Lappert, M.-F. *Chem. Commun.* **1999**, 705.
47. Radzewich, C. E.; Coles, M. P.; Jordan, R. F. *J. Am. Chem. Soc.* **1998**, *120*, 9384.
48. Vidovic, D.; Moore, J. A.; Jones, J. N.; Cowley, A. H. *J. Am. Chem. Soc.* **2005**, *127*, 4566.
49. Kopp, M. R.; Kräuter, T.; Dashti-Momertz, A.; Neumüller, B. *Organometallics*, **1998**, *17*, 4226.
50. Vidovic, D.; Lu, Z.; Reeske, G.; Moore, J.; Cowley, A. H. *Chem. Commun.* **2006**, 3501.
51. Paetzold, P.; Neyses, S.; G  ret, L. *Z. Anorg. Allg. Chem.* **1995**, *621*, 723.
52. Hanecker, E.; N  th, H.; Weitemann, U. *Chem. Ber.* **1986**, *119*, 1904.
53. (a) Pachaly, B.; West, R. *J. Am. Chem. Soc.* **1985**, *107*, 2987. (b) Groteklaes, M.; Paetzold, P. *Chem. Ber.* **1988**, *121*, 809. (c) Ito, M.; Tokitoh, N.; Okazaki, R. *Tetrahedron Lett.* **1997**, *38*, 4451. (d) Tokitoh, N. *Main Group Chem. News* **2000**, *7*, 27.
54. (a) Kuhn, N.; Kuhn, A.; Speis, M.; Bl  ser, D.; Boese, R. *Chem. Ber.* **1990**, *123*, 1301. (b) Qian, B.; Baek, S. W.; Smith, M. R. *Polyhedron* **1999**, *18*, 2405.
55. Kuhn, N.; Kuhn, A.; Lewandowski, J.; Spies, M. *Chem. Ber.* **1991**, *124*, 2197.
56. Akitt, J. W.; In *Multinuclear NMR*; Mason, J., Ed.; Plenum Press; New York, **1987**; Chapter 9.
57. Dewar, M. J.S.; Zoebisch, E. G.; Healy, E. F.; Steward, J. J. P. *J. Am. Chem. Soc.* **1985**, *107*, 3902; MOPAC (Version 5.0) QCPE 455.
58. Cowley, A. H.; Lu, Z.; Jones, J. N.; Moore, J. A. *J. Organomet. Chem.* **2004**, *689*, 2267.
59. Harris, R. K.; Mann, B. E. ed. *NMR and the Periodic Table*, Academic Press, London, **1978**.
60. Neculai, D.; Roesky, H. W.; Neculari, A. M.; Magull, J. M.; Walfort, B.; Stalke, D. *Angew. Chem. Int. Ed.* **2002**, *41*, 4294.
61. (a) Becke, A. D. *J. Chem. Phys.* **1992**, *96*, 2155. (b) Becke, A. D. *J. Chem. Phys.* **1993**, *98*, 5648.
62. Lesikar, L. A.; Richards A.F. *J. Organomet. Chem.* **2006**, *691*, 4250.
63. See, for example: (a) Nugent, W. A.; Mayer, J. M. *Metal Ligand Multiple Bonds*; Wiley-Interscience: New York, 1998. (b) Hendon, J. W. *Coord. Chem. Rev.* **2003**, *243*, 3.

64. See, for example: (a) Grumbine, S. K.; Tilley, T. D.; Arnold, F. P.; Rheingold, A. L. *J. Am. Chem. Soc.* **1993**, *115*, 7884. (b) Mitchell, G. P.; Tilley, T. D. *J. Am. Chem. Soc.* **1998**, *120*, 7635. (c) Wanadi, P. W.; Glaser, P. B.; Tilley, T. D. *J. Am. Chem. Soc.* **2000**, *122*, 972. (d) Mork, B. V.; Tilley, T. D. *Angew. Chem. Int. Ed.* **2003**, *42*, 357.
65. (a) Cowley, A. H.; Lomeli, V.; Voight, A. *J. Am. Chem. Soc.* **1998**, *120*, 6401. (b) Braunschweig, H.; Kollann, C.; Englert, U. *Angew. Chem. Int. Ed.* **1998**, *37*, 3179. (c) Irvine, G. J.; Rickard, C. E. F.; Roper, W. R.; Williamson, A.; Wright, L. J. *Angew. Chem. Int. Ed.* **2000**, *39*, 948. (d) Braunschweig, H.; Kollann, C.; Englert, U. *Angew. Chem. Int. Ed.* **2001**, *40*, 4198.
66. See, for example: (a) Braunschweig, H.; *Ad. Organomet. Chem.* **2004**, *51*, 163. Coombs, D. L.; (b) Aldridge, S.; Rossin, A.; Jones, C.; Willcok D. J. *Organometallics* **2004**, *23*, 2911 (c) Braunschweig, H.; Rais, D.; Kollann, C. *Angew. Chem. Int. Ed.* **2006**, *45*, 5254.
67. (a) Timms, P. L. *J. Am. Chem. Soc.* **1967**, *89*, 1629. (b) Timms, P. L. *Acc. Chem. Res.* **1973**, *6*, 118.
68. Pachaly, B.; West, R. *Angew. Chem. Int. Ed.* **1984**, *23*, 454.
69. (a) Baker, R. T.; Ovenall, D. W.; Calabrese, J. C.; Westcott, S. A.; Taylor, N. J.; Williams, I. D.; Marder, T. B. *J. Am. Chem. Soc.* **1990**, *112*, 9399. (b) Knorr, J. R.; Merola, J. S. *Organometallics* **1990**, *9*, 3008.
70. Braunschweig, H.; Wagner, T. *Angew. Chem. Int. Ed.* **1995**, *34*, 825.
71. (a) Bransuchweig, H.; Colling M.; Kollann C.; Stammmler H. G.; Neumann B. *Angew. Chem. Int. Ed.* **2001**, *40*, 2298. (b) Bransuchweig, H.; Colling M.; Hu, C.; Radacki, K. *Angew. Chem. Int. Ed.* **2003**, *42*, 205.
72. Coombs, D. L.; Aldridge, S.; Jones, C.; Willock, D. J. *J. Am. Chem. Soc.* **2003**, *125*, 6356.
73. Kays (née Coombs), D. L.; Day, J. K.; Ooi, L.-L.; Aldridge, S. *Angew. Chem. Int. Ed.* **2005**, *44*, 7457.
74. Aldridge, S.; Jones, C.; Gans-Eichler, T.; Stasch, A.; Keys (née Coombs), D. L.; Coombs, N. D.; Willock, D. J. *Angew. Chem. Int. Ed.* **2006**, *45*, 6118.
75. Macdonald, C. L.B.; Cowley, A. H. *J. Am. Chem. Soc.* **1999**, *121*, 12113.
76. Ohishi, T.; Shiotani, Y.; Yamashita, M. *J. Org. Chem.* **1994**, *59*, 250.
77. Jutzi, P.; Krato, B.; Hursthouse, M.; Howes, A. J. *Chem. Ber.* **1987**, *120*, 565.
78. NBO Version 3.1, Glendening, E. D.; Reed, A. E.; Carpenter, J. E.; Weinhold, F.
79. Burkhardt, E. R.; Matos, K. *Chem. Rev.* **2006**, *106*, 2617.
80. Eisch, J.J. In *Comprehensive Organometallic Chemistry II*; Abel, E. W., Stone, F. G. A., Wilkinson, G., Eds.; Elsevier: Oxford, UK, 1995; Vol 1, Chapter 10.
81. Piers, W. E.; Chivers, T. *Chem. Soc. Rev.* **1997**, *26*, 345.
82. (a) Sinn, J.; Karninsky, W.; Vollmer, H. J.; Woldt, R. *Angew. Chem., Int. Ed. Engl.* **1980**, *19*, 390. (b) Sinn, H.; Karninsky, W. *Adv. Organomet. Chem.* **1980**, *18*, 99.
83. (a) Piers, W. E.; Bourke, S. C.; Conroy, K. D. *Angew. Chem., Int. Ed. Engl.* **2005**, *44*, 5016. (b) Kölle, P.; Nöth, H. *Chem. Rev.* **1985**, *85*, 399.
84. Nöth, H.; Staudigl, R.; Wagner, H.-U. *Inorg. Chem.* **1982**, *21*, 706.

85. Courtenay, S.; Mutus, J. Y.; Schurko, R. W.; Stephan, D. W.; *Angew. Chem. Int. Ed.* **2002**, *41*, 498.
86. (a) Narula, C. K.; Nöth, H. *J. Chem. Soc. Chem. Commun.* **1984**, 1023. (b) Narula, C. K.; Nöth, H. *J. Inorg. Chem.* **1984**, *23*, 4147. (c) Narula, C. K.; Nöth, H. *J. Inorg. Chem.* **1985**, *24*, 2532.
87. Jutzi, P.; Karato, M.; Hursthouse, M.; Howers, A. J. *Chem. Ber.* **1987**, *120*, 1091.
88. Kuhn, N.; Kuhn, A. Lewandowski, J. *Chem. Ber.* **1991**, *124*, 2197.
89. (a) Cowley, A. H.; Lu, Z.; Jones, J. N.; Moore, J. A. *J. Organomet. Chem.* **2004**, *689*, 2267. (b) Vidovic, D.; Moore, J. A.; Jones, J. N.; Cowley, A. H. *J. Am. Chem. Soc.* **2005**, *127*, 4566.
90. Gates, D. P.; McWilliams, A. R.; Ziembinski, R.; Liable-Sands, L. M.; Guzei, I. A.; Yap, G. P. A.; Rheingold, A. L.; Manners, I. *Chem. Eur. J.* **1998**, *4*, 1489.
91. Ghesner, I. Piers, W.; E. McDonald, R. *Chem. Commun.* **2005**, 2480.
92. Davidson, M. G.; Fox, A.; Hibbert, T. G.; Howard, J. A. K.; Mackinnon, A.; Neretin, I. S.; Wade, K. *Chem. Commun.* **1999**, 1649.
93. De Biani, F. F.; Gmeinwieser, T.; Herdtweck, E.; Jäkle, F.; Laschi, F.; Wagner, M.; Zanello, P. *Organometallics* **1997**, *16*, 4776.
94. Wei, P.; Atwood, D. A. *Inorg. Chem.* **1998**, *37*, 4934.
95. (a) Kim, K.-C.; Reed, C. A. *J. Am. Chem. Soc.* **2002**, *124*, 7662. (b) Young, J. D.; Khan, M. A.; Wehmschulte, R. J. *Organometallics*, **2004**, *23*, 1965.
96. (a) Radzewich, C. E. Guzei, I. A.; Jordan R. F. *J. Am. Chem. Soc.* **1999**, *121*, 8673. (b) Masuda, J. D.; Stephan, D. W. *Dalton Trans.* **2006**, 2089.
97. (a) Coles, M. P.; Jordan, R. F. *J. Am. Chem. Soc.* **1997**, *119*, 8125. (b) Bruce, M.; Gibson, V. C.; Rredshaw, C.; Solan, G. A.; White, A. J. P.; Williams, D. J. *Chem. Commun.* **1998**, 2523. (c) Coslédan, F.; Hitchcock, P. B.; Lappert, M. F. *Chem. Commun.* **1999**, 705. (d) Kuhn, N.; Fuchs, S.; Maichle-Möbmer, Niquet, E. *Z. Anorg. Allg. Chem.* **2000**, *626*, 2248. (e) Baker, R. J.; Farley, R. D.; Jones, C.; Kloth, M.; Murphy, D. M. *J. Chem. Soc. Dalton Trans.* **2002**, 3844. (f) Wrobel, O.; Schaper, F.; Brintzinger, H. *Organometallics*, **2004**, *23*, 900. (g) Masuda, J. D.; Walsh, D. M.; Wei, P.; Stephan, D. W. *Organometallics*, **2004**, *23*, 1819. (h) Dagorne, S.; Bellemin-Laponnaz, S.; Welter, R. *Organometallics*, **2004**, *23*, 3053.
98. Atwood, J. L.; Bott, S. G.; Harvey, S.; Junk, P. C. *Organometallics*, **1994**, *13*, 4151.
99. (a) Bellavance, P. L.; Corey, E. R.; Corey, J. Y. Hey, G. W. *Inorg. Chem.* **1977**, *16*, 462. (b) Atwood, D. A.; Jegier, J. A.; Rutherford, D. *J. Am. Chem. Soc.* **1995**, *117*, 6779. (b) Atwood, D. A.; Jegier, J. A.; Rutherford, D. *Inorg. Chem.* **1996**, *35*, 63. (c) Jegier, J. A.; Muñoz-Hernández, M.-Á. Atwood, D. A. *J. Chem. Soc. Dalton Trans.* **1999**, 2583. (d) Sluka, R.; Nečas, M.; Šindelář, P. *Acta Cryst.* **2004**, *E60*, m447.
100. Bott, S. G.; Elgamal, H.; Atwood, J. L. *J. Am. Chem. Soc.* **1985**, *107*, 1797.
101. Korolev, A. V.; Guzei, I. A.; Jordan, R. F. *J. Am. Chem. Soc.* **1999**, *121*, 11605.
102. Atwood, D. A. *Coord. Chem. Rev.* **1998**, *176*, 407.

103. (a) Evans, D. A.; Chapman, K. T.; Bisaha, J. *J. Am. Chem. Soc.* **1988**, *110*, 1238. (b) Castellino, S.; Dwight, W. J. *J. Am. Chem. Soc.* **1993**, *115*, 2986.
104. Wehmschulte, R. J.; Steele, J. M.; Young, J. D.; Masood, A. K. *J. Am. Chem. Soc.* **2003**, *125*, 1470.
105. (a) Korolev, A. V.; Delpech, F.; Dagorne, S.; Guzei, I. A.; Jordan, R. F. *Organometallics*, 2001, *20*, 3369. (b) Bunn, N. R.; Aldridge, S.; Kays, D. L.; Coombs, N. D.; Rossin, A.; Willcock, D. J.; Day, J. K.; Jones, C.; Ooi, L. *Organometallics*, **2005**, *24*, 5891.
106. (a) Klosin, J.; Roof, G. R.; Chen, E. Y.-X. *Organometallics*, 2000, *19*, 4686. (b) Jenkins, H. A.; Dumaresque, C. L.; Vidovic, D.; Clyburne, J. A. C. *Can. J. Chem.* **2002**, *80*, 1398. (c) Dagorne, S.; Bellemin-Laponnaz, S.; Maisse-François, Rager, M.-N.; Jugé, L.; Welter, R. *Eur. J. Inorg. Chem.* **2005**, 4206.
107. (a) Cowley, A. H.; Gabbaï, F. P.; Atwood, D. A.; Carrano, C. J.; Mokry, L. M.; Bond, R. M. *J. Am. Chem. Soc.* 1994, *116*, 1159. (b) Baker, R. J.; Jones, C.; Kloth, M.; Mills, D. P. *New J. Chem.* **2004**, *28*, 207.
108. (a) Restivo, R.; Palenik, G. J. *J. Chem. Soc. Dalton Trans.* **1971**, 341. (b) Manessi, A.; Papaefstathiou, G. S.; Raptopoulou, C. P.; Terzis, A.; Zafiroopoulos, T. F. *J. Inorg. Biochem.* **2004**, *98*, 2052.
109. For example see : (a) Hardman, N. J.; Eichler, B. E.; Power, P. P. *Chem. Commun.* **2000**, 1991. (b) Baker, R. J.; Jones, C. *Coord. Chem. Rev.* **2005**, *249*, 1857. (c) Wiecko, M.; Roesky, P. W.; Nava, P.; Ahlrichs, R.; Konchenko, S. N. *Chem. Commun.* **2007**, 927. and the references within.
110. Kunze, A.; Gleiter, R.; Bethke, S.; Rominger, F. *Organometallics*, **2006**, *25*, 4787.
111. Buchin, B.; Gemel, C.; Cadenbach, T.; Fernández, I.; Frenking, G.; Fischer, R. A. *Angew. Chem. Int. Ed.* **2006**, *45*, 5207.
112. (a) Britovsek, G. J. P.; England, J.; White, A. J. P. *Inorg. Chem.* **2005**, *44*, 8134. (b) Vidovic, D.; Lu, Z.; Reeske, G.; Moore, J.; Cowley, A. H. *Chem. Commun.* **2006**, 3501.
113. (a) Olah, G. A.; Farooq, O.; Farina, S. M. F.; Olah, J. A. *J. Am. Chem. Soc.* **1988**, *110*, 2560. (b) Mayers, E. L.; Butts, C. P.; Aggarwal, V. K. *Chem. Commun.* **2006**, 4434. (c) Olah, G. A.; Farooq, O.; Li, C. X.; Morteza, Farina, M. A. F.; Aklonis, J. J. *J. App. Polym. Sci.* **1992**, *45*, 1355.
114. (a) Fringuelli, F.; Pizzo, F.; Tortoioli, S.; Vaccaro, L. *J. Org. Chem.* **2004**, *69*, 7754. (b) Williams, D. B. G.; Lawton, M. *Tetrahedron Lett.* **2006**, *47*, 6557. (c) Coulombel, L.; Rayzmann, M.; Pons, J.-M.; Olivero, S.; Duñach, E. *Chem. Eur. J.* **2006**, *12*, 6356. (d) Chaminade, X.; Coulombel, L.; Olivero, S.; Duñach, E. *Eur. J. Org. Chem.* **2006**, 3554. (e) Yang, Y.; Diederich, F.; Valentine, J. S. *J. Am. Chem. Soc.* **1991**, *113*, 7195. (f) Williams, D. B. G.; Lawton, M. *Org. Biomol. Chem.* **2005**, *3*, 3269.
115. (a) Prakash, G. K. S.; Yan, P.; Török, B.; Bucsi, I.; Tanaka, M.; Olah, G. A. *Catal. Lett.* **2003**, *85*, 1. (b) Yan, P.; Batamack, P.; Prakash, G. K. S.; Olah, G. A. *Catal. Lett.* **2005**, *103*, 165. (c) Li, H.-J.; Tian, H.-Y.; Chen, Y.-J.; Wang, D.; Li, C.-J. *Chem. Commun.* **2002**, 2994. (d) Yan, P.; Batamack, P.; Prakash, G. K. S.; Olah, G. A. *Catal. Lett.* **2005**, *101*, 141.

116. Bondi, A. *J. Phys. Chem.* **1964**, *68*, 441.
117. Ma, K.; Bats, J. W.; Wagner, M. *Acta Cryst.* **2001**, *E57*, 846.
118. Yamashita, M.; Yamamoto, Y.; Akiba, K.; Hashizume, D.; Iwasaki, F.; Takagi, N.; Nagase, S.; *J. Am. Chem. Soc.* **2005**, *127*, 4354.
119. Cowley, A. H.; Gabbai, F. P.; Atwood, D. A.; Carrano, C. J.; Mokry, L. M.; Bond, M. R. *J. Am. Chem. Soc.* **1994**, *116*, 1559.
120. Burford, N.; Ragogna, P. J.; Robertson, K. N.; Cameron, T. S. *J. Am. Chem. Soc.* **2002**, *124*, 382.
121. Sheldrick, G.M. *Shelxtl Pc*. 1994, Siemens Analytical X-ray Instruments Inc.
122. Frisch, M. J.; Trucks, G. W.; Schlegel, H. B.; Scuseria, G. E.; Robb, M. A.; Cheeseman, J. R.; Montgomery, Jr., J. A.; Vreven, T.; Kudin, K. N.; Burant, J. C.; Millam, J. M.; Iyengar, S. S.; Tomasi, J.; Barone, V.; Mennucci, B.; Cossi, M.; Scalmani, G.; Rega, N.; Petersson, G. A.; Nakatsuji, H.; Hada, M.; Ehara, M.; Toyota, K.; Fukuda, R.; Hasegawa, J.; Ishida, M.; Nakajima, T.; Honda, Y.; Kitao, O.; Nakai, H.; Klene, M.; Li, X.; Knox, J. E.; Hratchian, H. P.; Cross, J. B.; Adamo, C.; Jaramillo, J.; Gomperts, R.; Stratmann, R. E.; Yazyev, O.; Austin, A. J.; Cammi, R.; Pomelli, C.; Ochterski, J. W.; Ayala, P. Y.; Morokuma, K.; Voth, G. A.; Salvador, P.; Dannenberg, J. J.; Zakrzewski, V. G.; Dapprich, S.; Daniels, A. D.; Strain, M. C.; Farkas, O.; Malick, D. K.; Rabuck, A. D.; Raghavachari, K.; Foresman, J. B.; Ortiz, J. V.; Cui, Q.; Baboul, A. G.; Clifford, S.; Cioslowski, J.; Stefanov, B. B.; Liu, G.; Liashenko, A.; Piskorz, P.; Komaromi, I.; Martin, R. L.; Fox, D. J.; Keith, T.; Al-Laham, M. A.; Peng, C. Y.; Nanayakkara, A.; Challacombe, M.; Gill, P. M. W.; Johnson, B.; Chen, W.; Wong, M. W.; Gonzalez, C.; and Pople, J. A.; GAUSSIAN (B.04), Gaussian, Inc., Pittsburgh, PA, 2003.
123. Schaftenaar, G.; Noordik, J.H. *J. Comput.-Aided Mol. Design* **2000**, *14*, 123.

## VITA

Dragoslav Vidović was born in Mrkonjić Grad, Republic of Srpska, BiH on January 24<sup>th</sup> 1978, the son of Vlatko and Stana Vidović. In 1996, he left Serbia and moved to Vancouver, Canada. He entered Douglas College in 1998 and transferred to Simon Fraser University in 1999 where he graduated in 2002 with the degree of B.S. In September 2002, he enrolled in the doctoral program in Chemistry at the University of Texas at Austin where he received several awards including a Welch Research Fellowship (Summer 2005) and a Houston Endowment President's Excellence Scholarship (Fall 2006).

Permanent Address: Takovska 7  
Belgrade, Serbia

This dissertation was typed by the author.